Native mass spectrometry approaches to study zinc-binding plasma proteins

Esther Marie Martin

A thesis submitted in partial fulfilment of the requirements for the degree of Doctor of Philosophy in Chemistry

Department of Chemistry
University of Warwick

February 2013

Table of Contents

2 Experimental methods

List of Figures

1 Introduction

3 HSA-ligand complexes

4 Travelling-wave ion mobility mass spectrometry of HSA

5 Metal binding properties of a peptide mimic of HRG

List of Tables

Acknowledgements

Firstly, I would like to extend my gratitude to my supervisors, Dr Claudia Blindauer and Prof Peter Sadler for giving me the opportunity to undertake this research project and for their guidance over the past few years.

A big thank you to all the members of the Blindauer group both past and present for all their help: James, Amira, Maria, Tanvir, Greg, Fran, Jie, Oksana and Jin. I also thank the Dixon group for all our interesting discussions on proteins and in particular to Fay and Mike - all those lattes definitely helped!

I am extremely grateful to all the members of the Chemical Biology Research Facility for their help in the lab and for use of the equipment.

Also thanks must go to the Sadler group for making me feel so welcome on the fourth floor, particularly to Ruth McQuitty for her help with the HPLC.

I would also like to express my gratitude to Andrea Lopez-Clavijo for her mass spectrometry advice and useful discussions about albumin.

Thanks go to Dr Alan Stewart (University of St Andrews) for his valuable ideas on the project and the kind donation of protein samples.

Without the help of many people it would not have been possible to carry out this work so thank you to Dr Lijiang Song, Philip Aston, Dr Ivan Prokes, Edward Tunnah, Anne Smith, Dr Rod Watson (Bruker), Dr Julia Smith (Bruker) and Dr George McLeod (Bruker). Also thanks to Nick Barker for giving me the opportunity to help out with the Schools Outreach Program.

I would like to thank all my friends and family for all their love and encouragement (Mom and Dek, Dad and Jo, Em, Jon, Nanny Rose and Grandad John). And to Tom: thanks for your continued reassurance and cups of tea.

Finally, I dedicate this thesis to Nanny Marie and Grandad Walter.

Declaration

I hereby declare that this thesis, submitted in partial fulfilment for the degree of Doctor of Philosophy, represents my own work and has not been previously submitted to this or any other institution for another qualification. Work was carried out between October 2009 and December 2012 under the supervision of Dr Claudia Blindauer and Prof Peter Sadler.

Collaborative work contributes to Chapter 4 and parts of Chapter 5. In summary, ion-mobility mass spectrometry experiments were carried out in collaboration with Dr Frances Kondrat and electron transfer dissociation data with Dr Julia Smith (Bruker, Coventry, UK). In both cases, the data analysis was carried out by the author. Other contributions are explicitly stated throughout.

Esther Marie Martin
February 2013

Abstract

Human serum albumin (HSA) is a plasma protein that fulfils a wide range of biological functions and is thought to be the major Zn^{2+} transporter in blood plasma. The high affinity Zn^{2+} binding site (Site A) has recently been characterised and is located at an interdomain site. In addition to metal binding, HSA is also important in the transport of fatty acids. Previous work has shown that the binding of Zn^{2+} at Site A and the binding of myristate at fatty acid site 2 are mutually exclusive. It has been predicted that upon fatty acid binding, a conformational change occurs that can disrupt the residues that form Site A. This allosteric interaction could have an impact on the Zn^{2+} dependent activities of histidine-rich glycoprotein (HRG), a plasma protein involved in blood coagulation. The purpose of this work was to investigate the metal-binding properties of HSA and a peptide derived from HRG using a native MS approach. Furthermore, the possible Zn^{2+} transfer between the proteins was explored and also whether fatty acids influenced the Zn^{2+} distribution.

Native ESI-MS was able to detect Zn^{2+} ions associating with HSA although the interactions with fatty acids appeared to be broken upon entering the gas phase. No apparent loss of Zn^{2+} from HSA was observed by ESI-MS following incubation with myristate which was confirmed by elemental analysis in solution. Travelling wave ion mobility-MS showed no significant conformational changes between apo-HSA and holo-HSA although Zn^{2+} appears to have a role in stabilising the domain I/II interface. HSA incubated with myristate showed a larger collisional cross section that is in agreement with the X-ray crystal structures.

A peptide mimicking the His-rich region of HRG, HRGP330, was found to bind up to 5 Zn^{2+} ions by ESI-MS and evidence from a combination of circular dichroism spectroscopy, ion mobility and top-down MS/MS indicated that a conformational change occurs upon Zn^{2+} binding. During CID and ETD, Zn^{2+}-binding fragments were able to be detected in order

to map which residues Zn^{2+} was bound to. However, numerous fragments were detected and so it would appear that several possible binding sites in HRGP330 have a similar binding affinity for Zn^{2+}. Complementary ESI-MS and elemental analysis showed that up to 90% of Zn^{2+} was transferred from HSA to HRGP330 even in the absence of fatty acid. Cu^{2+} also preferentially bound to HRGP330 over the N-terminal peptide mimic of HSA. Overall this could have implications for how these metal ions are transported in blood plasma as it would appear from this evidence that HRG is a significant competitor for metal ions bound to HSA.

Abbreviations

1-D, 2-D, 3-D	One-. two-, three-dimensional
Å	Angstrom
ATCUN	Amino terminal Cu^{2+} and Ni^{2+} binding
ATD	Arrival time distribution
ATP	Adenine triphosphate
BSA	Bovine serum albumin
CD	Circular dichroism spectroscopy
CID	Collision induced dissociation fragmentation
DEPC	Diethyl pyrocarbonate
DSA	Dog serum albumin
DTNB	5,5-dithiobis (2-nitrobenzoic acid) or Ellman's reagent
DTT	Dithiothreitol
ECD	Electron capture dissociation fragmentation
EDTA	Ethylenediaminetetraacetic acid
ESI-MS	Electrospray ionisation-mass spectrometry
ETD	Electron transfer dissociation fragmentation
FA	Fatty acid
GGH	Gly-Gly-His peptide
HEPES	4-(2-Hydroxyethyl)piperazine-1-ethanesulfonic acid
HMWK	High molecular weight kininogen
HRG	Histidine-rich glycoprotein
HRGP330	Histidine-rich glycoprotein peptide, residues 330-365
HRGP335	Histidine-rich glycoprotein peptide, residues 335-365
HRR	His-rich region
HSA	Human serum albumin
ICP-MS	Inductively coupled plasma-mass spectrometry
ICP-OES	Inductively coupled plasma-optical emission spectroscopy
IM-MS	Ion mobility-mass spectrometry
ITC	Isothermal titration calorimetry
LCFA	Long chain fatty acid
MCFA	Medium chain fatty acid
MS	Mass spectrometry
MS/MS	Tandem mass spectrometry
MWCO	Molecular weight cut-off
NMR	Nuclear magnetic resonance
NOESY	Nuclear Overhauser enhancement spectroscopy
PFCA	Perfluorinated carboxylic acid
PFOA	Perfluorooctanoic acid

pI	Isoelectric point
ppb	Parts per billion
ppm	Parts per million
PRR	Pro-rich region
PTR	Proton transfer reaction
QTOF	Quadrupole-Time-of-Flight
RP-HPLC	Reverse phase-high pressure liquid chromatography
SCFA	Short chain fatty acid
SDS-PAGE	Sodium dodecyl sulphate-polyacrylamide gel electrophoresis
SEC	Size exclusion chromatography
TOCSY	Total correlated spectroscopy
TOF	Time of flight
TWIM-MS	Travelling wave ion mobility-mass spectrometry
UHR	Ultra-high resolution
Zincon	2-[5-(2-Hydroxy-5-sulfophenyl)-3-phenyl-1-formazyl] benzoic acid

Amino acid abbreviations

Single letter code	Three letter code	Full name
A	Ala	Alanine
C	Cys	Cysteine
D	Asp	Aspartic acid
E	Glu	Glutamic acid
F	Phe	Phenylalanine
G	Gly	Glycine
H	His	Histidine
I	Ile	Isoleucine
K	Lys	Lysine
L	Leu	Leucine
M	Met	Methionine
N	Asn	Asparagine
P	Pro	Proline
Q	Gln	Glutamine
R	Arg	Arginine
S	Ser	Serine
T	Thr	Threonine
V	Val	Valine
W	Trp	Tryptophan
Y	Tyr	Tyrosine

Chapter 1

Introduction

1.1 Metal ions in biological systems

Many transition metals play crucial roles in biology where they can enhance or even determine the activities of biomolecules. Approximately 50% of all enzymes require interaction with a metal ion to fulfil their biological function (Waldron *et al*., 2009). A delicate balance of these elements needs to be maintained as high concentrations can be toxic but too little can be equally damaging and have a detrimental effect on cells.

Metal ions can be classed as “essential” to the development of an organism or “non-essential”. One hundred years ago, Bertrand derived a mathematical relationship between the concentration of the nutrient and the effect on health as shown in Figure 1.1 (Bertrand, 1912). For those that are essential (e.g. Zn^{2+}) an optimal balance is needed and a deficiency can be detrimental to health. Essential metal ions can also become toxic when the concentration becomes excessive. Non-essential metal ions (e.g. Cd^{2+}) can only be tolerated at a low concentration, which is demonstrated by the sharp drop in beneficial effects as the concentration increases. This model highlights that every trace metal ion can be potentially toxic and it is the concentration that determines this toxicity (Mertz, 1981).

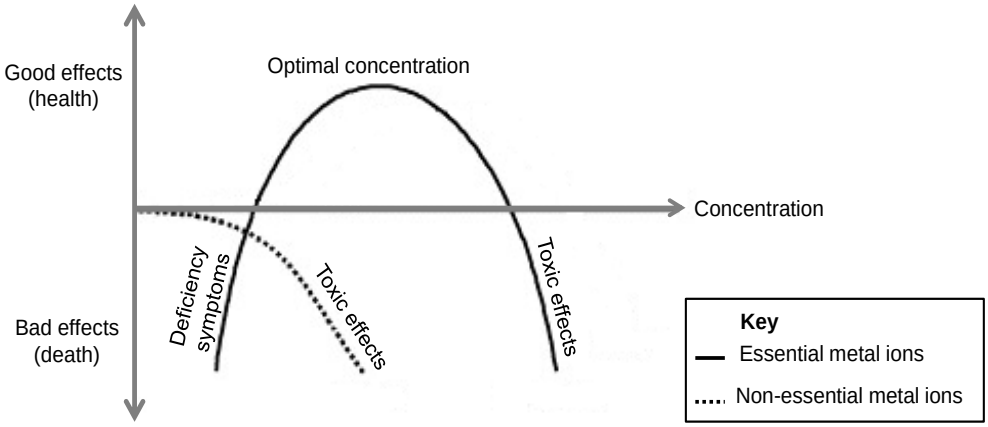

Figure 1.1 Essential vs. non-essential metal ions. The diagram illustrates that the effect of a metal ion on an organism is concentration dependent. Biologically essential metal ions can become toxic at high concentrations and non-essential metal ions can only be tolerated at low concentrations. Adapted from Bertrand (1912).

1.2 The importance of Zn^{2+}

Zn^{2+} is the second most abundant trace metal ion present in man after iron, with 2-3 g in adult humans (Haase and Rink, 2009). It is considered to be relatively non-toxic to humans (Fosmire, 1990) and studies administering the radioisotope ^{65}Zn to patients showed that 90% of the metal ion is stored in the bones and muscle (Wastney *et al*., 1986). In biology, Zn^{2+} exists only in a 2+ oxidation state and does not undergo redox reactions, a consequence of its filled d orbital. Furthermore, it is a borderline Lewis acid which allows it to interact with a variety of ligand donors including nitrogen, sulfur and oxygen. A study of 57 organisms in 2006 indicated that Zn^{2+}-binding proteins are extremely abundant, comprising 4-10% of proteomes (Andreini *et al*., 2006).

Zn^{2+} is vital for many cellular processes, and its roles in nature can be broadly placed into three categories: structural, catalytic and regulatory. It is involved in the transmission of genetic information, the development

of the immune system and as a signalling substance (Cousins *et al.*, 2006). On a cellular level it has critical roles in proliferation and apoptosis and therefore is essential for growth (Maret and Sandstead, 2006). Many enzymes require Zn^{2+} in order to be catalytically active, for example, carbonic anhydrase which allows the interconversion of carbon dioxide and water to bicarbonate and protons to proceed rapidly (Keilin and Mann, 1940). In addition, Zn^{2+} is required in so-called "Zn^{2+} finger proteins" where the protein chain arranges itself around the metal ion to form a stable fold. An example of this was first discovered in a transcription factor from *Xenopus Laevis*, TFIIIA, which contained a series of these small domains which were ordered in the presence of Zn^{2+} (Miller *et al*., 1985).

1.3 Blood plasma proteins

Blood plasma contains many different types of components including cells, low molecular weight compounds and proteins (Schaller *et al*., 2008). The concentrations of plasma proteins span a wide concentration range over 10 orders of magnitude (Anderson and Anderson, 2002). Lesser abundant proteins are often difficult to isolate and characterise due to the high content of albumin (55%) in blood which can cause interference. Globulins form the second most abundant fraction (38%) followed by fibrinogen which makes up around 7% of the total protein in plasma (Porth, 2002). Those proteins that are of much lower abundance include tissue leakage proteins and interleukins with concentrations as low as a few pg/ml (Anderson and Anderson, 2002). Proteins that are not

normally present in healthy plasma may accumulate as a biomarker for a particular disease which further complicates the system (Schaller *et al*., 2008). This study will focus on two particular plasma proteins: human serum albumin (HSA) and histidine-rich glycoprotein (HRG) with a focus on their metal-binding properties.

1.4 Human serum albumin (HSA)

1.4.1 Structure and function

HSA is the most abundant protein in blood plasma and is synthesised in the liver (Peters, 1995). It belongs to the albuminoid protein family along with α-fetoprotein and vitamin D-binding protein. Expression of HSA begins during foetal development and is at normal levels at birth. The protein is continuously turned over and typically found at concentrations of ~0.6 mM in plasma (Peters, 1995). It has the extraordinary ability to bind multiple types of ligand including metal ions, fatty acids, hormones and drug molecules (Kragh-Hansen *et al*., 2002; Fasano *et al.*, 2005). HSA has an isoelectric point (pI) of 5.67 which indicates it is negatively charged at physiological pH. This negative charge is important for its biological roles, which are summarised in Figure 1.2. For example, HSA maintains colloid osmotic pressure by preventing water from escaping from the intravascular compartment. The protein does this by attracting positively charged sodium ions across the capillary membrane which causes water to follow. Ultimately, this distribution of fluids is important for regulating body temperature.

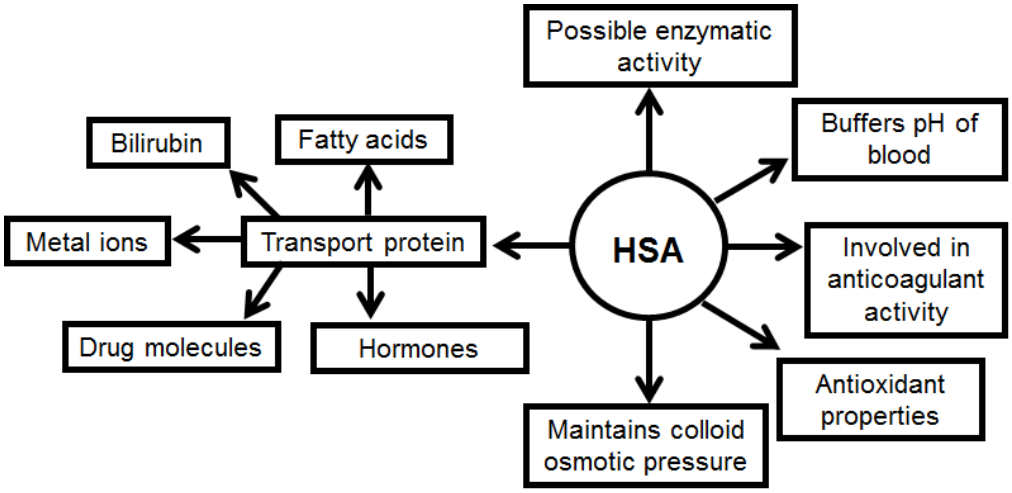

Figure 1.2 Summary of the biological functions of HSA.

The 66 kDa protein forms a heart-shaped structure with the dimensions 80 x 30 Å (He and Carter, 1992). The structure consists of three homologous domains as highlighted in Figure 1.3: domain I from residues 1-181 (blue), domain II from 188-373 (red) and domain III (green) from 380-571. Each of the domains is separated into two sub-domains that are given the notation “A” and “B” (He and Carter, 1992; Curry *et al*., 1998; Sugio *et al*., 1999). It is a largely helical protein (67%) with each of these three domains containing 10 principal helices as highlighted in Figure 1.3 (He and Carter, 1992; Peters, 1995). A common characteristic within the albumin family is the formation of 17 disulfide bridges which stabilise its folded structure and allow it to have a lengthy *in vivo* circulating half-life of approximately 19 days (Peters, 1995). Six of these bridges are formed in domains II and III, with domain I only having five disulfide bonds and a free thiol at Cys34. This residue is susceptible to oxidation and it can form disulfide bonds with other free thiols in plasma such as circulating glutathione.

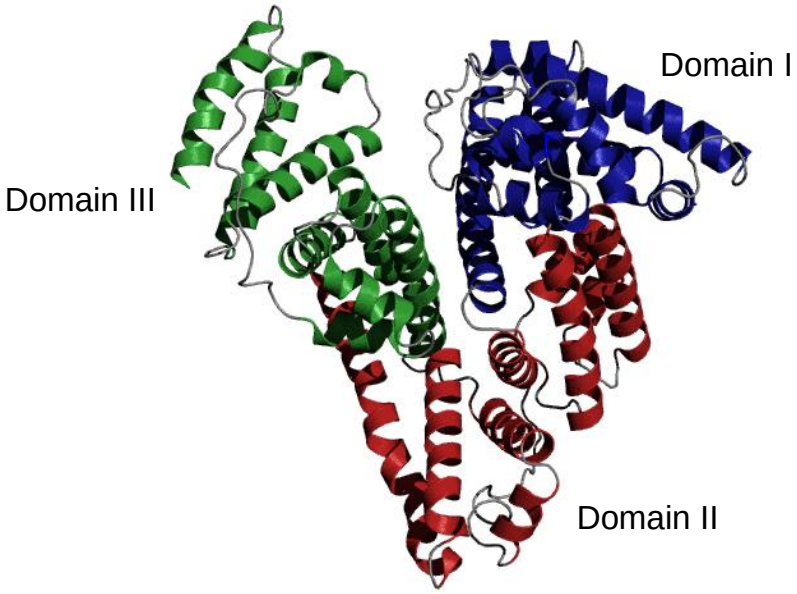

Figure 1.3 X-ray crystal structure of HSA. The three homologous domains are highlighted as follows: *blue* = domain I, *red* = domain II and *green* = domain III. The figure was created using PyMOL v1.3 and based on PDB 1AO6.

1.4.2 HSA-dimer formation

It has been well documented in the literature that HSA can form a dimer that is suggested to form through a covalent disulfide bond between Cys34 of two HSA molecules. Evidence against this, however, is that this residue is buried in a hydrophobic cavity 9.4 Å deep but it has been proposed that the pocket could flatten out to bring the residues closer together in space (Peters, 1995). A synthetic mercury bridged dimer was first produced by Straessle and co-workers in 1954 by linking the Cys34 residue of two HSA molecules, although it showed low stability (Edsall *et al*., 1954; Straessle, 1954). Other efforts with longer linker molecules to avoid strain on the protein molecules achieved high yields and a dimer that was stable for over a year at room temperature (Komatsu *et al.*, 1999). It is not known in great detail what biological significance a HSA dimer may have, although the possible clinical applications have recently

been reviewed (Taguchi *et al.*, 2012). These include its use as a plasma volume expander to treat conditions such as inflammation and as a drug carrier because it shows prolonged blood retention compared to the monomer.

1.4.3 HSA as a Zn^{2+} transporter

The concentration of Zn^{2+} in plasma is estimated to be ca. 15-20 μM (Kiilerich *et al*., 1980). It is thought that HSA is the major transporter of Zn^{2+} in blood plasma (Cousins, 1986) and binds approximately 80% of the metal ion present (Foote and Delves, 1984). The remainder is bound by α2-macroglobulin and low molecular weight compounds such as Cys and His which are able to compete for protein-bound Zn^{2+} (Giroux and Henkin, 1972). Although early studies implicated transferrin in Zn^{2+} transport this was found to be an insignificant amount (Chesters *et al*., 1981).

HSA has an important role in reducing the toxicity of Zn^{2+} to cells and it also influences the delivery of Zn^{2+}. At physiological concentrations HSA was capable of protecting human WRL-68 cells from toxic concentrations of Zn^{2+} as high as 600 μM (Blindauer *et al*., 2009). The presence of albumin reduced the amount of Zn^{2+} uptake into erythrocytes suggesting that it is involved in a regulation mechanism (Gálvez *et al*., 2001). The Zn^{2+}-albumin complex has also been shown to be important for Zn^{2+} acquisition by endothelial cells (Rowe and Bobilya, 2000; Tibaduiza and Bobilya, 1996). Cases of familial hyperzincemia, an excess Zn^{2+} disorder,

appear to be due to enhanced occupancy of the metal ion to HSA (Failla *et al*., 1982).

1.5 Ligand binding to HSA

1.5.1 Metal binding sites

HSA has the capacity to bind various metal ions, both essential and toxic, with different specificities at each binding site (Martins and Drakenberg, 1982; Bal *et al*., 1998). Although there is a lack of detailed structural information, four metal binding sites have been described in the literature:

a) Amino-Terminal Cu^{2+} and Ni^{2+} binding motif (ATCUN)

b) Site A

c) Site B

d) Free thiol on Cys34

Each of these binding sites is described below in further detail including their structural elements and metal specificity. The binding constants that have been determined for Zn^{2+} Cd^{2+}, Cu^{2+}, Co^{2+} and Ni^{2+} ions by various methods are summarised in Table 1.1. Overall, this demonstrates that Cu^{2+} and Ni^{2+} ions show stronger binding to HSA than Zn^{2+} Cd^{2+} or Co^{2+} ions. HSA has a moderate affinity for Zn^{2+} with affinity in the high nanomolar range. The differences in the binding affinities obtained from different research groups can be attributed to important factors such as ionic strength, temperature and pH.

Table 1.1 Stability constants for metal ion- HSA complexes.

Metal ion	pH of study	n[c]	logK_1	Reference
Zn	N/A	3	7.53[b]	Masuoka and Saltman, 1994
Zn	N/A	1	7.10[b]	Ohyoshi *et al.*, 1999
Zn	7.4	1	6.98[a]	Giroux and Henkin, 1972
Cd	7.4	2	5.30[a]	Goumakos *et al*., 1991
Cu	7.5	1	16.18[a]	Lau and Sarkar, 1971
Cu	N/A	3	11.18[b]	Masuoka and Saltman, 1994
Cu	7.4	1	12.00[a]	Rózga *et al*., 2007
Ni	7.5	1	9.57[a]	Glennon and Sarkar, 1982
Co	7.4	3	4.90[a]	Sokolowska *et al*., 2009

a. K_1 = apparent binding constant of the highest affinity binding site
b. K_1 = intrinsic binding constant of the highest affinity binding site. These are not dependent on pH.
c. Number of binding sites

Amino-Terminal Cu^{2+} and Ni^{2+} binding motif (ATCUN)

The first metal site to be identified was the N-terminus which is the primary binding site for Cu^{2+} and Ni^{2+} and is known as an ATCUN motif. (Glennon and Sarkar, 1982; Harford and Sarkar, 1997). The motif can also be found in other proteins such as histatins (Harford and Sarkar, 1997). This site at the N-terminus of HSA has been well characterised and four nitrogen ligands from Asp1, Ala2 and His3 coordinate to the central metal ion to form a square-planar structure as illustrated in Figure 1.4. There is also evidence to suggest that in intact HSA Lys4 may be involved in this site (Sadler *et al*, 1994). Although only 5-10% of Cu^{2+} in the blood is bound to HSA, it was suggested early on that a ternary albumin-Cu^{2+}-histidine complex was important for Cu^{2+} transport (Lau and Sarkar, 1971). The majority of Cu^{2+} in plasma is tightly-bound to ceruloplasmin, which is a non-exchangeable fraction, and the remainder

associated with circulating amino acids (Neumann and Sass-Kortsak, 1967).

In contrast, HSA is the major transporter of Ni^{2+} with 95% estimated to be bound to the protein *in vivo* (Lucassen and Sarkar, 1979) although Ni^{2+} is generally thought to be non-essential for human health. Intriguingly, this ATCUN motif does not occur in some albumins from mammalian species such as dog serum albumin (DSA) and as a result this protein does not show a specific binding site for the first equivalent of Cu^{2+}. This suggests that the mechanism of Cu^{2+} metabolism could differ across mammalian species (Appleton and Sarkar, 1971).

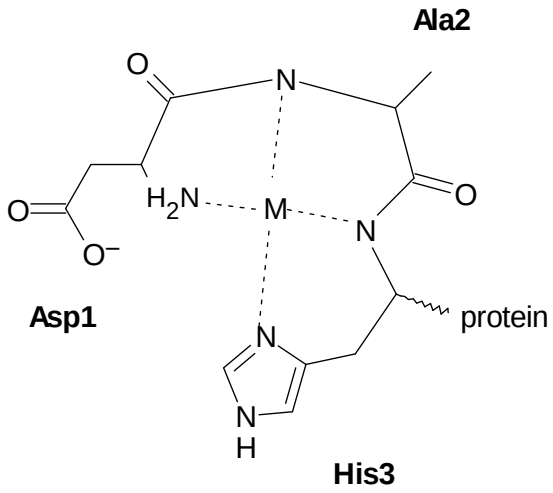

Figure 1.4 Structure of the ATCUN motif at the N-terminus of HSA. Asp1, Ala2 and His3 are involved in binding and M represents a Cu^{2+} or Ni^{2+} ion. Lys4 may also have a role in metal binding as proposed by Sadler *et al.* (1994)

Co^{2+} binding to HSA has attracted attention due to the albumin-cobalt binding assay (ACB assay), an FDA-approved test for myocardial ischemia (Bar-Or *et al*., 2000). In patients with acute coronary syndrome the binding of Co^{2+} in serum is significantly reduced (Bar-Or *et al*., 2001)

and this can be detected colorimetrically by measuring complex formation between Co^{2+} and dithiothreitol (DTT) which has absorbance at 470 nm. Early studies suggested that the N-terminal site was the primary binding site for Co^{2+} due to the fact that it was shown by potentiometry to interact with peptide mimics of the N-terminus (Lakusta and Sarkar, 1979). Sadler and co-workers (1994) provided further evidence for this by showing that addition of Co^{2+} to HSA reduced the intensity of the ^{1}H-NMR resonances observed for the N-terminal residues (Asp1, Ala2, His3 and also Lys4). However, it was not clear if the binding mode was the same as the square-planar arrangement formed with Cu^{2+} and Ni^{2+}. More recent studies have demonstrated that Co^{2+} actually competes with Zn^{2+} and Cd^{2+} for the occupation of Sites A and B and that only the third equivalent will be bound to the N-terminus (Mothes and Faller, 2007; Sokolowska *et al*., 2009). ITC and ^{111}Cd-NMR experiments have also confirmed that the primary binding site is not the N-terminus as the addition of Co^{2+} to $^{111}Cd^{2+}$ loaded HSA caused suppression of the peaks for Sites A and B as seen by NMR spectroscopy. This could have implications for the molecular mechanism of the ACB assay as the reduced Co^{2+} binding of plasma from ischemic patients may be due to elevated fatty acids (Lu *et al*., 2012a).

Site A

The location of the high affinity Zn^{2+} binding site has previously been reported (Stewart *et al.*, 2003), with increasing knowledge about the site being discovered over the past decade. The site is essentially pre-formed in HSA with little movement of the residues needed to accommodate the

metal ion. ^{111}Cd-NMR experiments of HSA yield two signals at ~ 25-30 ppm and another at 110-150 ppm, designated Site B and Site A respectively. Site A has been identified as the high affinity Zn^{2+} binding site on HSA and an interdomain location was proposed based on analysis of the albumin crystal structures available. The amino acids involved are from two domains: His67 and Asn99 from domain I and His247 and Asp249 from domain II. It is important to note that this ligand set has also been identified in other Zn^{2+}-binding enzymes such as human calcineurin, *E. coli* 5-endonucleotidase and kidney bean purple acid phosphatase (Stewart *et al.*, 2003). Compared to Asp, Cys and His, Asn is a relatively weak and uncommon ligand for metal ions in proteins. Further evidence for the residues involved in the Zn^{2+} binding site was obtained using X-ray absorption fine structure (EXAFS) spectroscopy (Blindauer *et al*., 2009) which characterised it as a 5-coordinate site with oxygen and nitrogen ligands (Figure 1.5). In addition, mutations at His67 and Asn99 clearly affected the Zn^{2+} binding affinity, further confirming that these residues participate in metal binding (Stewart *et al.*, 2003).

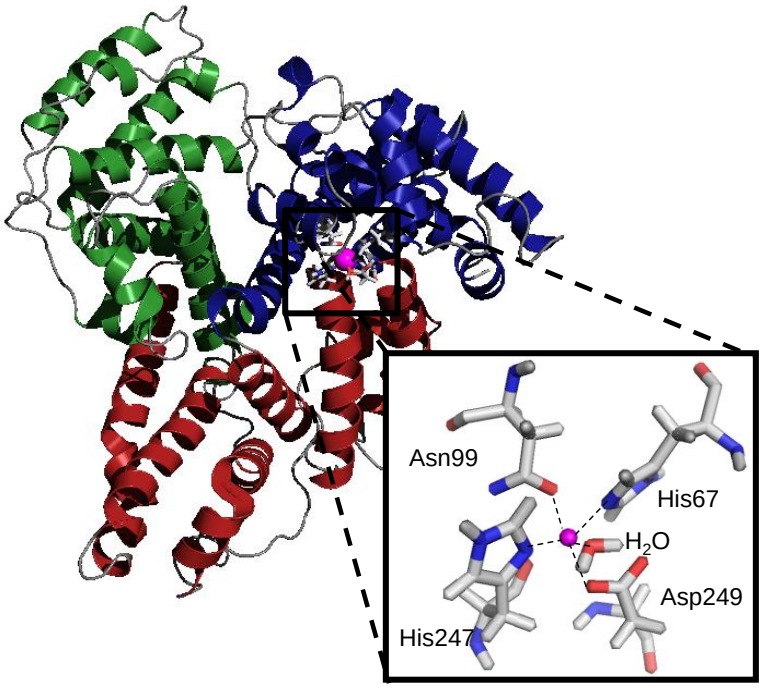

Figure 1.5 Zn^{2+} binding site located at the interface between domain I and domain II of HSA. Domain I is shown in *blue* and domain II is shown in *red* with the Zn^{2+} ion highlighted in *magenta*. The close-up image shows the 5-coordinate site composed of His67, Asn99, His247, Asp249 and a coordinating water molecule. The model was created using PyMOL v1.3 and based on the model published by Blindauer *et al*. (2009).

Cd^{2+} can also bind to Site A but is readily displaced by Zn^{2+} as shown by ^{113}Cd-NMR spectroscopy (Martins and Drakenberg, 1982; Goumakos *et al.*, 1991). Circular dichroism (CD) studies also indicated that it is a weaker binding site for Cu^{2+} and Ni^{2+} once the N-terminus has become saturated (Sadler and Viles, 1996) which was also confirmed by the work of Bal *et al*. (1998). This is consistent with the findings of Masuoka and Saltman (1994) who demonstrated by equilibrium dialysis that the first equivalents of Zn^{2+} and Cu^{2+} do not bind to the same site.

Site B

A high affinity Cd^{2+} site has been identified, Site B, but its location is yet to be fully characterised (Goumakos *et al*., 1991). The binding of Cu^{2+} or

Zn^{2+} to HSA did not reduce its affinity towards Cd^{2+} which supported the idea of a site that preferentially bound Cd^{2+} (Goumakos *et al*., 1991). This was later confirmed by ^{113}Cd-NMR data which showed that the peak for Site B was not supressed by the addition of 0.5-1.5 mol. equiv. of Zn^{2+} (Sadler and Viles, 1996). It has been proposed that the site consists of all oxygen ligands plus one or no nitrogen ligands, based on the fact that its ^{111}Cd chemical shift is 30 ppm (Öz *et al.*, 1998; Stewart *et al.*, 2003). A ^{13}C-NMR study with tripeptides suggested residues Asp35, Glu36 and His37 as good candidates for this binding site (Lakusta *et al*., 1980).

Free thiol located on Cys34

The final metal binding site that can be discussed is the only free thiol on the protein located at Cys34. The remaining 34 Cys residues are involved in the formation of disulfide bonds which are a characteristic trait of the albumin family. The sulfur has a high affinity for 'soft' acids for example Au^{+}, Ag^{+} and Hg^{2+}. Previous workers have reported that metallodrugs can bind at this site, for example Pt^{2+} anticancer drugs (Pizzo *et al.*, 1988; Esposito and Najjar, 2002) and also Au^{+} antiarthritic drugs (Christodoulou *et al*., 1994). Although Sadler and co-workers later showed that it was predominantly Met residues that were involved in cisplatin binding and only a minor amount of the drug was bound to Cys34 (Ivanov *et al.*, 1998). A more recent study found that cisplatin is able to form a cross-link between His67 and His247 and that there is competitive binding between Zn^{2+} and Pt^{2+} at this site (Hu *et al*., 2011).

1.5.2 Fatty acid transport by HSA

It was recognised as early as the 1940's that HSA extracted from serum contained fatty acids (Kendall, 1941) but it was not until over a decade later that researchers began to understand the physiological significance of this (Gordon and Cherkes, 1956). These acids are endogenous molecules which are insoluble in aqueous environments (Vorum *et al*., 1992) and therefore need to be transported around the blood by HSA. These molecules are the building blocks of fat in the body and a source of energy as their metabolism yields large quantities of adenine triphosphate (ATP). Few proteins are able to bind fatty acids and HSA has the ability to bind large amounts and with high affinity (Spector, 1975). Depending on the carbon chain length, they can be categorised as short-chain fatty acids (SCFA) with aliphatic tails of fewer than 8 carbon atoms, medium-chain fatty acids (MCFA) with 8-14 carbons atoms and long-chain fatty acids (LCFA) with greater than or equal to 16 carbon atoms (Beerman *et al*., 2003). The total concentration of fatty acids in blood plasma is approximately 300 μM (Van der Vusse, 2009) although only 5-10 nM are unbound (Richieri and Kleinfield, 1995). Typically the most common fatty acids found in the blood under normal conditions are oleic acid (18:1), palmitic acid (16:0) and linoleic acid (18:2) with 66% comprising of unsaturated acids (Saifer and Goldman, 1961). Importantly, fatty acids can dissociate from HSA very rapidly during circulation (Demant *et al.*, 2002) which allows HSA to work as an effective buffer against fluctuations in concentration. This also ensures that fatty acids bound to HSA are readily available to cells (Spector and Soboroff, 1971).

1.5.3 Fatty acid binding sites

Experimental evidence has indicated that fatty acid binding stabilises HSA against denaturation (Kragh-Hansen, 1981). Under normal physiological conditions, 0.1-2 moles of fatty acids are complexed to HSA, but seven sites have been identified by X-ray crystallography (Curry *et al*., 1998). Five of these sites are proposed to be of high to moderate affinity where the molecules are anchored into the protein by polar interactions (Bhattacharya *et al*, 2000). There is no evidence of such interactions at the other two sites and therefore these are thought to be weaker binding sites. Figure 1.6 shows the distribution of the high affinity binding sites occupied by myristate molecules. FA1 is located in subdomain IB and FA2 is at the interface between IA and IIA. FA3 and FA4 are both located in subdomain IIIA and FA5 is in subdomain IIIB. Sites FA6 and FA7 are not shown in Figure 1.6, but FA6 lies at the interface between IIA and IIB and FA7 in subdomain IIA (Curry, 2004).

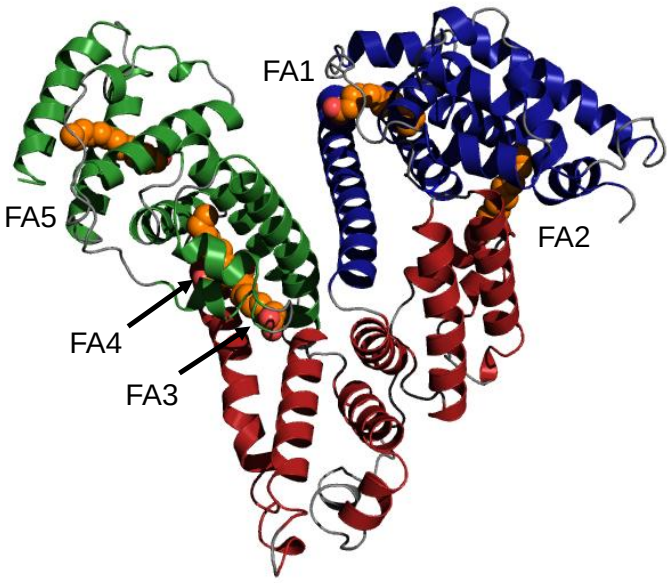

Figure 1.6 X-ray crystal structure of myristate-bound HSA. The protein structure is shown in the same colour scheme as previous figures. Myristate molecules are shown to occupy FA sites 1-5 (*orange*). The figure was created using PyMOL v1.3 and based on PDB 1BJ5 (Curry *et al*., 1998).

For many years, efforts have been directed towards quantifying the affinity of various fatty acids for HSA, even though difficulties occur as they are not readily soluble in aqueous media. Simard and co-workers carried out an NMR titration of HSA with ^{13}C-labelled palmitate, which revealed that FA sites 2, 4 and 5 are the high affinity binding sites whereas 1, 3, 6 and 7 are the low affinity binding sites (Simnard *et al*., 2006). This is most likely because sites 2, 4 and 5 provide the most enclosed environment and the aliphatic chain can sit in the pocket in almost a linear conformation (Van der Vusse, 2009).

1.6 Conformational changes of HSA

1.6.1 pH-induced conformational changes

HSA is a flexible molecule and can undergo several conformational changes. One trigger for this change is the pH of the environment (Carter and Ho, 1994; Peters, 1995) and this has an impact upon both the secondary and tertiary structure of HSA. The five structures described in the literature are summarised in Table 1.2. The N-(neutral) form is dominant at physiological relevant pH of 7.0-7.5. As the pH drops to 4.0, it is converted into the F-form which was shown by CD spectroscopy to involve a decrease in helical content (Era and Sogami, 1998). As the pH becomes more acidic further unfolding occurs to produce the E-form, until the molecule appears to have expanded to its full extent at pH 2.5. At alkaline pH, an N-to-B transition occurs which is thought to involve a loss of rigidity in the protein structure.

Table 1.2 Albumin conformations that are dependent on pH

Abbreviation	Name	pH of transition	Characteristics
E	Extended	2.7	Fully expanded form with disulfide bonds intact
F	Fast	4.3	Fast migrating form observed on gels
N	Neutral/Normal	7.0	Normal heart-shaped conformation observed at physiological pH.
B	Basic	8.0	Subtle change in molecule as it loses rigidity; physiologically relevant
A	Aged	10.0	Slower migrating form observed on gels

Dockal and co-workers demonstrated by CD spectroscopy and fluorescence measurements that during the N to B transition, domains I and II experienced an isomerisation in tertiary structure whereas domain III was unaffected (Dockal *et al*., 2000). The biological relevance of these isoforms has yet to be fully determined, although they are thought to be important for ligand binding and release.

1.6.2 Fatty acid-induced conformational changes

It has been shown that fatty acid binding is another trigger for a conformational change. Curry and co-workers compared myristate-bound HSA to unliganded HSA and found that substantial domain rotations occurred within the protein. Both domains I and III were moved considerably relative to domain II and a helix connecting domains I and II showed substantial bending (Curry *et al*., 1998). Later this conformational change was also found to occur with fatty acids of varying chain lengths from C10.0 to C18:0 (Bhattacharya *et al*., 2000). A combination of

chemical cross-linking and mass spectrometry has also been used to probe the effect of unsaturated fatty acid binding to HSA and the results correlated well with the changes observed in the crystal structures (Huang *et al*., 2005).

It is unclear whether these conformational changes have physiological significance, but one theory is that it could allow HSA receptors to differentiate between HSA molecules loaded with fatty acid and those that are fatty acid-free. This could have important implications for the delivery of fatty acids to cells (Curry *et al*., 1999). Overall, it is debatable whether HSA protein receptors on cells exist but there has been some evidence put forward (Schnitzer and Oh, 1994; de Château *et al*., 1996; Tiruppathi *et al*., 1996; Luiken *et al*., 1997). The conformational change could also be biologically important in that it may mediate the interactions with other molecules. An example that supports this is the case of thyroxine where 4 molecules of the hormone bind to fatty acid-free HSA, but upon myristate association, a fifth binding site for the hormone was identified in a new cleft created by movement of the domains (Petitpas *et al*., 2003). Interestingly, it appears that it is binding to fatty acid site 2 (FA2) that is mainly responsible for the conformational changes observed. This is discussed further with respect to implications for Zn^{2+} binding to Site A in section 1.7.2.

1.7 Interactive binding of metal ions and fatty acids

1.7.1 Evidence that fatty acid binding influences Zn^{2+} binding

Evidence to date that fatty acids influence the occupation of Site A has been obtained from combinations of ^{111}Cd-NMR spectroscopy, ^{1}H-NMR spectroscopy, isothermal titration calorimetry (ITC) and molecular modelling. Zn^{2+} is spectroscopically inactive, therefore it can usefully be replaced with isostructural Cd^{2+} in order to gain information about metal binding.

During early studies of ^{113}Cd binding to various mammalian albumins it was noted that there were differences in the appearance of the NMR peak corresponding to the major Zn^{2+} binding site (Sadler and Viles, 1996). It was realised that these differences could be attributed to the heterogeneity of the samples and that the relative affinity of Cd^{2+} for Site A was reduced in the presence of fatty acid. In light of this, Stewart and co-workers (2003) compared samples with high and low concentrations of octanoate by ^{111}Cd-NMR spectroscopy and found that the peak for Site A was supressed by fatty acid loading whereas Site B was not affected. Later experiments with myristate loading showed that both peaks observed in the ^{111}Cd-NMR spectrum of BSA were supressed indicating myristate binding had an impact upon metal binding to both Sites A and B (Figure 1.7, Lu *et al.*, 2012b).

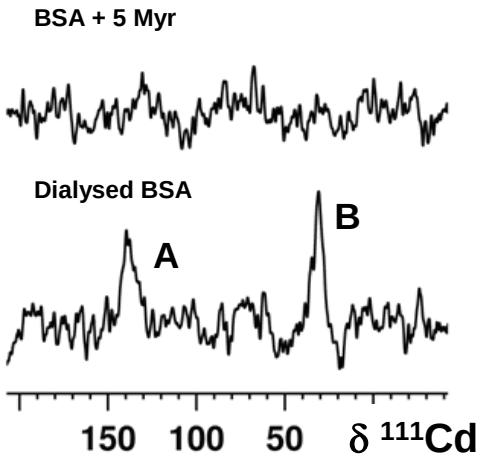

Figure 1.7 Influence of myristate loading on metal binding to BSA by ^{111}Cd-NMR spectroscopy. For dialysed BSA two peaks are observed: one for Site A and one for Site B. In the presence of myristate these peaks are significantly affected. (Lu *et al*., 2012b).

Further evidence for a relationship between fatty acids and Zn^{2+} was gained from ITC. Titrations with Zn^{2+} in the presence of 5 mol. equiv. octanoate gave similar data as titrations carried out in the absence of fatty acid. This was consistent with ^{1}H-NMR data showing simultaneous binding of Zn^{2+} and octanoate as although the Hε1 resonances for His67 and His247 were affected it was concluded that octanoate binding to FA2 does not abolish Zn^{2+} binding to BSA (Lu *et al.*, 2012b). In contrast, analysis of BSA-Zn^{2+} in the presence of myristate by ITC revealed that Zn^{2+} binding is dramatically decreased. This suggested that the chain length of the fatty acid is an important factor. One of the most important outcomes of ITC was the observation that Zn^{2+} binding was affected by the addition 1-2 molar equivalents of myristate which are physiologically relevant levels in plasma (Lu *et al.*, 2012b).

1.7.2 Disruption of Site A due to occupation of FA2

X-ray crystallography of fatty acid-bound albumin showed that the occupation of site FA2 was mainly responsible for the conformational change observed. Crucially, this is the only fatty acid site that is located between two domains (Curry *et al.*, 1998) and is also next to Site A, the major Zn^{2+} binding site. At this site, the carboxylate end of the molecule interacts with Arg257 and Ser287 in subdomain IIA and the aliphatic tail interacts with Tyr150 in subdomain IB. In order to accommodate the fatty acid anion, domains I and II have to move by 10 Å to form a cavity that is large enough. This causes significant disruption of the Zn^{2+} binding site as the His247/Asp249 pair from domain II and the His67/Asn99 pair from domain I are moved apart by 4-6 Å (Stewart *et al*., 2003).

Molecular modelling has given an insight into how fatty acids with different chain lengths could have an impact on the Zn^{2+} binding site. A model with octanoate bound shows that both the short-chain fatty acid and Zn^{2+} could be accommodated in their binding sites without the need for any conformational changes (Figure 1.8 B). As a result Site A is still observed to be intact as the C8 chain is too short to act as a pin between the two half sites. In contrast, when myristate is bound, a conformational change has to occur to accommodate the longer fatty acid chain and Zn^{2+} binding is lost (Figure 1.8 A, Lu *et al.*, 2012b).

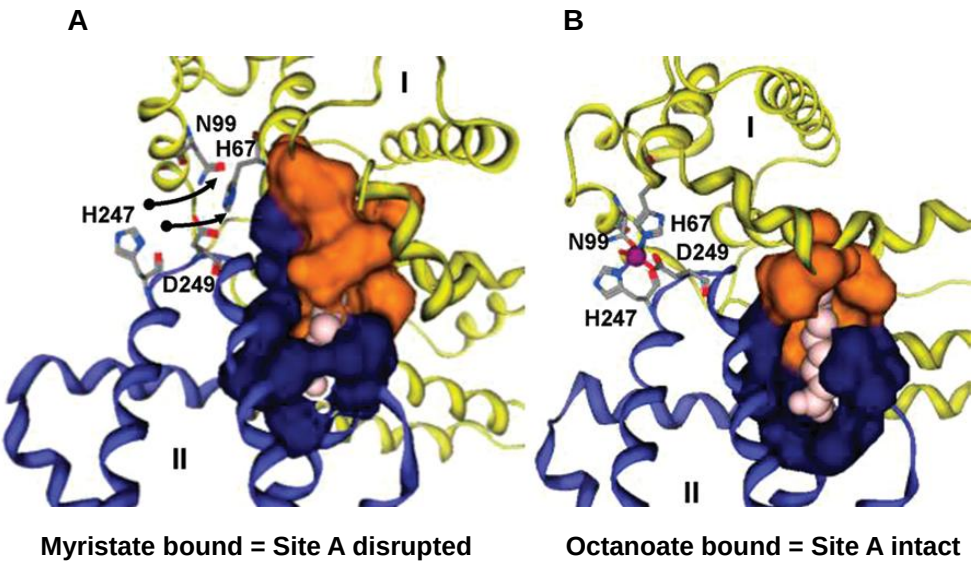

Figure 1.8 Molecular modelling shows binding modes of fatty acids with different chain lengths to FA2. When myristate is bound in FA2, Site A is disrupted (A) due to a significant conformational change whereas when octanoate occupies the site, the Zn^{2+}-binding site is still observed to be intact (B). Adapted from (Lu *et al.*, 2012b).

1.7.3 Biological significance

The experimental observations indicate that fatty acids could be a way of regulating Zn^{2+} speciation in blood plasma. HSA in healthy plasma carries 0.1-2 fatty acid molecules per protein, but some disease states including obesity, diabetes, cancer or cardiovascular disease are characterised by elevated fatty acid levels (Richieri *et al*., 1993). This is also a symptom of analbuminemia, which is a deficiency of HSA. Therefore this allosteric fatty acid "switch" mechanism may be a reason for shifts in Zn^{2+} distribution in plasma. The consequences of Zn^{2+} displacement from HSA are currently unknown, but predictions can be made. Zn^{2+} is potentially toxic to cells, so therefore an elevated fatty acid concentration could cause an increase in the unbound Zn^{2+} concentration in plasma which could be detrimental. A so-far unexplored link is the possibility that an increase in "free" Zn^{2+} concentration could have an impact on the

activities of other proteins that are Zn^{2+}-dependent such as histidine-rich glycoprotein (Stewart *et al*., 2009). This is the basis for this project and the hypothesis will be discussed later in this Chapter.

1.8 Histidine rich glycoprotein (HRG)

1.8.1 Structure and function

HRG is a 75 kDa plasma protein that was first isolated from human serum in 1972 (Heimburger *et al*., 1972) and belongs to the cystatin superfamily (Koide and Odani, 1987). It is synthesised in the liver and is present in blood at relatively abundant concentrations of 1.5-2 μM. The local concentration, however, could increase when it is released from activated platelets or close to thrombocytes activated during coagulation (Leung *et al*., 1983). During pregnancy HRG levels fall to half their normal concentration and then gradually return to normal after birth (Morgan *et al*., 1978a). It has been suggested that this may be related to delivering essential metal ions to the foetus during development (Morgan, 1981). At birth, the HRG concentration is 20% of that in adults and then increases with age (Corrigan *et al.*, 1990). Thrombophilia (or hypercoagulability), a condition that increases the risk of blood clots, has been shown to be a consequence of a HRG deficiency (Shigekiyo *et al*., 1998).

HRG is involved in the formation of multi-protein complexes that regulate numerous biological processes, which has earned it the title the “Swiss Army Knife” of mammalian plasma (Poon *et al.*, 2011). Its multidomain structure lends itself to being able to interact with many ligands including

heme (Morgan, 1978b; Katagiri *et al.*, 1987), Zn^{2+} (Morgan, 1978b), plasminogen (Lijnen *et al*., 1980), fibrinogen (Leung, 1986), thrombospondin (Leung *et al*., 1984), vasculostatin (Klenotic *et al*., 2010) immunoglobulin (Gorgani *et al*., 1997) and heparin (Lijnen *et al.*, 1983). Table 1.3 summarises the roles of HRG including comments on the supporting experimental evidence. With regards to the immune system, HRG is involved in the clearance of circulating immune complexes (ICs) whereby antibodies form complexes with target antigen and facilitate the clearance of invading microorganisms (Poon *et al*., 2010). If ICs are not cleared, deposition at tissues can occur, a consequence of which are diseases such as arthritis and vasculitis (Poon *et al*., 2011).

In vascular biology, HRG regulates angiogenesis, the formation of new blood vessels from ones that already exist (Olsson *et al.*, 2004). The process has to be tightly controlled in order to maintain the correct balance of oxygen and nutrients being delivered to cells in the organism. Unregulated angiogenesis can be extremely detrimental and is associated with a number of pathological conditions including ischemia, rheumatoid arthritis, thyroiditis and cancer (Folkman, 1995; Carmeliet and Jain, 2000). An additional function that has been found is that HRG shows antibacterial activity and that the His-rich region (HRR) is a requirement for this function (Rydengård *et al*., 2007).

Table 1.3 Biological functions of HRG.

Function	Comments	Reference(s)
Angiogenesis inhibitor	Tumour angiogenesis was reduced in mice in the presence of HRG and tumour growth was reduced by >60 %.	Olsson *et al*., 2004
	A peptide derived from the HRR showed antiangiogenic activity	Dixelius *et al*., 2006
Anticoagulant	Mice that were HRG-deficient showed increased blood coagulation and clotting	Tsuchida-Straeten *et al*., 2005
Antifibrinolytic effect	HRG deficient mice showed greater spontaneous fibrinolytic activity in clotted blood	Tsuchida-Straeten *et al*., 2005
Antibacterial	A peptide derived from the HRR, (GHHPH)4, had antibacterial effect against *E. faecalis* in the presence of Zn^{2+}	Rydengård *et al*., 2006
	HRG-deficient mice were more susceptible to *S. pyogenes* bacteria.	Shannon *et al*., 2010
Antifungal	HRG has significant antifungal action against Candida	Rydengård *et al*., 2008
Apoptotic and necrotic cell clearance	A complex consisting of both HRG and immunoglobulin G (IgG) was characterised and found necessary to aid necrotic cell uptake by monocytes	Poon *et al*., 2010
	HRG binds to cytoplasmic ligands exposed in necrotic cells – this interaction is mediated by the N-terminal domain.	Jones *et al*., 2005a
Endotoxin-neutralising effects	A 25-mer peptide from the HRR was shown to be an endotoxin lipopolysaccharide (LPS) antagonist	Bosshart and Heinzelmann., 2003
Formation of immune complexes	HRG regulates the binding of monomeric IgG and IC to monocytes.	Gorgani *et al*., 1999
	HRG binds to IgG and C1q as shown by ELISA	Gorgani *et al*., 1997
Regulates T-cell adhesion	HRG binds strongly to human T-cells with the interaction enhanced by Zn^{2+}	Olsen *et al*., 1996

No structure exists for HRG, however, suggestions have been made as to its domain structure from experimental observations. The different domains are illustrated in Figure 1.9 which is based on the models proposed in previous studies (Borza *et al*., 1996; Poon *et al*., 2011). The proposed structure contains 2 N-terminal regions which show homology to cystatin-like domains: N1 which consists of residues 1-112 and N2 from residues 113-225. The HRR occurs from residues 330-389 in the centre and is flanked by Pro-rich regions (PRRs). Finally, there is a C-terminal domain from residues 440-507. Four intradomain and two interdomain disulfide bonds are distributed across the protein as well as six predicted N-glycosylation sites at various Asn residues. Plasmin readily cleaves the multi-domain protein into various fragments ranging from 9-67 kDa and after 30 minutes none of the intact protein remained in patients undergoing thrombolytic therapy (Smith *et al*., 1985).

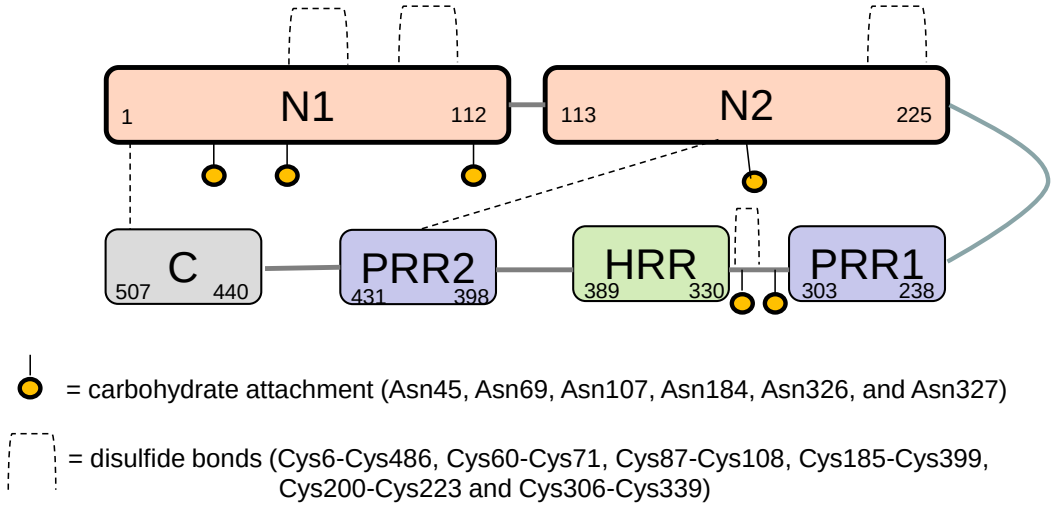

Figure 1.9 Multi-domain structure proposed for HRG. There are two cystatin-like N-terminal domains (*pink*) and a His-rich region (HRR) in the centre of the molecule (*green*). The HRR is flanked by Pro-rich regions (PRRs; *blue*) and finally a C-terminal domain with a disulfide bond linking it back to the N-terminus. Carbohydrate recognition sites and disulfide bonds are highlighted. This is based on models by Borza *et al.* (1996) and Poon *et al.* (2011).

A 30 kDa fragment containing the HRR is released upon cleavage while the N- and C-terminal domains remain linked by disulfide bond Cys6-Cys486 (Borza *et al*., 1996). Far UV CD spectroscopy revealed that the N-terminal regions are mainly comprised of β-sheet and some α-helices which are similar to the structure of cystatin. The C-terminal region and both the HRR and PRR regions show a lack of regular secondary structure which can be attributed to their high Pro content. In fact, the C-terminal appears to be predominantly random coil while a polyproline II helix has been suggested for the HRR and PRR which will be discussed in more detail below (Borza *et al*., 1996).

1.8.2 The His-rich region of HRG

Analysis of the primary structure shows that a quarter of the sequence is composed of His and Pro residues: 12.6 % His and 12.4 % Pro. The majority of these are found in the so-called HRR and PRR regions. The primary sequences of the HRR from mammalian species show conservation of the GHHPH pentapeptide with 12 tandem repeat units. This unusual domain shows some similarity to high molecular weight kininogen (HMWK), a protein from the blood circulation system which has a HRR that participates in coagulation and also has the ability to disrupt endothelial cell function (Zhang *et al*., 2000). The PRR shows similarity to Pro-rich proteins from parotid saliva, which have a repeating unit of QGPPP, with the sequence similarity between the two proteins being as high as 49% (Koide *et al*., 1986) Analysis of repeat units in protein sequences has shown that these are more common in eukaryotic

proteins than prokaryotic proteins and a reason for these could be that these proteins evolve quicker than those with non-repetitive units (Marcotte *et al*., 1998). In order for HRG to exert its anti-angiogenic properties the HRR is proteolytically released from the protein (Olsson *et al*., 2004) and smaller protein fragments have been found in preparations of HRG and identified by SDS-PAGE, which supports this idea (Kluszynski *et al*., 1997).

The HRR and PRR lack conventional secondary structure such as α-helices or β-sheet, probably due to the high Pro content. Borza and co-workers carried out CD-spectroscopy on the HRR region obtained from proteolytic cleavage, which indicated the formation of a polyproline II helix (Borza *et al*., 1996). This type of secondary structure is characterised by a large negative peak at 203 nm and a small positive peak at 226 nm. This structure formation is due to a lack of basic and hydrophobic amino acids which precludes more compact protein folding.

1.8.3 Metal binding to HRG

Contrary to earlier observations (Morgan, 1981; Guthans and Morgan, 1982) HRG does not appear to be a transporter for metal ions but there is inconsistent evidence for this. Analysis of hyperzincemic plasma showed that HRG concentrations were similar to that of normal plasma which is not in line with it being a major Zn^{2+} binder (Failla *et al*., 1982). Importantly however, its interactions with other binding partners are enhanced by Zn^{2+} but it is unclear how much Zn^{2+} would normally be

bound to HRG *in vivo*. Metal ion titrations and equilibrium dialysis have indicated that as many as 10 Zn^{2+} ions can bind to rabbit HRG (Morgan, 1981) and human HRG (Horne *et al*., 2001) with the His residues being involved in metal coordination (Morgan, 1981). Evidence for His involvement has been demonstrated by chemically modifying the His residues with diethyl pyrocarbonate (DEPC) which caused HRG to lose the ability to bind both Zn^{2+} (Morgan, 1981; Burch *et al*., 1987) and heparin (Borza and Morgan, 1998). At physiological pH the imidazole ring is partially deprotonated therefore it is readily available for metal binding. It is likely that Zn^{2+} binding modifies the protein structure of HRG in order to mediate interactions with other biomolecules (Jones *et al*., 2005b). The His residues provide a good "anchorage point" for metal ions, particularly in unstructured proteins where the residues are far more accessible (Rowinska-Zyrek *et al*., 2013). It is thought that the extended conformation of the HRR allows easier metal ion access to the imidazole rings of the His residues. It has also been demonstrated that the binding of Zn^{2+} to the HRR is cooperative, so that the binding of the first Zn^{2+} ion could make it more favourable for subsequent Zn^{2+} ions to bind (Morgan, 1981).

As shown in Figure 1.10 the HRR from different species are highly conserved. There are some slight differences, however, which could suggest that there are differences in Zn^{2+} binding affinity. For example, human HRG has 12 GHHPH repeats whereas rabbit HRG has 15, and overall a longer HRR, which indicates that the latter could have the

capacity to bind more metal ions. Moreover, the repeating unit GHHPH is predominant in bovine, human, mouse and rat HRG whereas GPPPH is more common in rabbit HRG.

```
HUMAN     PLLPMSCSSCQHATFGTNGAQRHSHNNNSS-----DLHPHKHHSHEQHPHGHHPHAHHPH 354
BOVINE    LPFPPPGLRCPHPPFGTKGNHRP----------------PHDHSSDE-------------- 263
RABBIT    PLSPPFRPRCRHRPFGTNETHRFPHHRISVNI-IHRPPPHGHHPHGPPPHGHHPHGPPPH 343
RAT       PQLPPGYP----PHSGANRTHRPSYNHSCNEHPCHGHRPHGHHPHSHHPPGHHSHGHHPH 346
MOUSE     PQMLPGHS----GPSGTNRSHRPPHNHSCNEHPCHGQHPHGHHPHGQHPHGHHPHGQHPH 346
                      *::  :*                ** * ..

HUMAN     ------------------EHDTHRQHPHGHHPHGHHPHGHHPHGHHPHGHHPHCHDFQD 395
BOVINE    ------------------------------HHPHGHHPHGHHPHGHHPHGHHPPDNDFYD 293
RABBIT    GHPPHGPPPRHPPHGPPPHGHPPHGPPPHGHPPHGPPPHGHPPHGPPPHGHPPHGHGFHD 403
RAT       G--------------HHPHSHHSHGHHPPGHHPHGHHPHGHHPHGHHPHGHHPHGHDFLD 392
MOUSE     G--------------HHPHGQHPHGHHPHGQHPHGHHPHGHHPHGDHPHGHHPHGHDFLD 392
                                      : ***  **** ***  **** *  :.* *
```

Figure 1.10 Sequence alignment of the HRR of HRG from various mammalian species. Amino acids are coloured according to their chemical properties: hydrophobic (*red*), acidic (*blue*), basic (*magenta*), hydroxyl/sulfhydryl/amines (*green*). Symbols represent conservation of amino acids: fully conserved (*****), conservation between groups with strongly similar properties (**:**) and conservation between groups of less similar properties (**.**).

In contrast, there is very little homology between the linker regions connecting the HRR and PRR thus highlighting the importance of these unusual domains with regards to the functionality of HRG (Hulett and Parish, 2002).

The binding affinity of HRG for metal ions has been addressed by a number of research groups as summarised in Table 1.4, These indicate that HRG binds Zn^{2+} with log*K* ~ 5-6 which suggests it is a weaker metal binder than HSA. Although the binding of Zn^{2+} and Cd^{2+} showed a similar binding affinity, Morgan (1981) demonstrated that Zn^{2+} is the strongest binder of the two as it was able to inhibit heme binding to a much greater extent than Cd^{2+}. The general consensus is that affinity data are difficult to obtain for HRG and these values may be underestimated due to the

fact that binding of Zn^{2+} and Cd^{2+} to the protein show cooperativity. Additionally, most work has been carried out using rabbit HRG, as the protein is more abundant in rabbit serum, but this has a longer HRR region compared to the human form.

Table 1.4 Stability constants for metal ion-HRG complexes

Metal ion	pH of study	Species	log*K*	Reference
Cu	7.4	Rabbit	6	Morgan, 1981
Cd	7.4	Rabbit	6[a]	Morgan, 1981
Zn	7.4	Rabbit	6[a]	Morgan, 1981
Zn	7.1	Rabbit	5	Guthans and Morgan, 1982
Zn	7.4	Rabbit	6-6.6	Burch and Morgan, 1985
Zn	7.4	Human	5.4	Horne *et al*., 2001

[a] Values must be taken with caution as due to cooperative binding of these metal ions the apparent K_d was qualitatively determined from competition experiments. However, these are still in good agreement with other estimations.

1.8.4 Zn^{2+} mediates HRG-ligand interactions

It has been recognised for some time that metal ions have a strong influence on the interactions between HRG and its binding partners. Binding to heparin was studied by Borza and Morgan (1998) who demonstrated that both Zn^{2+} and Cu^{2+} were effective at promoting this interaction. Ni^{2+} and Co^{2+} had some influence on the interaction, but not to the same extent as Zn^{2+} and Cu^{2+}. Other divalent metal ions including Mn^{2+}, Ca^{2+} and Mg^{2+} had no effect on promoting the binding of heparin. Additionally, this could have clinical significance as a combination of HRG and Zn^{2+} was shown to neutralise heparin although no appreciable effect was observed at normal plasma levels (Fu and Horne, 2002). The presence of Zn^{2+} ions enhanced the binding of a His-rich peptide to

tropomyosin with a suggested mechanism involving HRG becoming positively charged upon Zn^{2+} binding which facilitates its interaction with negatively charged tropomyosin (Doñate *et al*., 2004). Furthermore, the more recently discovered antibacterial activity of HRG was facilitated by low pH and Zn^{2+} (Rydengård *et al*., 2007). It has also been revealed that Zn^{2+} greatly increased the binding of HRG to platelets. As high concentrations of Zn^{2+} have been detected in activated platelets (Gorodetsky *et al*., 1993) this is a physiologically relevant function that could occur at blood clotting sites (Horne *et al*., 2001).

1.8.5 Could the fatty acid "switch" mechanism be involved in the regulation of HRG functions?

Elevated fatty acid levels may well result in an increase in plasma Zn^{2+} concentration through the fatty acid "switch" mechanism described above. An increase in the plasma Zn^{2+} concentration could allow more of the metal ion to associate with HRG and consequently trigger its interactions with its functional partners (Stewart *et al*., 2009). The proposed interplay between these two proteins is summarised in Figure 1.11. Even though HSA binds to Zn^{2+} with a greater affinity than HRG, the binding constants are not completely dissimilar so even small alterations in fatty acid levels could influence whether Zn^{2+} is bound to HSA and HRG. This suggested mechanism is biologically relevant as free fatty acids have been shown to be elevated during diseases such as cancer, diabetes and obesity (Brown *et al*., 1983; Richieri *et al*., 1993; Boden and Shulman, 2002).

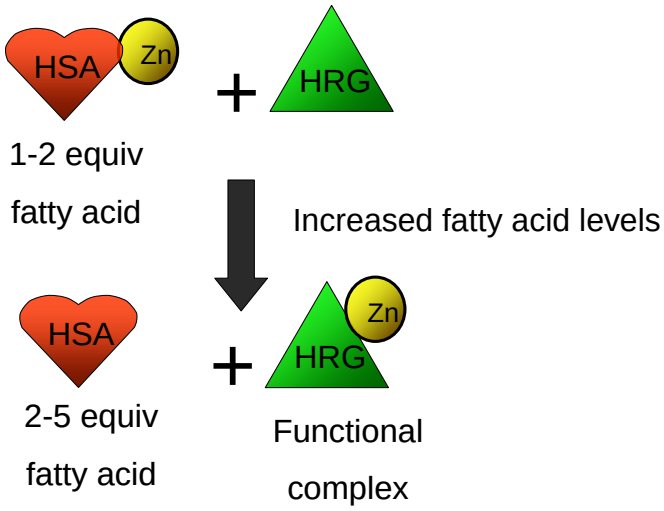

Figure 1.11 Mechanism of possible HRG regulation by the levels of plasma fatty acids. An increase in fatty acid levels could affect the Zn^{2+} distribution in blood plasma and cause more Zn^{2+} to associate with HRG (Stewart *et al*., 2009).

Additionally, an increase in fatty acids is also observed with myocardial ischemia, a heart disorder where a decrease in blood flow to the heart reduces its oxygen supply and hence fatty acid consumption (Hendrickson *et al*., 1997). When this is taken together with the fact that the local pH also drops during ischemia (Xia *et al*., 1996), which could cause HRG to become more protonated, then a scenario where fatty acids may affect the activities of HRG is even more viable.

This model is based on the assumption that HSA is the major Zn^{2+} carrier in plasma due to its abundance and HRG would only be Zn^{2+} bound if conditions in plasma became abnormal. However, there is conflicting evidence for this which needs to be taken into account. Indeed, Guthans and Morgan (1982) showed by equilibrium dialysis that when HSA was in 10-fold excess over HRG, 88 % of the Zn^{2+} present was found to be bound to rabbit HRG. Altering the HRG:HSA ratio to 1:100 still resulted in

equal concentrations of Zn^{2+} (29 μM) associating with both HSA and HRG. This led to the suggestion that HRG could also been an important competitor for Zn^{2+} in plasma although that fatty acid content of HSA used in this study is unclear.

1.9 Research motivation and aims

The aim of this work is to study the interactive binding of metal ions and fatty acids to albumin and to explore its biological significance. In particular native mass spectrometry will be used as a new approach to investigate metal ion binding to HSA directly. Overall, structural details on the biomolecular interactions of HRG are lacking although there have been numerous studies linking it to important physiological functions. The possible link between the fatty acid "switch" mechanism and the HRG-Zn^{2+} interaction could have implications for Zn^{2+} transport in blood plasma although there is no experimental evidence for this as yet. The reported binding constants for HSA and HRG give no clear answer as to whether Zn^{2+}-dependent HRG-complex formation would only occur as a result of elevated fatty acids and therefore this issue needs to be addressed.

Objectives:

1. To optimise mass spectrometry methods to study non-covalent HSA complexes under native conditions. This has mainly been applied in previous studies to investigate the binding of molecules that form covalent bonds with albumin (Chapter 3).

Can Zn^{2+} binding to HSA be observed in the gas phase? Do fatty acids have any effect on this?

2. To utilise travelling wave- ion mobility mass spectrometry as a novel technique to study HSA complexes (Chapter 4).

   Can any conformational changes be detected in the presence of metal ions or fatty acids?

3. To identify a suitable peptide mimic of the HRR of HRG and study its metal binding properties. There is currently very little structural information on HRG and its biomolecular interactions therefore this work will attempt to address this (Chapter 5).

   What are the metal binding properties of the HRGP330 peptide and can these be related to its biological functions? Do any structural changes occur upon metal binding?

4. To investigate the distribution of metal ions between the peptide mimic of HRG and HSA and explore if fatty acids have an effect on this (Chapter 6).

   Is the peptide mimic of HRG able to compete with HSA for metal ions? Do fatty acids have any effect on the distribution?

Chapter 2
Experimental Methods

2.1 Materials and chemicals

Wherever possible, reagents of the highest quality were used. If not stated, chemicals were obtained from either Fisher Scientific (UK) or Sigma Aldrich (UK).

2.2 Methods for defatting HSA

2.2.1 Dialysis of HSA

Recombinant HSA (Recombumin™) was a gift from Novozymes® (batch number PDP090078) containing 31.1 mM octanoic acid, 141 mM sodium chloride and 15 mg/L polysorbate 80. The dialysis tubing acquired from Medicell International Ltd was prepared by boiling in 10 mM ethylenediaminetetraacetic acid (EDTA) for 1 hour, followed by storage in a fresh EDTA solution. SnakeSkin™ dialysis tubing (Pierce Protein Biology Products, 10 KDa MWCO) was used without any further preparation. HSA stock solution (5 ml) was diluted to 20 ml in water and transferred to the tubing. Dialysis was carried out against 5 L of 100 mM ammonium bicarbonate for 24 hours at 4 °C with at least two buffer changes. Samples were frozen with liquid nitrogen, lyophilised by freeze-drying and stored at -20 °C.

2.2.2 Charcoal treatment

The method used was based on that described (Chen, 1967) with slight modifications. HSA in distilled water was acidified to pH 3.0 using microlitre aliquots 0.1 M HCl. An equal weight of activated charcoal was added and the mixture stirred on ice for 1 hour. Charcoal was removed from the solution by centrifugation (Sorvall RC6 floor standing centrifuge) at 30,000 x g for 20 minutes at 2 °C. The solution was filtered through a 0.22 μm filter and neutralised by addition of 0.2 M NaOH. Desalting into the appropriate buffer was achieved using a PD-10 column.

2.3 Characterisation of HSA

2.3.1 SDS-PAGE

Two kits were used: the NuPAGE® system from Invitrogen and Biorad. Pre-cast gels NuPAGE® gels (10 well, 4-12% gradient Bis-Tris gels) were assembled in the electrophoresis apparatus (OmniPAGE mini, Geneflow). Ten microlitres of SeeBlue2® pre-stained molecular weight marker was loaded into the first well. Samples were mixed 1:1 with NuPAGE 4 x LDS sample buffer and loaded onto additional sample wells. Gels were run at 200 mV for 35 minutes and then stained overnight with Coomassie Blue solution (0.25 g/L Coomassie Blue R-250, 10% acetic acid and 50% methanol). Gels were destained in distilled water overnight with agitation.

Mini-Protein TGX pre-cast gels were assembled in the Biorad apparatus. Ten microlitres of Precision Plus Protein™ Dual Colour Standard was used as a reference. Samples were mixed 1:1 with the Laemmli sample

buffer and loaded onto the gel. Gels were allowed to run for 35 minutes at 200 mV. Staining was achieved as described previously.

2.3.2 Determining HSA concentration

Protein concentration was estimated by measuring the absorption at 279 nm and using a value of A_{279} (1 mg/ml, 1 cm) = 0.556 for HSA (Sadler *et al*., 1994).

2.3.3 Assay for free thiol content

A modified colorimetric assay was used to determine the free thiol concentration (Ellman, 1958). HSA samples (100-200 μL) were diluted with 2.6 ml of 0.1 M Tris-Cl (pH 7.05 containing 1 mM EDTA) and 200 μL of 2.5 mM DTNB (dissolved in 50 mM ammonium acetate, pH 5.0, 1 mM EDTA) was added. Milli-Q water was used to make the total sample volume up to 3 ml. The solution was left to react for 10-15 minutes at room temperature before measuring the absorbance at 412 nm (Biomate 3 spectrophotometer, Fischer Scientific). An 800 μM cysteine stock, containing 1 mM EDTA, was used to prepare standards of known thiol concentration. Thiol concentration was calculated through calibration using these standard solutions. This was then divided by the protein concentration to give the free thiol content of the HSA sample.

2.3.4 Reaction with DTNB for ESI-MS analysis

Lyophilised HSA was dissolved in 2.5 ml potassium dihydrogen phosphate (100 mM, pH 8.0). Forty mol. equiv. of DTNB (5,5'-Dithio-

bis(2-nitrobenzoic acid) were added to a 30 μM solution of HSA and incubated at room temperature for an hour. Excess DTNB was removed using a PD-10 column. Confirmation that the free thiol of Cys-34 had been covalently modified was obtained using ESI-MS (theoretical mass of HSA-NTB = 66,635 Da).

2.4 ESI-MS of HSA

2.4.1 Desalting with PD-10 column

Lyophilised samples were reconstituted in 10 mM ammonium acetate (pH 7.4). The PD-10 column (Sephadex® G-25, Amersham Biosciences) was equilibrated with the appropriate buffer (25 ml) and loaded with 2.5 ml of protein sample. Elution was achieved with 3.5 ml of the buffer solution. The column was washed with a further 25 ml of buffer, and stored at 4 °C. If required, protein eluate fractions were concentrated using Amicon® Ultra-4 centrifugal filter units (Millipore) with a 30 kDa MWCO.

2.4.2 Sample preparation

Native HSA was prepared at a concentration of 2.5-5 μM in 10 mM ammonium acetate (~ pH 7.4) with 10% methanol (v/v). To denature the protein, 1 % formic acid and 50% organic solvent (methanol or acetonitrile) was used. All buffers used for sample preparation were filtered through a 0.22 μm sterile (Millipore) filter to prevent blocking of the electrospray needles. Prior to analysis, samples were centrifuged at 13,200 rpm for 2 minutes to ensure any precipitate was removed from solution.

2.4.3 Acquiring data: microTOF

Mass spectra were recorded on a microTOF instrument (Bruker Daltonics, Germany) operating in the positive mode. Samples were introduced into the syringe pump with injection into the instrument at a flow rate of 240 μL/hour. The following parameters were used: source temperature = 195 °C; capillary exit = 150 V; skimmer 1 = 50 V; skimmer 2 = 23.5 V; hexapole RF = 450 V; hexapole 1 = 24 V; hexapole 2 = 20.9 V; transfer time = 88 μs. Data were acquired for 1.2-1.5 minutes over an *m/z* range of 1500-5000. Raw data were averaged and deconvoluted using Bruker Daltonics Data Analysis v3.3.

2.4.4 Acquiring data: maXis-UHR-TOF

Positive electrospray mass spectra were acquired on a maXis ultra-high resolution time-of-flight (UHR-TOF) instrument (Bruker Daltonics, Germany) calibrated with Tune Mix for positive mode ESI (Bruker Daltonics). A syringe pump injected the sample into the mass spectrometer at a rate of 120 μL/hour. Data were collected for approximately 2 minutes over an *m/z* range of 1500-5000. This was extended to 7000 *m/z* to observe the dimer charge states. The following conditions were used for the Q-TOF mass spectrometer: dry gas = 4.0 L/min; source temperature = 200 °C; funnel RF = 400 Vpp; multipole RF = 400 Vpp; ISCID = 100 eV; collision cell energy = 10 eV; collision RF = 1800 Vpp; ion cooler = 650 Vpp; transfer time = 140.4 μs; pre pulse storage = 20 μs.

Online nanoESI was also used to record spectra using an TriVersa NanoMate® system (Advion Biosciences, Ithaca, NY, USA) coupled to the maXis instrument. Aliquots of 5 μM protein samples (20 μL) were pipetted into the wells on the sample-loading plate from which 5 μL was taken up by the tip, in an automated process, and infused at a flow rate of approximately 120 nL/min. Spraying voltages in the range of 1.65 – 1.75 kV were used and a gas pressure of 0.65 psi applied which gave ~ 100 nA current. Data were acquired in the positive mode over an *m/z* range of 1500-5000 and processed using the maximum entropy deconvolution algorithm (MaxEnt) within Bruker Compass Data Analysis v4.0.

2.4.5 Identifying fatty acids in the low mass range

To optimise the conditions for identifying small molecules in HSA samples, the conditions were adjusted as follows: dry gas = 4.0 L/min; source temperature = 200 °C; funnel RF = 400 Vpp; multipole RF = 400 Vpp; ISCID = 0 eV; collision cell energy = 10 eV; collision RF = 400 Vpp; ion cooler = 125 Vpp; transfer time = 100 μs; pre pulse storage = 5 μs.

2.5 Preparation of HSA complexes

2.5.1 Metal ion-bound HSA

HSA solutions were incubated with 1-2 molar equivalents of the appropriate metal ion from the following stock solutions: $Zn(CH_3COO)_2.2H_2O$, $Cd(CH_3COO)_2.2H_2O$, $Cu(CH_3COO)_2.H_2O$. Stock solutions were filtered through 0.22 μm filters prior to use. Following

incubation for 2 hours at 37 °C, unbound metal ions were removed by passage through a PD-10 column.

2.5.2 Fatty acid-bound HSA

Stock solutions of octanoic acid and myristic acid were prepared in Milli-Q water and heated to 60 °C in a water bath. The solution was cooled to 37 °C and 1-5 mol. equiv. of fatty acid were added to HSA and incubated at 37 °C in a water bath for 2-5 hours.

2.5.3 pH titration with HSA

A 5 μM sample of Zn-HSA was titrated with microlitre additions of 1 % acetic acid (v/v). An aliquot was taken in order to measure the pH (Hamilton Biotrode pH electrode) and the pH of the ESI-MS sample was measured directly following analysis.

2.6 Determination of metal: protein stoichiometry by ICP-OES

Following incubation with the appropriate ligands, HSA samples were buffer exchanged into 10 mM ammonium acetate (pH 7.4) using a PD-10 desalting column. ICP-OES (Inductively coupled plasma-optical emission spectroscopy) analyses were performed using an Optima 5300DV (Perkin Elmer). Ultrapure 72% nitric acid was obtained from in-house acid distillation. Samples were diluted with ultrapure 0.1 M HNO_3 and analysed for S, Zn, Cd and Cu. Standards of these elements were prepared gravimetrically from high grade 10,000 ppm stocks in the range of 0.2-5 ppm. The samples were measured in triplicate and then averaged. The

raw data (presented in mg/L) was divided by the atomic mass of the element to obtain the concentration in mmol/L. Protein concentration was estimated by dividing the sulfur concentration by the number of sulfur-containing residues (41 for HSA). Subsequently, the number of metal ions bound to the protein was calculated by dividing the metal concentration by the protein concentration.

2.7 NMR experiments with HSA

2.7.1 1-D ^{1}H NMR spectroscopy

Lyophilised samples of HSA were reconstituted in 100% D_2O and incubated at 4 °C overnight to minimise amide resonances. The sample was lyophilised again and stored at -20 °C. NMR samples were prepared to a concentration of 1 mM in 50 mM [D_{11}]Tris-Cl, 50 mM NaCl, 100% D_2O (v/v), pH 7.2. The pH* was measured using a pH meter calibrated with H_2O buffers and was not corrected for the effect of deuterium. The corresponding pD value can be calculated by adding 0.41 to the observed pH* (Glasoe and Long, 1960). Additions of ligands were made as stock solutions in the same buffer. The pH* values were monitored before and after addition of ligands. Spectra were obtained on a Bruker Avance 700 Ultrashield^{TM} spectrometer using 8k complex data points over 256 scans. The data was apodized, firstly with a squared-sinebell function followed by a Gaussian function for resolution enhancement and then Fourier-transformed.

2.7.2 ^{111}Cd-NMR spectroscopy

Dialysed HSA was solubilised into 50 mM Tris-Cl, 50 mM NaCl with 10% D_2O (pH 7.2). Proton decoupled 1-D ^{111}Cd-NMR spectra were obtained using a Bruker DRX500 spectrometer fitted with a broadband observe (BBO) probe. The operating frequency for ^{111}Cd is 106.037 MHz and the pulse sequence employed inverse gated decoupling. Data were acquired at 37 °C and a spectral width of 300 ppm was used with 8k complex data points and 98k scans. Spectra were referenced using an external standard of 0.1 M $Cd(ClO_4)_2$. The data was zero-filled to 32k data points and apodized using exponential multiplication with a line-broadening factor of 90 Hz. Spectra were processed using TOPSPIN 2.0 provided by Bruker.

2.8 TWIM-MS of HSA complexes

2.8.1 Experimental parameters

Samples of metal- and fatty acid-bound HSA were prepared according to sections 2.5.1 and 2.5.2. For TWIM-MS, 30 μM HSA samples were buffer exchanged into 200 mM ammonium acetate (pH 7.4). Ten microlitres was injected via a nanoflow source into a Synapt HDMS G2 system (Waters, Corporation, Milford, MA, USA). The instrument was operated in the positive mode with a source temperature of 90 °C. The following instrumental conditions were used: backing pressure 5 mBar; capillary voltage 1.5 kV; cone voltage 80 V; helium cell gas flow 180 mL/min; IMS cell gas flow 90 mL/min; travelling-wave height 40 V and travelling wave

velocity 700 m/s. A mass acquisition range of 500-5000 *m/z* was used. Data were processed using MassLynx v4.1 provided by Waters.

2.8.2 TWIM-MS calibration: sperm whale myoglobin

Arrival time distributions (ATDs) were extracted for each ion of interest. Calibration was achieved using 10 μM sperm whale myoglobin in 50% acetonitrile with 0.2% formic acid which was measured under the same conditions as in section 2.8.1. The calibration procedure followed has been described previously (Thalassinos *et al.,* 2009).

2.8.3 Estimation of theoretical cross sections using MOBCAL

Theoretical calculations for the rotationally-averaged collision cross-section were carried out using MOBCAL, a program to calculate mobilities (Mesleh *et al.,* 1996; Shvartsburg and Jarrold 1996). These were carried out by Matthew Edgeworth. PA and EHSS approximations were performed on published X-ray crystal structures 1AO6 (Sugio *et al*., 1999) and 1BJ5 (Curry *et al*., 1998) from the RCSB Protein Data Bank (www.rcsb.org, Berman *et al.* 2000).

2.9 Purification of the synthetic peptide HRGP330

2.9.1 Reverse phase-high performance liquid chromatography

A crude synthetic peptide from the His/Pro-rich region of HRG was synthesized at the Keck Biotechnology Research Facility (Yale University, USA). The sequence is shown below and included an acetylated N-terminus and amidated C-terminus.

Ac-DLHPHKHHSHEQHPHGHHPHAHHPHEHDTHRQHPH-$CONH_2$

The crude peptide was purified using reverse phase high performance liquid chromatography (RP-HPLC) on an Agilent 1100 instrument with HPLC grade solvents. Crude peptide (5 mg) was solubilised in 20% acetonitrile with 0.1% TFA. Aliquots of 50 μL were injected onto a Jupiter Proteo 90 Å C12 column (250 x 4.6 mm, Phenomenex) equilibrated with 95% of the aqueous mobile phase (H_20 + 0.1% TFA) and 5% organic mobile phase (Acetonitrile + 0.1% TFA). The peptides were eluted at 1 ml/min using the gradient in Table 2.1 and elution monitored at 220 nm. Fractions were analysed for HRGP330 using a microTOF instrument using the same parameters described in section 2.4.3 but over a mass range of 400-5000 *m/z*.

Table 2.1 Gradient used for purification of HRGP330 by RP-HPLC

Time (mins)	% Organic Mobile Phase
0	5
20	55
40	100
45	100
50	5

2.9.2 Lyophilisation of peptides

Fractions containing HRGP330 were combined in a round bottomed flask and the acetonitrile/TFA removed on a rotary evaporator for 10 minutes. The solution was aliquoted into acid-washed Eppendorfs and freeze-dried. The dried peptide was stored at -20 °C until required.

2.9.3 Estimating HRGP330 concentration

HRGP330 has no absorbance at 280 nm due to the lack of Cys, Trp and Tyr residues. Scopes' Equation (1) was used to estimate the concentration by measuring the absorbance at 205 nm (Scopes, 1974). The lyophilized peptide was reconstituted in the appropriate aqueous buffer before the absorbance was measured.

$$c\ (mg/ml) = \frac{A_{205}}{31\ x\ b}$$

c = concentration; A = absorbance; b = optical path length (cm)

Equation 1

2.10 Metal ion-binding experiments with HRGP330

2.10.1 Desalting HRGP330 samples

Lyophilized HRGP330 was reconstituted in 10 mM ammonium acetate (pH 7.4). Desalting was achieved using 5 ml polyacrylamide desalting columns with a 1.8 kDa exclusion limit (Pierce Protein Biology Products). The columns were inverted several times to resuspend the resin and then left to settle for 10 minutes. The storage solution (0.02% sodium azide) was removed from the column and it was equilibrated with 50 ml 10 mM ammonium acetate (pH 7.4). HRGP330 (0.5 ml) was loaded onto the column and 0.5 ml fractions collected. Emergence of peptide from the column was monitored by measuring the absorbance at 220 nm. The columns were regenerated by washing with 50 ml of buffer and stored at 4°C.

2.10.2 Metal ion titrations by ESI-MS

Metal stocks of $Zn(CH_3COO)_2.2H_2O$, $Cd(CH_3COO)_2.2H_2O$ and $Cu(CH_3COO)_2.H_2O$ were prepared in Milli-Q water at a concentration of 20 mM. Microlitre aliquots were added to HRGP330 samples to achieve varying metal:peptide ratios. Samples were incubated at room temperature for 2 hours. Spectra were acquired using a maXis-UHR-TOF, as outlined in section 2.4.4, with parameters adjusted to suit smaller proteins. A syringe pump injected the sample into the mass spectrometer at a rate of 90 μL/hour. Raw data were collected for approximately 1-1.5 minutes over a *m/z* range of 500-1500. The following conditions were used for the Q-TOF mass spectrometer: Dry gas = 4.0 L/min; dry gas temperature = 180 °C; funnel RF = 400 Vpp; multipole RF = 400 Vpp; collision cell energy = 10 eV; collision RF = 1300 Vpp; ion cooler = 650 Vpp; transfer time = 148.4 μs. The data were deconvoluted, smoothed and baseline subtracted using Bruker Compass Data Analysis v4.0.

2.10.3 pH titration of Zn_5-HRGP330 by ESI-MS

HRGP330 (20 μM) was incubated with 5 mol. equiv. of $Zn(CH_3COO)_2.2H_2O$ and desalted as described in section 2.10.1. Microlitre additions of 1% acetic acid were added to reduce the pH and spectra acquired for 2 minutes at each point. The pH range investigated was 2-7 and was double-checked for each sample following ESI-MS analysis.

2.10.4 CD spectroscopy of HRGP330

Lyophilized HRGP330 samples were reconstituted in 10 mM sodium phosphate buffer (pH 7.4) and diluted to a concentration of 11 μM. Far-UV CD spectra were measured on a J-720 spectropolarimeter (Jasco Inc, Easton, MD, USA) using quartz cuvettes with a 1 mm pathlength and a temperature of 20 °C. Spectra were recorded over a range of 180-260 nm with a data pitch of 0.2 nm, bandwidth of 1 nm, a scanning speed of 100 nm/min and a response time of 1 s. Sixteen scans were averaged and the spectrum of the buffer was subtracted to give the final corrected spectrum. Titrations were carried out by adding microlitre additions of $ZnCl_2$.

2.10.5 Comparison of apo- and holo-HRGP330 using TWIM-MS

Samples of Zn^{2+}-bound HRGP330 were prepared using the same procedure as described in section 2.10.2. Ten microlitres of 10 μM HRGP330 in 10 mM ammonium acetate (pH 7.4) was injected via a nanoflow source into a Synapt HDMS G2 system (Waters Corporation, Milford, MA, USA). The instrument was operated in the positive mode with a source temperature of 90 °C. The following instrumental conditions were used: backing pressure 2 mBar; capillary voltage 1.2 kV; cone voltage 40 V; helium cell gas flow 180 mL/min; IMS cell gas flow 90 mL/min; travelling-wave height 40 V and travelling wave velocity 700 m/s. A mass acquisition range of 200-1500 *m/z* was used. To calibrate the ion mobility data 10 μM polyalanine in 50% acetonitrile was used. Data were analysed and processed using MassLynx v4.1 provided by Waters.

2.11 Comparison of apo- and holo-HRGP330 by NMR spectroscopy

2.11.1 NMR sample preparation

Samples of HRGP330 (0.3-0.5 mM) were prepared in protein NMR buffer: 50 mM [D_{11}]Tris-Cl, 50 mM NaCl, 10% D_2O, pH 7.4. The pH was adjusted if necessary using 1 M DCl or 1 M NaOD and the pH measured prior to experiments. Aliquots of $ZnCl_2$ from a 55 mM stock solution were added to HRGP330 at varying metal ion:peptide ratio. The pH was adjusted with 1M DCl or NaOD and samples were allowed to equilibrate for 20 min before being spun to remove any aggregated protein.

2.11.2 1-D ^{1}H NMR spectroscopy

Spectra were recorded on a Bruker Avance 700 Ultrashield™ spectrometer which has an operating frequency of 700.13 MHz for ^{1}H. Suppression of the water signal was achieved using excitation sculpting with gradients (Hwang *et al.*, 1995). 1-D spectra were obtained over various temperatures (5-35 °C) using 65k complex data points, 128 scans and a spectral width of 15 ppm. Spectra were processed using TOPSPIN 2.0 provided by Bruker.

2.11.3 2-D homonuclear [^{1}H, ^{1}H] NMR spectroscopy

2-D [^{1}H,^{1}H] total correlation (TOCSY) and nuclear Overhauser (NOESY) spectra were acquired over 32 scans with 4k data points in the F2 dimension and 512 increments in F1. The spectral width was 13 ppm in both directions. A spin lock of 60 ms for the TOCSY and mixing time of 500 ms for the NOESY were used. The raw data were processed in

TOPSPIN 2.0 with apodization using a squared sine-bell function and Fourier-transformed with 2k x 2k data points in F2 and F1. Baseline correction was employed in both directions. Analysis was carried out using Sparky v3.114 (Goddard and Kneller, 2007).

2.11.4 Chemical shift referencing using residual water

The chemical shift of water is typically 4.766 at pH 7.0, 298 K and no salt (Wishart *et al*., 1995). This chemical shift is affected by temperature (-11.9 +/- 0.3 ppb/K), pH (-2 ppb/pH unit in the range of 2-7) and salt concentration (-9 ppb/100 mM salt). Residual water can be used as an internal standard and the shift is calculated according to Equation 2 (where pH = 6.20, temperature = 5 °C and salt concentration = 50 mM).

$$\delta = 4.766\ ppm - (0.009\ ppm\ x\ 0.5) - (-0.002\ ppm\ x\ 0.8) - (-0.0119\ ppm\ x\ 20)$$

Equation 2

2.12 Electrospray-tandem mass spectrometry (ESI-MS/MS)

MS/MS experiments were carried out on a dual ion funnel amazon speed ETD instrument (Bruker, Coventry, UK) operating in positive mode. HRGP330 was infused at a rate of 6 *μ*L/min and acquisitions were performed using a scan speed of 8,100 *m/z*/sec^{-1}. The following parameters were used: trap drive = 71.8; capillary exit = 140 V; source temperature = 180 °C. An isolation width of 4 *m/z* was used to select the ion of interest and CID was performed by applying an amplitude of 1.0 V. Fluoranthene was used as the electron transfer dissociation (ETD) reagent with an ETD reaction time of 100-120 ms followed by a proton

transfer reaction (PTR) time of 75 ms. Monoisotopic peaks were assigned using the SNAP™ peak detection algorithm. Spectra were analysed using BioTools v3.2 and Sequence Editor provided by Bruker.

2.13 Interaction of HRGP330 with a heparin dodecasaccharide

An ammonium salt of an unsaturated heparin dodecasaccharide was obtained from Dextra Laboratories (Reading, UK) which had been produced by enzyme cleavage (purity ≥ 95%). To observe the complex formation, the dodecasaccharide was reconstituted in 10 mM ammonium acetate (pH 7.4) and incubated with HRGP330 at a 1:1 ratio for 1 hour prior to mass spectrometry analysis. For the protein-heparin complex, spectra were obtained in the positive mode using the method previously described in section 2.10.2.

2.14 Determination of an apparent binding constant for HRGP330

5 μM $ZnCl_2$ was added to 10 μM Zincon in 50 mM HEPES and 100 mM NaCl at pH 7.4. Aliquots of HRGP330 in the same buffer were titrated in and the absorbance measured at 620 nm until a plateau was reached. The apparent binding constant was determined using Equation 3.

$$Kapp\ (Zn - HRGP330) = Kapp(Zn - Zincon)x\ \frac{[Zn{-}peptide]/[Zincon]}{[Peptide]/[Zn{-}Zincon]}$$

Equation 3

The absorbance values were converted to percentages with 100% relative absorbance corresponding to the maximum absorbance observed at 620 nm for the Zn^{2+}-Zincon complex.

2.15 Zn^{2+} binding to full length HRG

Rabbit HRG was a gift from Dr Alan Stewart (University of St Andrews). HRG was incubated with 10 mol. equiv. of $Zn(CH_3COO)_2.2H_2O$ for 2 hours at 37 °C. Samples were buffer exchanged into 10 mM ammonium acetate (pH 7.4) using a PD-10 column. The protein fraction that eluted was concentrated using Amicon-Ultra 4 centrifugal filters with a 30 kDa MWCO membrane. Samples were diluted with ultrapure 0.1 M HNO_3 and analysed using ICP-OES as described in section 2.6. HRG concentration was estimated by dividing the sulfur concentration by 13.

2.16 Metal binding to Gly-Gly-His peptide

2.16.1 ESI-MS

A peptide mimic for the N-terminus of HSA, Gly-Gly-His, was obtained from GenScript Corporation (USA) which had a purity of > 95%. The lyophilised peptide was reconstituted into sterile water, aliquoted and frozen at -20 °C. Aliquots were thawed on ice and 1 mol. equiv. of the appropriate metal ion added. The peptide was incubated for 2 hours followed by analysis on a maXis-UHR-TOF instrument in the positive mode over a mass range of 5-2000 *m/z*. The following parameters were used: dry gas = 4.0 L/min; source temperature = 200 °C; funnel RF = 100 Vpp; multipole RF = 300 Vpp; collision cell energy = 5 eV; collision RF =

600 Vpp; ion cooler = 200 Vpp; transfer time = 131.4 μs; pre pulse storage = 1 μs.

2.16.2 1-D ^{1}H NMR spectroscopy

2 mM peptide samples were prepared in 90% H_2O/ 10% D_2O at pH 7.35. ^{1}H-HMR was carried out on a Bruker-DRX550 instrument operating at a frequency of 500.13 MHz for ^{1}H. Data were obtained over 256 scans at a temperature of 25 °C. $ZnCl_2$ was titrated into the peptide from a 50 mM stock solution.

2.17 Metal ion transfer experiments

2.17.1 Zn^{2+} distribution between HSA and HRGP330

15 μM Zn-HSA (with or without 5 mol. equiv. myristate) was prepared as described in section 2.5.1 in 10 mM ammonium acetate (pH 7.4). Lyophilised HRGP330 was reconstituted in the same buffer and added to HSA at a concentration of 15 μM. The protein samples were incubated at 37 °C for 2 hours after which time they were diluted to 5 μM and analysed by ESI-MS as outlined in section 2.10.2.

2.17.2 Separation of HSA and HRGP330 with a MWCO filter

To investigate Zn^{2+} binding to HRGP330 in the presence of 600 μM HSA, a 30 kDa MWCO filter was used to retain the HSA on the membrane but allow any Zn^{2+}-bound HRGP330 to pass through. Zn-HSA (with or without 5 mol. equiv. myristate) was prepared as in section 2.5.1 in 10 mM ammonium acetate (pH 7.4) and concentrated to ~600 μM. 10-20 μM

HRGP330 was added followed by incubation at 37 °C for 2 hours. The peptide was separated from HSA by washing through an Amicon® Ultra-0.5 centrifugal filter unit (30 kDa MWCO) 3 times at 13,000 rpm for 10 minutes. The HRGP330 fraction was analysed by ESI-MS as outlined in 2.10.2 and the HSA fraction was prepared for ICP-OES analysis according to section 2.6.

2.17.3 Size exclusion chromatography

600 μM HSA, 20 μM HRGP330 and 25 μM $ZnCl_2$ (± 5 mol. equiv. myristate) were separated on a BioSep™-SEC-S2000 column (300 x 7.8 mm, Phenomenex) in 10 mM HEPES, 50 mM NaCl (pH 7.4) following incubation at 37 °C for 2 hours. Aliquots of the fractions where proteins eluted (200 μL) were diluted to 3 ml in 3% HNO_3 in acid-washed tubes and analysed for Zn on an Agilent 7500 ICP-MS instrument by Dr James Barnett. Protein concentration of the fractions was assessed using a BCA Protein Assay kit according to the manufacturer's instructions (Pierce Protein Biology Products).

2.17.3 Cu^{2+} transfer between Gly-Gly-His and HRGP330

The Cu^{2+}-Gly-Gly-His complex was formed by addition of 1:1 mol. equiv. $Cu(CH_3COO)_2.H_2O$ to the peptide in 10 mM ammonium acetate (pH 7.4). Addition of 0.2-1 mol. equiv. of HRGP330 was made from a stock in the same buffer. Following an equilibration period, samples were analysed on a maXis-UHR-TOF according to the same method in section 2.16.1.

2.18 Bioinformatic analysis

Primary sequences of HSA and HRG were obtained from the protein database, UniProtKB, accessed via ExPASy. Sequence alignments were carried out using ClusalW2 (Larkin *et al*., 2007). The Unimod database (Matrix Science Ltd, London) was used to identify protein modifications from mass spectrometry data. Structures from the protein databank (PDB) were manipulated using DeepView Swiss PDB-viewer v4.01 (Guex and Peitsch, 1997) and PyMOL Molecular Graphics System v1.3 (Schrödinger, LLC).

Chapter 3
HSA-ligand complexes

3.1 Introduction

In this Chapter, a high resolution Q-TOF instrument was used to optimise methods to study large protein complexes. Once weakly bound buffer and salt adducts were removed efficiently, this enabled production of data on metal binding to HSA. It was found that the interactions with biologically relevant fatty acids are removed on transfer into the gas phase. Conversely, perfluorinated fatty acids (PFCAs) were observed to bind in the gas phase and the data showed that Zn^{2+} remained bound to HSA even in the presence of perfluorinated octanoic acid (PFOA). This is consistent with the hypothesis proposed by Lu *et al*. (2012b) that Zn^{2+} is able to still bind in Site A when a short-chain fatty acid molecule is bound to FA2.

3.2 Electrospray-ionisation mass spectrometry (ESI-MS)

3.2.1 An overview of mass spectrometry

Mass spectrometry has been developed over the years to become an essential tool in the fields of both chemistry and biology. The mass of a molecule is an important characteristic and the ability to measure it precisely is necessary for a variety of scientific investigations. A mass spectrometer is an instrument that can measure the mass-to-charge ratio

(*m/z*) of ions in the gas phase. The instrument can be separated into five different components that are outlined in Figure 3.1. Firstly the sample of interest is injected into the mass spectrometer, followed by the formation of ions in the ion source. The ions are separated depending on their *m/z* by the mass analyser and the ion intensity at each different *m/z* value is registered by the detector. A digitizer allows this information to be converted into a user-friendly data format known as the mass spectrum. Typically, instruments have two mass analysers, for example the maXis-UHR-TOF used in this work has a quadrupole coupled to a time-of-flight analyser. A collision cell located between these allows MS/MS data to be obtained.

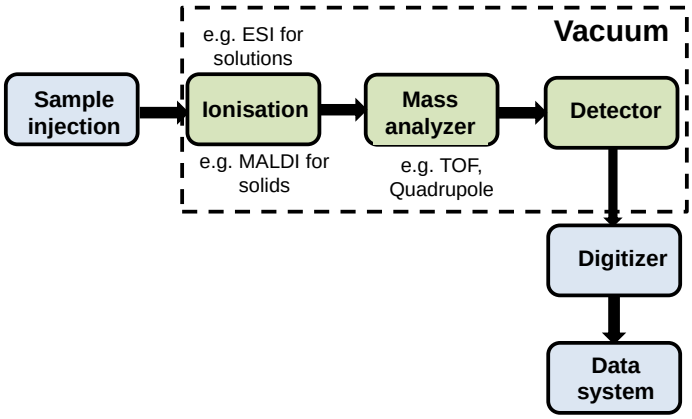

Figure 3.1 A general overview of a mass spectrometer. A schematic diagram of the components that make up a conventional mass spectrometer.

3.2.2 Development of ESI-MS for biomolecules

Until the late 1980's, researchers in the field of mass spectrometry believed that it was impossible to transfer large biomolecules from solution to the gas phase without breaking any covalent bonds and ultimately destroying the molecule. With the introduction of two new methods of ionisation, electrospray ionisation (ESI) and matrix assisted

laser desorption ionisation (MALDI), came the realisation that biomolecules could be preserved in the gas phase by using these soft ionisation techniques. ESI-MS is a technique that was first pioneered by John Fenn, who later received the Nobel Prize for the work. Firstly, the technique was employed for small molecules (Yamashita and Fenn, 1984), but then later extended to larger biomolecules such as oligonucleotides and proteins (Fenn *et al*., 1989). It has become an indispensable tool for analysing biomolecules of varying sizes and also their complexes. Early examples of ESI-MS to study non-covalent interactions include Zn^{2+} and Ca^{2+} binding to the metalloproteinase matrilysin (Feng *et al*., 1995) and the observation of a heme-myoglobin complex (Katta and Chait, 1991).

3.2.3 Mechanisms of ion formation

The sample is typically dissolved in a volatile buffer and/or organic solvent and infused continuously into the ion source. The solution is sprayed through a capillary needle which has a high electrical potential with respect to the entrance of the mass spectrometer. This electric field induces a charge accumulation on the surface of the solution at the end of the capillary, known as a Taylor cone (Figure 3.2). At a critical point the solution breaks away from the Taylor cone to form multiply charge droplets. A heated nebulising gas (typically nitrogen) flows around the outside of the capillary and directs the newly-released droplet towards the mass spectrometer in addition to aiding desolvation of the droplets.

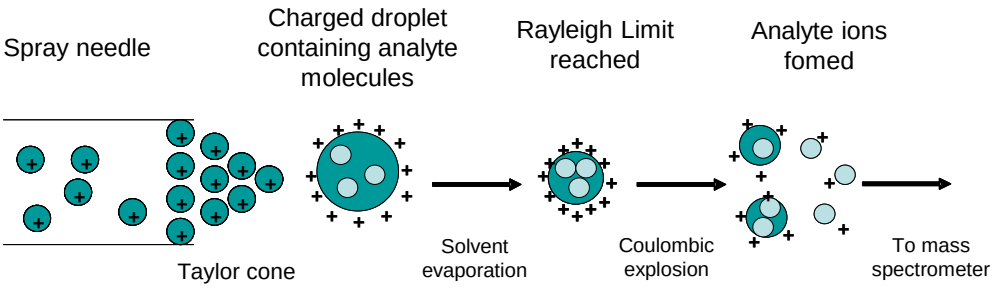

Figure 3.2 Ion formation during ESI-MS. A schematic diagram showing the steps involved in the CRM mechanism of ion formation during ESI-MS. Adapted from (Kebarle, 2000).

Gas phase ions form as solvent evaporates from the droplets. The mechanism of ion formation can be described using the two proposed models: the charge residue model (CRM) or the ion evaporation model (IEM). The CRM suggests that once the droplet is released from the Taylor cone, solvent evaporation occurs until the charge repulsion in the droplet exceeds the surface tension (or Rayleigh limit). The droplet can divide by means of a Coulombic explosion and this process is repeated until a single, multiply-charged, analyte ion is produced (Dole *et al*., 1968). In contrast, the IEM proposed by Iribarne and Thomson (1976) suggests that as the droplet reaches a particular radius the field strength of the surface of the ion becomes sufficiently large enough to eject the analyte ion out of the droplet. The IEM is thought to be the mechanism through which ions with a low mass are formed while the CRM is dominant for multiply charged ions with a high mass such as proteins (Kebarle, 2000; Kebarle and Verkerk, 2009).

3.3 Advantages of ESI-MS

A main advantage of ESI is that for instruments of limited *m/z* range, the production of the multiply-charged ions allows the observation of

molecules of higher masses at lower *m/z* values. It is also a particularly good technique for studying molecules that associate non-covalently because the gentle ionisation involved ensures that these complexes remain intact and can be detected. As proteins are proposed to form ions via the CRM model, non-covalent complexes are expected to survive in the gas phase due to a cooling effect as the solvent evaporates (Wilm, 2011). It is also an extremely sensitive technique that can analyse samples in a short time, requiring only low micromolar concentrations of the analyte. In addition, ESI-MS can be advantageous over other techniques for studying large proteins. NMR spectroscopy can provide detailed structural information on biomolecules as large as ribosomes although this requires large quantities of sample and hours, or even days, of instrument time (Cabrita *et al*., 2009). Furthermore, the protein may need to be isotopically labelled. X-ray crystallography is also an important technique in structural biology, however, some proteins can be difficult to crystallise and various conditions have to be screened in a trial and error process (Drenth, 2007).

3.4 Maintaining the native structure of proteins in the gas phase

3.4.1 Sample preparation

In the early days, mass spectrometry was mainly applied to proteomics, and routine analysis of intact proteins often used denaturing conditions (high concentrations of organic solvent or acidic solutions) in order to observe an accurate mass. With the development of instrumentation and methods for sample preparation it has become possible to study proteins

in their “native” state (Winston and Fitzgerald, 1997). This relies on proteins being prepared in volatile buffers at physiologically-relevant pH values. Purification of proteins by chromatography often utilises non-volatile buffers including Tris and HEPES and salts such as sodium chloride which are incompatible with mass spectrometry. The presence of these ionic substances will supress the ionisation of the analyte of interest (van Duijn, 2010). It is necessary for the protein samples to be buffer-exchanged into a volatile buffer and be as homogenous as possible. The sample concentration used for experiments is typically in the low micromolar range which prevents non-specific association of protein molecules, a common artefact at physiological pH.

3.4.2 Instrumental conditions

In addition to sample preparation, instrumental factors are also important. Time-of-flight mass analysers allow ions at a high *m/z* to be detected and the addition of a reflectron greatly increases the resolution (Mamyrin *et al*., 1973). Ion cooling is important for protein complexes as this removes excess energy that the ions may have acquired in the collision cell from interactions with neutral gas molecules (Chernushevich and Thomson, 2004). Lenses are then used to focus the ions into the mass analyser and the lower energy of the ions improves the resolution that is achieved. Transmission of the ions through the mass spectrometer under native conditions can also be problematic particularly for large protein complexes. One approach to improve this is to increase the backing

pressure because the low transmission is largely due to the high energy and energy-spread of high *m/z* ions (van den Heuvel and Heck, 2004).

3.5 How has ESI-MS previously been applied to albumin?

Although there are a variety of ligands that are transported around the blood by HSA, few of these interactions have been characterised using mass spectrometry. This is possibly because at the physiological conditions required to observe intact HSA complexes, the protein shows a weak spectrometric response (Henrotte *et al*., 2004) In particular, the binding of metal ions and fatty acids has not been investigated using this method although there has been success with drugs and other small molecules. Table 2 summarises the albumin-ligand interactions that have been investigated by ESI-MS to date, taking into account albumin proteins from various species. The majority of the ligands described here are exogenous. Combined with the extensive research on albumin, it would be interesting to apply mass spectrometry techniques to study endogenous molecules that bind to HSA.

Table 3.1. Non-covalent albumin complexes observed by ESI-MS.

Ligand	Albumin type	Comments	Reference
Anti-hepatitis B immune RNA	Human	Stoichiometric ratios calculated	Qi *et al*., 2007
Berberine	Human	Plant extract; determined binding constant	Cao *et al*., 2007a
Digitoxin	Human	Cardiac glycoside; used nanoESI-MS	Benkestock *et al*., 2005*
DNA	Bovine	K_D measured by ESI-MS	Greig *et al*., 2002
FK506 and FK520	Human	Immunosuppressant drugs	Ray and Stearns, 1995
Gd-DTPA Gd-C_4Me-DTPA Gd-EOB-DTPA MP-2269	Human	Gadolinium(III) chelates used as MRI contrast agents	Henrotte *et al*., 2004
Growth hormone releasing factor	Bovine	44 amino acid peptide	Baczynskyj *et al*., 1994
Glyburide	Human	Anti-diabetic drugs; used nanoESI-MS	Benkestock *et al*., 2005*
Iopanoic acid	Human	Iodine containing contrast agent; used nanoESI-MS	Benkestock *et al*., 2005*
Ketoprofen	Human	NSAID drug; used nanoESI-MS	Chen *et al*., 2006
KP1019 and KP418	Human	Ru(II) anticancer agents; negative electrospray	Groessl *et al*., 2006
Naproxen	Human	NSAID drug; used nanoESI-MS	Benkestock *et al*., 2005*
Oligonucleotide	Bovine	20mer phosphorothioate oligonucleotide; determined K_D	Shaw *et al*., 1991
Para-Sulfonato-Calix[n]arene derivatives	Bovine	Molecules of biological interest; K_A determined by ESI-MS	Da Silva *et al*., 2006
Puerarin	Human	Isoflavone of biological interest	Qi *et al*., 2006
Sodium aescinate	Human	Anti-inflammatory	Qi *et al*., 2006
Suramin	Human	Prostate cancer treatment undergoing clinical trials	Roboz *et al*., 1998
Tanshinone IIA	Human	Medicinal herb used in Chinese medicine	Liu *et al*., 2008
Tectoridin	Human	Isoflavone of biological interest; stoichiometric ratios calculated	Cao *et al*., 2007b
Tropane alkaloids	Human	Anticholinergic drugs; measured binding constant	Ma *et al*., 2008
Warfarin	Human	Anti-coagulant	Benkestock *et al*., 2005*; Liu *et al.,* 2008

*Indicates that although intact HSA was originally used, low mass resolution on the instrument mean published data were acquired using only Domain II.

3.6 Results and discussion

3.6.1 Native ESI-MS of HSA

A recombinant form of HSA was used in this work as this is typically more homogeneous with regards to the state of Cys34 and fatty acid content than HSA extracted from plasma. Furthermore, it is a safer alternative to handling plasma proteins extracted from human blood. The charge states that are observed under different conditions can be related to the protein conformation (Chowdhury *et al.*, 1990). Denaturation unfolds the protein and allows basic sites to become more accessible to protons and therefore highly charged states are observed. Under native conditions the protein is folded and as a result can accept fewer charges. The mass spectrum of HSA acidified with formic acid is shown in Figure 3.3 A where at least 3 bell-shaped charge state distributions were observed to overlap.

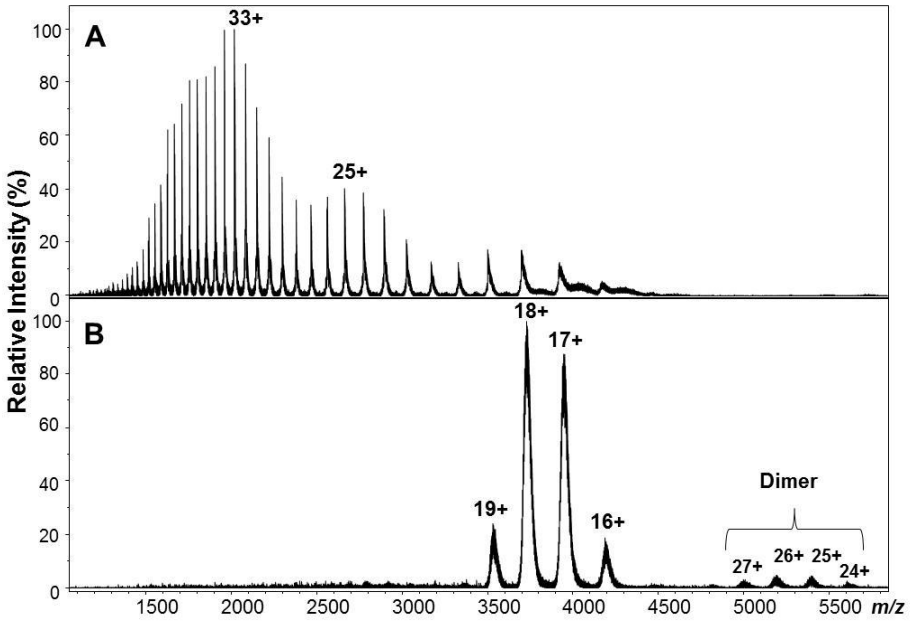

Figure 3.3 Comparison of the charge state distribution for denatured and native HSA. A) 5 μM HSA in 10 mM ammonium acetate with addition of 1% formic acid, pH 3.0 B) 5 μM HSA in 10 mM ammonium acetate (pH 6.90).

In contrast, using native conditions, four peaks were observed corresponding to the charge states 19+ through to 16+. (Figure 3.3 B). Deconvolution of the raw spectrum in Figure 3.3 A gave a clear indication of the components of the recombinant albumin sample which is shown in Figure 3.4. The most abundant peak observed was 66,437.38, in excellent agreement with the theoretical mass of 66,438.41 Da. A small proportion of Asp1-Ala2 truncation product was also observed at 66,253 Da (Chan *et al*., 1995). The second most abundant peak had a mass increase of 32 Da, possibly an oxidation product (+ 2O) of Cys34 or a Met residue. This has been observed before with recombinant HSA in borate buffer at pH 8.0 (Nicholls and Morton, 2010). Therefore it is possible that extensive dialysis in ammonium bicarbonate at pH 7.80-7.90 contributed to this oxidation. This was also not observed in early experiments, suggesting that storage time was a factor in the species occurring. The free thiol content of HSA was assessed using a cysteine assay with DTNB. The result indicated that there was 0.63 ± 0.04 mol SH mol^{-1} HSA in a fresh sample of HSA. The reported literature values for recombinant HSA are as high as 0.90 mol SH mol^{-1} HSA suggesting that the thiol had been partially oxidised (Ivanov *et al*., 1998). ESI-MS analysis following reaction of HSA with DTNB showed that 68% of the protein had been modified to produce a mass of 66,635 Da (Figure A2, Appendix). The only remaining species was that with +2O which suggests this is an oxidation occurring at Cys34 which subsequently blocks the residue from reaction with DTNB (Figure A2).

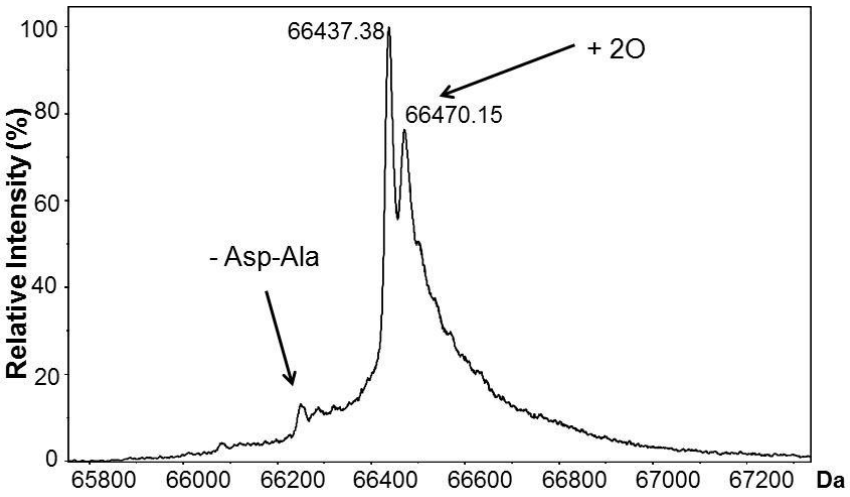

Figure 3.4 Deconvoluted spectrum of acid-denatured HSA. Two major species are observed with masses of 66,437.38 and 66,470.15 Da. A small proportion of HSA with Asp1 and Ala2 cleaved off is also present.

The HSA-dimer was observed with charge states from 27+ to 24+. The presence of the dimer was consistent but always of insufficient intensity to be studied in great detail. This formation of the dimer has been related to factors including the age of the sample, storage temperature and moisture content (Peters, 1995). Intriguingly, a dimeric species was only observed under native conditions which contradicts the idea that it is formed through a disulfide bond between to HSA molecules. At low pH, the protein would be denatured but would still allow the observation of an -S-S- bonded species therefore, based on this evidence it is likely to be a non-covalent dimer.

3.6.2 Incomplete desolvation of the analyte ions

The charge states observed at physiological pH under mild conditions were extremely broad which complicated the analysis i.e. the mass observed was not comparable to that predicted from the primary sequence. Further research into the limitations of ESI gave an indication

that the reason could be the formation of buffer adducts from the aqueous conditions used to preserve native protein complexes. Broad peaks are observed because the ion current is distributed over a heterogeneously solvated species as a result of an insufficient desolvation process (McKay *et al*., 2006) although manipulation of instrumental parameters can overcome this to some extent (Sobott and Robinson, 2004). Suggested approaches to improving desolvation include increasing the temperature of the counter flow gas, increasing the vacuum pressure and optimising the collision energies (Loo, 2000).

Collision induced dissociation (CID) is typically carried out in two areas of the instrument: the source region and the collision cell. Experiments were undertaken which involved varying the collision cell energy; it was typically set at 6-10 eV to give the large HSA ions enough energy for transmission. An increase to 20 eV reduced the peak broadness, however, at increased collision cell energy the intensity of peaks was considerably reduced and so the spectra were not improved. The other method to enhance the desolvation involves optimising the in-source collision induced dissociation (ISCID). Figure 3.5 shows spectra collected with various ISCID energies applied. An increase to 100 eV reduced the broadness of the peaks without changing the charge state distribution. This removed the unwanted buffer adducts and gave clear, well defined charge states with accurate masses without inducing fragmentation of the intact protein. In addition, the intensity of the signal was not compromised and enough data could be obtained for deconvolution.

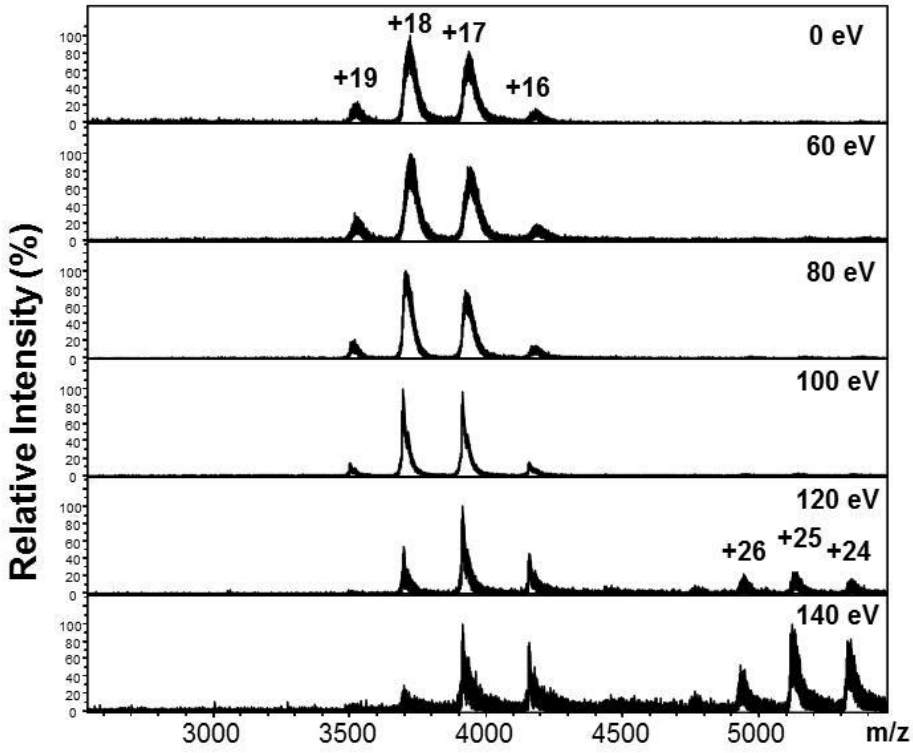

Figure 3.5 Effect of in-source CID on desolvation of protein complex ions. ESI mass spectrum of HSA with increasing ISCID energies ranging from 0-140 eV. Samples were 2.5 μM in 10 mM ammonium acetate.

Above 100 eV, the intensity for native HSA signals dropped and also the charge state distribution was shifted slightly to the right hand side of the spectrum. The charge state distribution for the dimer became considerably more abundant in relative intensity at 140 eV. An explanation for this could be that increasing the activation energy of the ions focuses them and as a result higher *m/z* ions are favoured (Loo, 1997). This could also support the idea that the dimeric form occurs through a covalent disulfide bond between Cys34 of two HSA molecules as a weaker interaction would be expected to break easily at the higher energy applied. These experiments highlighted the importance of finding a balance between removal of non-specific adducts and preserving the non-covalent complexes of interest.

3.6.3 NanoESI-MS of HSA

NanoESI-MS using a TriVersa Nanomate® (Advion) was also used as in NanoESI, initial droplet size is smaller which can improve sensitivity (Wilm and Mann, 1996). Higher order aggregates of HSA were observed in the spectra with charge state distributions of a trimer and tetramer centred around 6500 and 7500 *m/z* respectively (Figure 3.6 A). It is unclear as to what extent these oligomer formations are an artefact formed during the gentle ionisation process or if they are always present in HSA solutions as weak bands were detected for these assemblies on SDS gels as in Figure 3.6 B.

Observations of non-specific protein assemblies have been recently documented in the literature. Lane and co-workers attempted to improve the understanding of this phenomenon by modelling the number of molecules that would exist in a droplet, just before it is introduced into the mass spectrometer, using Monte Carlo methods (Lane *et al*., 2009). The model assumes that as the protein concentration increases, the probability of more than one biomolecule being contained within the droplet also increases. As it is most likely that desolvation of protein ions proceeds via the CRM model, non-specific association of the biomolecules may occur at the final stages of the ionisation process.

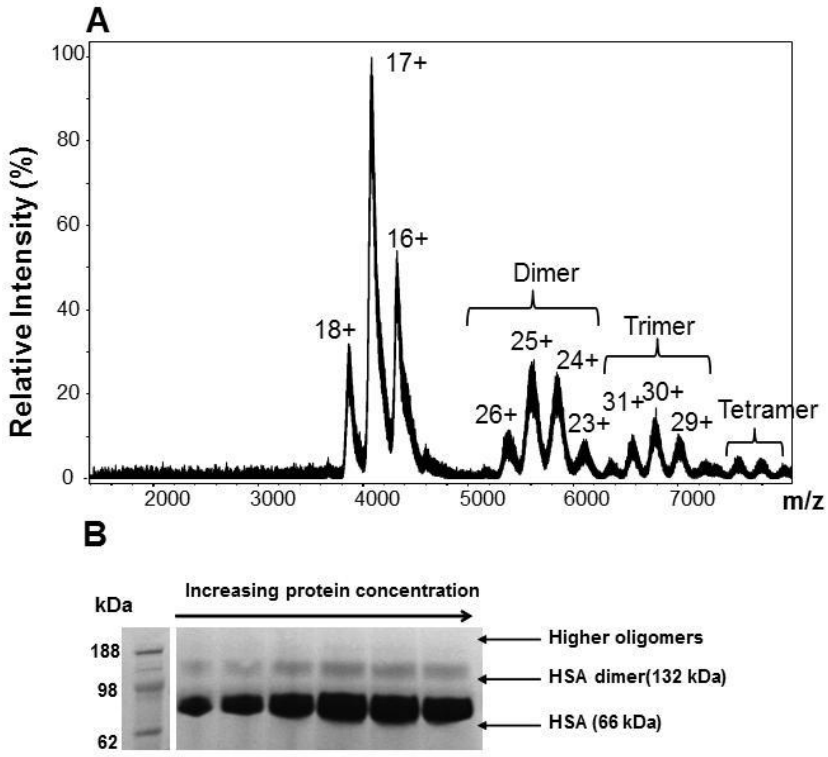

Figure 3.6 Observation of higher order oligomers of HSA during nano-ESI-MS and SDS-PAGE A) Samples (5 μL) were infused into a maXis-UHR-TOF mass spectrometer using a TriVersa Nanomate® (Advion) B) For SDS-PAGE samples were loaded onto a 4-12% SDS PAGE pre-cast gel (Invitrogen). As more concentrated samples are loaded the dimer and higher oligomers become more visible but dimers are clearly present even at the lowest concentration.

Although this model goes some way to explaining the observations of oligomers, at the experimental concentrations used (2.5-5 μM) the model predicts that the droplets should contain only one or even no molecules. This indicates that to a certain degree the assemblies are already formed in solution.

3.6.4 Analysis of Zn^{2+}-HSA

A comparison of the charge states for apo-HSA and Zn^{2+}-HSA is shown in Figure 3.7 A and B and there is no obvious difference between them. The close-up of the 18+ charge state shows two new peaks are observed in D compared to C: the first corresponds to the addition of a Zn^{2+} ion to

HSA (3695.11 *m/z*; theoretical = 3695.49 *m/z*) and a second which corresponds to the addition of Zn^{2+} to the oxidised species of HSA (3697.30 *m/z*). The difference compared to the theoretical values could be due to the broadness of the peaks. Only 1 Zn^{2+} ion was detected to be bound to HSA in the gas phase even when higher metal:protein ratios were used which suggests only binding to Site A is maintained during ESI-MS.

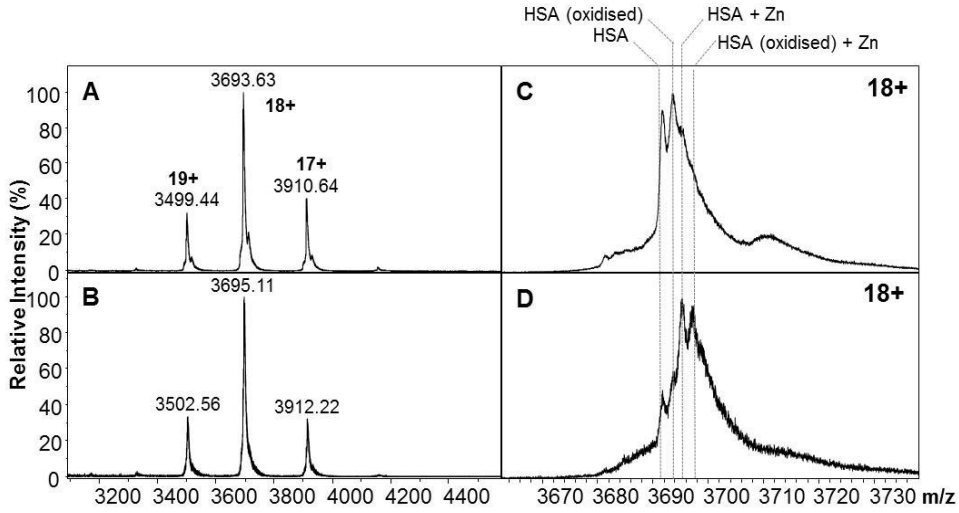

Figure 3.7 Native ESI-MS of HSA shows 1 Zn^{2+} ion bound. Charge state distribution of A) apo-HSA and B) Zn^{2+}-HSA. Close-up of the 18+ charge state of C) apo-HSA and D) Zn^{2+} HSA. Two new peaks are evident upon the addition of the metal ion.

To confirm the observations of experiments in the gas phase, samples were analysed in solution for inorganic elements. ICP-OES analysis indicated that 1.06 Zn^{2+} ions were bound per HSA molecule in these preparations which fits with the mass shifts observed. The data suggest that non-covalent metal complexes of HSA can be preserved in the gas phase even when less gentle conditions are used. This is consistent with the work of Gumerov *et al*. (2003) who found that studying Fe^{3+} binding to transferrin under extremely mild conditions was impractical. Interestingly,

a further peak centred around 3710 *m/z* is seen to be present for apo-HSA but not Zn^{2+}-HSA. It is possible that this is residual octanoic acid present in the sample as the mass is very close to the addition of two octanoate molecules. One line of evidence for this is that when a titration was carried out with increasing molar equivalents of octanoic acid, this peak increased in intensity. This will be discussed in more detail in section 3.6.6.

3.6.5 pH-induced Zn^{2+} release and unfolding of HSA

A sample of Zn^{2+}-bound HSA (0.95 Zn^{2+} ions per molecule as determined by ICP-OES) was titrated with varying amounts of acetic acid to achieve samples at varying pH which were analysed under the same conditions. The same four peaks were observed as in the previous section, however, at pH 7.36 the mass shift was greater than the addition of 1 Zn^{2+} ion and so it is possible that salt adducts contributed to this. At pH 6.15 the complex is still observed and the peaks are more resolved. As the pH was lowered to 5.46 there was little change to the Zn^{2+} binding although the protein began to partially unfold as higher charge states become visible. At pH 5.05 a clear bimodal distribution is observed as the charge states for partially unfolded HSA increase significantly in intensity. Below pH 5.0 Zn^{2+} has been released from the protein and only the peaks for HSA and HSA(oxidised) are visible.

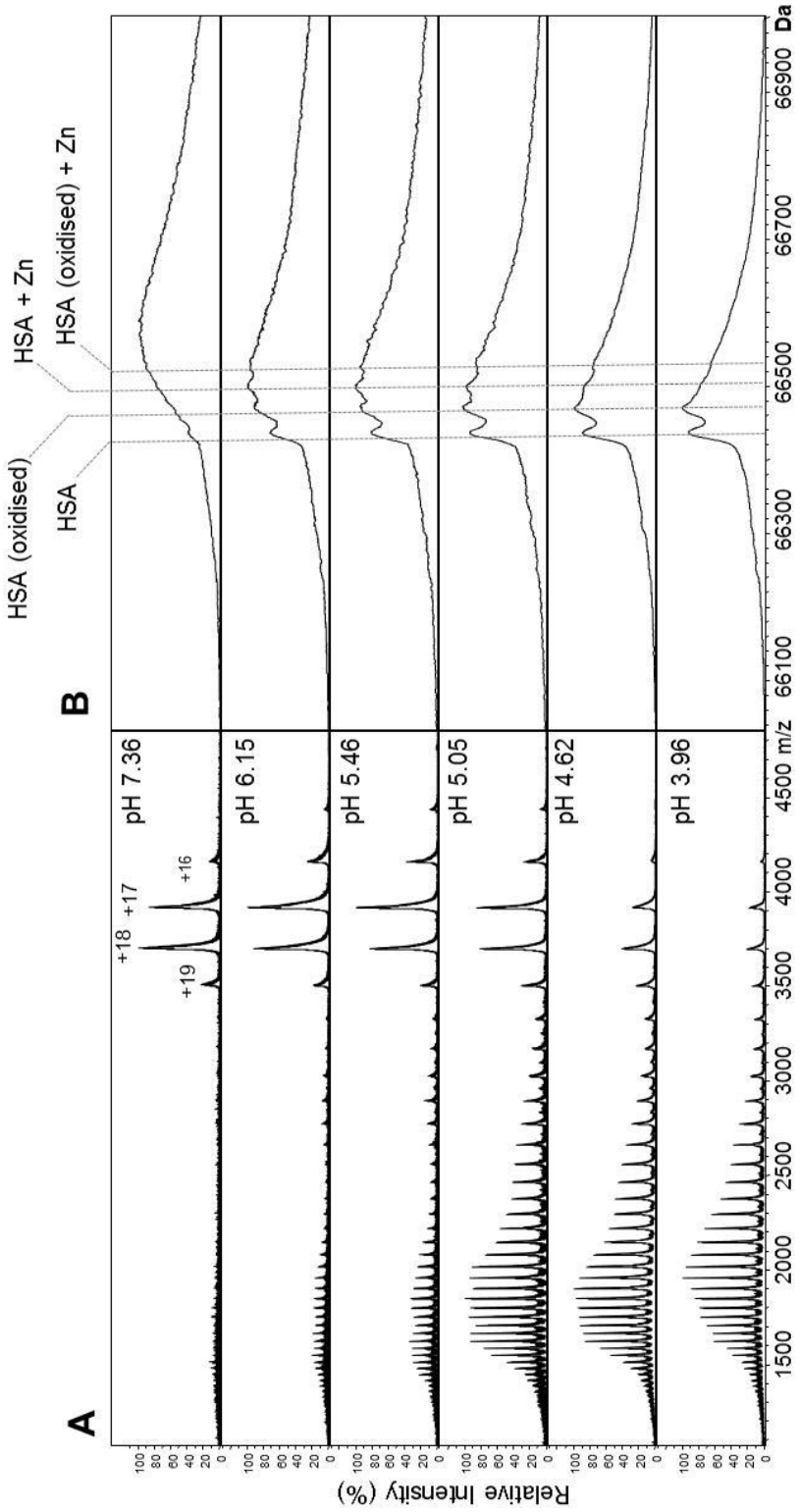

Figure 3.8 Acid-induced dissociation of Zn^{2+} from HSA. A) Charge state distribution observed at each pH B) Deconvoluted spectra with the different complexes highlighted with dashed lines.

The same observation is made at pH 3.96 although the charge states for native HSA are reduced in intensity. The increase in intensity of the higher charge states is concurrent with the loss of Zn^{2+} binding which indicates the metal ion could have a stabilising effect between domains I and II.

3.6.6 Analysis of HSA in the presence of fatty acids

To investigate the effect of fatty acids on HSA, titrations were carried out with both octanoate and myristate as shown in Figure 3.9 A and B. With increasing octanoate concentration, there was a substantial increase in the peak centred around 3710 *m/z*; the relative intensities at each point (1, 3 and 5 mol. equiv. octanoate) were 29%, 37% and 40% respectively. This peak was also evident in samples that had been dialysed which indicates it could be bound octanoate still remaining from the protein stock which originally contained 31 mM octanoic acid as a stabiliser. The data suggested that this was a non-covalent species as it was not visible once the protein was denatured (*cf*. Figure 3.4). This larger adduct had a mass of ~ 300 Da larger than HSA although an accurate mass could not be established due to the broadness of the peak.

In contrast, this peak was less apparent during the myristate titration and no change was visible. Clearly, this observation could be consistent with the interactions with myristate being broken in the gas phase although the larger adduct could be 2 molecules of octanoate-bound HSA (144.21 x 2 = 288.42 Da).

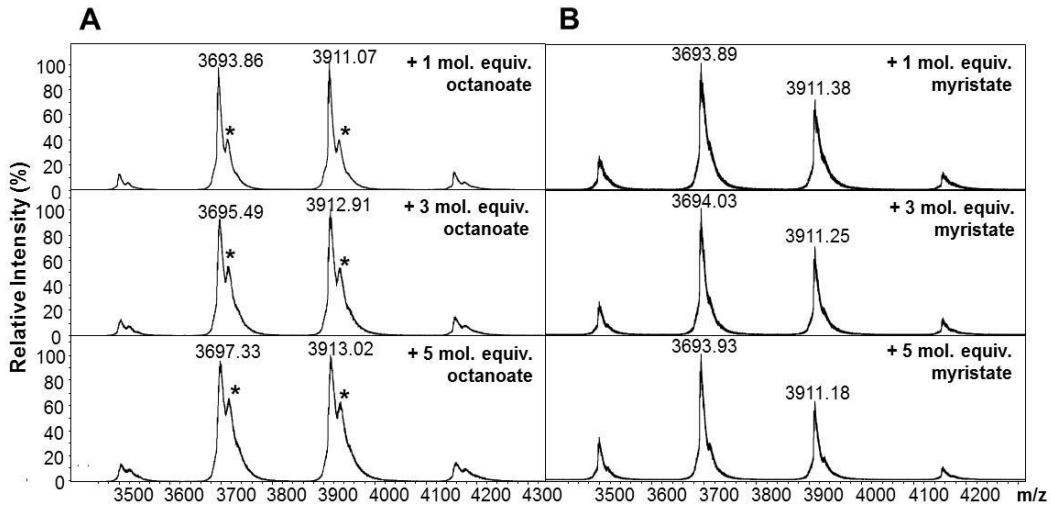

Figure 3.9 HSA titrated with varying amounts of fatty acid followed by ESI-MS. A) Aliquots of octanoate from a 0.5 mM stock solution were added to HSA and incubated at 37 °C for 2 hours B) Aliquots of myristate from a 1 mM stock solution were added to HSA at 37 °C for 2 hours. Mass spectra were obtained on a maXis-UHR-TOF instrument. A peak ~300 Da larger than HSA (*****) that was observed in native samples was observed to increase in intensity in the presence of increased octanoate.

Although fatty acids bind to HSA with relatively high affinity (K_d = 0.05-1 μM), it would appear that the interactions are too hydrophobic even though some polar side chains are thought to be involved at the high affinity binding sites. In the gas phase, hydrophobic binding partners are likely to dissociate as they are no longer being forced together as they would be in the presence of water molecules (Bich *et al*., 2010). Therefore, ESI-MS of HSA does not reflect the fatty acid binding that would occur in solution. More recently, Liu *et al*., (2009) have been able to characterise fatty acids binding to bovine β-lactoglobulin. However, it could be that the stabilisation of this hydrophobic protein-ligand interaction in the gas phase is due to the fatty acid being sterically trapped inside the cavity. The EF loops form a lid over the cavity, as can be observed in the crystal structure with myristate (3UEV), which may restrict movement of the ligand (Loch *et al*., 2012). The fatty acid binding

sites on HSA need to be less hindered in order to facilitate rapid dissociation of the molecules during transport.

3.6.7 Binding of PFCAs to HSA in the gas phase: a fatty acid mimic

PFCAs were chosen as a fatty acid mimic as the fatty acids investigated were not observed to remain bound in the gas phase. Fluorination of the molecules means they cannot be metabolised in the same way as their biologically relevant counterparts (D'eon *et al*., 2010). On a molecular level, HSA has been shown to be the most likely candidate for interaction of PFCAs that become present in blood serum at low levels (Han *et al*., 2003).

PFOA is an example of a C8 PFCA that is produced on an industrial scale and used in the production of Teflon® for cookware. It has been demonstrated by ^{19}F-NMR spectroscopy that PFOA, and other similar molecules, would bind in the same 7 hydrophobic cavities on HSA as fatty acids (D'eon *et al*., 2010) and it has been shown to bind to other fatty acid binding proteins. Han *et al.* (2003) reported the dissociation constant for PFOA binding to HSA as 0.38 mM, compared to 0.05-1 μM for fatty acids (Spector, 1975). Therefore, it is not thought that the PFOA molecule would be able to displace fatty acids once they are bound to HSA (Han *et al*., 2003). A native ESI-MS study identified the binding of up to 8 molecules (Henrotte *et al*, 2004) of PFOA to HSA in neutral ammonium acetate buffer. Following incubation with 5 mol. equiv. PFOA, and using the method developed on the maXis-UHR-TOF, 3 molecules of

PFOA were observed to be bound to HSA. Due to its impact on Zn^{2+} binding, the fatty acid site of the highest interest is FA2, which is one of the three highest affinity binding sites, therefore under these conditions it is likely to be occupied by PFOA. Additionally it has been demonstrated that FA2 becomes populated at HSA:FA concentrations as low as 1:1 (Simard *et al*., 2005). To obtain an optimum ISCID energy to observe non-covalent binding but remove buffer and salt adducts, mass spectra were obtained between 75 and 125 eV. The relative intensity for each complex was calculated and plotted to produce Figure 3.7. As the ISCID was increased the peak corresponding to HSA with no PFOA bound increased in a sigmoidal fashion. Non-covalent interactions with PFOA begin to significantly decrease at 105 eV, and a value of 100 eV appeared to be a good compromise between obtaining good spectra and preserving the complexes.

To ascertain if PFOA was a reasonable mimic for fatty acid binding and its impact on metal binding to HSA, ^{111}Cd NMR spectroscopy and ^{1}H NMR spectroscopy were carried out to probe the effect on metal binding and the histidine residues. In the presence of 5 mol. equiv. PFOA the ^{111}Cd NMR peak for Site A was supressed and the peak for Site B was still prominent albeit slightly reduced in intensity (Figure A3, Appendix). This is the same effect that has been previously observed for octanoate (Stewart *et al*., 2003). Figure A3 B (Appendix) shows the effect of PFOA on the ^{1}H-HMR spectrum of HSA where the His residues can clearly be seen.

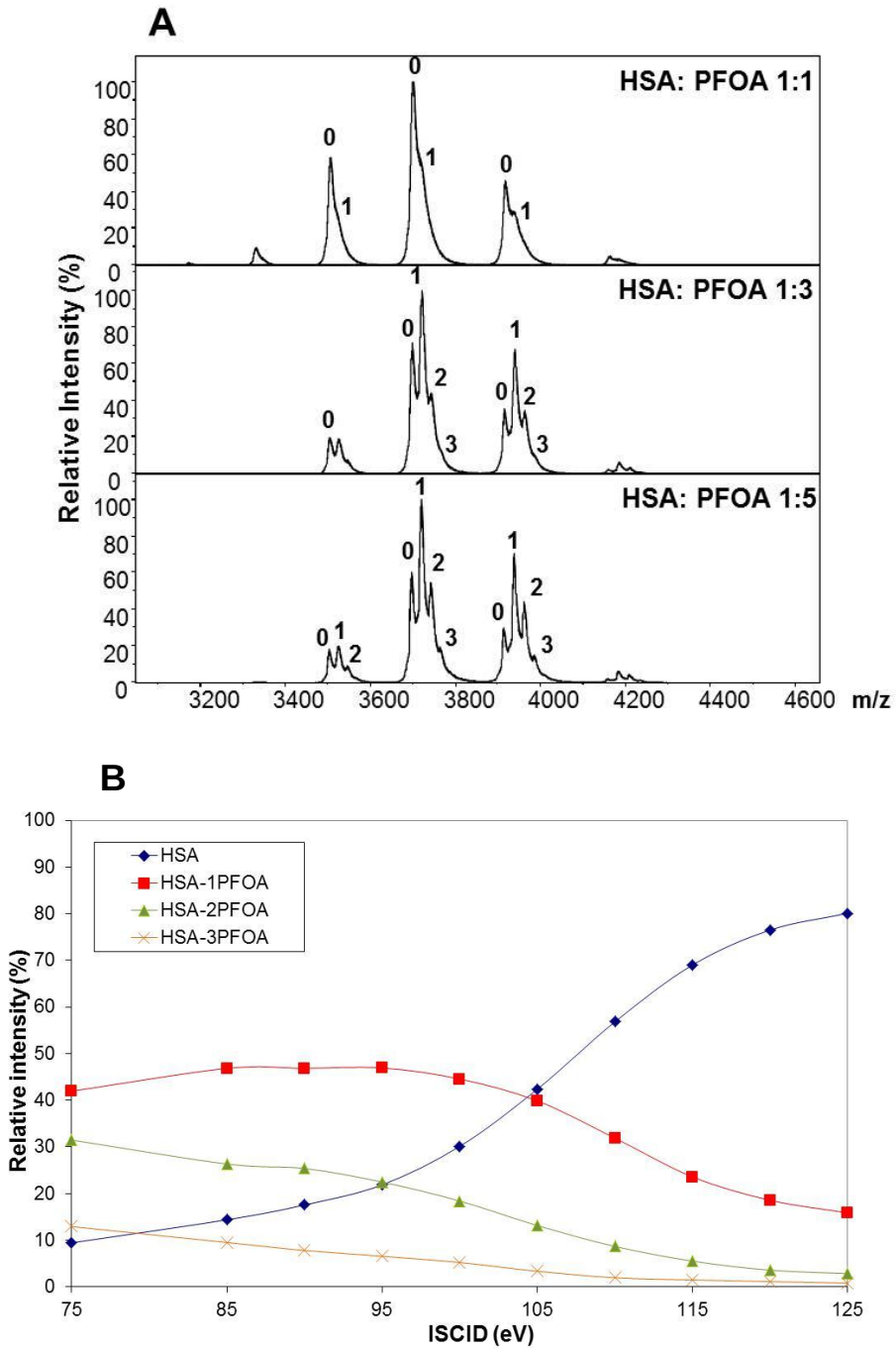

Figure 3.10 Binding of PFOA to HSA by ESI-MS. A) Spectra of HSA obtained with varying concentrations of PFOA. The numbers above the peaks correspond to number of PFOA molecules bound. B) Spectra were obtained at varying ISCID energies from 75-125 eV and the relative intensities plotted against the ISCID.

Peak 5 was unaffected by the addition of PFOA and also there was only a slight impact on peak 10. Peaks 6 and 6b disappeared completely and the intensity of peak 9 was also reduced considerably. Peaks 1 and 4,

which have been previously shown to correspond to His67 and His247, were no longer present once 5 mol. equiv. of PFOA were added. A previous titration with octanoate, showed that peak 4 became sharper which is different to that observed in the presence of PFOA, however, overall, the changes that occurred with both were largely similar indicating that the binding mode is the same. The fact that peaks 1 and 4 are affected by PFOA and also that Site A is perturbed in ^{111}Cd-NMR are both good indicators that PFOA binds in the vicinity of the Zn^{2+}-binding site. The evidence indicates that PFCAs are able to bind in the gas phase because the C-F bond is polar compared to a C-H bond which is non-polar. The hydrophilic fluorine atoms interact strongly with the lone pairs of polar amino acids and these associations are stabilised in the gas phase. However, fatty acid binding involves hydrophobic interactions which are not stabilised in the gas phase.

3.6.8 Concurrent PFOA and Zn^{2+} binding

As PFOA was shown to be a good model for octanoate, a sample incubated with both 5 mol. equiv. PFOA and Zn^{2+} was analysed by ESI-MS. Figure 3.12 shows the spectra obtained with an expansion of the most abundant 18+ charge state (Figure 3.12B). The two major peaks correspond to HSA-PFOA-Zn^{2+} (3718.44 *m/z*, theoretical mass = 3718.53 *m/z*) and also a HSA(oxidised)-PFOA-Zn^{2+} complex (3720.16 *m/z*, theoretical mass = 3720.30 *m/z*). The same set of peaks was also observed for the complex with 2 PFOA molecules bound (3741.60 *m/z*, theoretical mass = 3741.52 *m/z*). This would suggest that PFOA and Zn^{2+}

can bind simultaneously to HSA which would fit the hypothesis put forward for octanoate binding, i.e. that it does not disrupt Zn^{2+} binding in the same way predicted for myristate. ICP-OES evidence also suggested the ability of HSA to bind Zn^{2+} was not perturbed by the presence of PFOA. Zn-HSA was prepared in the absence and presence of PFOA in 10 mM ammonium acetate and subjected to gel filtration. Analysis of the solution showed Zn^{2+}-HSA had 1.48 Zn^{2+} per protein while following incubation with 5 mol. equiv. PFOA and gel filtration there was still 1.47 Zn^{2+} per protein. Therefore, neither in solution nor in the gas phase does PFOA perturb Zn^{2+} binding.

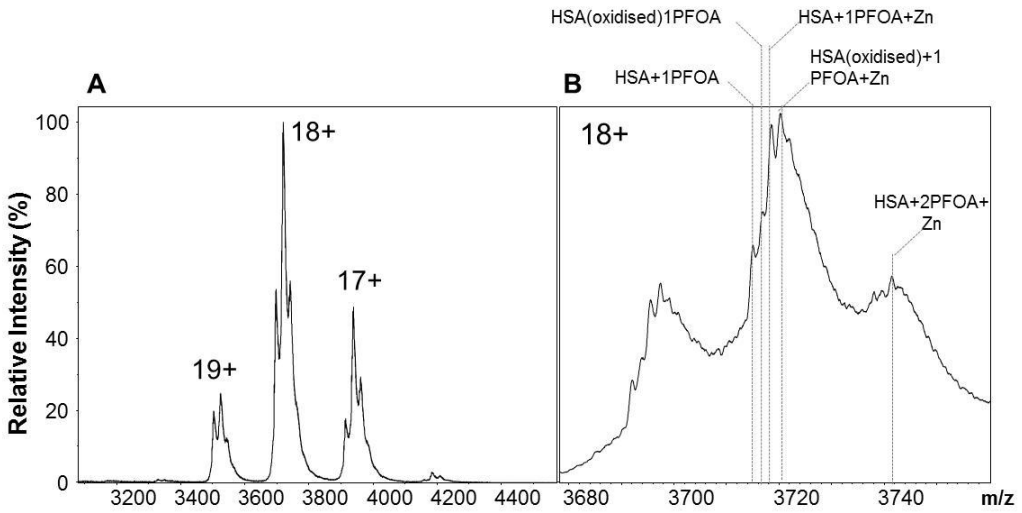

Figure 3.11 Simultaneous binding of PFOA and Zn^{2+} to HSA observed by ESI-MS. A) Charge states observed B) Expansion of the 18+ charge state showing peaks corresponding to the mass of Zn^{2+} bound to a PFOA complex.

Interestingly, Wu *et al*. (2009) carried out CD and fluorescence spectroscopy of PFOA-bound HSA and this indicated a conformational change occurred as is also observed with normal fatty acids. Although as with octanoate the conformational change may not be significant enough to disrupt the interdomain Zn^{2+} binding site.

3.6.9 Analysis of Zn^{2+} binding in the presence of myristate

Figure 3.8C shows the effect of myristate on the Zn^{2+}-HSA complex. The peaks are much broader than those observed in the presence of Zn^{2+} only. The average mass of the peak hinted that Zn^{2+} binding had not been lost from HSA and ICP-OES analysis of the same sample in solution confirmed that 1.21 Zn^{2+} ions were still bound. This does not support the hypothesis that myristate would induce a conformational change that disrupts Zn^{2+} binding.

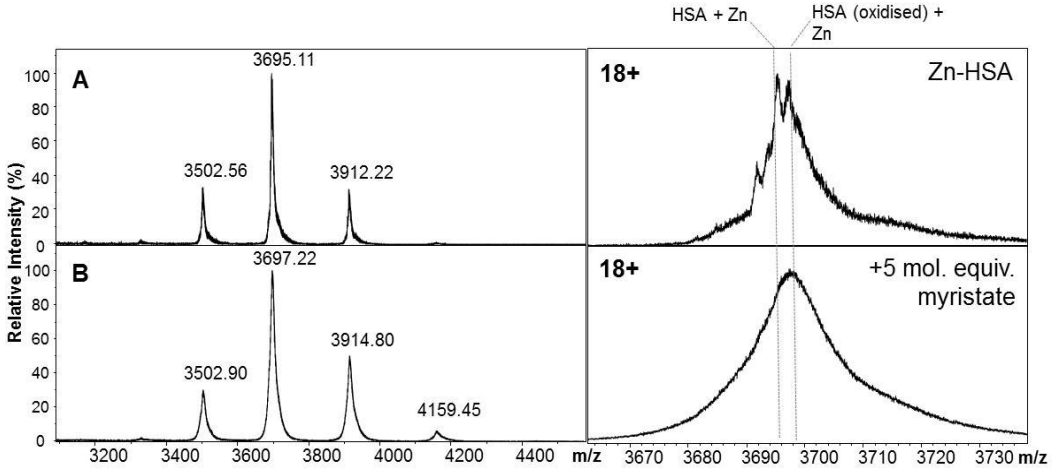

Figure 3.12 Effect of myristate on Zn^{2+} binding to HSA. A) HSA with the addition of Zn^{2+} B) HSA with the addition of Zn^{2+} and 5 mol. equiv. myristate. The spectra on the right hand side are zoomed in on the 18+ charge state.

One explanation for this could be that myristate binding may displace the Zn^{2+} from Site A to another site on HSA as there are two further sites that can accommodate Zn^{2+}. Evidence for this is that Goumakos *et al*. (1991) showed that HSA became saturated at 3.3 ± 0.2 Zn^{2+} ions which would indicate that there are two further binding sites in addition to Site A. Furthermore, ICP-OES analysis during this work showed > 2 mol. equiv. of Zn^{2+} remaining associated with HSA following passage through a gel filtration column. These other two binding sites are proposed to be Site B

and the N-terminus. Additionally, myristate has also been shown to displace metal ions from Site B (Lu *et al*., 2012b) which may result in increased binding at the N-terminus. This would rationalise why the ICP-OES results show a similar Zn^{2+}:HSA stoichiometry in the absence and presence of myristate as ICP-OES cannot provide information on to which of the three potential sites the Zn^{2+} is bound. Another explanation for there being no decrease in the Zn^{2+} binding ability of HSA in the presence of myristate could be that the buffer conditions are different as ESI-MS is not compatible with high concentrations of non-volatile buffers and salts.

One important question to address is could Zn^{2+} bind to the N-terminus if fatty acids displaced it from Sites A and B? To investigate if Zn^{2+} binding to the N-terminus is possible, 1 mol. equiv. of Zn^{2+} was added to a peptide mimic of this site that has been well characterised (Lau *et al*., 1974) which is shown in Figure 3.13 B. No evidence of an interaction was observed by ESI-MS while the control sample with 1 mol. equiv. of Cu^{2+} did show an intense peak corresponding to the Cu^{2+}-Gly-Gly-His complex (Figure 3.13 A). It was thought that perhaps the interaction with Zn^{2+} was simply too weak to be observed by ESI-MS and a previous study using ^{13}C-NMR spectroscopy did suggest that Zn^{2+} can form a complex with the tripeptide (Lakusta *et al*.,1980). Therefore the Zn^{2+}-Gly-Gly-His interaction was also studied by ^{1}H NMR spectroscopy.

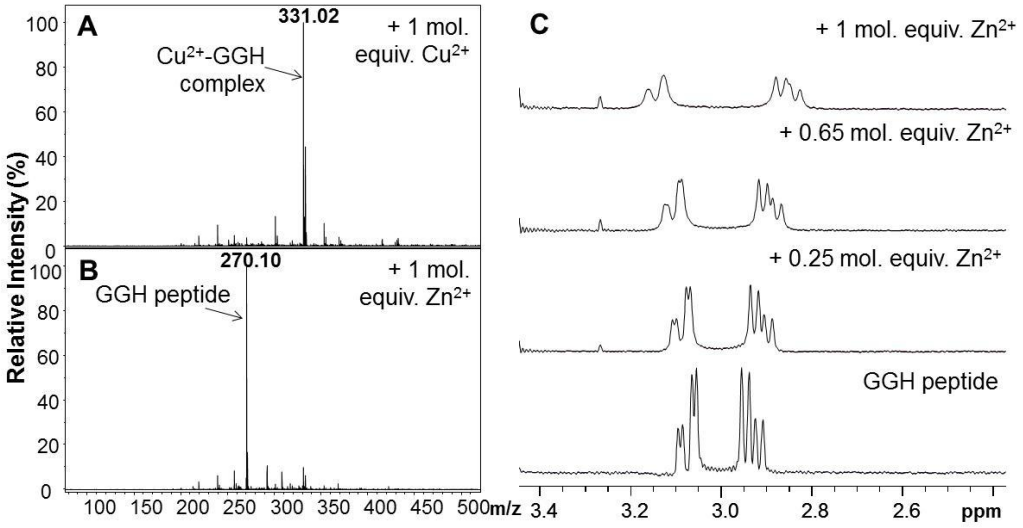

Figure 3.13 Comparison of Zn^{2+} binding to Gly-Gy-His peptide by ESI-MS and ^{1}H NMR spectroscopy. A) ESI-MS spectra of Gly-Gly-His in the presence of 1 mol. equiv. Cu^{2+} or B) 1 mol. equiv. Zn^{2+} C) 1-D ^{1}H NMR spectra of Gly-Gly-His titrated with varying amounts of $ZnCl_2$.

Substantial changes to lineshapes were observed and Figure 3.13 C shows the broadening that occurs to the CH_2 group of the His residue which suggests that there is an interaction with Zn^{2+} in solution. Overall, this indicates that Zn^{2+} may bind to the N-terminus of HSA if the other sites are saturated or no longer available due to the fatty acid-induced conformational change, even though this interaction may be too weak to be detected by ESI-MS.

3.6.10 Identification of myristic acid in low mass range

Additional evidence for fatty acid interactions being broken in the gas phase was obtained by scanning the low mass range while HSA samples were being injected. This has been shown with other molecules; for example Jones and co-workers detected perfluorooctane sulfonic acid (PFOS) at 499 *m/z* when BSA was subjected to high collision energy and the interaction between the protein and the compound was lost (Jones *et*

al., 2003). Once the conditions were optimised for smaller molecules, a peak at 229.21 *m/z* for protonated myristic acid was observed (Figure 3.14 B). Using Smart Formula 3D a molecular formula and theoretical isotopic distribution was generated for the molecule which matched that of myristic acid (Figure 3.14 C).

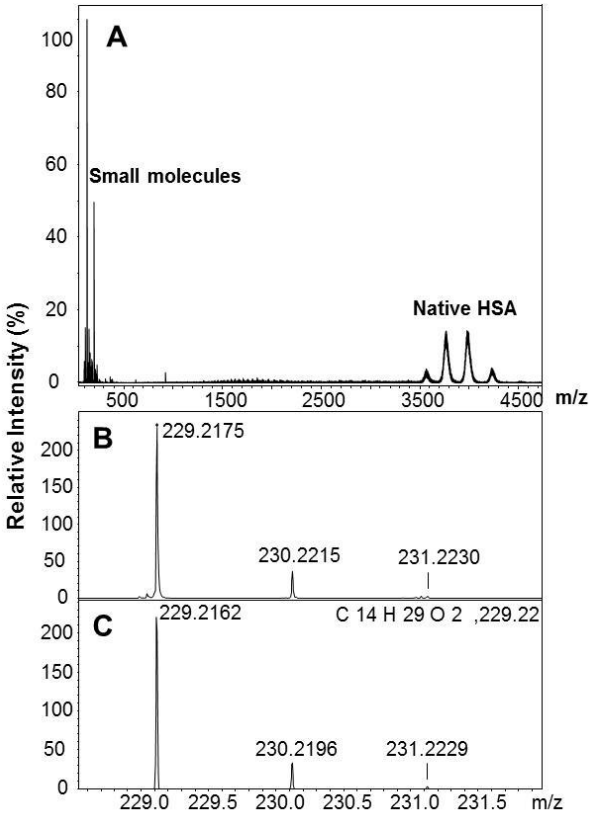

Figure 3.14 Detection of protonated myristic acid in the low *m/z* range of HSA. A) Full spectrum showing small molecules and native HSA peaks B) Expansion of the low *m/z* range shows protonated myristic acid C) This is confirmed by the formula and theoretical isotopic distribution calculated from Smart Formula 3D. The isotopic distributions are in close agreement.

Importantly, no extra collision energy was needed to observe this peak supporting the idea that the interaction of the fatty acid was broken during the transition to the gas phase. This experiment was repeated on two different maXis-UHR-TOF instruments (Instrument 2 at Bruker, Coventry, UK) to ensure the reproducibility of the data and the unbound myristic acid was detected on both indicating that it was present in the sample.

3.7 Conclusion

Experimental conditions were optimised using the maXis-UHR-TOF to study large proteins. A balance between stripping the protein of weakly-bound buffer molecules and being able to investigate ligand binding to HSA meant binding of 1 metal ion to HSA could be resolved. Evidence for only 1 Zn^{2+} ion being bound to HSA was observed by ESI-MS which is likely to be Site A. The interactions of HSA with myristate were disrupted in the gas phase resulting in no significant mass increase observed for these complexes, although, a larger HSA species was in agreement with the addition of 2 octanoate molecules. This could suggest that for two binding sites at least the interactions with octanoate are not completely abolished. For myristate bound samples, protonated myristic acid was detectable in the low mass range confirming that the ligands were too hydrophobic to remain bound in the gas phase. PFOA was used as a model compound to mimic a natural fatty acid as this interaction was preserved in the gas phase due to the more hydrophilic nature of fluorine. The ESI-MS data indicated that 1 Zn^{2+} ion can bind to HSA in the presence of PFOA which would fit with the hypothesis that this size molecule can fit in FA2 along with Zn^{2+} being bound in Site A. With addition of myristate to the Zn^{2+}-complex it appeared from the mass observed that Zn^{2+} was still bound. This was also confirmed in solution which does not support the overall hypothesis that myristate binding to HSA at FA2 displaces Zn^{2+} from its major binding site.

Chapter 4
Travelling-wave ion mobility mass spectrometry of HSA

4.1 Introduction

In this chapter, travelling wave ion mobility mass spectrometry (TWIM-MS) was applied as a novel technique to study HSA complexes with metal ions and fatty acids. Instrumental conditions were optimised to prevent unfolding of the protein, although this gave an insight into how metal ions may influence the conformational flexibility of HSA. The data obtained were compared to theoretical cross sections obtained from published crystal structures.

4.2 Ion mobility-mass spectrometry

4.2.1 Development of IM-MS

Ion-mobility-mass spectrometry (IM-MS) is an analytical technique whereby the conformation of molecules can be studied. It was first introduced in the 1970's under the name plasma chromatography as a method to separate ions (Cohen and Karasek, 1970) and was soon recognised as a powerful tool that could be used to analyse a whole host of molecules (Collins and Lee, 2001). During the 1990's the technique was applied to larger biomolecules with Clemmer demonstrating protein conformer separation using cytochrome c (Clemmer *et al*., 1995). The development of high resolution IM-MS over the past decade has further

enabled the separation of structural isomers that have an identical mass (Wu *et al.*, 2000).

As described previously conventional mass spectrometry involves four processes: sample introduction, sample ionisation, mass separation and detection. The addition of an IM cell to a mass spectrometer allows for an extra separation step which is dependent on the mobility of the ions (Kanu *et al.,* 2008). The mobility of an ion is measured by the time it takes to pass through a buffer gas which is subjected to a weak electric field (drift time). The mobility can be dependent on many factors including molecular mass, charge on the ion, size of the ion and the polarizability of the drift gas used (Karasek, 1974).

4.2.2 TWIM-MS

Four types of IM-MS are available but only one will be discussed here: TWIM-MS (Pringle *et al*., 2007). Unlike other traditional IM-MS methods where the electric field is applied constantly, a high electric field is applied to one part of the cell and is swept sequentially through the cell in the direction that the ions are moving. This is achieved by using a stacked ring ion guide (SRIG) (Giles *et al*., 2004) which consists of a series of ring electrodes stacked orthogonally to the axis on which the ions travel. Ions are propelled down the SRIG in pulses or “waves” and it is therefore given the name “travelling wave”. The ions exit the IM cell at unequal times because the time it takes for the ion to exit the cell is dependent on its mobility through an inert gas as it travels along the travelling voltage

wave. Separation of ions is then achieved as ions that have a high mobility can keep up with the wave and exit the IM cell faster. Ions that have a lower mobility have more interactions with the buffer gas, roll over the top of the wave and have to wait for ensuing waves to propel them through the cell. As a consequence these ions exit the cell later (Giles *et al*., 2004). A longer drift time through the IM cell indicates that the ion has a larger collisional cross section (Jarrold, 1999). The quantity of ions exiting the cell is plotted as a function of time, known as the arrival time distribution (ATD).

4.2.3 A commercially available TWIM-MS instrument: Synapt HDMS

The travelling wave ion guide has been integrated into a conventional hybrid Q-TOF mass spectrometer to produce the Synapt HDMS instrument which is manufactured by Waters (Pringle *et al.*, 2007). The IM cell is located between two mass analysers, namely a quadrupole and a TOF. A close-up view of the TriWave cell is shown in Figure 4.1. The IM cell contains three travelling wave-enabled SRIGs: trap, IM and transfer cell. Ions first accumulate in the trap, are released into the IM ion guide for the actual separation and then pass into the transfer region to allow them to travel to the TOF mass analyser (Pringle *et al.*, 2007). Although suggested flow rates for the buffer gas in this region are indicated on the diagram, these can be optimised depending on the sample. The presence of a helium cell prior to the nitrogen region maximises the transmission of the ions into the IM cell.

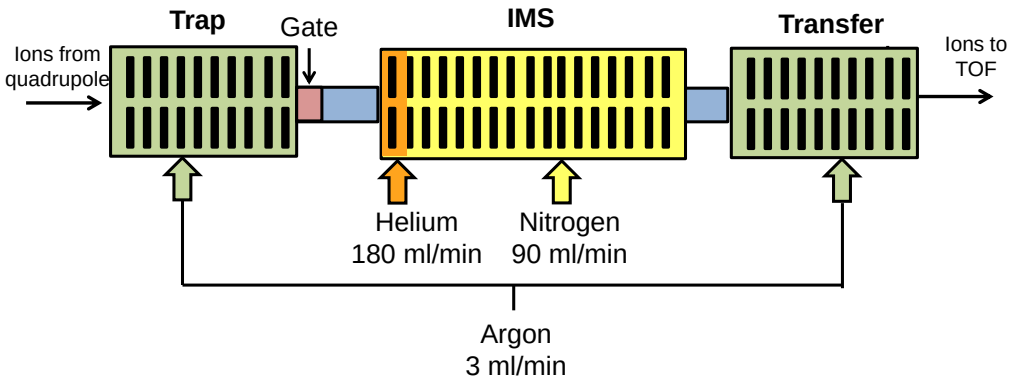

Figure 4.1 An outline of the ion mobility cell in the Synapt G2 instrument. This is a schematic view of the TriWave cell where the separation of the ions according to their mobility takes place. The three main regions of the IM cell (trap, IM separation and transfer) and labelled on the diagram. The *black* lines represent the electrode pairs. Adapted from Pringle *et al*. (2007).

In the transfer region a travelling wave voltage is continuously applied in order to maintain the mobility separation of the ions as they travel to the TOF and then the detector. A main advantage of this instrument is that it allows the simultaneous collection of both ATD data and mass spectra which is achieved by synchronising the TOF acquisition with the release of ions from the trap SRIG into the IM SRIG (Pringle *et al.*, 2007).

4.2.4 Calibration of TWIM-MS data

In order to obtain a good estimate of the collisional cross section from ATD values for an unknown molecule, the ATD data must be calibrated using the mobilities of standards for which there are established cross sections. Different research groups have developed various approaches to calibrating ATD data. A calibration method has been previously published by the Scrivens group (Thalassinos *et al.,* 2009) and was used throughout this work. The size of the unknown molecule dictates which standard will be used for calibration and for the experiments on HSA

reported here, sperm whale myoglobin was used as a calibration standard. Importantly the calibration standard must be analysed under the same conditions as the unknown sample (Leary *et al*., 2009) as the buffer gas, T-wave height and wave velocity can have an impact on the ATD of an ion. For the estimation of protein cross sections, a power fit series has been shown to be the most appropriate (Thalassinos *et al*., 2009).

4.3 Results and discussion

4.3.1 TWIM-MS of recombinant HSA at physiological pH

TWIM-MS was used as a novel technique to study the conformation of HSA and its binary and ternary complexes. Preliminary experiments with 10 mM ammonium acetate as in Chapter 3 did not yield reliable data as the ion transmission through the IM cell was insufficient. To overcome this, the buffer concentration was increased to 200 mM ammonium acetate as higher concentrations have been shown to stabilise large proteins (Sterling *et al*., 2010). In addition a high backing pressure was used, as Ruotolo *et al.* (2008) suggested that for IM experiments of proteins between 50-200 kDa a backing pressure of 5.5 mbar was optimal. Using the Synapt G2, the charge states observed were 14+ to 17+ for apo-HSA. These are slightly different charge states than observed from standard electrospray in Chapter 3 (16+ to 19+) because the Synapt G2 has a nanospray source. As collisional activation had been shown to be beneficial on other instruments, cone voltages of 60, 80 and 100 V were investigated and the conformations of the protein compared.

Although all three conditions appeared to produce the same charge state distribution associated with the monomeric folded form of the protein, shown in Figure 4.2 A, the ATD suggested otherwise.

At 60 and 80 V, one conformation was observed, but when the cone voltage was increased to 100 V, a significant change occurred and three different conformations were observed in the ATD plot. The single observed conformation in both the 60 V and 80 V spectra had an arrival time of 8.71 ms and 8.85 ms respectively for the 16+ charge state. It was established that this was the heart-shaped, folded form of HSA as the values were in close agreement with the theoretical collisional cross section, 3847 $Å^2$, calculated from the PDB structure of HSA (see Figure 4.8 B for details).

As the cone voltage was increased, less of this species was observed and two more extended conformations were seen at 10.03 and 11.47 ms (16+ charge state, Figure 4.2 B). For the 15+ charge state, extended conformations were observed at 12.50 and also at 10.03 ms, which dominated at 100 V, while the native conformation had an arrival time of 9.54 ms at both 60 and 80 V. The calculated cross sections for these, provided in Figure 4.2 C, indicated that the ions with longer arrival times were extended forms of the protein and their dominance at higher cone voltages is in line with expectations.

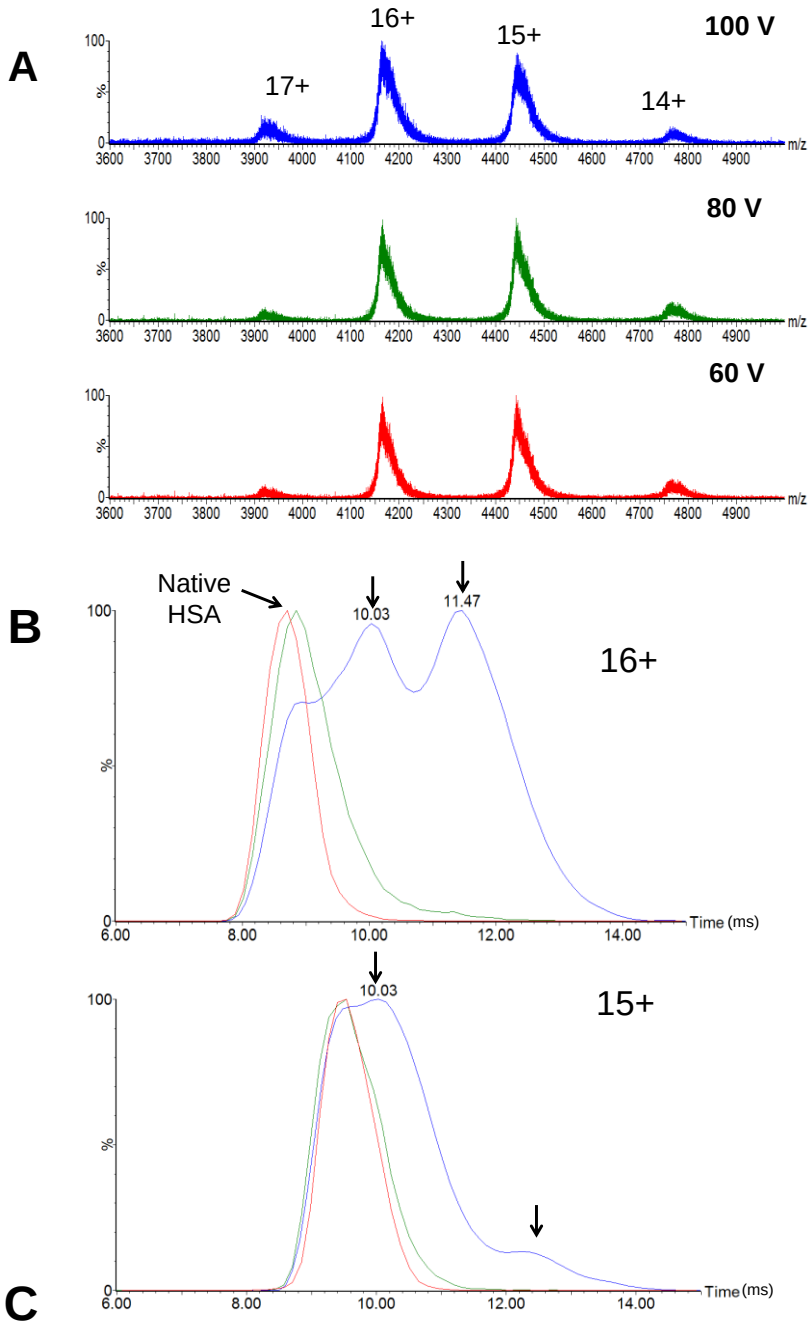

Cone voltage	Charge state	
(V)	15+	16+
60	3928 Å^2	3935 Å^2
80	3920 Å^2	3976 Å^2
100	3918 Å^2 4067 Å^2 4702 Å^2	3986 Å^2 4339 Å^2 4740 Å^2

Figure 4.2 Comparison of ATD for the 16+ and 15+ charge states of apo-HSA at varying cone voltages of 60, 80 and 100 V. A**)** ATD at cone voltage = 60 V (*red*), 80 V (*green*) and 100 V (*blue*). Arrows highlight the new conformations observed as the cone voltage is increased. B) Table showing the estimated collisional cross sections of conformations observed for each cone voltage. Partially unfolded conformations are highlighted (*blue*).

A larger number of solvent clusters are stripped away from the protein at 100 V compared to lower cone voltages which could explain these additional conformations. These unfolded conformations are novel observations and could reflect intermediates between the N and F-forms of HSA, which are described in detail in section 1.6.1. As a result of these findings, subsequent experiments were carried out with a cone voltage of 80 V where only one conformation was observed.

4.3.2 Comparison of N- and F-forms of HSA

In order to see if altered conformations of HSA at different pH values could be identified by TWIM-MS, a sample of HSA at pH 4.0 was analysed. The N-form is thought to be a compact, heart shape structure whereas conversion to the F-form is characterised by elongation of the protein structure. It has previously been shown that at least two steps of isomerisation occur to the N form before full expansion of the protein occurs (Leonard and Foster, 1961). At pH 4.0 the charge states showed that HSA is denatured to some extent as more highly charged states are observed. In this experiment the charge states at pH 7.4 ranged from 15+ to 18+. Two particular charge states, 17+ and 18+, were present at both pH 7.4 and 4.0 which allowed a comparison of the ATDs (Figure 4.3). At pH 7.4 two peaks were observed in the ATD which represent the native-like conformations that travel through the gas relatively quickly. At pH 4.0 the single peak observed for each charge state has a much longer arrival time (20.88 and 17.97 ms) indicating that it is a more extended conformation of HSA.

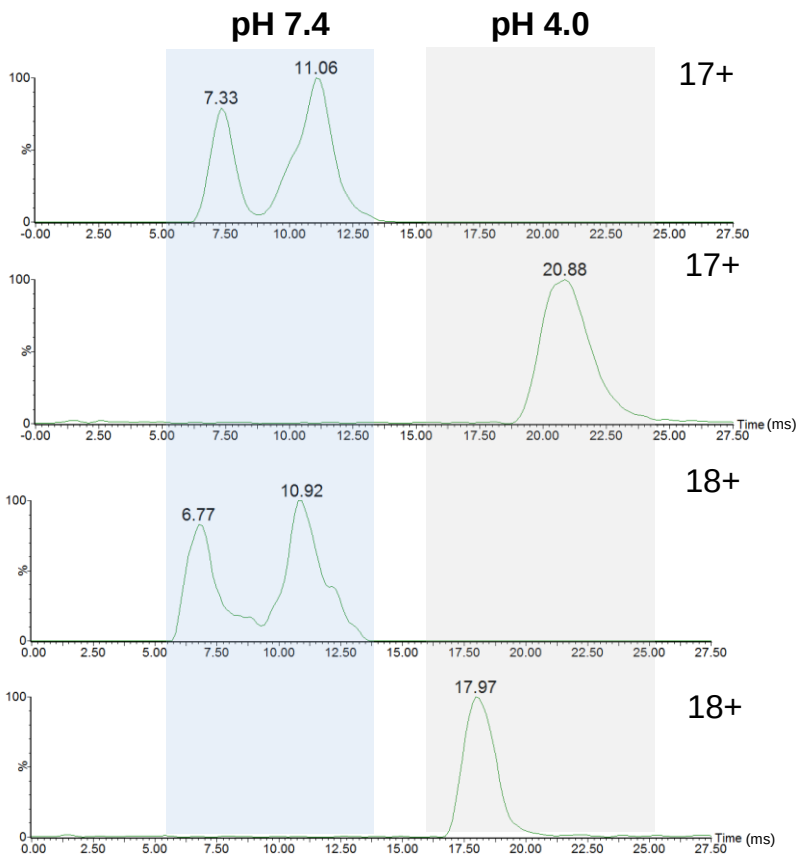

Figure 4.3 ATDs for the 17+ and 18+ charge states of HSA measured at pH 7.4 and pH 4.0. The blue shaded region indicates the conformations at pH 7.4 and the grey shaded region indicates conformations at pH 4.0. The cone voltage was 100 V which explains why there are two conformations observed at pH 7.4.

Therefore, it can be seen that at pH 4.0 there is a large amount of unfolding which could correspond to the F-form of the protein. Carter and Ho (1994) suggested that the F-form was a separation of two halves of the molecule from each other. Differences in the mobility of ions under native and denatured conditions have been previously recognised. An example is the case of cytochrome c where the 9+ ion observed from an aqueous solution was much smaller than that observed using a denaturing buffer (Hudgins *et al*., 1997). Furthermore, Faull *et al*. (2008) demonstrated that haemoglobin at pH 4.5 had a greater collisional cross section than those measured at neutral pH. Both of these studies are in

agreement with what is observed in this work and so it would appear that pH-dependent conformations of HSA can be observed even when the species have the same number of charges.

4.3.3 Comparison of the conformations of apo- and holo-HSA

The effect of Zn^{2+} and Cd^{2+} binding on protein conformation was investigated using TWIM-MS. The same charge state distribution (14+-17+) was observed for the metal bound forms of HSA as for apo-HSA. The ATDs for the most abundant charge states showed no difference between apo-HSA, Zn_2-HSA and Cd_2-HSA as shown in Figure 4.4. The ATD for Cd_2-HSA showed a very slight increase in drift time suggesting it had a less compact structure than apo-HSA and Zn_2-HSA. It has not yet been determined where the other high affinity binding site for Cd^{2+}, Site B, is located although ^{111}Cd-NMR spectroscopy suggests a ligand set containing one or less nitrogen atoms, different to that for the high affinity Zn^{2+} site. This could account for the small differences in ATD for this particular complex. The 17+ charge state shows evidence of another conformation beginning to appear in both the apo- and holo- HSA complexes. As this charge state is the most highly charged out of those observed, this more elongated conformation could be due to partial unfolding of the protein. This observation could indicate that a partially unfolded conformation is present under mild conditions as well as when the collisional activation is higher.

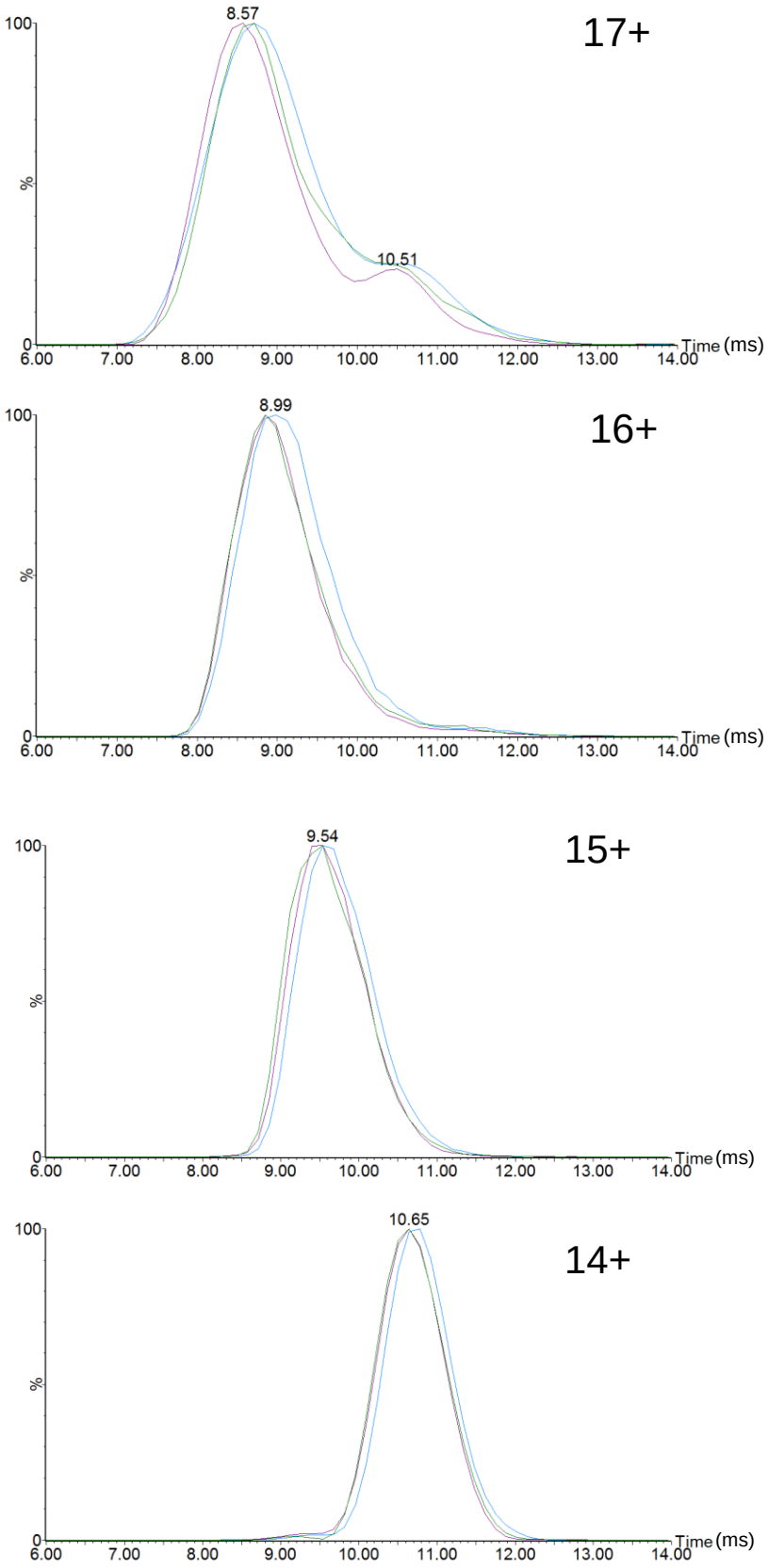

Figure 4.4 Comparison of ATD for the 17+, 16+, 15+ and 14+ charge states of apo-HSA, Zn_2-HSA and Cd_2-HSA. *Green* = apo-HSA, *Purple* = Zn_2-HSA and *Blue* = Cd_2-HSA. The cone voltage was 80 V in all experiments.

Using these IM data, estimated collisional cross sections were obtained by calibration with sperm whale myoglobin. The experimentally-determined collisional cross sections were plotted against charge state (Figure 4.5) and show the expected trend of more highly charged ions having a less compact structure. For the apo- and metal forms, no significant differences are observed although Cd_2-HSA showed a slightly larger collisional cross section for all of the charge states, consistent with the slightly longer arrival times. Site A only undergoes minor re-arrangements to accommodate a Zn^{2+} ion therefore no great change in cross section is in agreement with the proposed model for the interdomain site. In the case of Cd_2-HSA, the protein structure may be slightly less compact.

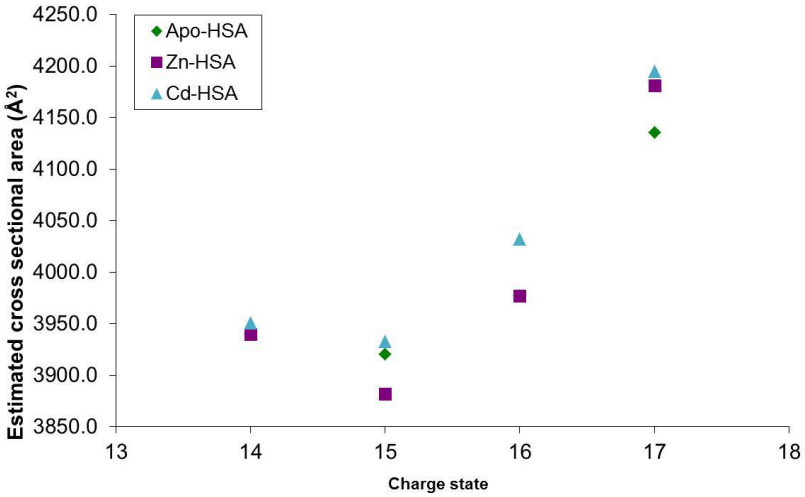

Figure 4.5 Dependence of the estimated collisional cross section on charge state for apo-HSA, Zn_2-HSA and Cd_2-HSA. There is no major difference in the cross sections calculated for the apo- or holo-HSA complexes.

Although the collisional cross sections of apo- and holo-HSA were similar, the partially unfolded conformations of HSA observed in Figure 4.2 were

able to give an indication of how the metal ions influenced the conformational flexibility of HSA. The high affinity Zn^{2+} site, Site A, involves residues from both domains I and II, as illustrated previously (Chapter 1, Figure 1.5). Therefore metal ion binding at this site has been speculated to make the domain interface more rigid. Figure 4.6 shows the ATD for the 16+ and 15+ charge state of Zn_2-HSA measured at 60, 80 and 100 V. Comparison to the ATD to Figure 4.2 shows some interesting differences.

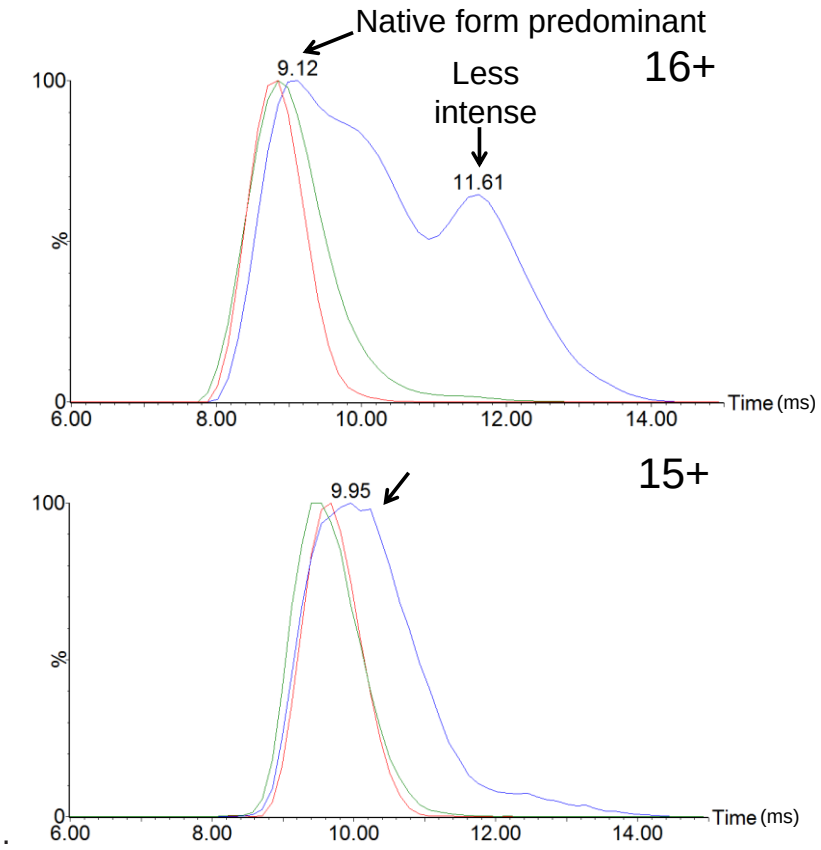

Figure 4.6 Comparison of ATD for the 16+ and 15+ charge states of Zn_2.HSA at varying cone voltages of 60, 80 and 100 V. Cone voltage = 60 V (*red*), 80 V (*green*) and 100 V (*blue*). Arrows highlight the new conformations observed as the cone voltage is increased.

The two extended conformations of the protein are considerably less intense for the 16+ charge state and do not dominate the ATD as was

observed for apo-HSA. In fact the native form of HSA is the most prominent peak in the ATD at 9.12 ms. For the 15+ charge state the difference is more subtle although the unfolded conformation observed at 12.50 ms for apo-HSA is not visible in Figure 4.6. These observations are experimental evidence that occupation of Site A by Zn^{2+} has a stabilising effect on the domain I/domain II interface. This outcome can also be used to explain why in the ^{1}H-NMR spectroscopy of HSA other His residues, apart from the Zn^{2+} ligands His67 and His247, broaden when 1 mol. equiv. of Zn^{2+} is added (Blindauer *et al*., 2009) as the stabilisation of the interface means the sidechains are less flexible. Other interdomain His residues appear to be affected by metal ion binding even though they are not directly involved in coordination which would support the idea that Zn^{2+} binding locks domain I and II in place.

4.3.4 Conformational changes induced by fatty acids

Previous studies indicate that a conformational change occurs when fatty acids bind to HSA (Curry *et al*., 1998; Bhattacharya *et al*., 2000). This causes the relative movement between domains I and II and results in disruption of the Zn^{2+} binding site as His67/Asn99 and His247/Asp249 are no longer in close proximity to each other (see Figure 1.5). Previously, conformational changes induced by fatty acid binding have been studied by other approaches including cross linking of Lys residues followed by tryptic digestion and analysis of the peptides produced (Huang *et al*., 2005). TWIM-MS was used to compare the mobility of HSA samples that had been extensively dialysed to samples that had high concentrations of

myristate present. The HSA was studied in the presence of myristate and not myristate/Zn^{2+} so the experimental cross section could be directly compared to the theoretical value calculated from the structure deposited in the PDB. Although the Synapt used a much gentler nanospray source, a HSA-myristate complex could not be preserved as no significant increase in mass was observed (*cf.* Chapter 3). However, HSA in the presence myristate showed an increased collisional cross section compared to apo-HSA under the same conditions. The sample that had been incubated with myristate had a large increase in cross section which was estimated to be 87 $Å^2$ for the 15+ charge state (Figure 4.7).

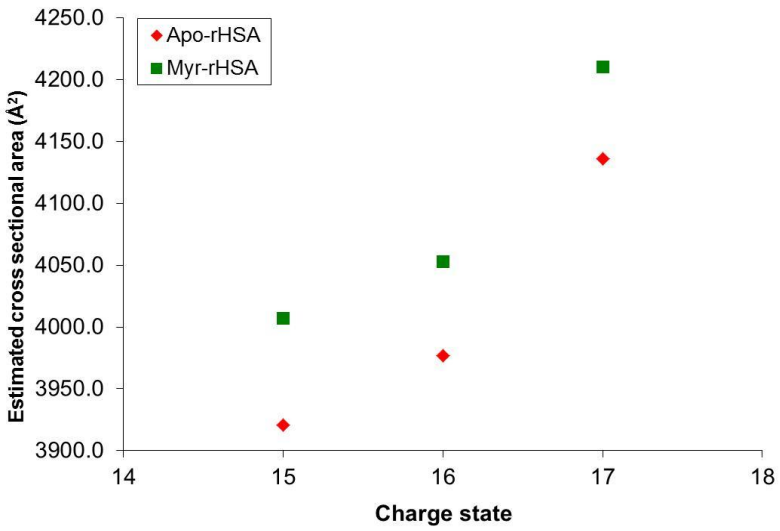

Figure 4.7 Dependence of charge state for the estimated collisional cross sections of apo-HSA and HSA in the presence of 5 mol. equiv. myristate. There are large differences in cross sections observed for each protein sample.

In order to validate these experimental data, theoretical cross sections were calculated using MOBCAL, an open source program (Mesleh *et al.*, 1996; Shvartsburg and Jarrold, 1996). X-ray crystal structures are available for apo-HSA and myristate bound HSA, files 1AO6 and 1BJ5 in

the Protein Data Bank, respectively. Theoretical cross sections are calculated based on projection approximation (PA) and exact hard sphere scattering (EHSS) approximation. The PA method can underestimate the cross sections of more complex molecules such as proteins as they undergo more interactions with the buffer gas. The EHSS method takes into account the scattering between the ion and the buffer gas correctly but can overestimate cross sections (Jarrold, 1999). However, these models are used because they take substantially less computational time than others such as the more accurate trajectory method (TJ) (Jarrold, 1999).

The PA and EHSS cross sections for 1AO6 and 1BJ5 are outlined in Figure 4.8 B. The experimentally-determined cross sections fall between the theoretical values for the PA and EHSS. There is good agreement between the experimental values and those calculated from the PA method but the EHSS method overestimates the cross section of HSA significantly. Some examples of native gas phase conformations have smaller estimated cross sections than those obtained from the EHSS method, for example in the case of bovine pancreatic trypsin inhibitor (BPTI) (Shelimov *et al*., 1997). This could be due to a lack of water molecules which would otherwise occupy cavities in the protein structure and increase its size. Furthermore, polar side chains, which would usually extend out into the solvent, collapse onto the protein surface in the gas phase (Shelimov *et al*., 1997).

A

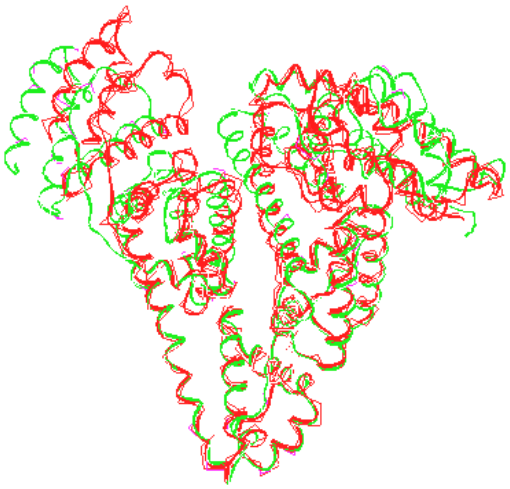

B

Complex	HSA (1AO6)	HSA-5Myr (1BJ5)
Experimental	3920 Å²	4007 Å²
PA	3847 Å²	3923 Å²
EHSS	5054 Å²	5127 Å²

Figure 4.8 Comparison of experimental and theoretical collisional cross sections for HSA complexes. A) Overlay of the protein structures from 1AO6 (*red*; FA free) and 1BJ5 (*green*; 5 myristates) B) Table summarising the experimental cross sections and those obtained from the PA and EHSS methods.

The theoretical difference between the cross sections calculated from the PA method is 76 $Å^2$ which compares well with the experimental difference of 87 $Å^2$. An overlay of 1AO6 and 1BJ5 is also shown in Figure 4.8 A which indicates the structural changes induced by fatty acid binding. The crevice in the centre of the protein is considerably expanded and domains I and III are moved away from each other.

Taking into account the experimental and theoretical results, it can be suggested that even though the interactions with fatty acids were broken on entering the gas phase, the expanded conformation induced by fatty-acid binding in solution was apparently retained in the gas phase during the time in which the experiment was performed. This can be rationalised

as it has been shown that gas phase structures reflect the native structure of proteins in solution over short time scales (Hoaglund-Hyzer, 1991; Breuker and McLafferty, 2008). A study of cytochrome c that involved trapping the ions for various periods of time prior to IM experiments showed that protein native structure was retained for 30-60 ms. Trapping the ions for longer than this resulted in unfolded conformations being observed (Badman *et al*., 2005). Other reports have indicated that structural features can be retained for longer than 100 ms (Wyttenbach *et al*., 2009). The TWIM-MS experiments in this work were carried out on a shorter timescale of 10-20 ms therefore there is less chance for the solution structure to rearrange into the most stable FA-free conformation in the gas phase.

4.4 Conclusion

In summary, this chapter has described efforts to study HSA complexes using TWIM-MS. The estimated collisional cross section of HSA at physiologically relevant pH was in good agreement with theoretical values obtained from the crystal structures. At pH 4.0 a significantly elongated conformation was observed, providing evidence for a pH-induced conformational change. This could reflect two halves of the molecule becoming separated which results in a longer arrival time. No significant increase in the collisional cross sections for metal-bound forms of HSA was seen compared to the apo-form. However, the Cd_2-HSA form had a consistently larger collisional cross section. In the presence of Zn^{2+} less unfolding to extended protein conformations was observed, compared to the apo-form, which could indicate Zn^{2+} having a stabilisation effect on

the domain I/domain II interface. Even though HSA-myristate interactions appeared to be broken in the gas phase, an increased collisional cross section was still detected for myristate-HSA compared to apo-HSA, which could mean on the timescale of the IM-MS experiment the protein had not returned to its most stable FA-free conformation in the gas phase. Overall, this evidence has indicated that TWIM-MS can be applied to study native HSA using a method that hasn't been attempted previously and has given an important insight into how ligand binding can influence the conformation of HSA.

Chapter 5
Metal binding properties of a peptide mimic from HRG

5.1 Introduction

In this Chapter, the metal binding properties of a peptide mimic (HRGP330) from the HRR of HRG were explored by native ESI-MS, NMR spectroscopy and tandem MS/MS. Although some potential biological roles for HRG have been acknowledged, there is a shortfall on structural information as to how it might fulfil these. Additionally, many studies have utilised rabbit HRG, which may have different metal-binding properties, whereas the peptide sequence used here is derived from the human form.

5.2 HRGP330: a peptide mimic of the His/Pro-rich region

Histidine rich glycoprotein (HRG) contains a His/Pro-rich region which shows some similarities to high-molecular-weight kininogen (HMWK) (Nordahl *et al.*, 2005), a 72 kDa protein from the blood coagulation system, with which it shows 17% sequence similarity. HRGP330, a 35 amino acid peptide derived from the HRR was selected to mimic the Zn^{2+} binding properties and Zn^{2+}-mediated interactions of HRG. The primary sequence consists of amino acids 330-365 from the full length HRG sequence which is highlighted in Figure 5.1. The nomenclature used by Dixelius *et al.* (2006) does not count the signal peptide and only the main chain hence the position of HRGP330 in Figure 5.1 is shifted by 18

residues to 348-383 as highlighted in red. This peptide has been shown to be biologically active and has been used for *in vivo* experiments confirming that it is suitable for mimicking physiological conditions. It has been demonstrated that HRGP330 shows antiangiogenic properties both *in vitro* and *in vivo* (Dixelius *et al*., 2006). HRGP330 at a concentration of 23 nM was able to inhibit chemotaxis of primary endothelial cells which had been induced by vascular endothelial growth factor. Also in 2006, Vanwildemeersch *et al.* (2006) showed that HRGP330 can bind to both heparin and heparan sulphate in a Zn^{2+}-dependent manner.

```
        10         20         30         40         50         60
MKALIAALLL ITLQYSCAVS PTDCSAVEPE AEKALDLINK RRRDGYLFQL LRIADAHLDR

        70         80         90        100        110        120
VENTTVYYLV LDVQESDCSV LSRKYWNDCE PPDSRRPSEI VIGQCKVIAT RHSHESQDLR

       130        140        150        160        170        180
VIDFNCTTSS VSSALANTKD SPVLIDFFED TERYRKQANK ALEKYKEEND DFASFRVDRI

       190        200        210        220        230        240
ERVARVRGGE GTGYFVDFSV RNCPRHHFPR HPNVFGFCRA DLFYDVEALD LESPKNLVIN

       250        260        270        280        290        300
CEVFDPQEHE NINGVPPHLG HPFHWGGHER SSTTKPPFKP HGSRDHHHPH KPHEHGPPPP

       310        320        330        340        350        360
PDERDHSHGP PLPQGPPPLL PMSCSSCQHA TFGTNGAQRH SHNNNSSDLH PHKHHSHEQH

       370        380        390        400        410        420
PHGHHPHAHH PHEHDTHRQH PHGHHPHGHH PHGHHPHGHH PHGHHPHCHD FQDYGPCDPP

       430        440        450        460        470        480
PHNQGHCCHG HGPPPGHLRR RGPGKGPRPF HCRQIGSVYR LPPLRKGEVL PLPEANFPSF

       490        500        510        520
PLPHHKHPLK PDNQPFPQSV SESCPGKFKS GFPQVSMFFT HTFPK
```

Figure 5.1 Location of HRGP330 in the full-length sequence of human HRG. The red residues indicate the sequence of HRGP330. The residues coloured in blue are the signal peptide.

HRGP335, a related 26 amino acid peptide (residues 353-378; Arg378 is replaced by Gly), was shown to bind to defined heparin oligomers in the presence of Zn^{2+} with increased binding observed with increasing

oligomer length. This reached maximum binding with the heparin dodecasaccharide and tetradecasaccharide (Vanwildemeersch *et al.*, 2006). Modifications to HRGP330 used in this work included C-terminal amidation and an N-terminal acetylation to avoid metal binding occurring at these sites. HRGP330 was selected as it has been previously shown to be a minimal active domain of HRG (Dixelius *et al*., 2006). Furthermore, its relatively small size (4.3 kDa) allows it to be studied by techniques such as MS, MS/MS and NMR spectroscopy. The peptide has no aromatic residues and furthermore Zn^{2+} is spectroscopically inactive therefore ESI-MS is an invaluable tool that can be used to study the peptide-metal ion interactions.

5.3 Results and discussion

5.3.1 Purification of HRGP330 by HPLC

HRGP330 typically eluted from the HPLC column at 9.2 min (Figure 5.2). This corresponded to an acetonitrile concentration of 25% which shows that it was the least hydrophobic component of the sample. The peak that eluted slightly later at 9.6 min was shown by ESI-MS to correspond to HRGP330 with a mass increase of 56 Da (Figure A5, Appendix). This was attributed to a *t*-butyl protecting group still remaining from the synthesis. As a result, it was beneficial to use TFA in the separation as this cleaves protecting groups although ESI-MS data indicated that this modification did not appear to interfere with metal binding. The identity of the peptide was confirmed by ESI-MS as shown in Figure 5.3. The HPLC fractions were infused directly into the instrument and therefore the

samples had a low pH of 2.0. As a result a range of charge states were observed with 5+ being predominant.

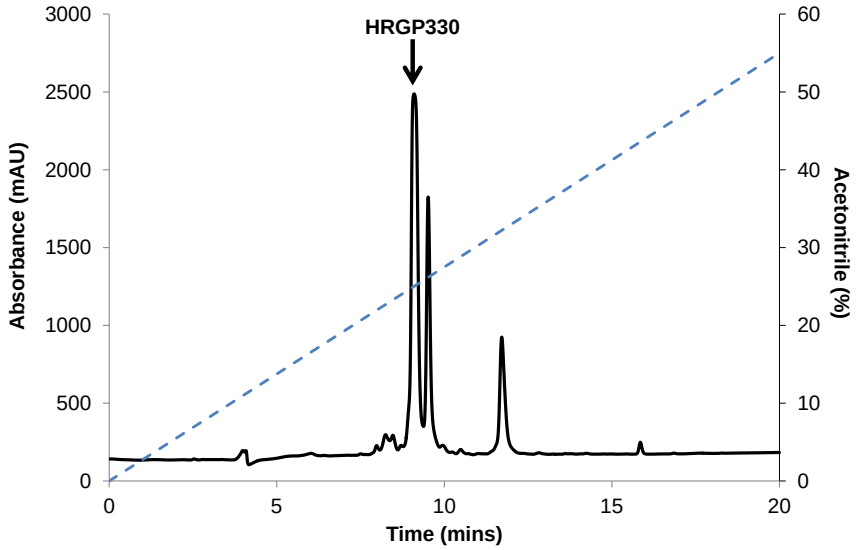

Figure 5.2 Purification of crude HRGP330 with RP-HPLC. Example of a chromatogram obtained from loading crude HRGP330 onto a Jupiter Proteo 90 Å column using an Agilent 1100 instrument. The blue line shows an increasing gradient of acetonitrile containing 0.1% TFA.

Following deconvolution of the raw data, the experimental mass of 4333.98 Da was observed (theoretical mass = 4334.58 Da) which was the most abundant peak. The mass of the peptide eluting at 9.6 min was 4390.0 Da and this fraction contained more impurities (Figure A5). SDS-PAGE was also used to check the purity and HRGP330 was observed just below the 10 kDa standard. This is at a higher position than expected indicating it migrates more slowly through the gel. One reason for this could be that the unusual composition of the peptide means it may not take up as many SDS molecules. After the peptide had been buffer-

exchanged into a neutral buffer, the predominant charge states were +4 and +5.

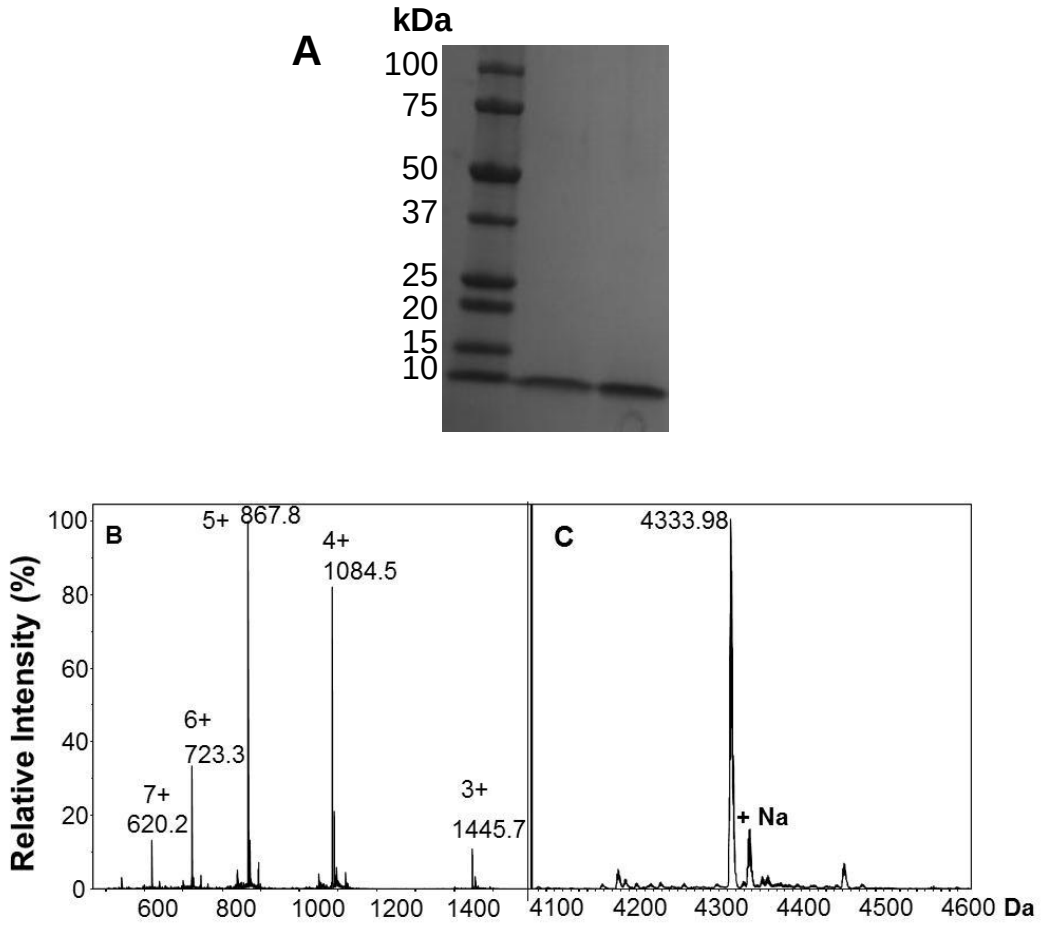

Figure 5.3 Identification of purified HRGP330 by SDS-PAGE and ESI-MS. A) SDS PAGE of HRGP330 fractions. B) Charge state envelope C) Deconvoluted mass spectrum. The HPLC fraction that eluted at 9.2 minutes was injected directly into the mass spectrometer to produce the spectrum.

At physiologically-relevant pH, a small amount of Zn^{2+} contamination was sometimes observed in the samples that had been purified. The peak corresponding to the Zn^{2+}-bound species had a relative intensity of ~ 5% and so was not significant. This could be from contamination during the purification process. To avoid this contamination, once the peptide was brought up to neutral pH, the containers used for experiments were acid-washed. It could also not be ruled out that that the source of contamination was the mass spectrometer. In order to test this, a sample

was tested on two different mass spectrometers (Figure 5.4). This confirmed that at least on one of these, the sample was binding metal ions upon injection into the instrument and not as a result of contamination in the laboratory. This phenomenon has previously been reported by Mattapalli *et al.* (2009) who found evidence that the apo-form of a model Zn^{2+} finger peptide became Zn^{2+}-bound on infusion into the mass spectrometer even after rigorous cleaning.

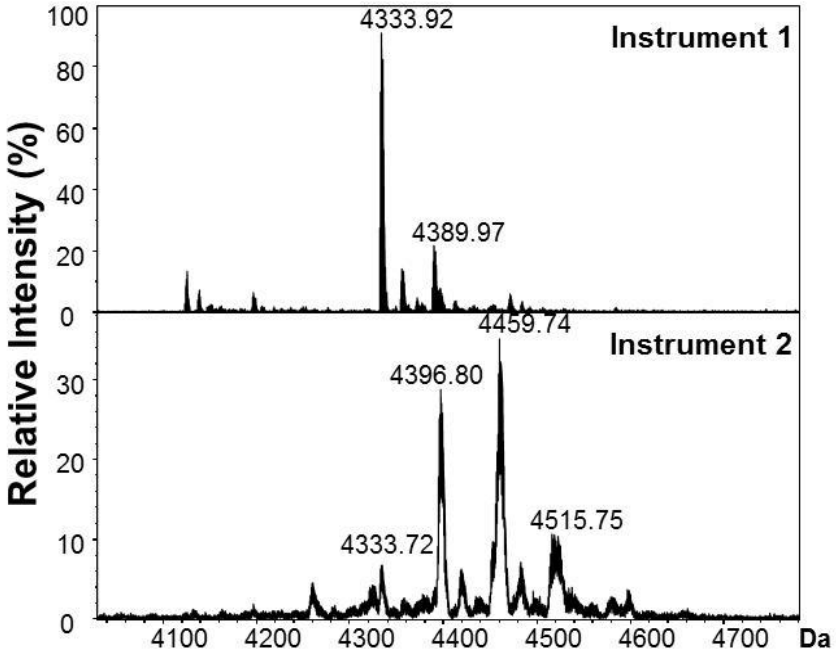

Figure 5.4 Comparison of apo-HRGP330 spectra from two different mass spectrometers. Two new peaks became apparent in the second spectrum which have a mass shift of 63 Da and 126 Da compared to HRGP330 i.e. addition of 1 or 2 Cu^{2+} or Zn^{2+} ions. The low resolution results in difficulty in assigning these unambiguously.

They concluded that Zn^{2+} from previous experiments was being deposited in the stainless steel emitter of the instrument and then detected in other samples (Mattapalli *et al*., 2009). Although this example showed a particularly extreme amount of contamination, it highlighted how the peptide can readily bind trace metal ions from the environment.

5.3.2 Metal binding properties of HRGP330 investigated by ESI-MS

Prior to the addition of metal ions, the peptide was desalted and buffer exchanged into 10 mM ammonium acetate (pH 7.4). The literature suggests that up to 10 Zn^{2+} ions could bind in the HRR (Morgan, 1981). The region characterised as the HRR is 59 amino acids in length and HRGP330 spans approximately half this region. Therefore, 1, 2 and 5 mol. equiv. of metal ion were titrated into the peptide. The spectra for three titrations with $Zn(CH_3COO)_2.2H_2O$ (A), $Cd(CH_3COO)_2.2H_2O$ (B) and $Cu(CH_3COO)_2.H_2O$ (C) are shown in Figure 5.5. The masses of Zn^{2+} and Cu^{2+} are within 1 Da of each other and so high resolution MS allows the unambiguous assignment of which metal ion is present. The highlighted peak on the right hand side shows the experimental isotopic distribution of HRGP330 with 1 metal ion bound with a comparison to the theoretical model. At a HRGP330:Zn^{2+} ratio of 1:1, Zn_1-HRGP330 was observed at a low intensity but the most abundant peak was apo-HRGP330. Similarly, once 2 mol. equiv. of Zn^{2+} were added, a peak for Zn_2-HRGP330 was observed but the apo-form was still present in substantial quantities. Once 5 mol. equiv. Zn^{2+} were present, the apo-form disappeared from the spectrum completely and a range of metallated species were observed. The most abundant metalloform was Zn_4-HRGP330. Mangani *et al*., (2003) carried out EXAFS on a Zn^{2+}-bound complex of HRG associated with rabbit skeletal muscle AMP deaminase, a protein that has similarities to HRG but has a unique extended N-terminal region (Ranieri-Raggi *et al*., 1997). The possible models of Zn^{2+} coordination proposed were 3 coordinating His imidazole rings, with an additional sulfur from Cys or a

Cl^- ligand, in a mononuclear or dinuclear site. There is only one Cys residue in the HRR not involved in disulfide bonds therefore a $CysHis_3$ site could potentially form. However, HRGP330 contains no Cys residues and still binds a number of metal ions. Assuming that 3 His residues coordinate to Zn^{2+} then 5 metal ions would be able to coordinate to HRGP330 which is in agreement with the ESI-MS data.

The titration with Cd^{2+} also resulted in a range of metallated peptide species but notably the apo-HRGP330 was present throughout the experiment, even when 5 mol. equiv. Cd^{2+} were present. The most abundant species was the Cd_2-HRGP330 form which could indicate that this metal ion has a lower affinity for HRGP330 than Zn^{2+} and this fits with previous observations made in the literature (Morgan, 1981).

The titration with Cu^{2+} followed a similar course to the titration with Zn^{2+} with a Cu_4-HRGP330 species being the most abundant. The only difference was that apo-HRGP330 was no longer observed once 1 mol. equiv. of Cu^{2+} was present which indicates that HRGP330 has a high affinity for this metal ion. It has been suggested that HRG could be involved in Cu^{2+} transport and indeed some studies have found the protein has a higher affinity for Cu^{2+} than Zn^{2+} (Morgan, 1981; Guthans and Morgan, 1982) . Although it is mainly Zn^{2+} that is thought to mediate the interactions of HRG with heparin, Cu^{2+} could also have an influence (Borza and Morgan, 1998).

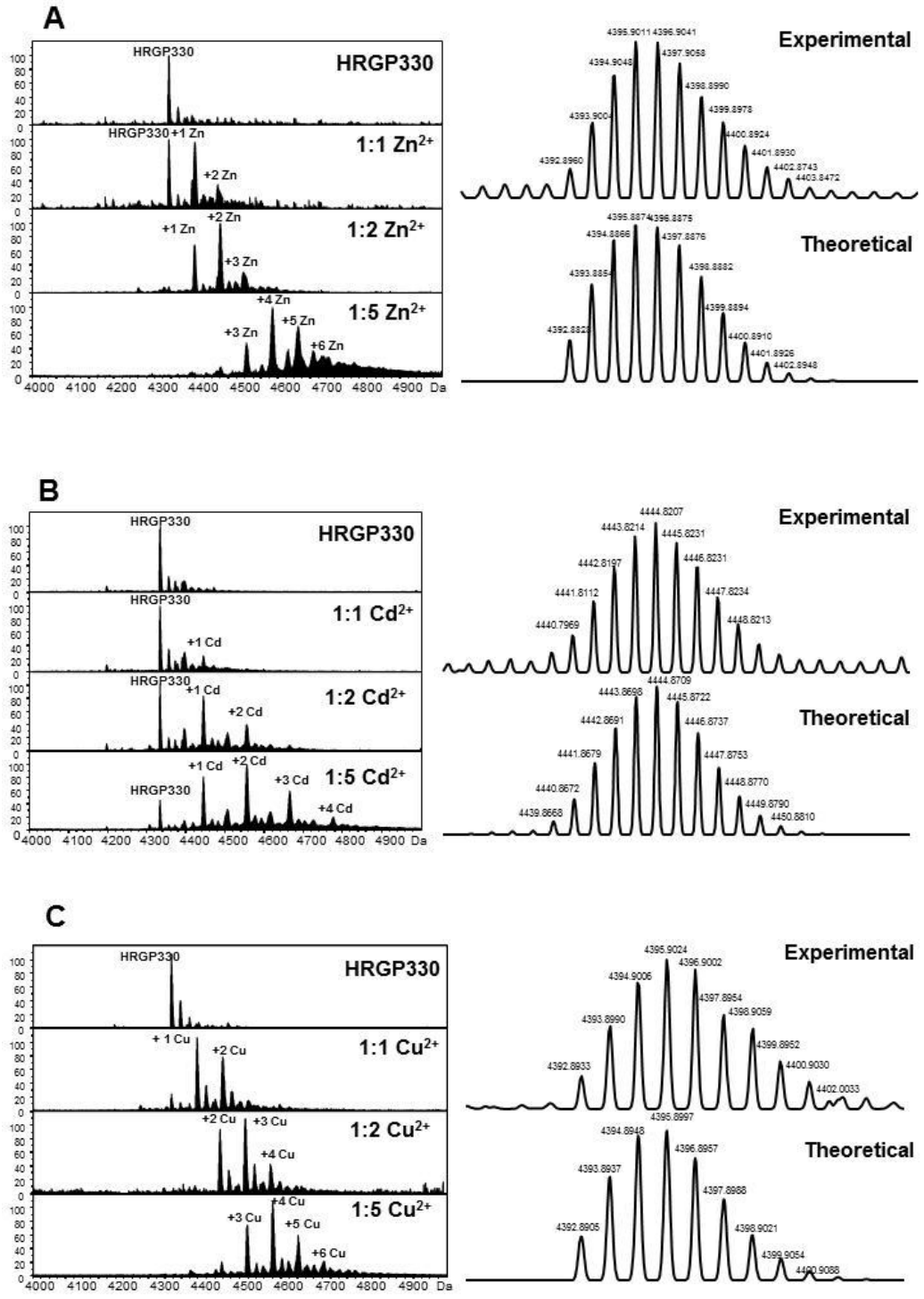

Figure 5.5 Metal binding properties of HRGP330. 15 μM HRGP330 was titrated with 1, 2 and 5 mol. equiv. of A) $Zn(CH_3COO)_2.2H_2O$ B) $Cd(CH_3COO)_2.2H_2O$ and C) $Cu(CH_3COO)_2.H_2O$. The buffer was 10 mM ammonium acetate at pH 7.4. The isotopic distribution for 1 mol. equiv. of the metal ion bound to HRGP330 is shown on the right hand side together with a comparison to the theoretical model.

Some groups have investigated small His-containing peptides and their interaction with Cu^{2+} including an MS study of the oligopeptide $(GHHPG)_5G$ which found that one Cu^{2+} binds per GHHPH moiety (Hutchens *et al*., 1992). It is unsurprising that Cu^{2+} binds more strongly than other metal ions as it is able to deprotonate backbone amides to a much greater extent than Zn^{2+}. La Mendola *et al*. (2012) suggested a model where only two His residues in the peptide Ac-HGHH-NH_2 were involved in Cu^{2+} coordination.

As shown in Figure 5.5, there was a preference for forming the [Metal ion]$_2$-HRGP330 species before fully saturating the apo-HRGP330 with one metal ion. An explanation for this is that the binding of metal ions to HRG is cooperative and so the addition of the first Zn^{2+} ion could induce a conformational change that makes it easier for the second Zn^{2+} ion to bind. This was demonstrated previously using small peptides where two Zn^{2+} ions bound to the sequence Ac-$(HHPHG)_2$-NH_2 with higher stability compared to one Zn^{2+} binding to Ac-(HHPHG)-NH_2 (Jancsó *et al*., 2009). Cooperativity has also been observed for Zn^{2+} and Cd^{2+} binding to full length HRG (Morgan, 1981).

5.3.3 Comparison of Zn^{2+} binding to intact HRG

Attempts were made to study rabbit HRG under native MS conditions however, the charge states were of too low intensity to interpret and small peptides were observed which could be the result of protein degradation (Figure A6, Appendix). To gain an understanding of the Zn^{2+} binding

properties, the sample was analysed by ICP-OES which indicated 8.4 Zn^{2+} per HRG molecule. This is consistent with previous literature that 10 metal ions can bind per protein (Morgan, 1981) and the slight discrepancy could be Zn^{2+} loss occurring during the gel filtration column. As yet it is unclear as to how many Zn^{2+} ions are required to be bound to HRG in order for the protein to have an anti-angiogenic effect but some authors have shown that only one Zn^{2+} may be bound per 10 HRG molecules endogenously (Horne *et al*., 2001; Fu and Horne, 2002).

5.3.4 pH titration of Zn_5-HRGP330

In order to understand how metal binding to HRGP330 facilitates its biological function, it is necessary to study the Zn^{2+} binding and release properties of the His-rich domain. One way in which HRG could become positively charged is through acidic conditions and the protein has been proposed to be a plasma pH sensor (Borza and Morgan, 1998). The pH dependence of Zn^{2+} binding to HRGP330 was explored using a pH titration as shown in Figure 5.6. At a physiologically relevant pH (7.36), a range of metallated states were observed as described previously. As the pH was lowered to 6.33, a complete loss of Zn_5-HRGP330 was observed indicating the loss of a Zn^{2+} ion from a low affinity binding site. A small peak for Zn_4-HRGP330 was still present, however, this has drastically reduced in intensity. As the conditions became more acidic (pH 5.05) the most abundant species was Zn_1-HRGP330 with a sharp increase in the apo form. The apo-form became most abundant at pH 4.66 but Zn_1-HRGP330 could still be observed at pH 3.31. Interestingly, from this data

there appears to be one metal binding site that is more stable at low pH whereas a significant drop in the intensity of Zn_4- and Zn_5-HRGP330 occurs across a relatively small change in pH.

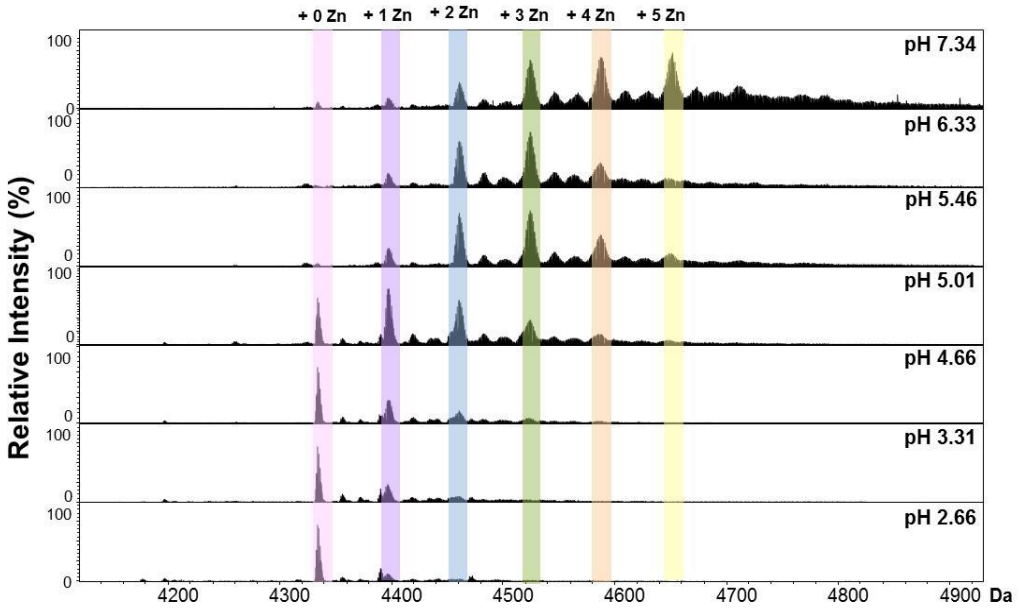

Figure 5.6 pH titration of Zn_5-HRGP330. Zn_5-HRGP330 (20 μM) was titrated with microlitre additions of 1% acetic acid followed by analysis using ESI-MS

5.3.5 CD spectroscopy of HRGP330

CD spectroscopy can be used to study the conformation of proteins and any conformational changes that are induced by ligands. This technique was used to study samples of HRGP330 in the absence and presence of metal ions (Figure 5.7). It is useful to have complementary solution phase data to compare with mass spectrometry experiments where the protein is in the gas phase. In the HRR of HRG there is a lack of conventional secondary structure such as α-helices and β-sheets. The high His and Pro content in this region indicates that formation of a polyproline type II helix with numerous His residues could occur. Previously a limited proteolysis approach isolated a 30 kDa fragment containing the HRR and

this showed evidence for a polyproline II helix (Borza *et al.*, 1996). The spectrum for apo-HRGP330 shows a negative band at 198 nm and a slight positive band with a maximum at 221 nm indicated by the black line in Figure 5.7. These bands are characteristic of a polyproline II helix (Ronish & Krimm, 1974). In the presence of 2 mol. equiv. Zn^{2+}, an increase in the negative band was observed and also a slight increase in the positive band. The same observation was seen when the Zn^{2+} concentration was increased to 5 mol. equiv. with respect to HRGP330.

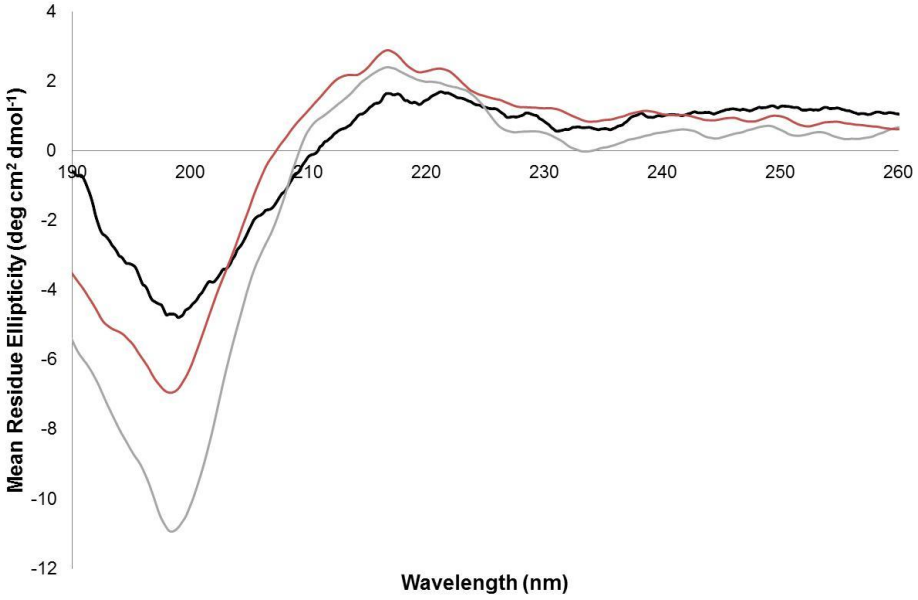

Figure 5.7 Far-UV region CD spectrum of HRGP330 in the presence and absence of Zn^{2+}. The *black* line represents the signal for HRGP330 (11 μM in 10 mM potassium phosphate, pH 7.4). The *red* line was observed after addition of 2 mol. equiv. $ZnCl_2$ and the *grey* line after addition of 5 mol. equiv. $ZnCl_2$.

An increase in the negative band upon metal ion binding has been reported for His-rich antimicrobial peptides from histatin which could indicate similarity between the structural features occurring in both peptides (Brewer and Lajoie, 2000). The interpretation of CD spectra in terms of polyproline II helical content can be difficult because its CD spectrum can be similar to that of a random coil and also there is not yet

an established way to quantify the amount of polyproline II helix structure within the peptide. Nevertheless, the substantial change in band intensities suggests that a conformational change occurs upon Zn^{2+} binding.

5.3.6 TWIM-MS of HRGP330

As described in Chapter 4, TWIM-MS is an invaluable technique for studying the conformation of biomolecules. The distinctive negative band in the CD spectrum (Figure 5.7) indicated a lack of traditional secondary structure elements and this could be due to the abundance of Pro residues. This makes HRGP330 an interesting candidate for IM-MS studies as the effect of coordinating metal ions on the peptide structure can be probed in more detail.

Firstly, apo-HRGP330 was analysed in 10 mM ammonium acetate (pH 7.4) on a Synapt HDMS G2 instrument. The ATDs observed for charge states ranging from 6+ to 3+ are shown in Figure 5.8 A. The ATDs are used to estimate the collisional cross section of the peptide for each charge state in Figure 5.8 B. The charge states 6+, 5+ and 4+ appear to show one conformation, however, the 4+ charge state has an unusually small collisional cross section and does not fit the linear trend where increasing charge leads to increasing collisional cross section.

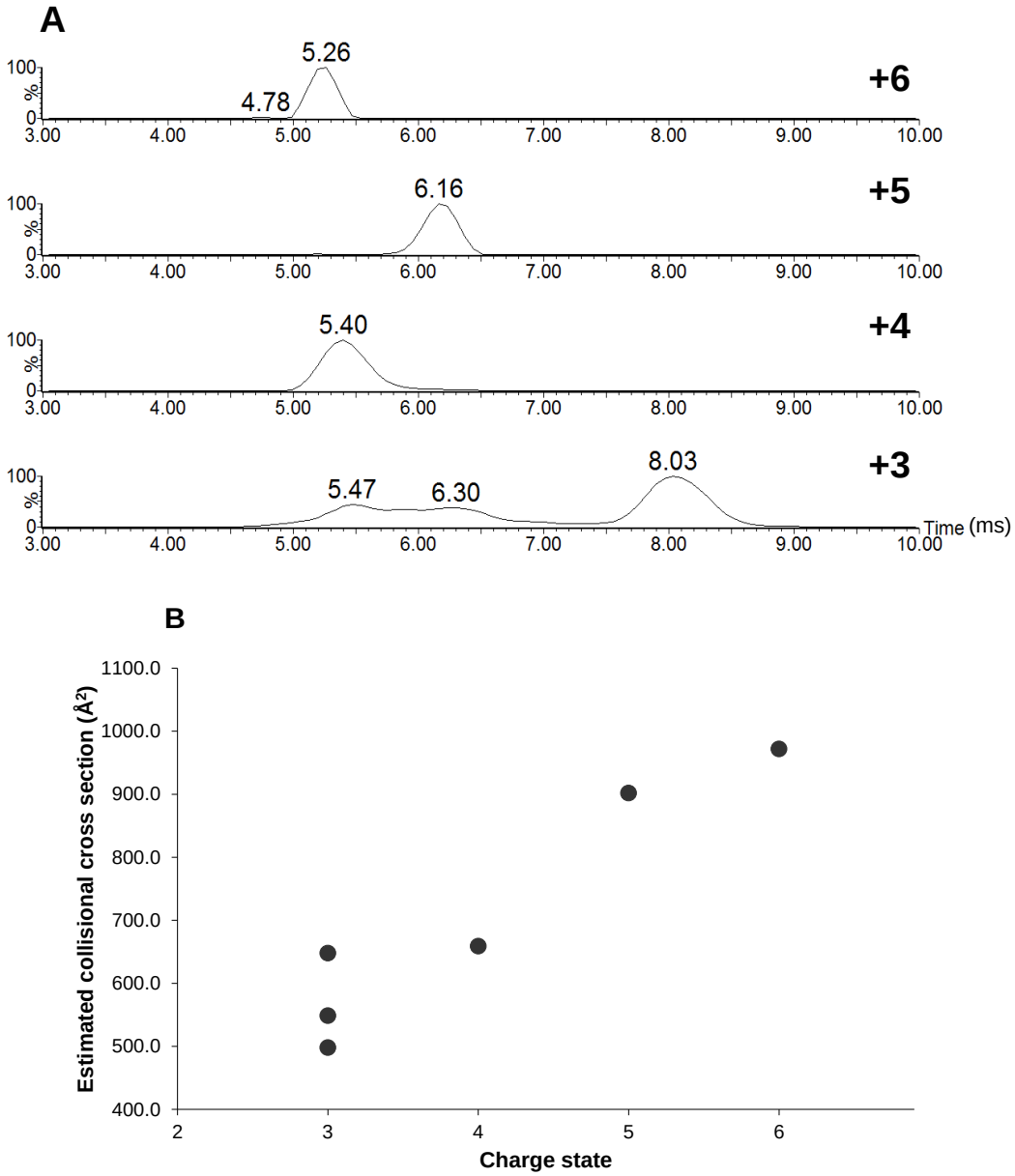

Figure 5.8 ATDs and estimated collisional cross sections of the charge states observed for apo-HRGP330. A) ATDs for the charge states observed which are given in ms B) Estimated collisional cross sections calculated from the ATDs. The samples were 10 μM HRGP330 in 10 mM ammonium acetate (pH 7.4). There are 3 points for the 3+ charge state representing the 3 different conformations observed. The estimated cross sections were the same across two datasets.

Furthermore, the 3+ charge state shows the presence of at least 3 different conformers, two of which have a more compact structure, as each peak in the ATD represents at least one gas phase conformation of the ion. A possible explanation for this could be the difference in the

conformation of HRGP330 as it reaches a more native (more folded) charge state.

5.3.7 Comparison of apo- and Zn^{2+} bound HRGP330 by TWIM-MS

The ATDs for the 5+ charge state of Zn^{2+}-HRGP330 are compared in Figure 5.9 A and the width of the ATD can be related to the number of different conformations that contribute to the area under the peak. A relatively sharp ATD is observed in the plot for apo-HRG330, compared to the Zn^{2+}-bound forms, suggesting one defined conformation dominates in this case. In contrast the ATDs for Zn_2-HRGP330, Zn_3-HRGP330, Zn_4-HRGP330 and Zn_5-HRGP330 are broader indicating multiple conformations. The peak for Zn_1-HRGP330 was of too low intensity to produce reliable data. Furthermore as the number of Zn^{2+} ions interacting with HRGP330 increases, the ATD moves to a shorter arrival time indicating that the peptide structure becomes more compact.

Calculation of the estimated cross sections for the 5+ charge state is shown in in Figure 5.9 B. Apo-HRGP330 has a larger estimated cross section than the holo-forms and a decrease in estimated cross section is observed for all the Zn^{2+}-bound forms. The 5+ charge state shows a clear trend of the decrease in the collisional cross section as more Zn^{2+} becomes bound. This suggests that the Zn^{2+} bound forms have a more compact structure. This correlates well with the hypothesis that Zn^{2+} alters the conformation of the HRR of HRG to mediate interactions with ligands.

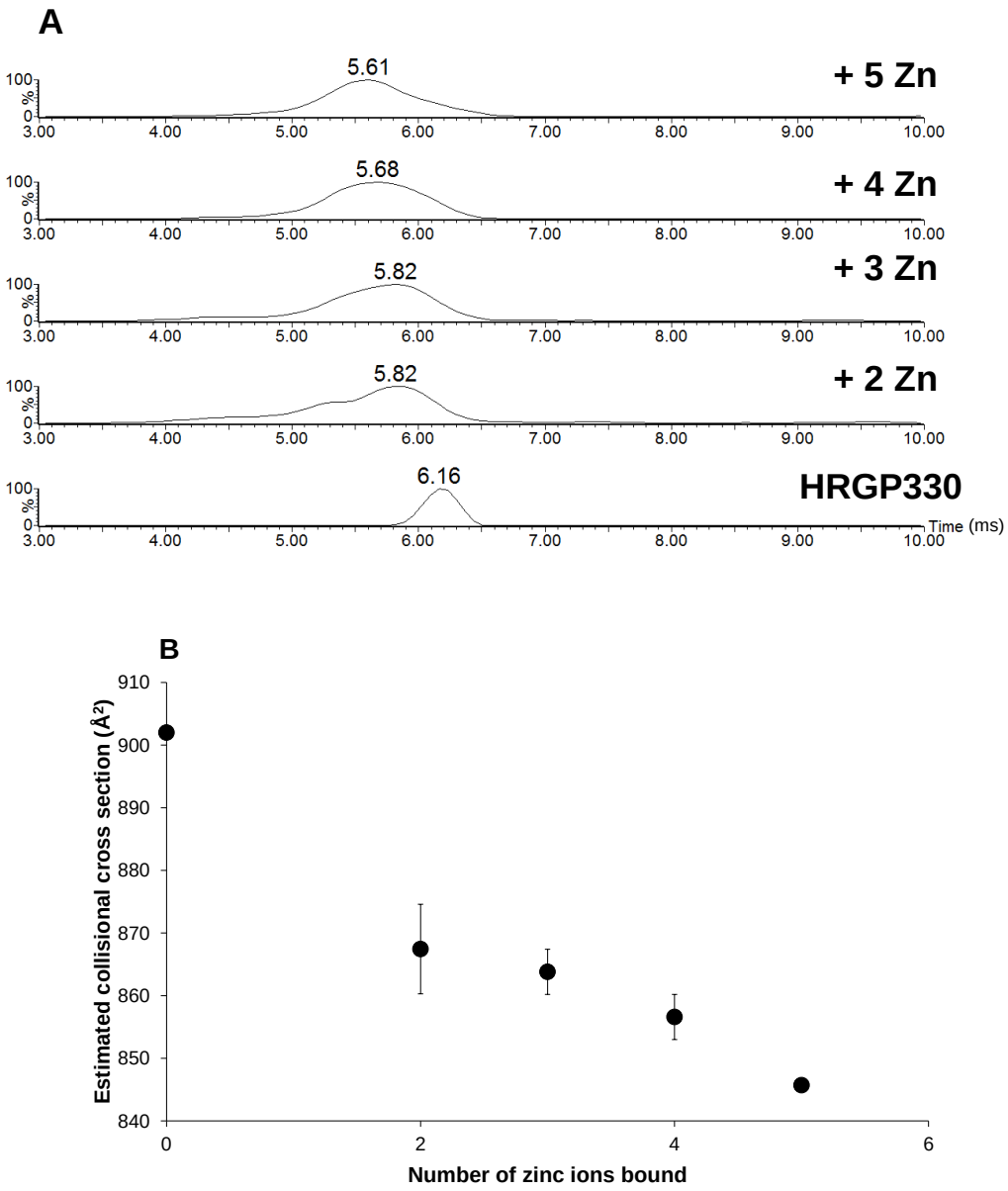

Figure 5.9 Effect of Zn^{2+} binding on the ATD and collisional cross section of the 5+ charge state of HRGP330. A) ATDs of Zn^{2+} bound species which are given in ms B) Estimated collisional cross sections calculated. The sample was 10 μM HRGP330 in 10 mM ammonium acetate (pH 7.4). The error bars represent the standard error in the two datasets obtained in the presence of Zn^{2+} ions.

5.4 NMR spectroscopy of HRGP330

5.4.1 1-D and 2-D NMR spectroscopy of apo-HRGP330

1-D ^{1}H NMR spectroscopy of apo-HRGP330 at 25 °C showed a mixture of sharp and broad peaks, suggesting an unfolded structure. Various temperatures from 5-35 °C were investigated in order to gain more

information from the spectra and improve the resolution. Figure 5.10 shows that as the temperature is decreased, a greater dispersion of the peaks in the fingerprint region is observed, indicating that at 5 °C the peptide appears to have a more ordered structure. Consequently, all subsequent experiments were performed at 5 °C.

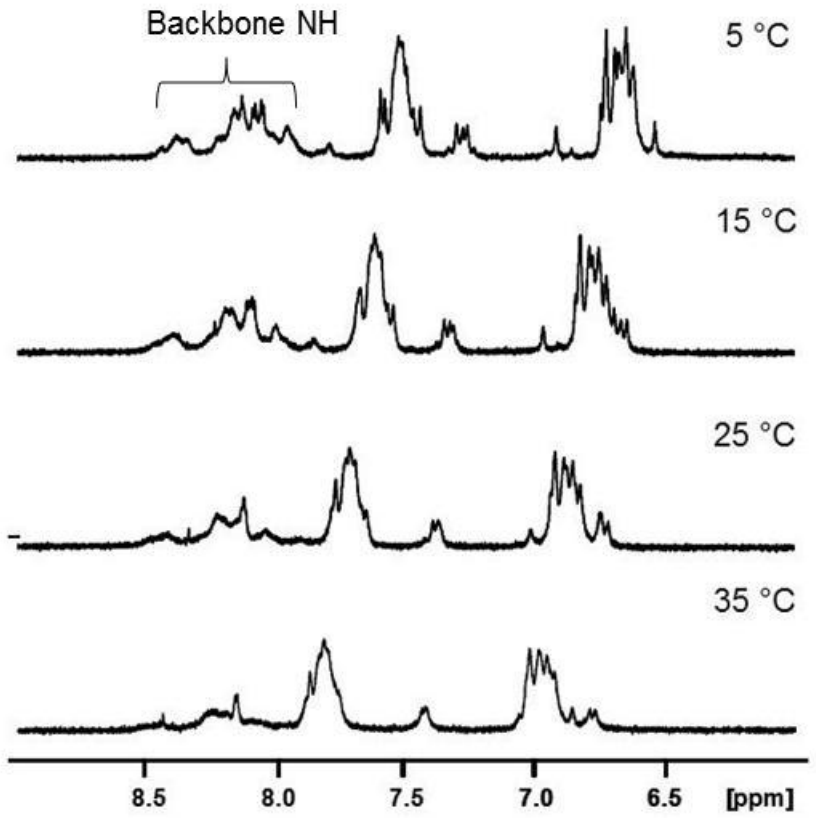

Figure 5.10 Stacked plot of 700 MHz 1-D ^{1}H-NMR spectra showing fingerprint region of HRGP330 obtained at varying temperatures from 5-35 °C. ~0.7 mM sample was prepared in 50 mM Tris[D_{11}], 50 mM NaCl with 10% D_2O at pH 7.4.

To obtain information on the peptide folding, 2-D TOCSY and NOESY were employed. These experiments give information about through-bond and through-space ^{1}H-^{1}H interactions, respectively. An overlay of the TOCSY (blue) and NOESY (red) spectra are shown in Figure 5.11 A. The distribution of backbone amide proton peaks spans the range 6.9-8.9

ppm which indicates a lack of conventional protein folding and secondary structure. For the apo-form of HRGP330, partial assignment was achieved at pH 6.20 and 5°C (Figure 5.11 A). Full details of chemical shifts are provided in Table A4 (Appendix). Approximately 27 NH-CH(α) crosspeaks can be detected in the fingerprint region of the TOCSY whereas 30 would be expected therefore it is clear some residues are not observed. A significant number of crosspeaks are observed in the NOESY which indicates that the structure is not completely random coil. The nomenclature used for the imidazole protons of His (Hε1 and Hδ2) is shown in Figure 5.11 B and these can be clearly observed in the TOCSY spectrum. The His Hδ2 protons are observed at 7.0 ppm and the Hε1 protons centred around 8.0 ppm at 5 °C. On closer inspection the His residues are resolved in the NH direction and approximately 11 can be distinguished although they cannot be assigned unambiguously (Figure 5.11 C). Three that could be identified are His3, His7 and His30 which are highlighted.

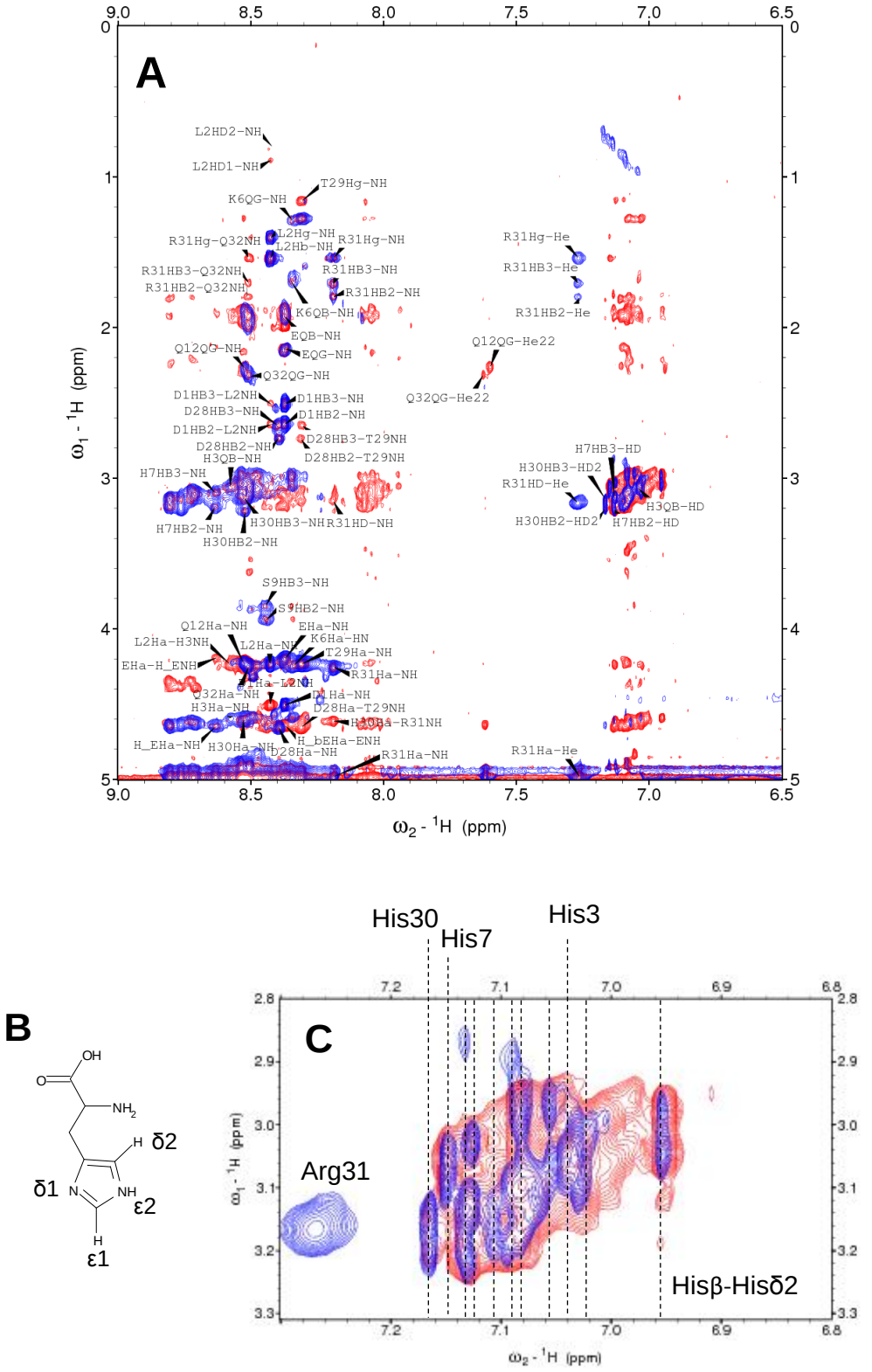

Figure 5.11 Fingerprint region of [^{1}H,^{1}H] TOCSY and NOESY spectra of HRGP330 obtained at 700 MHz. A) Full fingerprint region showing assigned peaks. B) Chemical structure of His showing nomenclature of resonances. C) Identification of approximately 11 His residues from their Hisβ-Hisδ2 crosspeaks, each distinguished with a dashed line. Sample concentration was ~0.4 mM in 50 mM Tris[D_{11}], 50 mM NaCl with 10% D_2O. The pH was 6.20 and the spectra were obtained at 5 °C. The TOCSY spectrum (*blue)* is overlaid onto the NOESY spectrum (*red*).

5.4.2 1-D and 2-D NMR spectroscopy of Zn^{2+}-HRGP330

A Zn^{2+} titration was carried out by addition of microlitre aliquots of $ZnCl_2$ to HRGP330 followed by the recording of 1-D ^1H spectra which are shown in Figure 5.12. Upon addition of 1 mol. equiv. Zn^{2+} the His residues in the aromatic region broadened considerably which indicates they are participating in metal binding. When 2 mol. equiv. were added, the peaks had broadened significantly into the baseline and no further change was seen at 3 mol. equiv. Zn^{2+}. Some of the peaks, however, remain relatively sharp for example Gln12, Gln32 and Arg31 which are annotated in the spectrum. Asp1 and Leu2 are also still visible in the presence of 3 mol. equiv. Zn^{2+} although are much broader. These amino acids are not thought to be involved in metal binding although some broadening could be due to their close proximity to Zn^{2+} binding residues.

It must also be noted that broadening of residues other than His may mean Zn^{2+} is promoting the formation of oligomers. With greater than 3 mol. equiv. $ZnCl_2$, aggregation of the peptide was visible as white precipitate in the NMR tube. This could be due to high peptide concentrations used for NMR spectroscopy as only a small amount of dimer was observed in ESI-MS and only in the presence of metal ions. As shown in Figure A7 (Appendix), this was a minor species and the relative abundance compared to the HRGP330 monomer was 1.5-2% relative intensity in the samples.

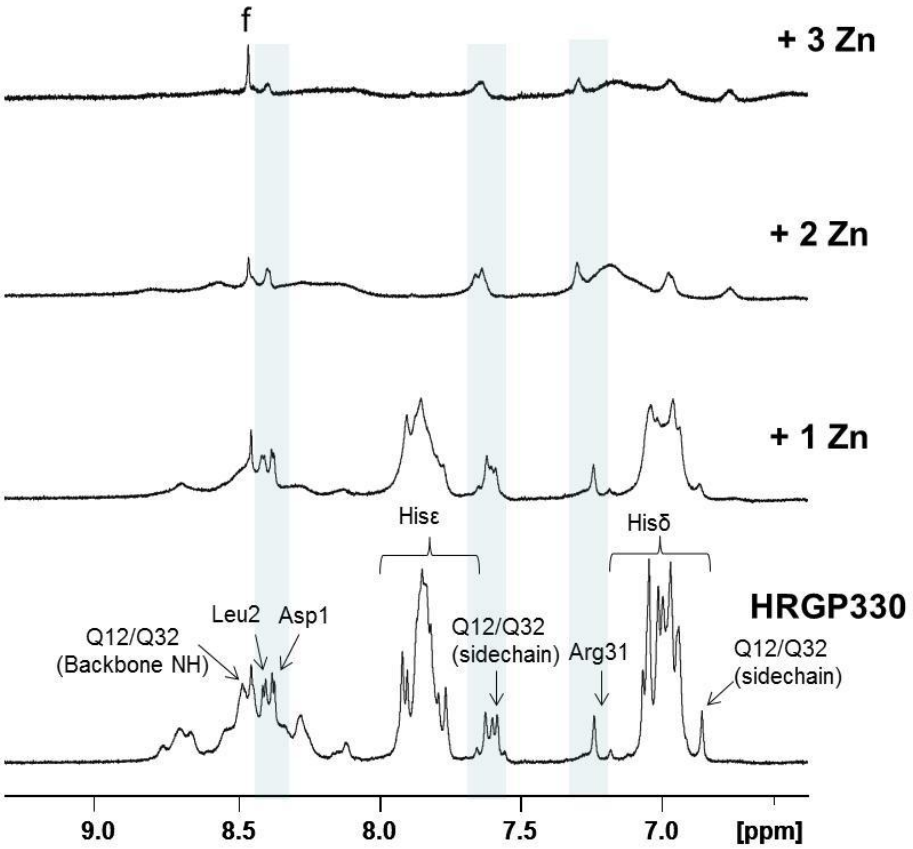

Figure 5.12 Stacked plot of 700 MHz 1-D ^{1}H-NMR spectra showing fingerprint region of HRGP330 in the presence of varying mol. equiv. $ZnCl_2$. Sample was prepared in 50 mM Tris[D_{11}], 50 mM NaCl with 10% D_2O at pH 7.4 and 278 K. The His protons are annotated but significant overlapping meant they could not be assigned unambiguously. f denotes formate.

Intriguingly, this oligomerisation of HRGP330 in the presence of Zn^{2+} may have physiological relevance as Jones *et al*. (2004) hypothesised that Zn^{2+} may be able to crosslink the HRR regions of HRG molecules. This would form a functional oligomeric complex that would have an enhanced binding affinity towards cell surfaces. From the NMR data it can be suggested that a number of Zn^{2+}-bound complexes were present which are in intermediate exchange with each other. It cannot be said conclusively from the NMR data that Zn^{2+} alters the peptide structure, however, TWIM-MS did suggest a more compact conformation was formed upon Zn^{2+} binding. Furthermore, both NMR data and the

broadness of the ATDs support that fact that there are a number of complexes present once Zn^{2+} is bound.

Figure 5.13 shows an overlay of the TOCSY spectra obtained for HRGP330 in the absence and presence of Zn^{2+}. Upon Zn^{2+} binding, most of the residues disappear completely which is clearly seen by the overall lack of orange peaks (with Zn^{2+}) compared to the blue peaks (no Zn^{2+}). Interestingly, some spin systems remain unaffected as highlighted in Figure 5.13 A. Peaks for the amino acids Asp1 and Leu2 are still relatively strong which indicates they have similar behaviour in the presence of Zn^{2+}. In this case, the amino group at the N-terminus has been modified to an amide group which lowers its exchange rate with water and allows it to be observed. The Arg31Hδ-Hε crosspeak is also still prominent which could indicate residues at both ends of the peptide are generally less affected by Zn^{2+} binding. This is further supported by the observation that Gln32 can be seen in the aromatic region of the spectrum even when the His crosspeaks are significantly broadened (Figure 5.13 B).

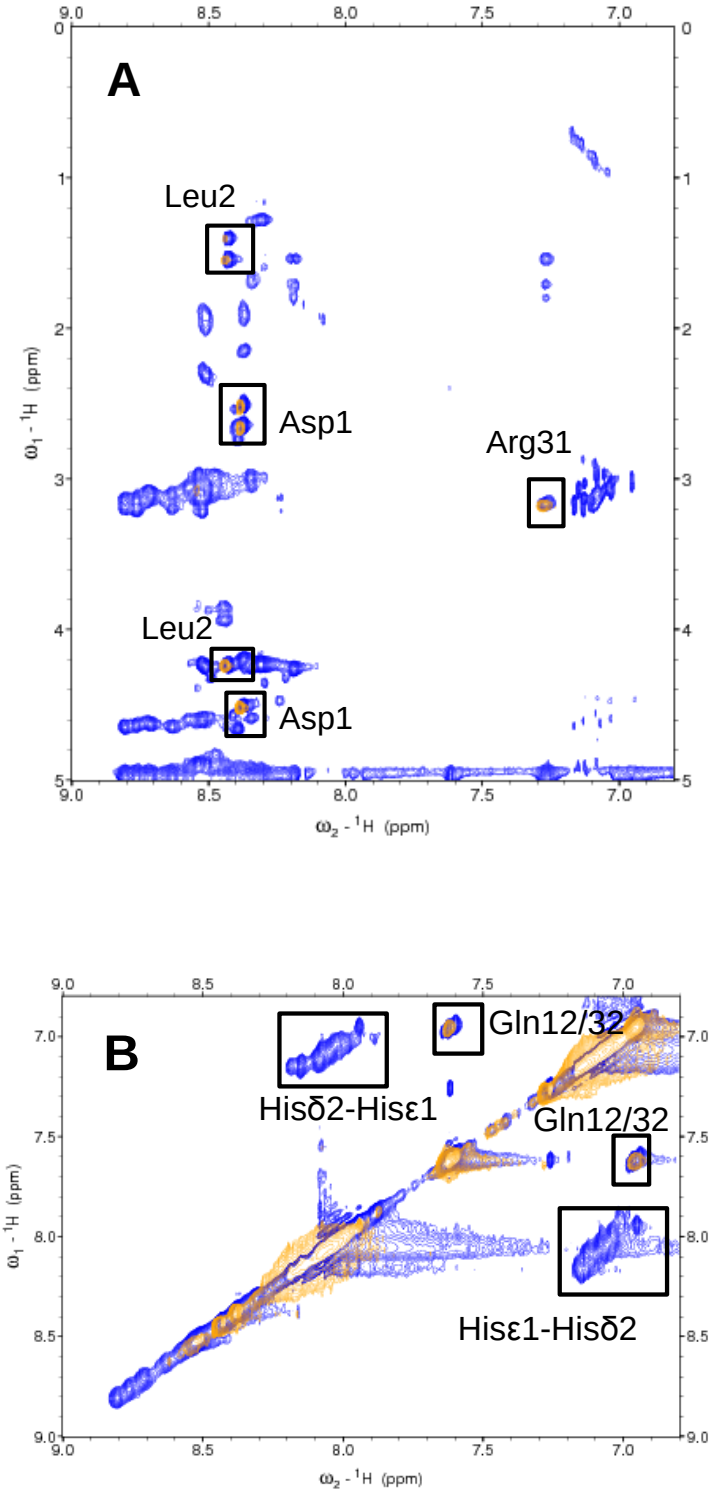

Figure 5.13 Effect of Zn^{2+} on TOCSY spectrum of HRGP330 at 700 MHz. A) Fingerprint region B) Aromatic region. The TOCSY spectrum of Zn-HRGP330 (*orange*) is overlaid onto the TOCSY spectrum of apo-HRGP330 (*blue*). ~0.5 mM samples were prepared in 50 mM Tris[D_{11}], 50 mM NaCl with 10% D_2O at pH 6.20 and 278 K. The peaks that remain upon Zn^{2+} binding are annotated. The His crosspeaks are labelled to show that they are no longer observed when Zn^{2+} is bound.

5.5 Tandem mass spectrometry

5.5.1 An overview of MS/MS

Tandem mass spectrometry (MS/MS) involves at least two steps of mass analysis and is a valuable tool for gaining structural information about biomolecules. Typically, an ion of interest is isolated using a first mass analyser (known as the precursor or parent ion) and then fragmented to yield ions of smaller masses which are detected by a second mass analyser. Fragmentation of a protein provides information about the amino acid sequence and depending on the MS/MS technique used, different types of ions can be formed. Assignment of these product ions is carried out using the Biemann nomenclature which is summarised in Figure 5.14 (Biemann, 1982; Roepstorff and Fohlmann, 1984; Johnson *et al*., 1988). If the charge on the ion is retained on the N-terminal fragment then the ion is denoted a, b or c and if it is on the C-terminal fragment the assignment is x, y and z.

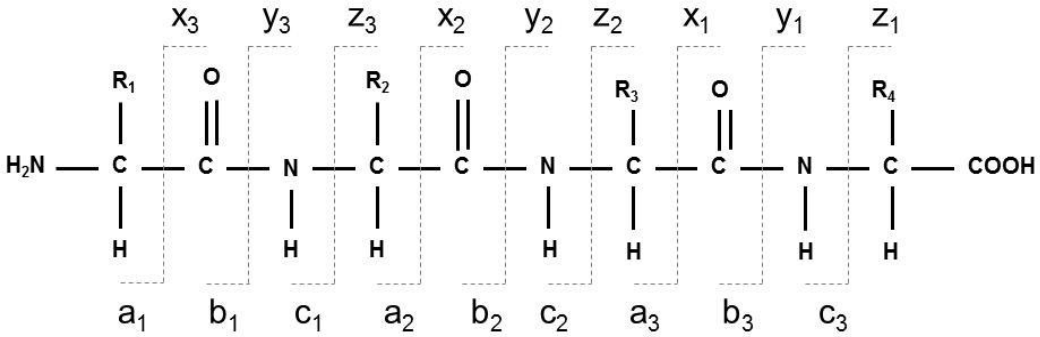

Figure 5.14 Schematic showing the nomenclature of peptide ions formed from tandem MS/MS experiments. This notation is based on the Biemann method (Biemann, 1982; Roepstorff and Fohlmann, 1984; Johnson *et al.*, 1988). The numbers in subscript next to the letters represent the number of residues in the fragment ion.

5.5.2 Collision-induced dissociation (CID)

Collision-induced dissociation (CID[1]) was first introduced by Jennings and McLafferty and carried out on small organic molecules (Jennings, 1968; McLafferty *et al*., 1973). During CID the ion of interest is subjected to high energy collisions with inert gas molecules (Ar, N_2, He etc.) in a collision cell and the internal energy within the molecule increases until fragmentation occurs. With the advent of new mass spectrometry techniques to study biomolecules, CID was soon applied to peptides and proteins and was able to provide valuable information about post translational modifications (Hunt *et al*., 1986). As a result of CID, cleavage occurs at the amide bond and predominantly b and y ions are formed. CID experiments are dependent on the size of the biological molecule as with large proteins the efficiency of energy transfer is considerably reduced which results in individual collisions being less effective.

5.5.3 Electron Capture Dissociation and Electron Transfer Dissociation

Other more recently developed techniques include electron capture dissociation (ECD) and electron transfer dissociation (ETD) and in both cases fragmentation is driven by free radicals. Zubarev was first to apply ECD to proteins in 1998 and the technique involves electrons being captured by ions which induces fragmentation (Zubarev *et al.*, 1998). More efficient fragmentation is achieved and a predictable series of c and

[1] Also known as collisonally activation dissociation (CAD)

z ions is produced following cleavage of the N-Cα bond. Other ions such as y can be generated from secondary reactions but these are less abundant. One disadvantage of ECD is that it can only be used with highly expensive FT-ICR instrumentation which is not readily available. This drove the development of the analogous technique ETD for lower resolution ion-trap instruments (Syka *et al*., 2004).

During ETD protein ions that are positively charged are allowed to react with radical anions (e.g. fluoranthene). This can be followed by Proton transfer reaction (PTR) which reduces the charge on the resulting fragments and simplifies the spectra to allow easier interpretation of the data (Coon *et al*., 2005). The mechanisms by which ECD and ETD occur are not fully understood but they do have some advantages over CID. Firstly, these techniques are more site-specific and labile modifications or "weak linkages" are able to be retained (e.g phosphorylation) which may not be the case during CID (Zubarev, 2004; Zhou *et al*., 2011). Secondly, they are independent of the size of the peptide/protein and so are suited to the analysis of larger biomolecules (Coon *et al*., 2005).

The majority of examples in the literature on non-covalent protein complexes utilise ECD and not ETD which is due to the accuracy and high resolution that FT-ICR instruments afford. A study on non-covalently bonded peptide-antibiotic complexes using ECD showed that the interactions were preserved (Haselmann *et al*., 2002) and binding site information has also been obtained from ECD of larger protein-ligand

complexes (Xie *et al*., 2006; Clarke *et al*., 2011; Breuker and McLafferty, 2003) . This is a good indication that ECD and ETD could be used to study metalloproteins as the metal-protein interactions occur through non-covalent bonds. Although it is not entirely clear what effect the positively charged metal ion may have on these processes.

5.5.4 MS/MS of non-covalent protein complexes: metalloproteins

It is of much interest to develop the application of different fragmentation techniques that allow identification of metal ions on peptide fragments and which could be a good indication of high affinity binding sites. It is challenging to maintain metal binding during fragmentation and carry out experiments under non-denaturing conditions which will preserve any non-covalent interactions, however, a limited number of studies have been able to achieve this. Loo *et al.* (1994) investigated the interaction of Zn^{2+} ions with an angiotensin peptide of 8 residues in size and were able to gain evidence of how the metal ion was coordinating to the peptide. A year later Hu and Loo extended this work by comparing the fragmentation chemistry of angiotensin peptides in the presence of Zn^{2+}, Co^{2+} and Ni^{2+} (Hu and Loo, 1995). More recently, the Zn^{2+} binding site of a 23-residue histidine-rich peptide, H5WYG, was investigated using CID and it was shown that the metal ion was associated with three out of the five histidine residues (Buré *et al.*, 2009a), even though conclusive evidence required the generation of mutant peptides (Buré *et al.*, 2009b). A similar experiment was used to map the site of Cu^{2+} binding on CP12, a protein originating from *Chlamydomonas reinhardtii* that is involved in the Calvin

cycle (Erales *et al.*, 2009). The largest metalloprotein to be studied by tandem MS in a native state is carbonic anhydrase (29 kDa) although this utilised supercharging with m-nitrobenzyl alcohol. Yin and Loo (2011) did not obtain good sequence coverage but were able to identify some Zn^{2+}-bound fragments. One recent example utilised ETD/PTR to study a bacterial metallothionein and showed that folded dimeric Zn_4SmtB_2 yielded few fragments while the monomeric form did produce some Zn^{2+}-bound fragments which contained residues thought to be Zn^{2+} ligands within the intact protein (Kondrat *et al*., 2012).

5.5.5 MS/MS of HRGP330

The 5+ charge state was selected for study as this showed the greatest intensity (Figure A8, Appendix) and so the 867 *m/z* ion was isolated and fragmented using CID and ETD. ETD was followed by PTR which allowed the isotopic pattern of many of the ions to be clearly observed and facilitates easier identification of metal-containing fragments. As shown in Figures 5.15 A and 5.16 A, good sequence coverage was achieved for apo-HRGP330 in both experiments: 82.9% achieved in the ETD fragmentation compared to a slightly lower value of 74.6% for CID. The Biemann nomenclature was used to annotate the fragments and fragmentation schemes in Figure 5.15 B and 5.16 B summarise the cleavages that occurred in each experiment. CID tends to give lower sequence coverage than ETD because while ETD produces a defined ion series that is independent of the protein size, CID induces more random fragmentation along the backbone.

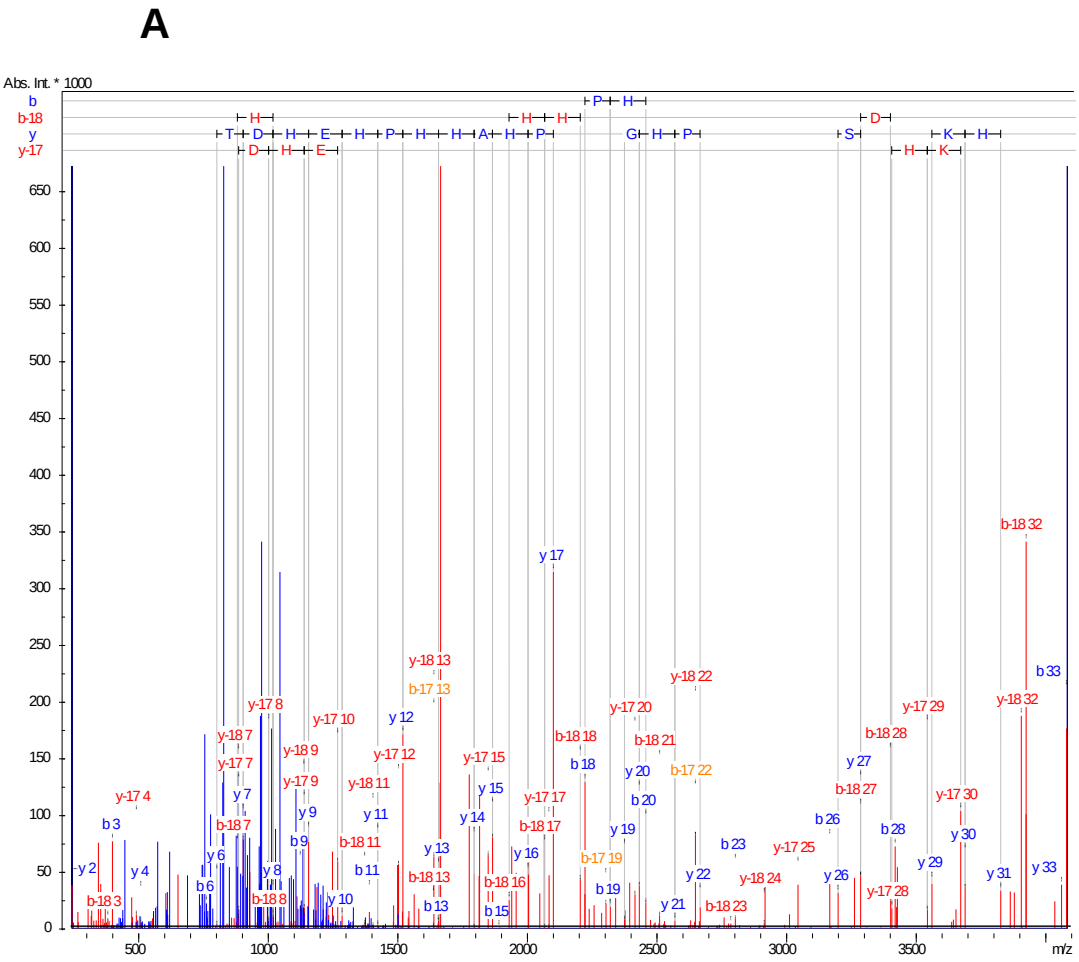

Figure 5.15 CID spectrum of apo-HRGP330. A) CID spectrum of 867 *m/z* B) Fragmentation scheme showing the b and y ions produced. The b-18 and y-17 ions correspond to the loss of water and ammonia respectively. Analysis was carried out using Biotools v3.2 and Sequence Editor v3.2. Sequence coverage of 74.6% was obtained.

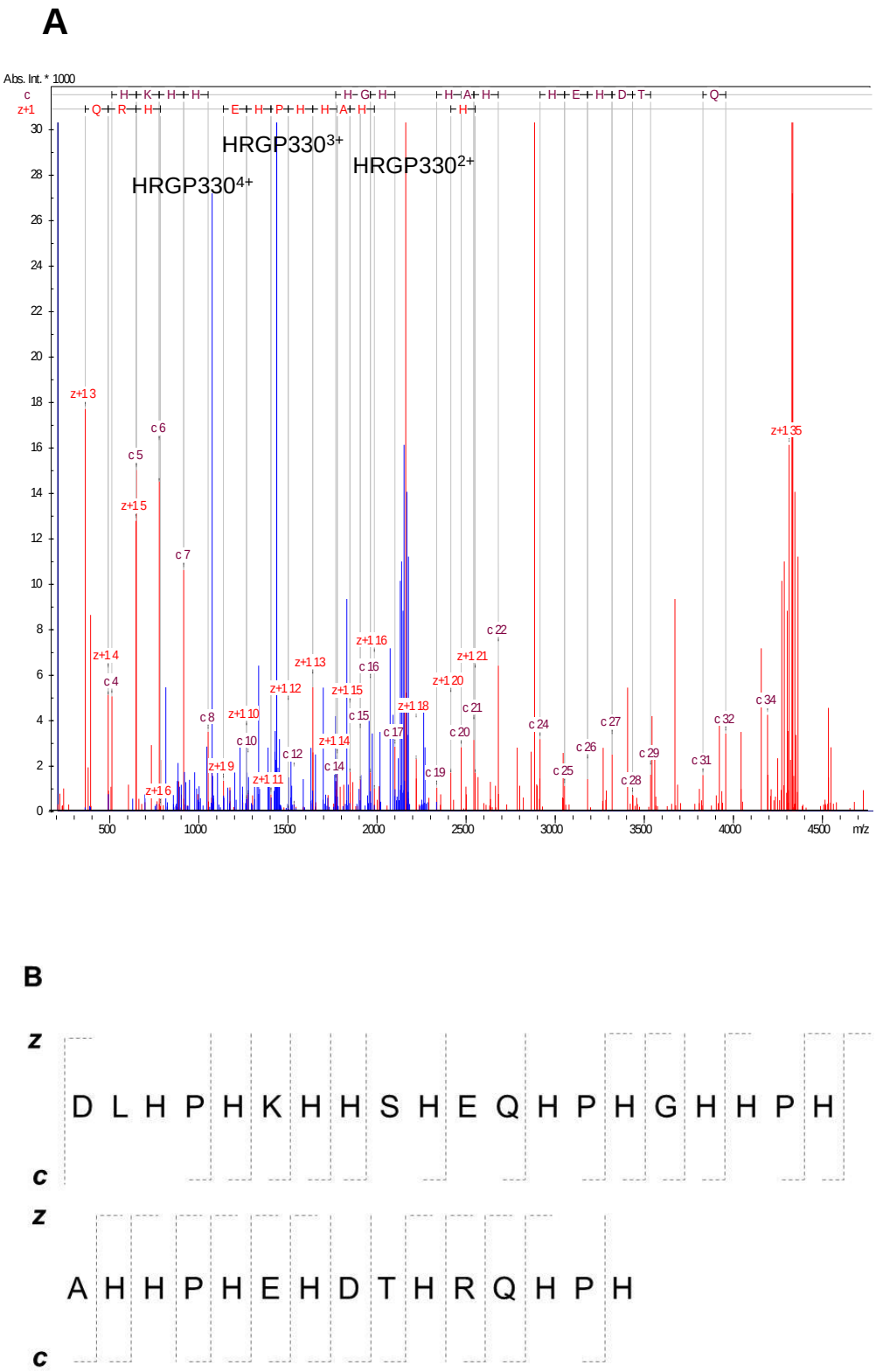

Figure 5.16 ETD spectrum of apo-HRGP330. A) ETD spectrum of 867 *m/z* B) Fragmentation scheme showing the c and z ions produced. Analysis was carried out using Biotools v3.2 and Sequence Editor v3.2. Sequence coverage of 82.9% was obtained.

Full sequence coverage was still not expected for ETD because HRGP330 contains 5 Pro residues and cleavage of the N-Cα bond in the N-terminal direction cannot occur due to its cyclic structure. This precludes the observation of c_3, c_{13}, c_{18} c_{23}, c_{33}, z_2, z_{12}, z_{17}, z_{22} and z_{32}. In addition to c and z ions, a number of y ions were also detected in the ETD spectra which can be produced from secondary reactions. An important feature of the ETD spectrum is the charge-reduced states of the parent ion (4+, 3+ and even 2+) which are visible at high intensity and are labelled on Figure 5.16 A.

5.5.6 MS/MS of Zn^{2+}-bound HRGP330

The intact spectrum prior to isolation and fragmentation is provided in Figure A8 (Appendix). Comparison of the CID spectra for fragmentation of 867 *m/z* (apo-HRGP330) and 880 *m/z* (Zn_1-HRGP330) showed that a significant number of peaks were produced in each case. This is evident from the spectra shown in Figures 5.15 A and 5.17 A. In fact, there also appeared to be more fragmentation once the Zn^{2+} was bound (Figure 5.17 A) which suggested that additional fragment peaks with Zn^{2+} ions bound were likely. Immediately a number of possible Zn^{2+} binding fragments could be identified from the isotopic distribution. A summary of the fragments that were Zn^{2+}-adducts is given in the fragmentation scheme in Figure 5.17 B (A table of the mass list with comparison to theoretical values is provided in Table A5, Appendix).

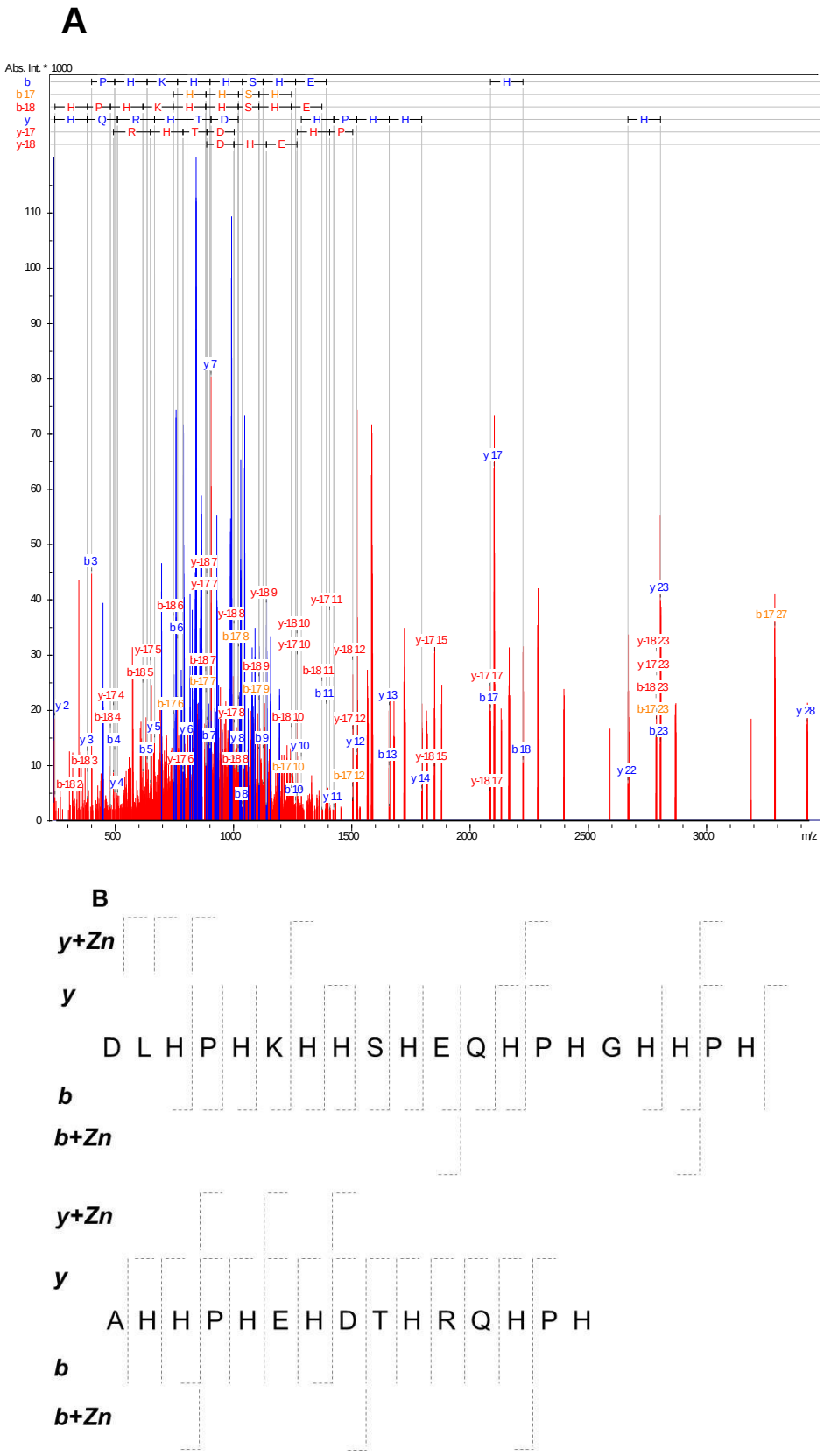

Figure 5.17 CID spectrum of Zn-HRGP330. A) CID spectrum of 880 *m/z* B) Fragmentation scheme showing the b and y ions produced and those that were identified to be Zn^{2+}-adducts. Analysis was carried out using Biotools v3.2 and Sequence Editor v3.2.

In some cases these were observed as a mixture of the Zn^{2+}-free and Zn^{2+}-bound fragments. Many of them identified were large fragments which did not provide useful information about the specific interactions that are occurring. In order to confirm that the new peaks were observed as a result of Zn^{2+} binding, the 893 *m/z* (+2 Zn^{2+} ions) peak was fragmented as this was also observed in the intact spectrum (Figure A8, Appendix). A comparison of the mass range 540-740 *m/z* from the CID spectra of 867 *m/z*, 880 *m/z* and 893 *m/z* is shown in Figure 5.18. This showed that in the CID spectrum of 893 *m/z* the same peaks were present as in that for 880 *m/z*, however, the intensity was increased.

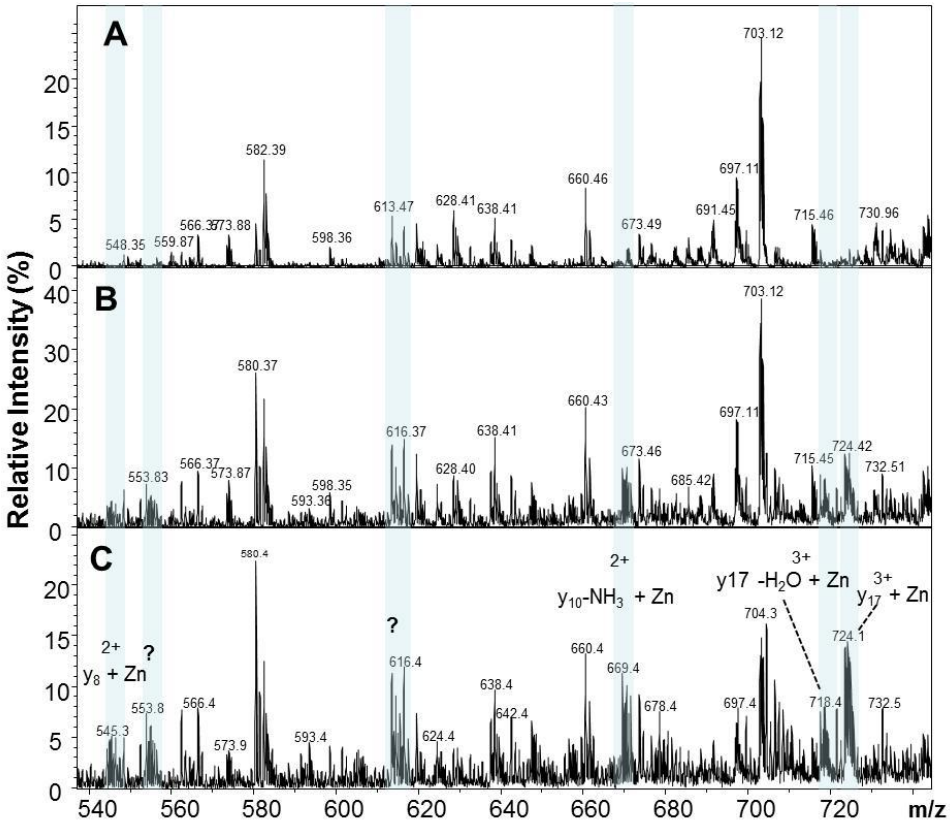

Figure 5.18 Comparison of the MS/MS spectra of apo-HRGP330 (867 *m/z*), Zn_1-HRGP330 (880 *m/z*) and Zn_2-HRGP330 (893 *m/z*). The highlighted regions indicate the new peaks that appear in the Zn^{2+}-bound samples. Those that could be assigned are labelled and those that were not conclusive are marked with a **?**

These peaks were clearly not observed in the CID spectrum of apo-HRGP330, 867 *m/z*. The blue regions highlight the new Zn^{2+}-bound peaks that appear and illustrate how they increase in intensity at a higher concentration of Zn^{2+}. Two of the small fragments identified to bind Zn^{2+} were y_8 and y_{10} which are highlighted in Figure 5.18. The y_{10} fragment had a mass loss of 17 Da indicating that ammonia had been lost. In the case of the y_8 ion these data suggest that the metal ion is interacting with His35, His33, and His27. This is in good agreement with the proposal that three His residues are involved in Zn^{2+} ion ligation. Additionally His25 could also be involved in the case of the y_{10} ion. The Zn^{2+}-bound ions were characterised by their distinctive isotopic distribution. The isotopic patterns for the y_{12}^{1+} ion and y_{10}-NH_3^{2+} ion are shown in Figure 5.19 A and C respectively.

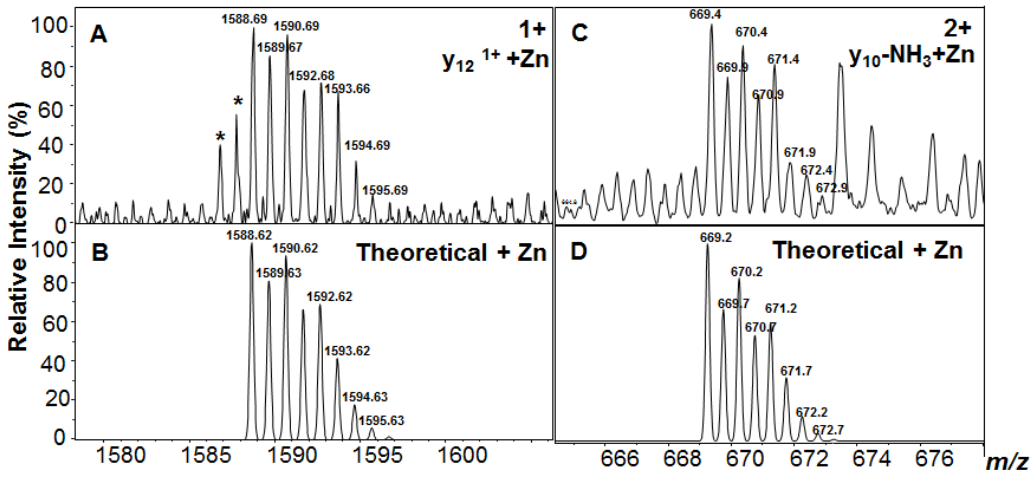

Figure 5.19 Comparison of experimental and theoretical isotopic patterns for the Zn^{2+} adducts of y_{12} and y_{10} generated from CID. A) Experimental isotopic distribution of the y_{12}^{1+} ion with Zn^{2+} bound B) Theoretical isotopic distribution of the y_{12}^{1+} ion with Zn^{2+} bound. C) Experimental isotopic distribution of the y_{10}^{2+} ion with a loss of NH_3 and Zn^{2+} bound D) Theoretical isotopic distribution of the y_{10}^{2+} ion with a loss of NH_3 and Zn^{2+} bound. The peaks marked with * are contaminating peaks.

The experimental isotopic distributions are in agreement with the theoretical simulations (Figure 5.19 B and D) which is evidence that the Zn^{2+} was bound in this location in the full-length HRGP330. Furthermore, the doubly charged ion for the y_{12} fragment with Zn^{2+} bound was also identified which provides further confirmation. Although the masses of the ions identified to be Zn^{2+}-adducts proved that a metal ion was bound, the intensities for some of the peaks in the isotopic distribution did not exactly match those of the simulation which could be because there is considerable overlap in the complex spectra.

As shown in the fragmentation scheme in Figure 5.17 B, fragments from the N-terminal end of the molecule were also observed to be interacting with Zn^{2+}. The smallest fragment was b_{11} which indicates that any of the five His residues in the sequence DLHPHKHHSHE could be coordinating to a Zn^{2+} ion. Interestingly, compared to the CID of apo-HRGP330, Zn-HRGP330 showed a considerable lack of fragmentation around the GHHPH pentapeptide unit. This could be due to a conformational change upon Zn^{2+} binding which means the central residues of the peptide are less predisposed to collisions with the gas molecules.

In contrast to CID, the ETD spectrum of Zn^{2+}-HRGP330 showed considerably less fragment ions as illustrated by Figure 5.20. Overall, the spectrum in Figure 5.20 A is noisier and the peaks throughout are less well resolved. The fragmentation scheme in Figure 5.20 B shows predominantly low mass c and z ion which suggests that only the two

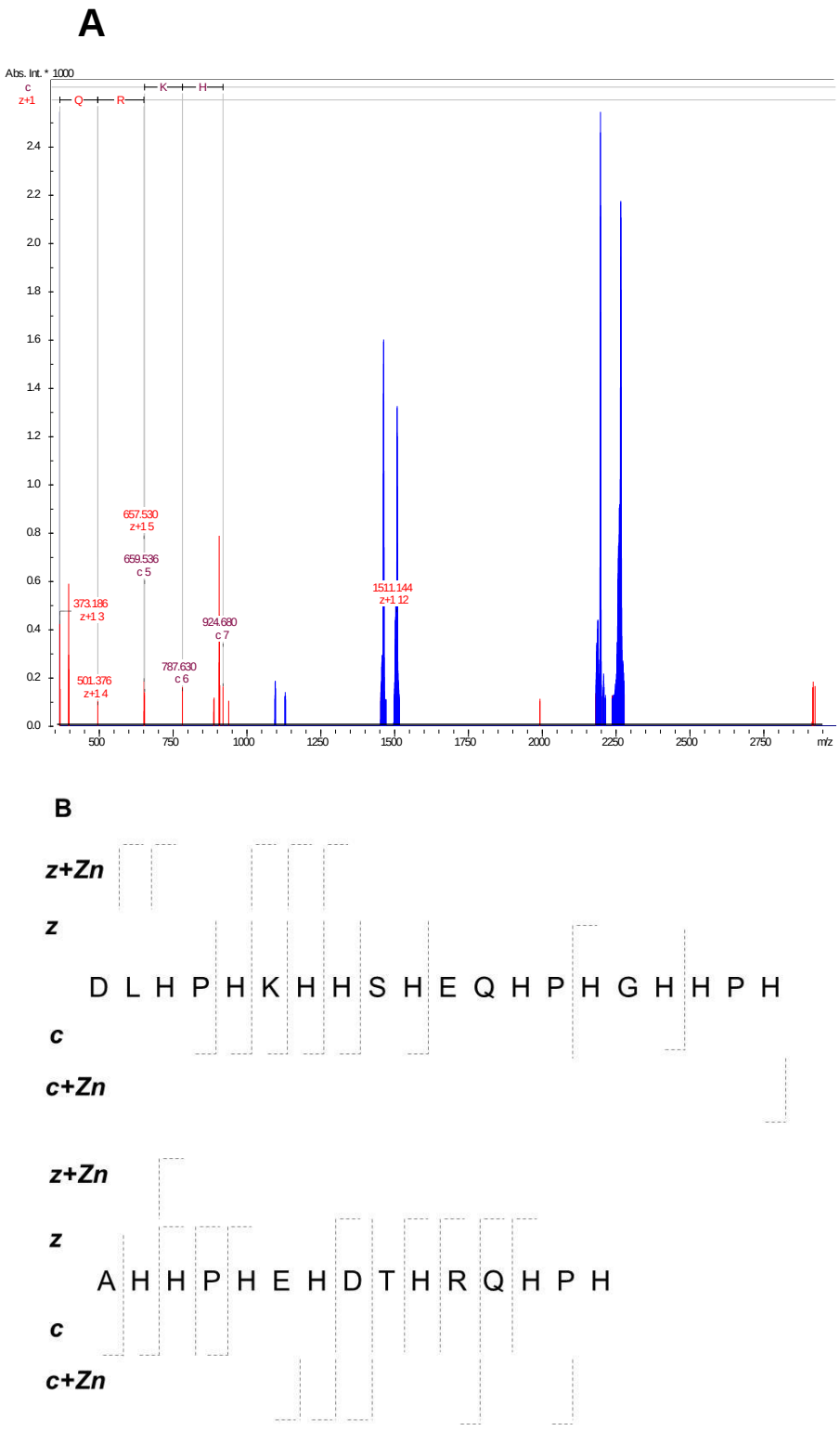

Figure 5.20 ETD spectrum of Zn-HRGP330. A) ETD spectrum of 880 *m/z* B) Fragmentation scheme showing the c and z ions produced and those that were identified to be Zn^{2+} adducts. Analysis was carried out using Biotools v3.2 and Sequence Editor v3.2. The spectrum does not show many peaks compared to the fragmentation scheme because most of the peaks were of too low intensity to be recognised by the software. Therefore, the raw data was manually interrogated to produce the fragmentation scheme.

ends of the peptide can be fragmented by ETD when Zn^{2+} is attached. Intriguingly, fragments around the GHHPH pentapeptide are noticeably absent as was the case for the CID spectrum. There is a significant increase in the intensity of the y_7 ion (911.61*m/z*) once Zn^{2+} is present as shown in Figure 5.21. A concomitant decrease in the intensity of the c_7 ion (924.66 *m/z*) is also observed which could indicate a conformational change upon Zn^{2+} binding that has an impact on the way the molecule fragments.

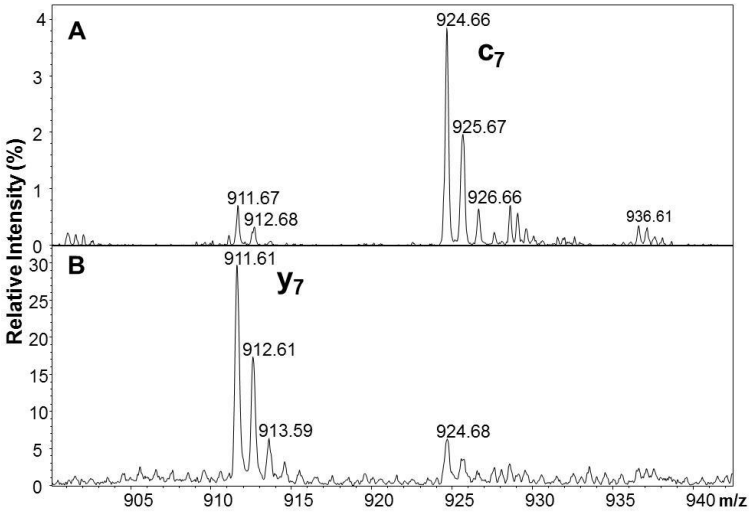

Figure 5.21 Zn^{2+} binding to HRGP330 has an effect on the intensity of different ions produced by ETD. A) c_7 ion observed in the ETD spectrum of 867 *m/z* B) y_7 ion observed in the ETD spectrum of 880 *m/z*. The y ion is produced from a secondary reaction.

It appeared as though a number of Zn^{2+}-bound peaks appeared in the ETD spectrum of 880 *m/z* although the complex spectrum did not allow all of these to be assigned. Those that were distinguishable with the most certainty are described in Table A6 (Appendix). The smallest ion identified to have a Zn^{2+} ion bound was z_{13}*, although this was of low intensity, which would suggest that any of the six His residues could be

involved in binding: His35, His33, His30, His27, His25 or His23 (Figure 5.22 B). This correlates well with the observation that the y_{12} ion detected in CID also associated with Zn^{2+}. Figure 5.22 C illustrates the well resolved peaks for ETD of 867 *m/z* compared to that for 880 *m/z* in D.

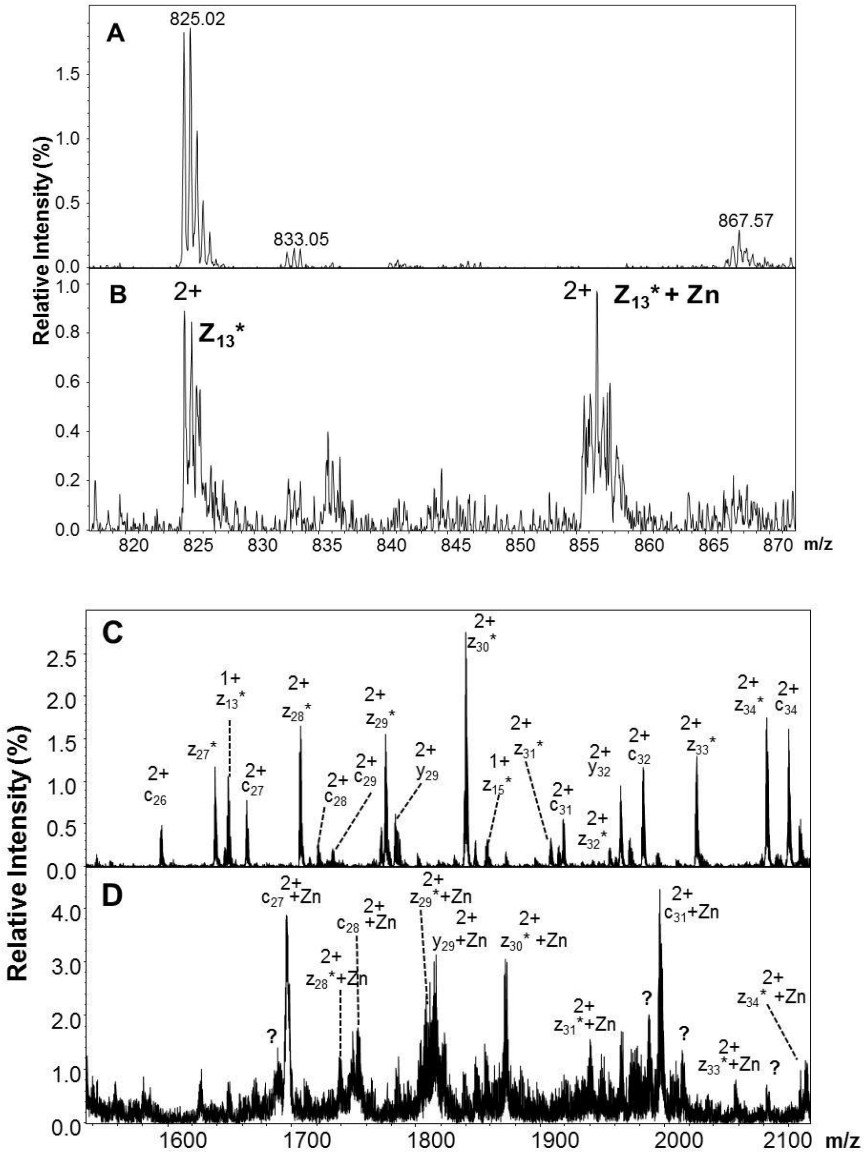

Figure 5.22 Identification of Zn^{2+}-adducts in the ETD spectrum of Zn_1-HRGP330. A) ETD spectrum of apo-HRGP330 showing z_{13}* B) Observation of a Zn^{2+} ion bound to z_{13}* C) ETD spectrum of apo-HRGP330 shows a number of clearly resolved peaks between 1500-2100 *m/z* D) ETD spectrum of Zn_1-HRGP330 shows a number of peaks identified to be Zn^{2+}-adducts although the spectrum is much noisier. Those peaks that appear to coordinate Zn^{2+} but not assigned are marked with a **?**

There appears to be many Zn^{2+} adducts but these cannot all be fully assigned with confidence. The lack of fragments for the ETD spectrum of the Zn_1-HRGP330 compared to those produced in the absence of Zn^{2+}, could indicate that the molecule undergoes a conformational change to form a less flexible structure that is less susceptible to fragmentation. ETD has in principle the advantage of leaving more labile interactions intact so it is possible that the ETD mechanism cannot fragment Zn^{2+}-HRGP330 as efficiently whereas CID is a higher energy fragmentation and can overcome the structural changes to some extent to still produce b and y ions effectively. This is supported by the IM data which indicated that the HRGP330 structure becomes more compact when Zn^{2+} binding occurs. The contribution of the Zn^{2+} ion to the electron transfer process, however, can also not be ignored as two earlier studies reported that the cation may act as an electron sink. Zubarev *et al*. (2000) demonstrated through ECD of cytochrome c that the region around the heme, with bound Fe^{3+}, was resistant to backbone cleavage. Similarly, ECD of an angiotensin peptide produced fewer fragments in its Zn^{2+}-bound form (Zubarev *et al*., 2002). This would rationalise the lack of fragmentation around the GHHPH region if Zn^{2+} was indeed bound there, however, the observation of Zn^{2+} adducts not containing this pentapeptide would point towards the partial occupation of different sites.

Taking into account the findings of the MS/MS data it would appear that there is not a single preferred binding site for Zn^{2+} to HRGP330 as fragments from both N-terminal and C-terminal ends of the molecule were

observed in a Zn^{2+}-bound form. This would suggest that several of the His residues, and the binding sites they may form, have a similar affinity for Zn^{2+} ions and that at sub-stoichiometric Zn^{2+}:HRGP330 ratios they are likely to be partially occupied. However, it was noticed that in the presence of Zn^{2+} the least fragmentation occurred around the GHHPH unit. Further work is needed to rationalise this observation fully which could involve fragmentation of other metal ion-HRGP330 complexes and a comparison of the data.

5.6 Conclusion

The biologically-active peptide from the HRR of HRG was shown to bind up to 5 Zn^{2+} ions by native ESI-MS. Broadening of the proton signals and aggregation of the peptide did not allow any significant information to be gained from ^{1}H-NMR spectroscopy although the large number of NOESY cross peaks suggested it was not completely random coil structure. TWIM-MS showed that a number of complexes were present in the Zn^{2+}-bound forms which could not be resolved. Interestingly, the collisional cross sections that were estimated showed that the peptide complexes with Zn^{2+} had a more compact structure. Furthermore, CD spectroscopy showed evidence of a polyproline II helix and a substantial change upon addition of Zn^{2+}. These results give an insight into how active multimeric HRG complexes could form and it would appear significant changes occur in the HRR in order to facilitate this.

Top down MS/MS was utilised to map the sites for Zn^{2+} binding. HRGP330 was able to be sequenced by CID and ETD with high levels of

sequence coverage, most likely due to its extended conformation which allowed it to fragment easily. When Zn^{2+} was bound to HRGP330, less sequence coverage was achieved, indicating that a conformational change may have taken place. Zn^{2+} binding fragments were identified in both CID and ETD data and it was found that the metal ion was primarily associating with y fragments from the C terminus although some Zn^{2+}-binding fragments from the N-terminus were also identified. ETD was not able to efficiently fragment the Zn^{2+}-bound HRGP330 to the same extent as CID indicating that a conformational change had occurred that ETD was not able to overcome. Overall, the observation of Zn^{2+}-peptides has important implications for the field of top-down MS/MS of metalloproteins as few studies have attempted this.

Chapter 6

Investigating metal ion distribution between HSA and HRGP330

6.1 Introduction

The hypothesis being investigated in this chapter is that the fatty acid "switch" mechanism could have implications for other Zn^{2+} binding proteins in plasma. If the balance of fatty acids in plasma were perturbed, during a disease for example, then other proteins may play a role in protecting the cells from toxic concentrations of Zn^{2+}. This chapter investigates if Zn^{2+} can transfer between HSA and HRGP330. Furthermore, the effect of fatty acid is investigated to establish if this could facilitate Zn^{2+} binding to HRG. It also explores if HRGP330 could acquire Cu^{2+} from the N-terminal site on HSA as Cu^{2+} may also have an effect on the antiangiogenic activity of HRG.

6.2 Results and discussion

6.2.1 Zn^{2+} transfer occurs between HSA and HRGP330

Reports addressing interactions between HSA and HRG are lacking apart from two examples where Zn^{2+} distribution between rabbit HRG and HSA was investigated using equilibrium dialysis (Guthans and Morgan, 1982) and also the effect of HRG on heme binding to HSA was probed (Morgan, 1981). It has been demonstrated that small molecules such as histidine

can affect Zn^{2+} distribution between the two proteins (Guthans and Morgan, 1982), therefore, this work sought to address if fatty acids can also have an effect. First, Zn^{2+} transfer from HSA to HRGP330 at a 1:1 ration and in the absence of fatty acids was probed. Separation of HSA and HRGP330 was achieved using a molecular weight cut-off filter, retaining the HSA on the membrane but allowing the HRGP330 to pass through. Analysis of the HRGP330 fraction by ESI-MS showed that compared to the control sample, HRGP330 had obtained Zn^{2+} from HSA (Figure 6.1 A).

A

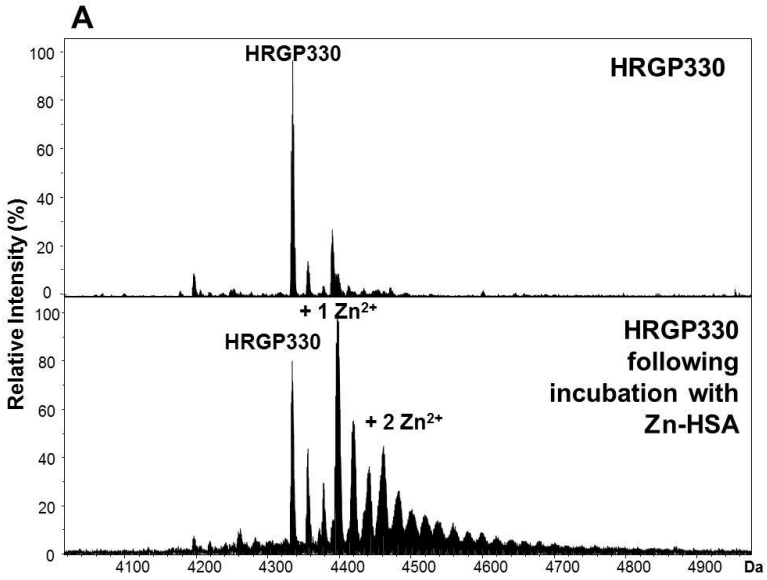

B

Sample	Zn^{2+}:HSA stoichiometry
Zn-HSA	0.96
Zn-HSA following incubation with HRGP330	0.12

Figure 6.1 ESI-MS of HRGP330 and ICP-OES of HSA as evidence for Zn^{2+} transfer having occurred. A) Mass spectra of HRGP330 before and after incubation with Zn-HSA B) ICP-OES analysis of the HSA fraction confirms a significant loss of Zn^{2+} in the presence of HRGP330. Analysis was carried out on a maXis-UHR-TOF in 10 mM ammonium acetate (pH 7.4). HSA samples were diluted in 0.1 M HNO_3 and analysed on a Perkin Elmer Optima 7500 DV.

The fact that the majority of Zn^{2+} is removed from HSA is an indicator that HRG has a higher binding affinity for Zn^{2+} than any site on HSA under the conditions employed. Furthermore, high resolution ESI-MS allowed the metal ion to be unambiguously assigned as Zn^{2+} as opposed to Cu^{2+}. In order to confirm that the source of Zn^{2+} was HSA, the protein fraction retained on the membrane was diluted and subjected to ICP-OES analysis. Figure 6.1 B shows that the Zn^{2+} bound to HSA had reduced by 87% from 0.96 to 0.12 Zn^{2+} ions per HSA molecule. Analysis of the buffer also failed to detect any Zn^{2+}; giving strong evidence that Zn^{2+} transfer occurred between HSA and HRGP330. Additionally, the preparation of Zn-HSA involved passing the sample through a PD-10 column prior to incubation with HRGP330 to ensure no unbound metal ions were present in the solution.

6.2.2 Does Zn^{2+} transfer occur from HRGP330 to HSA?

To confirm the findings of the previous experiment, the reverse Zn^{2+} transfer reaction was carried out. HRGP330 was incubated with 5 equivalents of $Zn(CH_3COO)_2.2H_2O$ and then excess metal ions were removed. Four different species were observed (apo-HRGP330, Zn_1-HRGP330, Zn_2-HRGP330 and Zn_3-HRGP330) as shown in Figure 6.2. This sample was combined with dialysed HSA in a 1:1 molar ratio and infused into the mass spectrometer. The conditions were optimised to favour observation of HRGP330 over HSA. Following incubation with dialysed HSA the distribution of metallated species in HRGP330 did not

change perceptibly. This demonstrates that at a 1:1 molar ratio, the Zn^{2+} ions have a higher affinity for HRGP330 rather than for HSA.

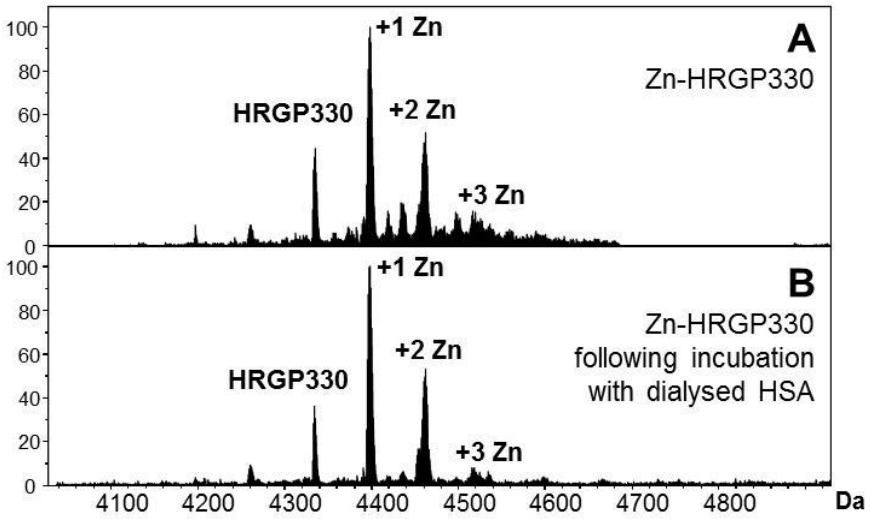

Figure 6.2 Direct infusion of a 1:1 mixture of dialysed HSA and Zn-HRGP330. Mass spectrometry was carried out on a maXis-UHR-TOF in 10 mM ammonium acetate (pH 7.4) with conditions optimised for HRGP330.

The experiments suggested that HRGP330 has a higher affinity for Zn^{2+} than HSA and this is not in agreement with the hypothesis that HRG could only obtain Zn^{2+} if it was displaced from HSA. The next step was to ascertain if fatty acid had any further effect on the Zn^{2+} distribution.

6.2.3 Effect of fatty acid on Zn^{2+} distribution

Although it appeared that HRGP330 was able to readily obtain Zn^{2+} from HSA under the conditions used for ESI-MS, the effect of myristate was investigated to try and identify any perceptible differences. One of the samples was supplemented with 5 mol. equiv. myristate and the other with no fatty acid. The instrumental parameters were optimised in order to observe HRGP330 as a probe for Zn^{2+} binding. A charge state distribution

for HRGP330 was observed including the +5 and +4 which were of the highest intensity (Figure 6.3 A). A charge state distribution for native HSA could be observed but this was of low intensity and the peaks were extremely broad. Compared to the starting HRGP330 sample that was analysed (Figure 6.3 A), two new peaks for Zn_1-HRGP330 and Zn_2-HRGP330 became present as shown in the deconvoluted spectrum in Figure 6.3 B. A Zn_2-HRGP330 species was also formed before the apo-HRGP330 was saturated with one metal ion. This is the same result described in section 6.2.2 which confirms reproducibility.

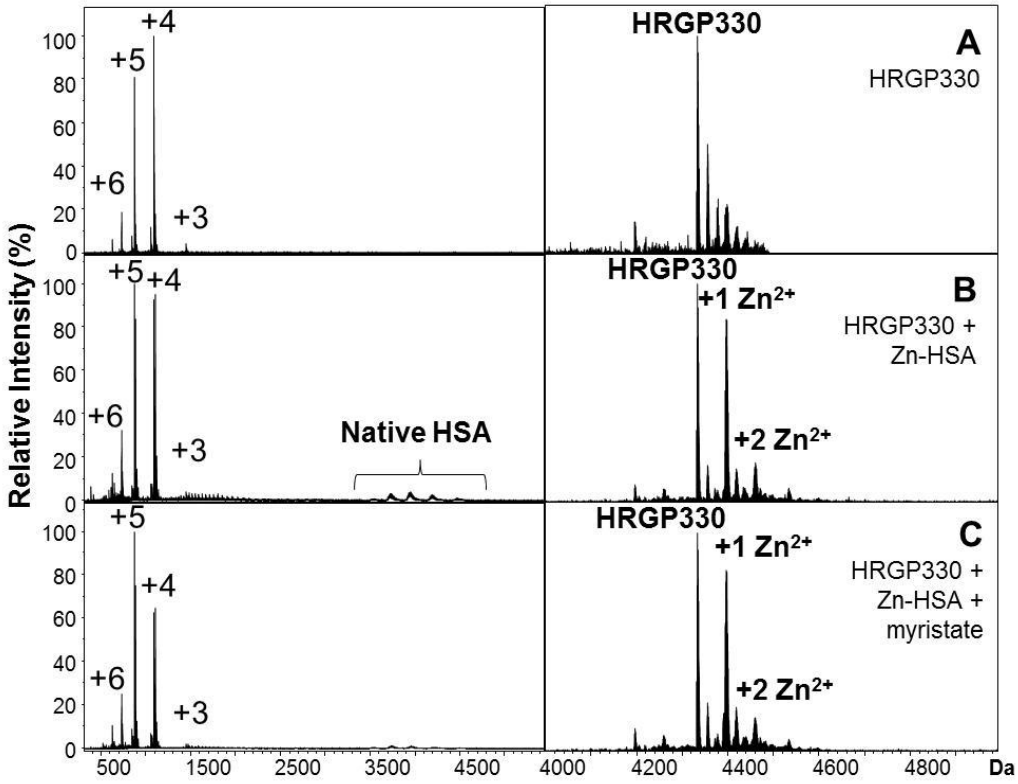

Figure 6.3 Direct infusion of a 1:1 mixture of Zn-HSA and HRGP330 in the absence and presence of myristate. A) HRGP330 control sample B) HRGP330 incubated with Zn-HSA at a 1:1 ratio C) HRGP330 incubated with Zn-HSA at a 1:1 ratio with 5 mol. equiv. myristate. The spectra on the left show the charge states and the spectra on the right are the deconvolution of the HRGP330 peaks. Mass spectrometry was carried out on a maXis-UHR-TOF in 10 mM ammonium acetate (pH 7.4) with conditions optimised for HRGP330. Native HSA peaks can be observed but at low intensity.

The sample analysed with addition of myristate is shown in Figure 6.3 C. The same amount of Zn^{2+} was bound to HRGP330 in both cases as evidence by similar intensity peaks in the mass spectrum corresponding to the Zn_1-HRGP330 and Zn_2-HRGP330 complexes. This indicates that the myristate had no effect on the distribution of Zn^{2+} between HSA and HRGP330 in this case because HRGP330 was already an effective competitor for the metal ion.

To corroborate the findings of the previous section and investigate the ternary system in more detail, HSA was incubated with the various ligands followed by separation from HRGP330. A summary of the ICP-OES measurements is provided in Figure 6.4.

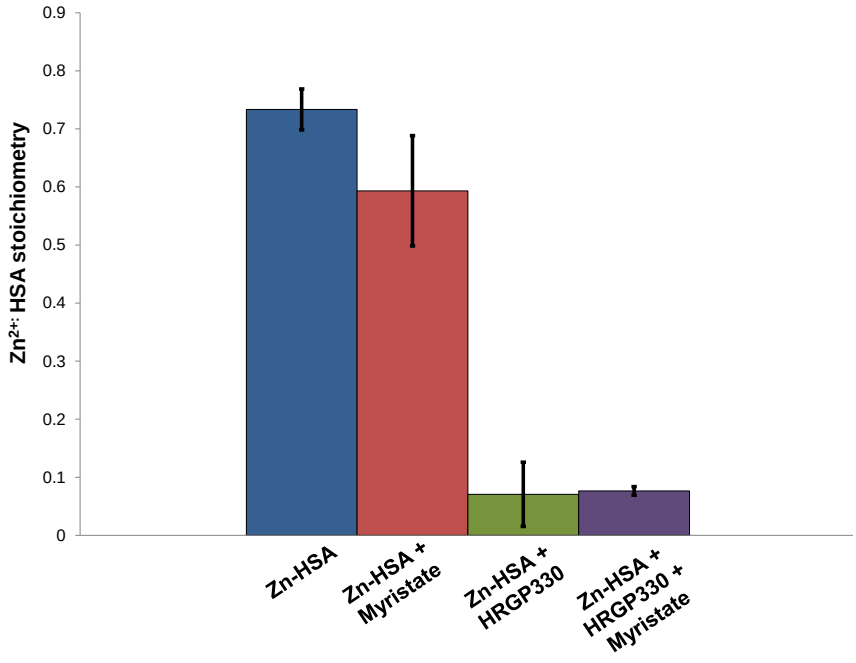

Figure 6.4 HSA:Zn^{2+} stoichiometry in the presence of 1 mol. equiv. HRGP330 (± myristate). Samples were prepared in 10 mM ammonium acetate at pH 7.4. Following incubation with the ligands HSA was separated from HRGP330. HSA fractions were diluted in 0.1 M HNO_3 and analysed on a Perkin Elmer Optima 7500 DV.

The control sample of only HSA showed less than the expected 1 Zn^{2+} bound, likely due to some loss during gel filtration. In the presence of myristate no change in the Zn^{2+} bound to HSA was observed which is consistent with the findings in Chapter 3. With the addition of HRGP330, a substantial loss of Zn^{2+} occurred (82%) and the same effect was also observed for the sample with myristate where 81% of the HSA-bound Zn^{2+} is transferred to HRGP330. There is only a small difference in Zn^{2+} content between the samples with and without myristate, therefore it can be concluded that the myristate appears to have no effect on whether the Zn^{2+} is bound to HSA or HRGP330.

6.2.4 Effect of excess HSA on Zn^{2+} distribution

To determine if the presence of HRGP330 had an impact on Zn^{2+} binding when HSA was in significant excess, as in blood plasma, the Zn^{2+} distribution between 600 μM HSA and 20 μM HRGP330 was investigated. This was used because the concentration of HRGP330 in blood plasma is ~2.5 μM, however, the effective concentration could be 10 times higher due to the proposed HRG: metal stoichiometry of 1:10. Additionally, a higher concentration had to be used in these experiments in order to obtain sufficient signal for ESI-MS following separation from HSA. Although good quality spectra of HRGP330 were obtained from 5 μM samples, it was found that a small proportion of contaminating HSA, following the separation of the proteins, supressed the ionisation of the HRGP330 signals when lower concentrations were used (Appendix, Figure A9).

Following incubation with 600 μM Zn-HSA (± myristate) an increase in the relative intensity of the Zn_1-HRGP330 was observed as shown in Figure 6.5. The control HRGP330 sample (Figure 6.5 A) showed a slight amount of Zn^{2+} contamination (34%) most likely from the purification procedure. Following incubation with Zn-HSA the relative intensity of this peak increased by 7% compared to the control sample indicating that some Zn^{2+} had been obtained from HSA. This supports the data in the previous section of HRGP330 being a good competitor for Zn^{2+} even without fatty acid-induced Zn^{2+} release. In the presence of myristate there was a further increase of 4% in the relative intensity of the peak. Overall, this may indicate that slightly more Zn^{2+} was transferred from HSA to HRGP330 in the presence of fatty acids, but this could not be confirmed by ICP-OES analysis (see below).

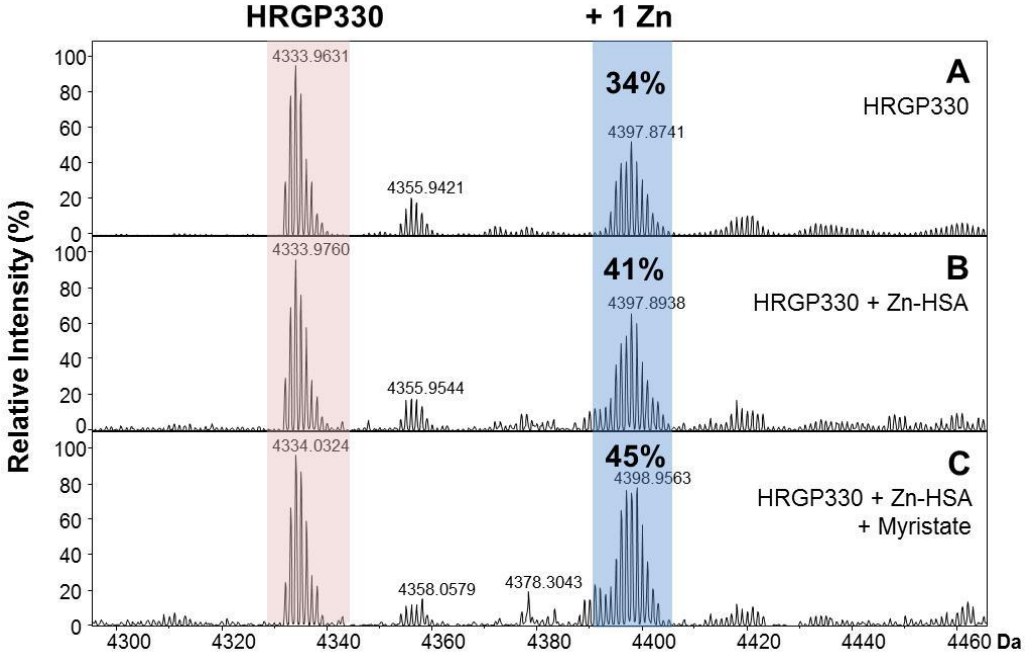

Figure 6.5 Relative intensity of Zn_1-HRGP330 following incubation with Zn-HSA (± myristate). A) HRGP330 control sample B) 20 μM HRGP330 incubated with 600 μM Zn-HSA C) 20 μM HRGP330 incubated with 600 μM Zn-HSA with 5 mol. equiv. myristate. Mass spectrometry was carried out on a maXis-UHR-TOF in 10 mM ammonium acetate (pH 7.4)

Elemental analysis was carried out on the HSA fractions. The results in Figure 6.6 showed a greater amount of Zn^{2+} associating with HSA in the presence of myristate: 0.74 Zn^{2+} ions per HSA compared to 0.66 Zn^{2+} determined for the control sample. With the addition of HRGP330 there was a decrease of the Zn^{2+} interacting with HSA which is consistent with an increased amount bound to HRGP330 as demonstrated by ESI-MS (Figure 6.5 B).

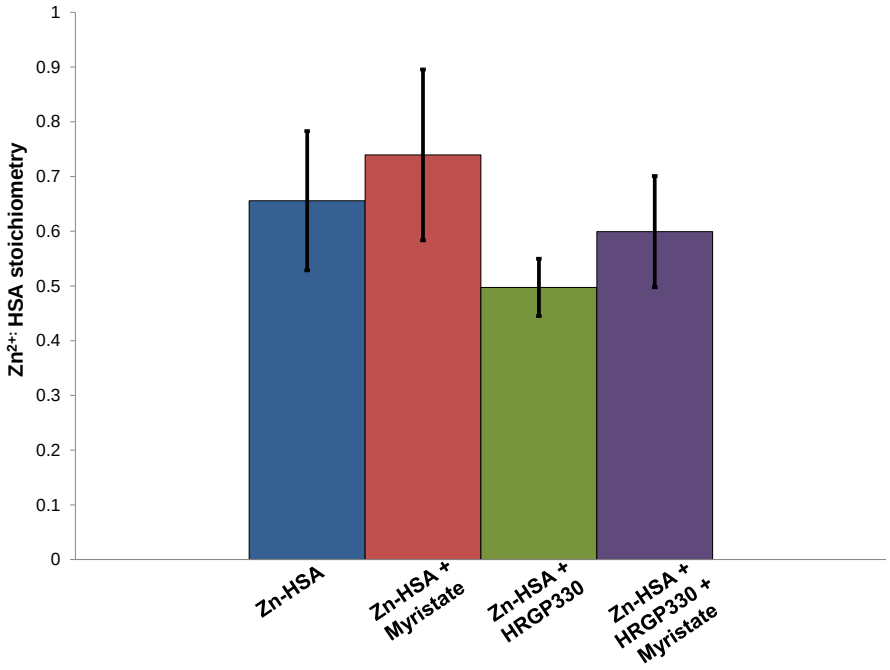

Figure 6.6 HSA:Zn^{2+} stoichiometry (600 μM) in the presence of 20 μM HRGP330 (± myristate). Samples were prepared in 10 mM ammonium acetate at pH 7.4. Following incubation with the ligands HSA was separated from HRGP330, diluted in 0.1 M HNO_3 and analysed on a Perkin Elmer Optima 7500 DV.

The quaternary system, with the addition of myristate, showed slightly more Zn^{2+} bound to HSA than only with HRGP330: 0.60 Zn^{2+} per HSA with myristate compared to 0.50 Zn^{2+} with no myristate. Importantly, both HSA samples allowed to react with HRGP330 had less Zn^{2+} bound than those without HRGP330 which is good agreement with the increases in

Zn^{2+}-bound HRGP330 shown in Figure 6.5 B and C. Overall, this would indicate that even when HSA is in significant excess, as in plasma, a small proportion of Zn^{2+} becomes bound to HRG.

ESI-MS and ICP-OES results indicate that HRGP330 can readily compete for Zn^{2+} under these conditions. This is in good agreement with the work by Guthans and Morgan (1982). Based on the original hypothesis it was expected that Zn^{2+} transfer would only occur between HSA and HRGP330 in the presence of fatty acids. Therefore, the question to address is would HRG carry Zn^{2+} endogenously or would it only come into play if Zn^{2+} was displaced from another protein i.e. through elevated fatty acids? Overall this work is in agreement with the former conclusion. Although HRG is present at relatively low abundance in comparison to other proteins thought to be major Zn^{2+} transporters, it could be able to compete with these because of its high number of potential metal binding sites. If it is assumed that HRG binds 10 metal ions and is 2 μM in human plasma (Morgan *et al*., 1978) then the effective binding site concentration is as high as 20 μM. This could be an explanation as to why HRGP330 binds preferentially to Zn^{2+} in the presence of HSA *in vitro* although it is unclear as to if this is something that could occur *in vivo*. It is important to note that these experiments were carried out at low ionic strength due to the low tolerance of ESI-MS to salts, however, changes in ionic strength could affect the stability of the metal:protein complexes.

6.2.5 Investigation of metal binding between HSA and HRGP330 at plasma Zn^{2+} concentrations

Experiments were carried out with physiologically relevant Zn^{2+} concentrations using a combination of size exclusion chromatography (SEC) and inductively coupled plasma mass spectrometry (ICP-MS). These techniques are also more amenable to high concentrations of salt and so the effect of this can be probed. Calibration of the column was achieved using HSA (66.5 kDa) and insulin B chain (3.5 kDa) as shown in Figure 6.7. The two proteins eluted at 7 ml and 9 ml respectively.

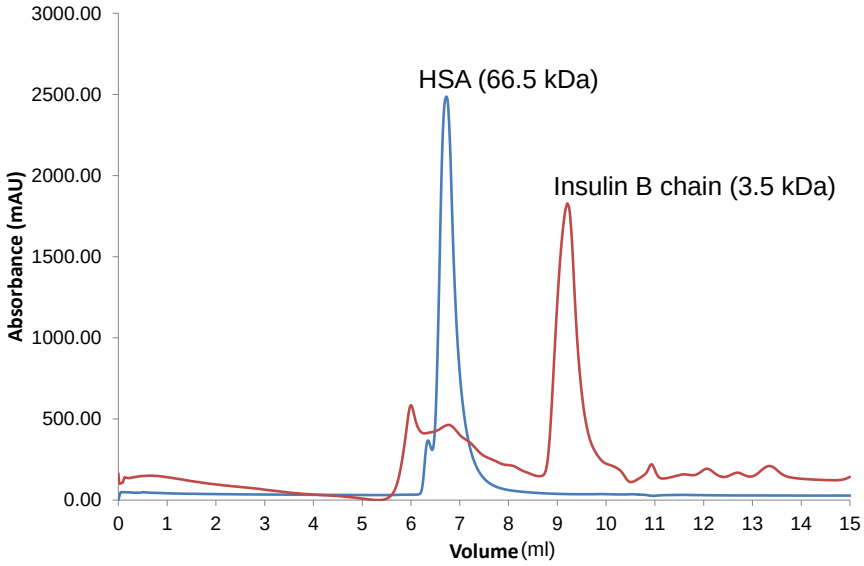

Figure 6.7 Elution of HSA and insulin B chain on a BioSep-SEC-2000 column. HSA eluted at 7 ml (*blue*) which is 66 kDa. Insulin B chain which is 3.5 kDa eluted at 9-10 ml (*red*) which indicates HRGP330 (4.3 kDa) should elute in similar fractions. The buffer was 10 mM HEPES, 50 mM NaCl (pH 7.4).

Insulin B-chain has a similar size to HRGP330, therefore they would be expected to elute around the same volume. Surprisingly, when a concentrated HRGP330 sample was loaded onto the column, an increase in absorbance at 220 nm at an elution volume of 11-12 ml was observed (blue trace of Figure 6.8 A). The fact that this fraction has absorbance at

220 nm but not 280 nm also suggests that this is HRGP330 as it has a lack of aromatic residues (inset of Figure 6.8 A). Some residual HSA from a previous run was also observed at a lower intensity in the HRGP330 sample (sharp peak in blue trace at 7.40 ml). Therefore it would appear that HRGP330 elutes ~1 ml later than expected.

To investigate plasma concentrations of Zn^{2+} with respect to HSA and HRGP330, samples of HSA (600 μM) and HRGP330 (20 μM) were incubated at 37 °C with 25 μM $ZnCl_2$ and one sample included the addition of 5 mol. equiv. myristate. The proteins were applied to a BioSep- SEC-2000 gel filtration column and the fractions were analysed for Zn^{2+} content (ICP-MS) and protein content (BCA assay). As can be seen in Figure 6.8 B the Zn^{2+} detected at ppb levels eluted with the HSA across the fractions labelled 7 and 8. This is consistent with chromatographic separation of both human and rabbit plasma which has shown that the majority of Zn^{2+} elutes with HSA (Muñiz *et al*., 2001; Manley *et al*., 2009). The HRGP330 could not be observed in the UV chromatogram due to the lower concentration used in these samples. Interestingly, in the presence of myristate, the concentration of Zn^{2+} eluting with HSA was considerably reduced to 300 ppb (Figure 6.8 C) compared to 600 ppb without myristate. This is one piece of evidence that myristate could shift the Zn^{2+} distribution from HSA at physiologically relevant Zn^{2+} levels. One reason for this result could be the presence of salt in the buffer, as ionic strength may affect the stability of the

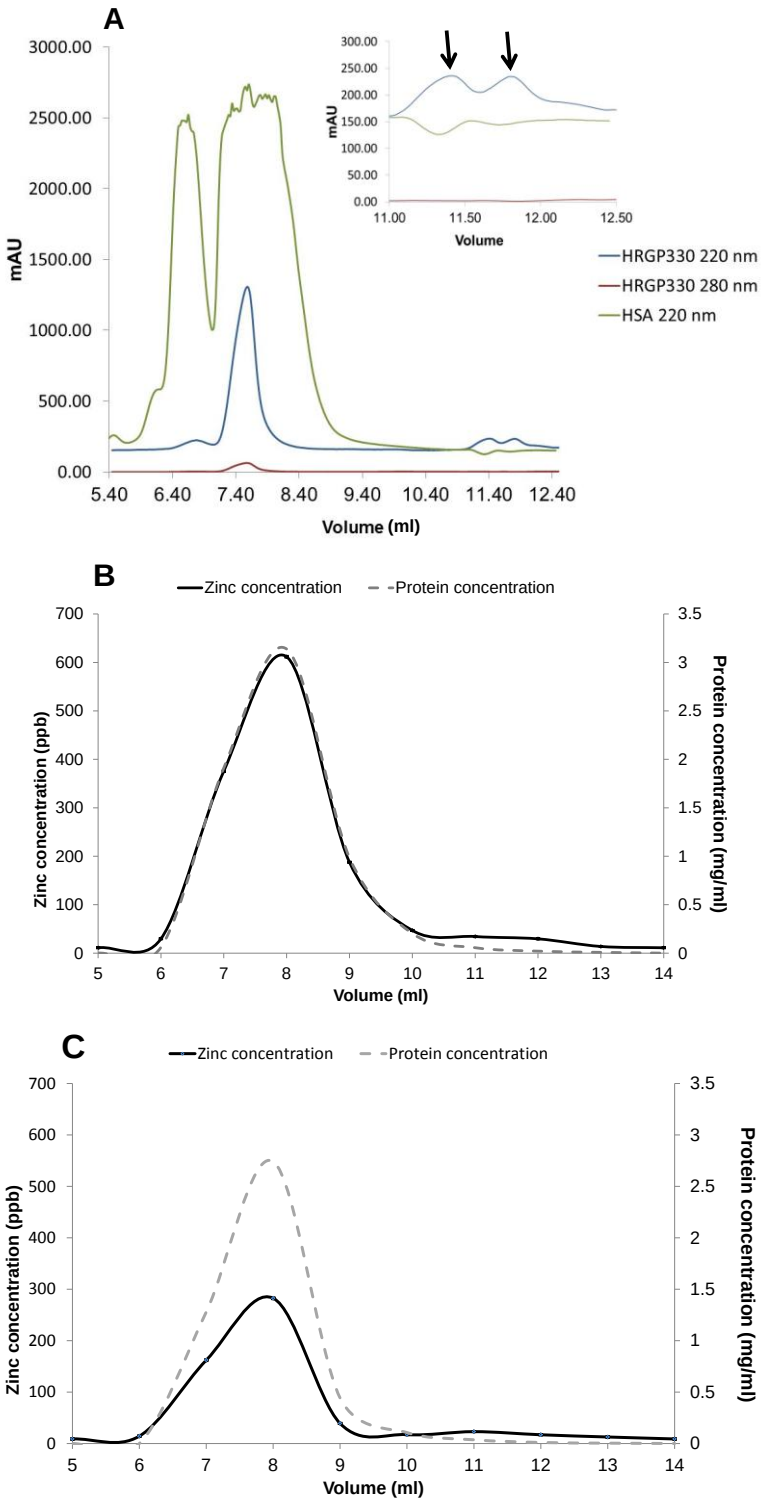

Figure 6.8 Elution of HSA and HRGP330 from a BioSep-SEC-2000 column. A) Chromatograms for HSA (*green*), HRGP330 at 220 nm (*blue*) and HRGP330 at 280 nm (*red*). The inset shows an increase in absorbance at 220 nm at 11.50 ml which could correspond to elution of HRGP330. B) Zn^{2+} concentration (*black*) and corresponding protein concentration (*grey, dashed line*) of fractions when a sample of 600 μM HSA, 20 μM HRGP330 and 25 μM $ZnCl_2$ was applied to the column C) 600 μM HSA, 20 μM HRGP330 and 25 μM $ZnCl_2$ with 5 mol. equiv. myristate. The buffer was 10 mM HEPES, 50 mM NaCl (pH 7.4).

metal:protein complex, although this is a further avenue that needs exploring. On analysis of the Zn^{2+} content of fractions eluting at 11-12 ml there does appear to be a small peak in Zn^{2+} concentration at 11-12 ml, however, no significant difference was observed between the samples with or without myristate. One possibility is that free Zn^{2+} that had been shifted from HSA may elute in another fraction although this could not be concluded from this experiment. It would appear that under these conditions, myristate was able to perturb metal binding although other work has provided non-conclusive evidence for this.

6.2.6 Estimation of the apparent binding constant for Zn-HRGP330

Zincon was used in a competition assay to determine an apparent binding constant (K_{app}) for HRGP330. Complexation of Zincon with Zn^{2+} produces a 1:1 complex with a blue colour and a characteristic absorbance at 620 nm. This absorbance can be exploited to assess the binding of Zn^{2+} to peptides and proteins (Shaw *et al*., 1990; Mekmouche *et al*., 2005; Armas *et al*., 2006; Talmard et al., 2007).

Titrating increasing amounts of HRGP330 into the Zn^{2+}-Zincon complex produced a decrease in the absorbance at 620 nm (Figure 6.9). Approximately 4.8 μM HRGP330 was required to reduce the absorbance at 620 nm by 50% which indicates that half of the Zn^{2+} originally bound to Zincon had been transferred to HRGP330. A plateau in the absorbance is reached relatively quickly which demonstrates that Zn^{2+} exchange between HRGP330 and Zincon is rapid. The results indicate that the

binding constants are globally similar but HRGP330 is a slightly stronger Zn^{2+} binder than Zincon. The K_{app} for Zincon has previously been determined to be 7.9 x 10^4 M^{-1} at pH 7.4 (Shaw *et al*., 1990) and more recently a slightly different value of 8.5 x 10^4 M^{-1} was found by Mekmouche *et al*. (2006) under 50 mM HEPES, 100 mM NaCl at pH 7.4. Using this value, Equation 3 in the experimental methods can be used which results in a K_{app} for HRGP330 of 2.7 x 10^5 M^{-1}

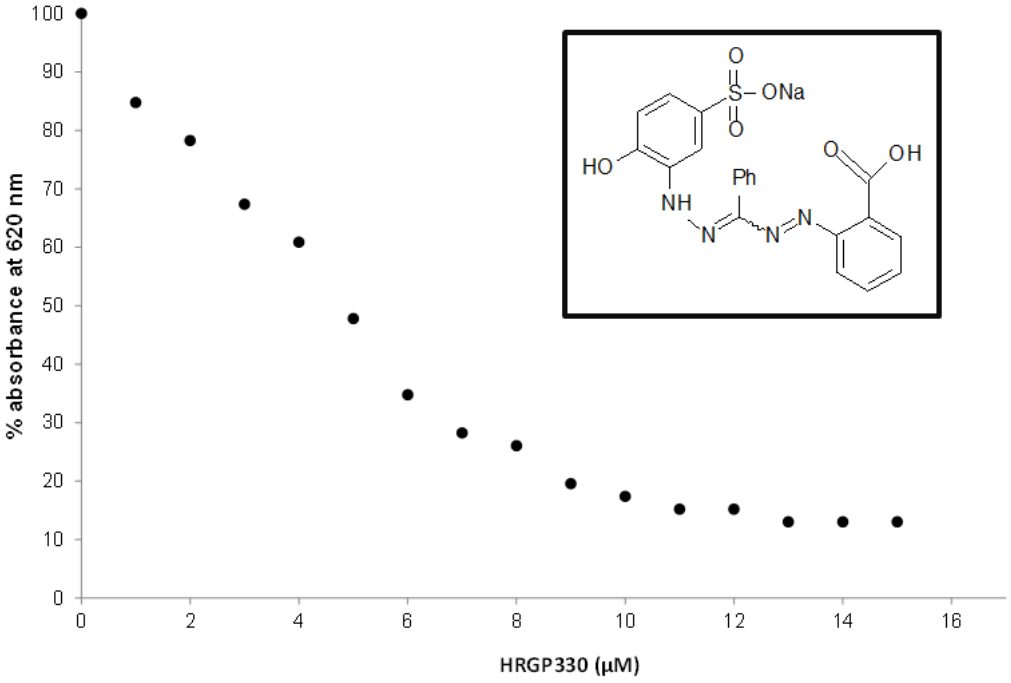

Figure 6.9 Estimation of the apparent binding constant of Zn^{2+} and HRGP330 using competition with Zincon. HRGP330 was titrated into a solution of 10 μM Zincon and 5 μM $ZnCl_2$ in 50 mM HEPES, 100 mM NaCl, pH 7.4. 100% relative absorbance corresponds to the maximum absorbance observed at 620 nm at t=0 and t=∞. The inset shows the structure of Zincon.

As HRGP330 is able to obtain Zn^{2+} from the 1:1 Zn^{2+}-Zincon complex this would suggest it is also able to rapidly acquire Zn^{2+} from other available donors, including HSA under appropriate conditions. This result yields an apparent log*K* of 5.43 which is in the same range as the values published

for full length HRG (Table 1.4) therefore it would appear that HRGP330 has a similar binding affinity to the intact protein. Differences will be due to the different buffer conditions and ionic strengths used. Recently, our laboratory has determined an apparent log*K* of 5.67 for Zn^{2+} binding to BSA in 50 mM Tris, 50 mM NaCl at pH 7.2 (Lu *et al*., 2012b). Therefore, although BSA or HSA would bind Zn^{2+} with greater affinity than HRG, the high number of potential binding sites may mean the binding capacity of HRG is underestimated. It would be invaluable to assess the binding affinity of HSA and human HRG under the same conditions by a method such as ITC although there may be difficulties in comparing a cooperative binder (HRG) to a non-cooperative binder (HSA).

6.2.7 Cu^{2+} transfer between Gly-Gly-His and HRGP330

The major Cu^{2+} binding site on HSA is the N-terminal ATCUN-motif. Gly-Gly-His is a peptide mimic of this site that has been previously studied as a model for the N-terminal site (Figure 6.10). The apparent stability constant for the Cu^{2+}-peptide complex has been shown to be log*K* = 16 compared to 16.2 for Cu^{2+}-HSA (Lau *et al*., 1974). Although most of the ligands that interact with HRG are thought to be mediated by Zn^{2+} binding to the HRR, these associations could also be influenced by the concentration of Cu^{2+}. Borza and Morgan (1998) confirmed that the only other transition metal apart from Zn^{2+} to be effective at promoting heparin binding to HRG at physiological pH was Cu^{2+}. Binding of Cu^{2+} to rabbit HRG has also been shown to be stronger than Zn^{2+} (Morgan, 1981). In fact, analysis of serum indicates that while the concentration of Zn^{2+} is

reduced in human cancers (Kuo *et al*., 2002), plasma Cu^{2+} levels are actually increased (Coates *et al*., 1989). Therefore, it must be acknowledged that Cu^{2+} could potentially be biologically relevant for HRG although the question still remains as to whether it contributes significantly to anti-angiogenic activity.

ESI-MS experiments of Gly-Gly-His showed binding of 1 equivalent of Cu^{2+} which is consistent with the literature. Cu^{2+} distribution between Gly-Gly-His and HRGP330 was also studied using this technique. First the Cu^{2+}-Gly-Gly-His complex was formed which can be observed at 331 *m/z* in spectra A and C in Figure 6.11.

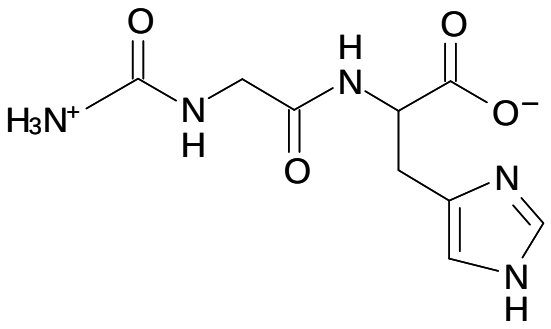

Figure 6.10 Structure of Gly-Gly-His. The peptide mimic for the N terminus of HSA.

This was reacted with 1 or 0.2 mol. equiv. of HRGP330, shown in Figure 6.11 B and D respectively. With addition of 1 mol. equiv. of HRGP330, the intensity of ESI-MS peaks corresponding to the Cu^{2+}-Gly-Gly-His species reduced considerably to 10% relative intensity from 69% and the peak at 270 *m/z*, corresponding to Gly-Gly-His without a metal ion, became the most abundant species (Figure 6.11 B). This showed that

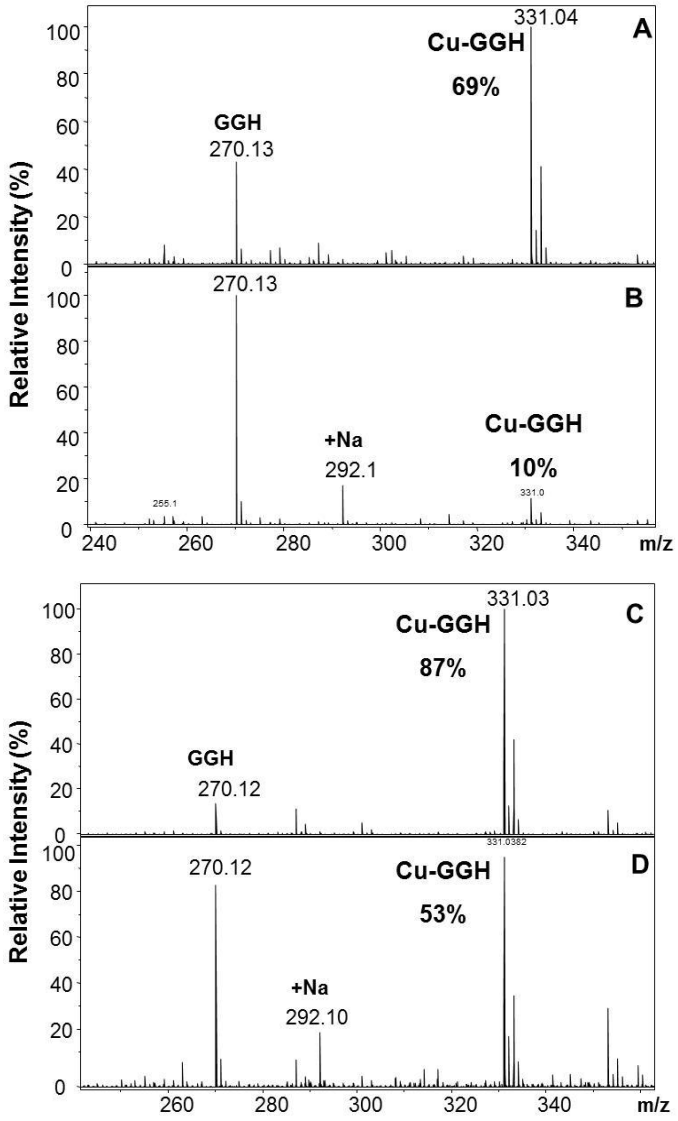

Figure 6.11 Effect of HRGP330 on Cu^{2+} binding to Gly-Gly-His. Cu^{2+} was allowed to react with Gly-Gly-His producing the spectra in A and C. HRGP330 was added at concentrations of 1 mol. equiv. (B) and 0.2 mol. equiv. (D). Samples were prepared in 10 mM ammonium acetate at pH 7.4 and analysed on a maXis-UHR-TOFinstrument.

Cu^{2+} transfer had occurred to HRGP330. A similar approach was to add 1 mol. equiv. of Cu^{2+} to a 1:1 HRGP330:Gly-Gly-His: the same result was achieved as the metal ion preferentially bound to HRGP330 over Gly-Gly-His. As HRGP330 was clearly shown to be able to bind up to 5 metal ions in Chapter 5, this reaction was repeated with 0.2 mol. equiv. HRGP330. This means that the potential binding sites between the two peptides are approximately equal. At this concentration there was a significant

increase in the 270 *m/z* peak to the point where a 50:50 ratio of Gly-Gly-His and Cu^{2+}-Gly-Gly-His was observed. This experiment indicated that not all of the Cu^{2+} had been transferred to HRGP330. At this point it can be assumed that globally the binding affinities are roughly similar as approximately half of Cu^{2+} is bound to each peptide. This result is surprising as Gly-Gly-His binds to Cu^{2+} with a much stronger affinity than proposed for HRG: log*K* = 16 for Cu^{2+}-Gly-Gly-His (Lau et al., 1974) compared to ~6.70 for Cu^{2+}-HRG (Morgan, 1981). Therefore, it may be that case that the large number of potential binding sites makes Cu^{2+} binding to HRGP330 more favourable. These results indicate that one route through which HRG may obtain Cu^{2+} in plasma could be through transfer from HSA. Furthermore, as Cu^{2+} binds to HRG more strongly than Zn^{2+} then it would be feasible that Cu^{2+} would sufficiently block metal binding sites and this might have consequences for the Zn^{2+}-dependent activities of HRG.

6.2.8 Implications of Zn^{2+} transfer to HRG: effect of Zn^{2+} on HRGP330 binding to heparin

The results described in this chapter have suggested that, using HRGP330 as a mimic, Zn^{2+} would transfer from HSA even without elevated fatty acid levels to displace Zn^{2+} from HSA under the conditions used. One consequence of Zn^{2+} being transferred to HRG would be an increase in its biological activities as evidence has suggested that its interactions with other biomolecules are enhanced by Zn^{2+}. Native HRG has a pI of 6.45 so will be negatively charged at physiological pH.

However, through interactions with metal ions it can acquire positive charges which facilitate complex formation with other ligands such as heparin. It has been demonstrated that HRG is the only plasma protein that can compete with antithrombin for heparin which gives an insight into the importance of this interaction. This is likely because the dissociation constant of heparin binding to human HRG has been reported to be 7 nM (Lijnen *et al*., 1983). To investigate one biological implication of HRG obtaining Zn^{2+} from HSA, the interaction of HRGP330 with a heparin dodecasaccharide (Figure 6.12) was investigated by ESI-MS. Previous data have shown that this gives maximal binding to a related peptide, HRGP335 (Vanwildemeersch *et al*., 2006).

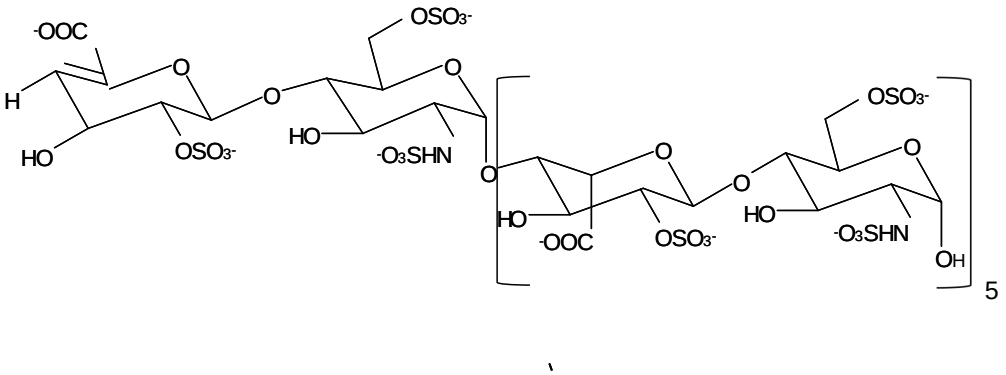

Figure 6.12 Chemical structure of the heparin dodecasaccharide (dp12) used in this work.

There are examples of work where ESI-MS has be used to observe complexes of heparin with a fibroblast growth factor (Harmer *et al*., 2004; Harmer *et al*., 2006) and a chemokine (Przybylski *et al*., 2010). The average mass of the heparin dodecasaccharide (dp12) was 3550 Da. Following incubation of dp12 with HRGP330 at a 1:1 mol. ratio, a new group of peaks became visible that were centred around 1550 and 1950

m/z (Figure 6.13 A). These corresponded to the 5+ and 4+ charge states of a 1:1 HRGP330:dp12 complex which has a theoretical mass of 7883 Da. Low intensity peaks for unbound dp12 were also observed between these charge states. Although some complex formation was detected between the peptide and the heparin, in the presence of 1 mol. equiv. Zn^{2+}, the intensity of the complex was increased more than two-fold : 18% relative intensity of the complex compared to 7% without Zn^{2+} (Figure 6.13 B).

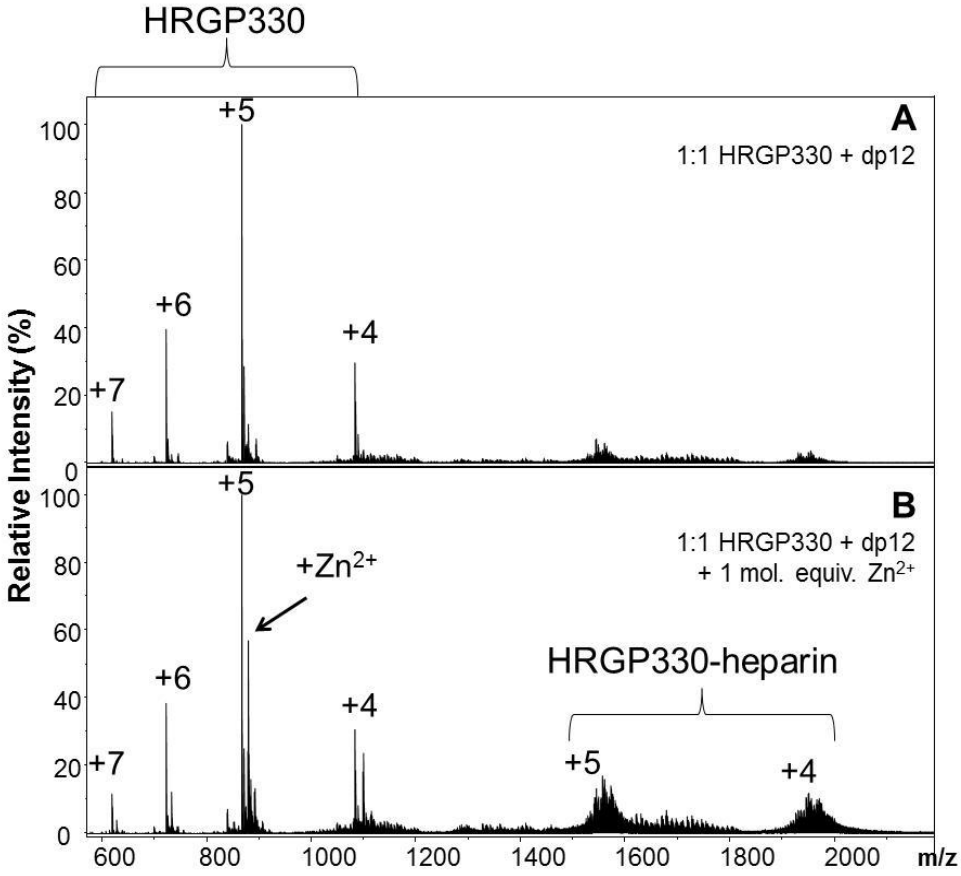

Figure 6.13 ESI-MS shows increased HRGP330:dp12 complex in the presence of Zn^{2+}. A) HRGP330 was incubated with 1 mol. equiv. of heparin dodecasaccharide B) HRGP330 was incubated with Zn^{2+} prior to addition of dp12. A greater amount of the complex was formed with Zn^{2+} as judged by the relative intensities of the peaks.

This is the first ESI-MS evidence of heparin binding to a HRG-derived peptide. Currently, there are no examples of His-rich peptides binding to

heparin in the gas phase, therefore, this result indicates that the complexes are strong enough to be detected. Furthermore, this adds support to the argument that heparin binding occurs at the HRR. There has been much debate over this in recent years with one study demonstrating that the N-terminal domain bound to immobilised heparin and cell-surface heparan sulphate while no interaction was observed with HRR-derived peptides (Jones *et al*., 2004). It is surprising that such a large fragment of heparin can bind to a relatively small peptide, however, longer fragments may have multiple sites that can interact with the peptide and stabilise the association. The fact that the formation of the complex appears to be enhanced by the presence of Zn^{2+} is in good agreement with the literature. The complex spectra contained many overlapping peaks although a close-up view of the 5+ charge state provides evidence for the fact that Zn^{2+} is bound to the complex (Figure 6.14). Two sets of abundant peaks (marked with * and †) are visible in Figure 6.14 A and the difference between them is an SO_3 group (80 Da). The other peaks are attributed to ammonia and sodium adduction. In the presence of Zn^{2+} these peaks are clearly shifted by 63 Da (Figure 6.14 B) therefore it is indeed possible that a ternary complex of HRGP330-Zn^{2+}-dp12 exists in the gas phase. This observation is consistent with the suggested mechanism that the interaction is mediated by metal ions bound to HRG and the addition of EDTA completely abolishes complex formation (Lijnen *et al*., 1983).

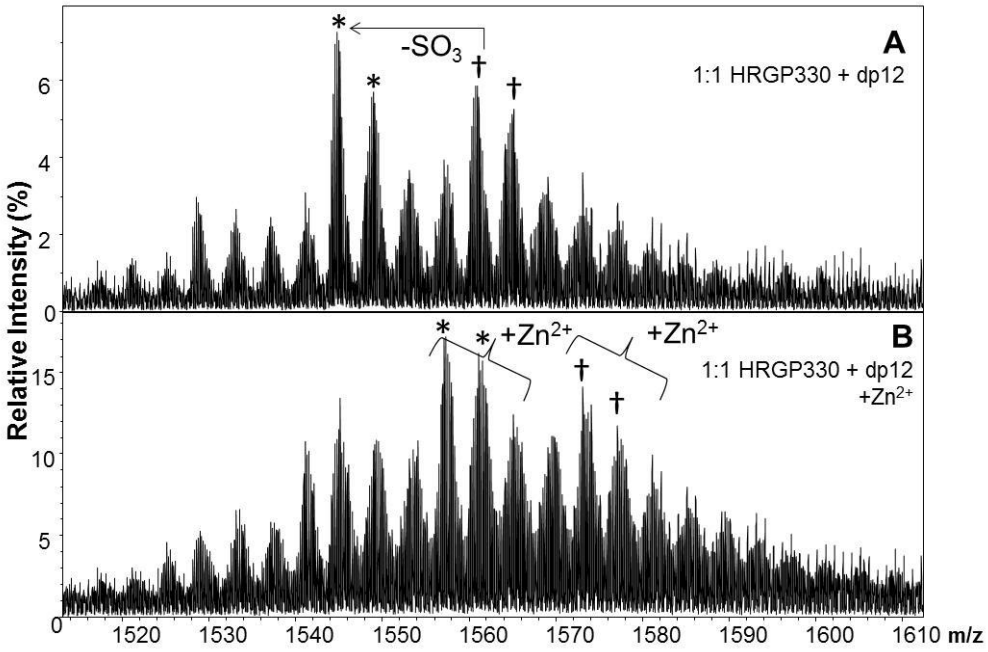

Figure 6.14 Close-up view of the 5+ charge state of HRGP330:heparin complex. A) HRGP330 incubated with 1 mol. equiv. of heparin dodecasaccharide shows two sets of abundant peaks marked with * and †. The difference between them is 80 Da which corresponds to loss of an SO_3 group. B) The complex with addition of Zn^{2+} shows that these peaks are still most abundant and shifted by the mass of 63 Da i.e. addition of a Zn^{2+} ion.

6.9 Conclusion

ESI-MS has demonstrated that Zn^{2+} transfer can occur from HSA to HRGP330 even in the absence of fatty acids. Even with HSA in significant excess, as would be in plasma, an increase in Zn^{2+} bound to HRGP330 was still detected. This indicates that the affinities of HSA and HRG are very close to each other, however, this could depend on the solution conditions. At low ionic strength, HRG displays higher affinity, whilst the data presented in section 6.2.5 suggest that at higher ionic strength, HSA retains bound Zn^{2+}. Therefore, the question remains: is HRG carrying Zn^{2+} endogenously or would it only obtain Zn^{2+} if there was a change in the plasma conditions? This work provides support for the former conclusion. The apparent dissociation constant determined

appeared to be in good agreement with these experimental observations although further work, such as ITC, is warranted to make direct comparisons with full length HRG. HRGP330 is also able to compete for HSA-bound Cu^{2+} which could have implications for the activities of HRG as this metal ion has been shown to mediate some HRG-ligand interactions.

SEC revealed that at physiologically relevant Zn^{2+} concentrations, the metal ion eluted with HSA and no increase in Zn^{2+} was observed in the fractions corresponding to HRGP330. This SEC approach could be utilised to analyse whole plasma samples and detect less abundant Zn^{2+} binding plasma proteins although a higher resolution separation method may be desirable to separate HSA and HRG which are close in size (66 kDa compared to 75 kDa). With regards to biological consequences of Zn^{2+} transfer to HRG, experiments with heparin as a model ligand showed a larger amount of HRGP330:heparin complex formation with Zn^{2+} as assessed by ESI-MS. This is the first ESI-MS evidence of a heparin complex with a peptide derived from HRG.

Chapter 7

Conclusion

7.1 Summary of observations

7.1.1 Native ESI-MS of HSA-ligand complexes

In Chapter 3, methods were developed to study HSA in its native form using ESI-MS. This proved challenging as the gentle conditions allowed buffer and salt adducts to remain bound to the protein. However, once these could be effectively removed, single metal ion binding to HSA was detected. The addition of fatty acids to HSA did not yield any significant mass increase, therefore, it was concluded that the interactions with these must be broken on entering the gas phase. Evidence to support this was obtained by observing a protonated myristic acid molecule in the low mass range while infusing HSA-myristate complexes into the mass spectrometer.

In contrast, a perfluorinated derivative of octanoic acid was found to remain bound in the gas phase and also a ternary HSA-PFOA-Zn^{2+} complex was detected. This is in agreement with molecular modelling that indicates the binding of octanoate does not induce a conformational change great enough to abolish metal binding at Site A (Lu *et al*., 2012b). Recently, a perfluorinated derivative of myristic acid has become commercially available and so this could be tested in the future. It would appear that these molecules are good fatty acid mimics and the

hydrophilic nature of fluorine can be exploited to preserve the binding of these molecules in the gas phase.

TWIM-MS was also used as a novel technique to study the conformation of HSA and its complexes in Chapter 4. The estimated collisional cross section for apo-HSA was in good agreement with that calculated from the X-ray crystal structure (1AO6). No change in conformation was seen in the presence of Zn^{2+} or Cd^{2+} although the collisional cross section was slightly larger upon Cd^{2+} binding. Increasing the cone voltage provided sufficient energy for HSA to begin to unfold although with the addition of Zn^{2+}, less of these extended conformations were detected which is evidence that occupation of Site A confers some stability onto the domain I/domain II interface. Although the fatty acids appeared to dissociate from HSA in the gas phase, the myristate-bound sample showed an increased collisional cross section compared to that to fatty acid-free HSA. This could indicate that a conformational change takes place within the protein upon fatty acid binding but that the protein doesn't revert back to its normal fatty acid-free conformation during the timescale of the IM experiment.

7.1.2 Metal binding properties of HRGP330

In the work reported in Chapter 5, a peptide derived from the HRR of HRG was studied by various techniques. Complexes with Zn^{2+}, Cd^{2+} and Cu^{2+} were able to be observed in the gas phase and CD spectroscopy suggested a conformational change occurs upon Zn^{2+} binding. A dimeric

form of HRGP330 was identified only in the presence of Zn^{2+} which could give an important insight as to how multimeric complexes of HRG form in plasma. To obtain further information on residues involved in metal binding, NMR analysis was carried out in the absence and presence of Zn^{2+}. The addition of the metal ion ligand significantly broadened the signals suggesting that the binding to the peptide is dynamic. This precluded gaining any structural information from NMR spectroscopy although using sub-stoichiometric quantities may allow this to a greater extent.

TWIM-MS confirmed that a change occurred to the peptide upon Zn^{2+} binding as the estimated cross sectional area of the Zn^{2+}-bound complexes were observed to be significantly more compact than apo-HRGP330. Top-down ESI-MS was then utilised to map the Zn^{2+} binding sites within the peptide. High sequence coverage was obtained from both CID and ETD/PTR of HRGP330 which could be due to a lack of conventional secondary structure which allows it to fragment easily. Zn^{2+}-bound fragments from both N- and C- terminal ends of the molecule were detected which implies several His residues have a similar affinity for the metal ion. During the ETD/PTR experiment the sequence coverage was dramatically reduced and fewer fragments were identified. Intriguingly, the most pronounced loss of fragments was observed around the GHHPH pentapeptide although further studies are required to completely rationalise this.

Overall the data suggest that a conformational change within the peptide could have occurred upon Zn^{2+} binding that was unable to be overcome by the ETD mechanism which can maintain weaker linkages. This work could have implications for the study of His-rich proteins by mass spectrometry as interestingly one of the other studies to retain Zn^{2+} binding during MS/MS also concerns a His-rich protein (Buré *et al*, 2009a and 2009b). There has also been little research into how metal cations may affect the processes involved in the ECD or ETD mechanisms although it has been suggested that they may act as an electron sink (Zubarev *et al*., 2002). This could be another explanation for the significant decrease in fragmentation upon Zn^{2+} binding, although further investigation is needed.

7.1.3 Metal ion distribution between HSA and HRGP330

Competition experiments between HSA and HRGP330 showed that the majority of Zn^{2+} was transferred to HRGP330. The presence of fatty acids had no further effect on this distribution, which indicates that HRG could be an important competitor for Zn^{2+} in normal plasma. However, this is in agreement with Chapter 3 which showed no loss of Zn^{2+} in the presence of myristate under the conditions used. Competition with Zincon suggested the apparent binding constant for Zn-HRGP330 was similar to that for full-length HRG which validated the potential biological significance of the observations in Chapter 6. The exact role of HRG is uncertain although it would appear from these results that it would be

found in a Zn^{2+}-bound state endogenously even with high concentrations of HSA.

It is also important to note that other factors may trigger an increase in Zn^{2+} concentration in plasma which could affect the activities of HRG, for example at sites of injury degranulating platelets can release high concentrations of Zn^{2+} that are 30-60 times higher than plasma levels with the metal ion distributed between the cytoplasm and α-granules (Gorodetsky *et al*., 1993; Marx *et al*., 1993). Taken together with the information that HRG is also released from human platelets (Leung *et al*., 1983) then this could clearly be another route through which the Zn^{2+}-dependent activities of HRG are modulated. More recent evidence has indicated that activated platelets contained the antiangiogenic fragment of the HRR with one possibility being that the large increase in Zn^{2+} concentration could stimulate proteolysis to release this active domain. In the tissue of cancer patients, this peptide was also found to associate with the vessel wall but no binding was observed in healthy patients (Thulin *et al*., 2009).

Additionally HRG could become activated through low pH to the extent that Borza and Morgan (1998) suggested an important role as a plasma pH sensor. During hypoxia or ischemia an onset of acidosis can occur which could be extremely detrimental to tissues (Levine, 1993). This would cause the His sidechains to become protonated and would enhance the interaction with negatively charged glycosaminoglycans on

the cell surface. Apart from HMWK, HRG appears to be the only plasma protein that can be regulated in this way. Some parallels can be drawn between HMWK, a cofactor in blood coagulation, and HRG as numerous reports have found that binding of HMWK to endothelial cells is Zn^{2+}-dependent (van Iwaarden *et al*., 1988; Schmaier *et al*., 1988; Joseph *et al*., 1996). Although, HMWK may not act as a pH sensor to the same extent as HRG as the His-rich region contains a greater number of Arg and Lys which are permanently protonated at physiological pH. As a whole, this evidence points toward HRG being a unique protein whose multi-domain structure and polycationic nature are extremely important for the formation of functional complexes in plasma.

More recently it has been acknowledged that Cu^{2+} could be biologically relevant for HRG, although given the fact that only 5-10% of exchangeable serum Cu^{2+} is bound to HSA it is questionable whether a proportion would be bound to HRG. The competition experiments with the N-terminal peptide mimic of HSA in Chapter 6 showed that HRG is able to compete with the N-terminus even though Gly-Gly-His has a higher binding affinity for Cu^{2+} than HRG. This could be due to the large number of possible binding sites as Cu^{2+} can deprotonate backbone amides and may only require two additional imidazole side chains for stable binding. This could have important consequences for Cu^{2+} homeostasis, because if the levels of Cu^{2+} are increased in tumours then the expression of Cu^{2+}-carrying proteins may be upregulated (Lowndes and Harris, 2005). There is ongoing work to use Cu^{2+}-chelators as a therapeutic strategy to combat

tumour angiogenesis, one example being Tetrathiomolybdate (TM) which significantly reduced Cu^{2+} levels in clinical trials (Redman *et al*., 2003).

7.2 Future directions

1. Native mass spectrometry of full-length HRG

No detailed structural information is available on HRG and suggestions have only been made based on analysis of the fragments obtained from proteolysis. Analysis of HRGP330 by TWIM-MS highlighted a possible conformational change upon Zn^{2+} binding therefore this could be verified by gas-phase studies of full-length HRG. Most of the observations in the literature have been made using *in vitro* model peptides although many of these show the same biological activity of HRG therefore it could be argued that in this case these studies are relevant.

2. Investigate the binding of other fatty acid molecules to HSA using TWIM-MS

As TWIM-MS was able to identify an increased collisional cross section for myristate-HSA, it would be of interest to study the conformational changes induced by fatty acids of different chain lengths. Furthermore, a titration could be carried out with varying fatty acid concentrations to follow the changes that occur to the protein structure.

3. Zn^{2+} distribution between HSA and HRG

This work has utilised a peptide derived from the His-rich region as there are challenges associated with isolating sufficient amounts of human

HRG from plasma. Further investigations are warranted using a direct comparison between human HSA and HRG which would have more relevance than the studies using rabbit HRG. The influence of different buffers and ionic strengths also needs to be explored as this may impact upon binding affinities.

4. A metalloproteomics approach to characterising Zn^{2+} binding proteins in plasma: does Zn^{2+} associate with HRG endogenously?

It would be of great interest to develop protocols in order to isolate HRG from human plasma and determine the amount of Zn^{2+} associated with it. This is associated with difficulties as HSA is so abundant. Previous strategies to identifying less abundant proteins have involved targeted depletion of highly concentrated plasma proteins with antibody columns. A metallopoteomics approach to fractionating metal binding proteins in the marine cyanobacterium *Synechococcus* sp. WH8102 has recently been developed in our laboratory which could be applied to plasma samples (Barnett *et al*., 2012). It is important to note that due to its large number of binding partners in serum it is possible that HRG could be isolated in a complex with another biomolecule. It would also be interesting to achieve this from the point of view of Cu^{2+} to establish whether any Cu^{2+} is associated with HRG *in vivo*, considering it might be a stronger binder. Plasma samples could then be supplemented with fatty acids of varying chain lengths to see what effect this has on the metal ion distribution.

5. Analysis of clinical samples: can a correlation between fatty acids and Zn^{2+} be observed *in vivo*?

An important future direction would be to study clinical samples from patients with conditions known to be associated with elevated fatty acid levels. There is a growing body of evidence that indicates serum Zn^{2+} levels are reduced during diseases such as diabetes (Kinlaw *et al*., 1983; Chausmer, 1998) and cardiovascular disease (Shokrzadeh *et al*., 2009; Little *et al*., 2010). The fact that elevated fatty acids are also associated with diabetes, obesity (Boden and Shulman, 2002) and cardiovascular disease (Bhagavan *et al*., 2009) makes it even more pertinent that the relationship between these two nutrients is addressed. The allosteric binding of fatty/acid Zn^{2+} to HSA may go some way to explaining shifts in Zn^{2+} distribution observed during disease. Although many studies have analysed plasma levels of Zn^{2+} or fatty acid, testing needs to be carried out for both to assess if there is any correlation between them.

References

Anderson N.L. and Anderson N.G. (2002) The human plasma proteome: history, character, and diagnostic prospects. *Mol. Cell. Proteomics* **1**(11): 845-867.

Andreini C., Banci L., Bertini I. and Rosato A. (2006) Zinc through the three domains of life. *J. Proteome Res.* **5**(11): 3173-3178.

Appleton D.W. and Sarkar B. (1971) The absence of specific copper(II)-binding site in dog albumin: a comparative study of human and dog albumins*. J. Biol. Chem.* **246**(16): 5040-5046.

Armas A., Sonois V., Mothes E., Mazarguil H. and Faller P. (2006). Zinc(II) binds to the neuroprotective peptide humanin. *J. Inorg. Biochem.* **100**(10): 1672-1678.

Baczynskyj L., Bronson G.E. and Kubiak, T.M. (1994) Application of thermally assisted electrospray ionization mass spectrometry for detection of noncovalent complexes of bovine serum albumin with growth hormone releasing factor and other biologically active peptides. *Rapid Commun. Mass Spectrom.* **8**(3): 280-286.

Badman E.R, Myung S. and Clemmer D.E. (2005) Evidence for unfolding and refolding of gas-phase cytochrome c ions in a Paul trap. *J. Am. Soc. Mass Spectrom.* **16**(9): 1493-1497.

Bal W., Christodoulou J., Sadler P.J. and Tucker A. (1998) Multi-metal binding site of serum albumin. *J. Inorg. Biochem.* **70**(1): 33-39.

Barnett J.P., Scanlan D.J and Blindauer C.A. (2012) Fractionation and identification of metalloproteins from a marine cyanobacterium. *Anal. Bioanal. Chem.* **402**(10): 3371-3377.

Bar-Or D., Lau E. and Winkler J.V. (2000) A novel assay for cobalt-albumin binding and its potential as a marker for myocardial ischemia-a preliminary report. *J. Emerg. Med.* **19**(4): 311-315.

Bar-Or D., Winkler J.V., VanBenthuysen K., Harris L., Lau E. and Hetzel F.W. (2001) Reduced albumin-cobalt binding with transient myocardial ischemia after elective percutaneous transluminal coronary angioplasty: A preliminary comparison to creatine kinase-MB, myoglobin, and troponin I. *Am. Heart J.* **141**(6): 985-991.

Beermann C., Jelinek J., Reinecker T., Hauenschild A., Boehm G. and Klor H.U. (2003) Short term effects of dietary medium-chain fatty acids and n-3 long-chain polyunsaturated fatty acids on the fat metabolism of healthy volunteers. *Lipids Health Dis*. **2**(1): 10.

Benkestock K., Edlund P.O. and Roeraade J. (2005) Electrospray ionization mass spectrometry as a tool for determination of drug binding sites to human serum albumin by noncovalent interaction. *Rapid Commun. Mass Spectrom.* **19**(12): 1637-1643.

Berman H., Henrick K. and Nakamura H. (2003) Announcing the worldwide Protein Data Bank. *Nat. Struct. Mol. Biol.* **10**(12): 980.

Bertrand G. (1912) *8th Int. Congr. Appl. Chem.* New York. **28:** 30.

Bhagavan N.V., Ha, J.-S., Park J.-H., Honda S.A., Rios C.N., Sugiyama C., Fujitani G.K., Takeuchi I.K. and Ha C.-E. (2009) Utility of serum fatty acid concentrations as a marker for acute myocardial infarction and their potential role in the formation of ischemia-modified albumin: a pilot study. *Clin. Chem.* **55**(8): 1588-1590.

Bhattacharya A.A., Grune T. and Curry S. (2000) Crystallographic analysis reveals common modes of binding of medium and long-chain fatty acids to human serum albumin. *J. Mol. Biol.* **303**: 721-732.

Biemann K. (1982). Sequencing of proteins. *Int. J. Mass Spectrom. Ion Phys.* **45**: 183-194.

Biemann, K. (1992). Mass spectrometry of peptides and proteins. *Annu. Rev. Biochem.* **61**(1): 977-1010.

Bich C., Baer S., Jecklin M.C and Zenobi R. (2010) Probing the hydrophobic effect of noncovalent complexes by mass spectrometry. *J. Am. Soc. Mass Spectrom.* **21**(2): 286-289.

Blindauer C.A., Harvey I., Bunyan K.E., Stewart A.J., Sleep D., Harrison D.J., Berezenko S. and Sadler P.J. (2009) Structure, properties and engineering of the major zinc binding site on albumin. *J. Biol. Chem.* **284**(34): 23116-23124.

Boden G. and Shulman G.I. (2002) Free fatty acids in obesity and type 2 diabetes: defining their role in the development of insulin resistance and β-cell dysfunction. *Euro. J. Clin. Invest.* **32**: 14-23.

Borza D.-B., Tatum F.M and Morgan W.T. (1996) Domain structure and conformation of histidine-proline-rich glycoprotein. *Biochemistry* **35**(6): 1925-1934.

Borza D.-B. and Morgan W.T. (1998) Histidine-proline-rich glycoprotein as a plasma pH sensor. *J. Biol. Chem.* **273**(10): 5493-5499.

Bosshart H. and Heinzelmann M. (2003) Endotoxin-neutralizing effects of histidine-rich peptides. *FEBS Lett.* **553**(1-2): 135-140.

Breuker K. and McLafferty F.W (2003) Native electron capture dissociation for the structural characterization of noncovalent interactions in native cytochrome c. *Angew. Chem. Int. Ed.* **42**(40): 4900-4904.

Breuker K. and McLafferty F.W. (2008) Stepwise evolution of protein native structure with electrospray into the gas phase, 10^{-12} to 10^{-2} s. *Proc. Natl. Acad. Sci*. USA **105**(47): 18145-18152.

Brewer D. and Lajoie G. (2000) Evaluation of the metal binding properties of the histidine-rich antimicrobial peptides histatin 3 and 5 by electrospray ionization mass spectrometry. *Rapid. Commun. Mass Spectrom.* **14**(19): 1736-1745.

Brown R.E., Steele R.W., Marmer D.J., Hudson J L. and Brewster M.A. (1983) Fatty acids and the inhibition of mitogen-induced lymphocyte transformation by leukemic serum. *J. Immunol.* **131**(2): 1011-1016.

Burch M. K. and Morgan W.T (1985) Preferred heme binding sites of histidine-rich glycoprotein. *Biochemistry* **24**(21): 5919-5924.

Burch M.K., Blackburn M.N. and Morgan W.T. (1987) Further characterization of the interaction of histidine-rich glycoprotein with heparin: evidence for the binding of two molecules of histidine-rich glycoprotein by high molecular weight heparin and for the involvement of histidine residues in heparin binding. *Biochemistry* **26**(23): 7477-7482.

Buré C., Maget R., Delmas A.F., Pichon C., Midoux P. (2009a) Histidine-rich peptide: evidence for a single zinc-binding site on H5WYG peptide that promotes membrane fusion at neutral pH. *J. Mass Spectrom.* **44**(1):81-89.

Buré C., Pichon C., Midoux P. (2009b) Involvement of histidines 11, 15 and 19 in the binding of zinc to the fusogenic H5WYG peptide. *J. Mass Spectrom.* **44**(8): 1163-1170.

Cabrita L.D., Hsu S.-T. D., Launay H., Dobson C.M. and Christodoulou J. (2009) Probing ribosome-nascent chain complexes produced *in vivo* by NMR spectroscopy. *Proc. Natl. Acad. Sci. USA.* **106**(52): 22239-22244.

Cao Y., Han F.-M. and Chen, Y. (2007a) Studies on the non-covalent binding between berberine and human serum albumin by electrospray ion trap mass spectrometry. *Fenxi Kexue Xuebao* **23**(4): 389-392.

Cao Y., Han F. and Chen, Y. (2007b) Non-covalent binding between tectoridin and plasma proteins by electrospray ion trap mass spectrometry. *Zhongcaoyao* **38**(10): 1473-1476.

Carmeliet P. and Jain R.K. (2000) Angiogenesis in cancer and other diseases. *Nature* **407**(6801): 249-257.

Carter D.C. and Ho J.X. (1994) Structure of serum albumin. *Adv. Protein Chem.* **45:** 153-203.

Chan B., Dodsworth N., Woodrow J., Tucker A. and Harris R. (1995) Site-specific N-terminal auto-degradation of human serum albumin. *Eur. J. Biochem.* **227**(1-2): 524-528.

de Château M., Holst E. and Björck L. (1996) Protein PAB, an albumin-binding bacterial surface protein promoting growth and virulence. *J. Biol. Chem* **271**(43): 26609-26615.

Chausmer A. B. (1998) Zinc, insulin and diabetes. *J. Am. Coll. Nutr.* **17**(2): 109-115.

Chen R.F. (1967) Removal of fatty acids from serum albumin by charcoal treatment. *J. Biol. Chem.* **242**(2): 173-181.

Chen Y., Qi C., Chen H. and Han F. (2006) Study on noncovalent binding between ketoprofen and plasma protein by electrospray ion trap mass spectrometry. *Zhongguo Yaoxue Zazhi* **41**(6): 460-462.

Chernushevich I.V. and Thomson B.A. (2004) Collisional cooling of large ions in electrospray mass spectrometry. *Anal. Chem.* **76**(6): 1754-1760.

Chesters J.K. and Will M. (1981). Zinc transport proteins in plasma, *Br. J. Nutr.* **46**: 111-118.

Christodoulou J., Sadler P.J. and Tucker A. (1994) A new structural transition of serum albumin dependent on the state of Cys34. *Eur. J. Biochem.* **225**(1): 363-368.

Chowdhury S.K., Katta V. and Chait B.T. (1990) Probing conformational changes in proteins by mass spectrometry. *J. Am. Chem. Soc.* **112**(24): 9012-9013.

Clarke D.J, Murray E., Hupp T., Mackay C.L. and Langridge-Smith P.R.R. (2011) Mapping a noncovalent protein-peptide interface by top-down FTICR mass spectrometry using electron capture dissociation. *J. Am. Soc. Mass Spectrom.* **22**(8): 1432-1440.

Clemmer D.E., Hudgins R.R. and Jarrold M.F. (1995) Naked protein conformations: Cytochrome c in the gas phase. *J. Am. Chem. Soc.* **117**(40): 10141-10142.

Coates R.J., Weiss N.S., Daling J.R., Rettmer R.L. and Warnick G.R. (1989) Cancer risk in relation to serum copper levels. *Cancer Res.* **49**(15): 4353-4356.

Cohen M.J. and Karasek F. W. (1970) Plasma Chromatography™ - a new dimension for gas chromatography and mass spectrometry. *J. Chromatogr. Sci.* **8**(6): 330-337.

Coleman J.E. (1992) Zinc proteins: enzymes, storage proteins, transcription factors and replication proteins. *Annu. Rev. Biochem.* **61**(1):897-946.

Collins D. and Lee M. (2002) Developments in ion mobility spectrometry-mass spectrometry. *Anal. Bioanal. Chem.* **372**(1): 66-73.

Coon J.J., Ueberheide B., Syka, J.E.P., Dryhurst D.D., Ausio J., Shabanowitz J. and Hunt D.F. (2005) Protein identification using sequential ion/ion reactions and tandem mass spectrometry. *Proc. Natl. Acad. Sci USA.* **102**(27): 9463-9468.

Corrigan J.J., Jeter M.A., Bruck D., Feinberg W.M. (1990) Histidine-rich glycoprotein levels in children: the effect of age. *Thromb. Res.* **59**(3): 681–686.

Cousins R.J. (1986) Toward a molecular understanding of zinc metabolism. *Clin. Physiol. Biochem.* **4**(1): 20-30.

Cousins R.J., Liuzzi J.P. and Lichten L.A. (2006) Mammalian zinc transport, trafficking, and signals. *J. Biol. Chem.* **281**(34): 24085-24089.

Curry S., Mandelkow H., Brick P. and Franks N. (1998) Crystal structure of human serum albumin complexed with fatty acid reveals an asymmetric distribution of binding sites. *Nat. Struct. Mol. Biol.* **5**(9): 827-835.

Curry S., Brick P. and Franks N.P. (1999) Fatty acid binding to human serum albumin: new insights from crystallographic studies. *Biochim. Biophys. Acta* **1441**(2-3): 131-140.

Curry S. (2004) *Plasma albumin as a fatty acid carrier.* Advances in Molecular and Cell Biology, Elsevier **33:** 29-46.

Da Silva E., Rousseau C., Zanella-Cléon I., Becchi M. and Coleman A.W (2006) Mass spectrometric determination of association constants of bovine serum albumin (BSA) with para-sulphonato-calix[n]arene derivatives. *J. Incl. Phenom. Macro.* **54**(1): 53-59.

Demant E.J.F., Richieri G.V. and Kleinfeld A.M. (2002). Stopped-flow kinetic analysis of long-chain fatty acid dissociation from bovine serum albumin. *Biochem. J.* **363**(3): 809-815.

D'eon J.C., Simpson A.J., Kumar R., Baer A.J. and Mabury S.A. (2010) Determining the molecular interactions of perfluorinated carboxylic acids with human sera and isolated human serum albumin using nuclear magnetic resonance spectroscopy. *Environ. Toxicol. Chem.* **28**(8): 1678-1688.

Dixelius J., Olsson A.-K., Thulin A., Lee C., Johansson I. and Claesson-Welsh L. (2006) Minimal active domain and mechanism of action of the angiogenesis inhibitor histidine-rich glycoprotein. *Cancer Res.* **66**(4):2089-2097.

Dockal M., Carter D.C. and Rüker F. (2000) Conformational transitions of the three recombinant domains of human serum albumin depending on pH. *J. Biol. Chem*. **275**(5): 3042-3050.

Dole M. Mack L.L., Hines R.L., Mobley R.C., Ferguson L.D and Ferguson and Alice M. B. (1968) Molecular beams of macroions. *J. Chem. Phys.* **49**(5): 2240-2249.

Doñate F., Juarez J.C., Guan X., Shipulina N.V., Plunkett M.L., Tel-Tsur Z., Shaw D.E., Morgan W.T. and Mazar A.P. (2004) Peptides derived from the histidine-proline domain of the histidine-proline-rich glycoprotein bind to tropomyosin and have antiangiogenic and antitumor activities. *Cancer Res.* **64**(16): 5812-5817.

Drenth J. (2007) *Principles of Protein X-Ray Crystallography.* New York: Springer

van Duijn E. (2010) Current limitations in native mass spectrometry based structural biology. *J. Am. Soc. Mass Spectrom*. **21**(6): 971-978.

Edsall J.T., Maybury, R.H., Simpson R.B. and Straessle R. (1954). Dimerization of serum mercaptalbumin in presence of mercurials. II. studies with a bifunctional organic mercurial 1a,b,c. *J. Am. Chem. Soc.* **76**(12): 3131-3138.

Ellman G.L. (1958) A colorimetric method for determining low concentrations of mercaptans. *Arch. Biochem. Biophys*. **74**(2): 443-450.

Era S. and Sogami M. (1998) ^{1}H-NMR and CD studies on the structural transition of serum albumin in the acidic region—the N→F transition. *J. Pept. Res. **52**(6):* 431-442.

Erales J., Gontero B., Whitelegge J. and Halgand F. (2009) Mapping of a copper-binding site on the small CP12 chloroplastic protein of Chlamydomonas reinhardtii using top-down mass spectrometry and site-directed mutagenesis, *Biochem. J.* **419**(1): 75-82.

Esposito B.P. and Najjar R. (2002) Interactions of antitumoral platinum-group metallodrugs with albumin. *Coord. Chem. Rev.* **232**(1): 137-149.

Evans L., Hughes M., Waters J., Cameron J., Dodsworth N., Tooth D., Greenfield A. and Sleep D. (2010) The production, characterisation and enhanced pharmacokinetics of scFv-albumin fusions expressed in Saccharomyces cerevisiae. *Protein Expr. Purif.* **73**(2): 113-124.

Failla M. L., Van de Veerdonk M., Morgan W. T. and Smith J.C. (1982) Characterization of zinc-binding proteins of plasma in familial hyperzincemia. *J. Lab. Clin. Med*. **100**(6): 943-952.

Fasano M., Curry S., Terreno E., Galliano M., Fanali G., Narciso P., Notari S., Ascenzi P. (2005) The extraordinary ligand binding properties of human serum albumin. *IUBMB Life* **57**(12): 787-796.

Faull P.A., Korkeila K.E.. Kalapothakis J.M., Gray A., McCullough B.J. and Barran P.E. (2009) Gas-phase metalloprotein complexes interrogated by ion mobility-mass spectrometry. *Int. J. Mass Spectrom.* **283**(1-3): 140-148.

Feng R., Castelhano A., Billedeau R., Yuan Z. (1995) Study of noncovalent enzyme inhibitor complexes and metal binding stoichiometry of matrilysin by electrospray ionization mass spectrometry. *J. Am. Soc. Mass Spectrom.* **6**(11): 1105-1111.

Fenn J.B., Mann M., Meng C.K., Wong S.F., and Whitehouse C.M. (1989) Electrospray ionization for mass spectrometry of large biomolecules. *Science* **246**(4926): 64-71.

Folkman, J. (1995) Angiogenesis in cancer, vascular, rheumatoid and other disease. *Nat. Med.* **1**(1): 27-30.

Foote J.W and Delves H.T (1984) Albumin bound and α_2-macroglobulin bound zinc concentrations in the sera of healthy adults. *J. Clin. Pathol.* **37**(9): 1050-1054.

Fosmire G.J. (1990) Zinc toxicity. *Am. J. Clin. Nutr.* **51**(2): 225-7.

Fu C.-L. and Horne M.K. (2002) Histidine-rich glycoprotein plus zinc to neutralize heparin*. J. Lab. Clin. Med.* **139**(4): 211-217.

Gálvez M., Moreno J.A., Elósegui L.M. and Escanero J.F. (2001). Zinc uptake by human erythrocytes with and without serum albumins in the medium. *Biol. Trace Elem. Res*. **84**(1-3): 45-56.

Giles K., Pringle S.D., Worthington K.R., Little D., Wildgoose J.L. and Bateman, R.H. (2004) Applications of a travelling wave-based radio-frequency-only stacked ring ion guide. *Rapid Commun. Mass Spectrom.* **18**(20): 2401-2414.

Giroux E.L. and Henkin R.I. (1972) Competition for zinc among serum albumin and amino acids. *Biochim. Biophys. Acta* **273**(1): 64-72.

Glasoe P.K and Long F.A. (1960) Use of glass electrodes to measure acidities in deuterium oxide. *J. Phys. Chem*. **64**: 188-190.

Glennon J.D. and Sarkar B. (1982) Nickel(II) transport in human blood serum. *Biochem. J.* **203**(1): 15-23.

Goddard T.D. and Kneller D.G. (2007). SPARKY 3 San Francisco, University of California.

Gorgani N.N., Parish, C.R., Easterbrook Smith S.B. and Altin J.G. (1997). Histidine-rich glycoprotein binds to human IgG and C1q and inhibits the formation of insoluble immune complexes. *Biochemistry* **36**(22): 6653-6662.

Gorgani N.N., Altin J.G. and Parish C.R. (1999) Histidine-rich glycoprotein regulates the binding of monomeric IgG and immune complexes to monocytes. *Int. Immunol.* **11**(8): 1275-1282.

Gordon R.S. and Cherkes A. (1956) Unesterified fatty acid in human blood plasma. *J. Clin. Invest.* **35**(2): 206-212.

Gorodetsky R., Mou X., Blankenfeld A. and Marx G. (1993) Platelet multielemental composition, lability, and subcellular localization. *Am. J. Hematol.* **42**(3): 278-283.

Goumakos W., Laussac J.P., Sarkar B. (1991) Binding of cadmium(II) and zinc(II) to human and dog serum albumins. An equilibrium dialysis and ^{113}Cd-NMR study, *Biochem. Cell Biol.* **69**(12): 809-20.

Greig M.J., Gaus H., Cummins L.L., Sasmor H. and Griffey R.H. (2002) Measurement of macromolecular binding using electrospray mass spectrometry. Determination of dissociation constants for oligonucleotide: serum albumin complexes. *J. Am. Chem. Soc.* **117**(43): 10765-10766.

Groessl M., Hartinger C.G., Egger A., Keppler B.K. (2006) The binding of ruthenium(III) anticancer complexes to serum proteins: an ESI-MS study *Metal Ions in Biology and Medicine* **9**: 111-116.

Guex N. and Peitsch M.C. (1997) SWISS-MODEL and the Swiss-PdbViewer: an environment for comparative protein modelling. *Electrophoresis* **18**(15): 2714-2723.

Gumerov D.R., Mason A.B. and Kaltashov I.A. (2003) Interlobe communication in human serum transferrin: metal binding and conformational dynamics investigated by electrospray ionization mass spectrometry. *Biochemistry* **42**(18): 5421-5428.

Guthans S.L. and Morgan W.T. (1982) The interaction of zinc, nickel and cadmium with serum albumin and histidine-rich glycoprotein assessed by equilibrium dialysis and immunoadsorbent chromatography. *Arch. Biochem. Biophys.* **218**(1): 320-328.

Haase H. and Rink L. (2009) The immune system and the impact of zinc during aging. *Immun. Ageing* **6**(1): 9.

Han X., Snow T.A., Kemper R.A. and Jepson G.W. (2003) Binding of perfluorooctanoic acid to rat and human plasma proteins. *Chem. Res. Toxicol.* **16**(6): 775-781.

Harford C. and Sarkar B. (1997) Amino Terminal Cu(II)- and Ni(II)-Binding (ATCUN) motif of proteins and peptides: metal binding, DNA cleavage, and other properties, *Acc. Chem. Res.* **30**(3): 123-130.

Harmer N.J., Ilag L.L., Mulloy B., Pellegrini L., Robinson C.V., Blundell T.L.. (2004) Towards a Resolution of the stoichiometry of the fibroblast growth factor (FGF)-FGF receptor-heparin complex. *J. Mol. Biol.* **339**(4): 821-834.

Harmer N.J., Robinson C.J., Adam L.E., Ilag L.L., Robinson C.V., Gallagher J.T., Blundell T.L. (2006). Multimers of the fibroblast growth factor (FGF)-FGF receptor-saccharide complex are formed on long oligomers of heparin. *Biochem. J*. **393**(3): 741-748.

Haselmann K.F., Jørgensen T.J.D., Budnik B.A. Jensen F. and Zubarev R.A. (2002) Electron capture dissociation of weakly bound polypeptide polycationic complexes. *Rapid Commun. Mass Spectrom.* **16**(24): 2260-2265.

He X.M and Carter D.C. (1992) Atomic structure and chemistry of human serum albumin. *Nature* **358**(6383): 209-215.

Heimburger N., Haupt H., Kranz T. and Baudner S. (1972) Human serum proteins with high affinity to carboxymethylcellulose.II. Physicochemical and immunological characterization of a histidine-rich 3,8S- 2-glycoportein (CM-protein I) [in German] *Hoppe Seylers Z Physiol. Chem.* **353**(7): 1133-1140.

Hendrickson S.C., St. Louis J.D., Lowe J.E., Abdel-aleem S. (1997). Free fatty acid metabolism during myocardial ischemia and reperfusion. *Mol. Cell. Biochem.* **166**(1-2): 85-94.

Henrotte V., Laurent S., Gabelica V., Elst L.V., Depauw E. and Muller, R.N. (2004) Investigation of non-covalent interactions between paramagnetic complexes and human serum albumin by electrospray mass spectrometry. *Rapid Commun. Mass Spectrom.* **18**(17): 1919-1924.

van den Heuvel R.H.H. and Heck A.J.R. (2004) Native protein mass spectrometry: from intact oligomers to functional machineries. *Curr. Opin. Chem. Biol.* **8**(5): 519-526.

Hoaglund-Hyzer C.S., Counterman A.E. and Clemmer, D.E. (1999) Anhydrous protein ions. *Chem. Rev*. **99**(10): 3037-3080.

Horne M.K., Merryman P.K. and Cullinane A.M. (2001) Histidine-proline-rich glycoprotein binding to platelets mediated by transition metals. *Thromb. Haemost.* **85**(5): 890-895.

Hu P. and Loo J.A. (1995) Gas-phase coordination properties of Zn^{2+}, Cu^{2+}, Ni^{2+}, and Co^{2+} with histidine-containing peptides. *J. Am. Chem Soc.* **117**(45): 11314-11319.

Hu W., Luo Q., Wu K., Li X., Wang F., Chen Y., Ma X., Wang J., Liu J., Xiong S. and Sadler P.J. (2011) The anticancer drug cisplatin can cross-link the interdomain zinc site on human albumin. *Chem. Comm.* **47**(21): 6006-6008.

Huang B.X., Dass C. and Kim H.-Y. (2005) Probing conformational changes of human serum albumin due to unsaturated fatty acid binding by chemical cross-linking and mass spectrometry. *Biochem. J.* **387**(3): 695-702.

Hudgins R.R., Woenckhaus J. and Jarrold M.F. (1997) High resolution ion mobility measurements for gas phase proteins: correlation between solution phase and gas phase conformations. *Int. J. Mass Spectrom.***165-166**: 497-507.

Hughes W.L. and Dintzis H.M. (1964) Crystallization of the mercury dimers of human and bovine mercaptalbumin, *J. Biol. Chem.* **239**(3): 845-849.

Hulett M.D. and Parish C.R. (2000) Murine histidine-rich glycoprotein: Cloning, characterization and cellular origin. *Immunol. Cell Biol.* **78**(3): 280-287.

Hunt D.F., Yates J.R., Shabanowitz J., Winston S. and Hauer C.R. (1986) Protein sequencing by tandem mass spectrometry. *Proc. Natl. Acad. Sci. USA* **83**(17): 6233-6237.

Hutchens T.W., Nelson R.W., Allen M.H. Li C.M. and Yip T.-T. (1992). Peptide-metal ion interactions in solution: Detection by laser desorption time-of-flight mass spectrometry and electrospray ionization mass spectrometry. *Biol. Mass Spectrom.* **21**(3): 151-159.

Hwang T.-L. and Shaka A.J. (1995) Water suppression that works. excitation sculpting using arbitrary wave-forms and pulsed-field gradients. *J. Magn. Reson. A* **112**(2): 275-279.

Iribarne J.V. and Thomson B.A. (1976) On the evaporation of small ions from charged droplets. *J. Chem. Phys.* **64**(6): 2287-2294.

Ivanov A.I., Christodoulou J., Parkinson J.A., Barnham, K.J., Tucker A.,Woodrow J., Sadler P.J. (1998) Cisplatin binding sites on human albumin, *J. Biol. Chem.* **273**(24): 14721-14730.

van Iwaarden F., de Groo, P.G. and Bouma B.N. (1988) The binding of high molecular weight kininogen to cultured human endothelial cells. *J. Biol. Chem.* **263**(10): 4698-4703.

Jancsó. A., Kolozsi A., Gyurcsik B., Nagy N.V. and Gajda T. (2009) Probing the Cu^{2+} and Zn^{2+} binding affinity of histidine-rich glycoprotein. *J. Inorg Biochem.* **103**(12): 1634-1643.

Jarrold, M. F (1999) Unfolding, refolding, and hydration of proteins in the gas phase. *Acc. Chem. Res.* **32**(4): 360-367.

Jennings K.R. (1968) Collision-induced decompositions of aromatic molecular ions. *Int. J. Mass Spectrom. Ion Phys.* **1**(3): 227-235.

Johnson R.S., Martin S.A. and Biemann K. (1988) Collision-induced fragmentation of (M + H)+ ions of peptides. Side chain specific sequence ions*. Int J. Mass Spectrom. Ion Processes* **86**: 137-154.

Jones P.D, Hu W., De Coen W., Newsted J.L., Giesy J.P. (2003) Binding of perfluorinated fatty acids to serum proteins. *Environ. Toxicol. Chem.* **22**(11): 2639-2649.

Jones A.L., Hulett M.D. and Parish C.R. (2004) Histidine-rich glycoprotein binds to cell-surface heparan sulfate via its N-terminal domain following Zn^{2+} chelation. *J. Biol. Chem.* **279**(29): 30114-30122.

Jones A.L., Poon I.K H., Hulett M.D. and Parish C.R. (2005a). Histidine-rich glycoprotein specifically binds to necrotic cells via its amino-terminal domain and facilitates necrotic cell phagocytosis. *J. Biol. Chem* **280**(42): 35733-35741.

Jones A.L., Hulett M.D. and Parish C.R. (2005b) Histidine-rich glycoprotein: A novel adaptor protein in plasma that modulates the immune, vascular and coagulation systems. *Immunol. Cell. Biol.* **83**(2): 106-118.

Joseph K., Ghebrehiwet B., Peerschke E.I., Reid K.B. and Kaplan A.P. (1996) Identification of the zinc-dependent endothelial cell binding protein for high molecular weight kininogen and factor XII: identity with the receptor that binds to the globular "heads" of C1q (gC1q-R)." *Proc. Natl. Acad. Sci. USA* ***93***(16): 8552-8557.

Kanu A.B., Dwivedi P., Tam M., Matz L. and Hill H.H. (2008) Ion mobility–mass spectrometry. *J. Mass Spectrom.* **43**(1): 1-22.

Karasek F.W. (1974) Plasma Chromatography. *Anal. Chem.* **46**(8): 710A-720A.

Katagiri M., Tsutsui K. Yamano T., Shimonishi, Y., Ishibashi F. (1987) Interaction of heme with a synthetic peptide mimicking the putative heme-binding site of histidine-rich glycoprotein, *Biochem. Biophys. Res. Commun.* **149**(3): 1070-1076.

Katta V. and Chait B.T. (1991) Observation of the heme-globin complex in native myoglobin by electrospray-ionization mass spectrometry. *J. Am. Chem. Soc.* **113**(22): 8534-8535.

Kebarle P. (2000) A brief overview of the present status of the mechanisms involved in electrospray mass spectrometry. *J. Mass Spectrom.* **35**(7): 804-817.

Kebarle P. and Verkerk U.H. (2009) Electrospray: from ions in solution to ions in the gas phase, what we know now*. Mass Spectrom. Rev.* **28**(6): 898-917.

Keilin D. and Mann T. (1940). Carbonic anhydrase. Purification and nature of the enzyme. *Biochem. J.* **34**(8-9): 1163-1176.

Kendall F.E. (1941) Studies of human serum proteins II. Crysallization of human serum albumin*. J. Biol. Chem.* **138**(1): 97-109.

Kiilerich S., Christensen M.S., Naestoft J. and Christiansen C. (1980). Determination of zinc in serum and urine by atomic absorption spectrophotometry; Relationship between serum levels of zinc and proteins in 104 normal subjects. *Clin. Chim. Acta* **105**(2): 231-239.

Kinlaw W.B., Levine A.S., Morley JE., Silvis S.E. and McClain C.J. (1983) Abnormal zinc metabolism in type II diabetes mellitus. *Am. J. Med.* **75**(2): 273-277.

Klenotic P.A., Huang P., Palomo J., Kaur B., Van Meir E.G., Vogelbaum M.A., Febbraio, M., Gladson, C.L. and Silverstein, R.L. (2010) Histidine-rich glycoprotein modulates the anti-angiogenic effects of vasculostatin, *Am. J. Pathol*. **176**(4): 2039-2050.

Kluszynski B.A., Kim C and Faulk W.P. (1997) Zinc as a cofactor for heparin neutralization by histidine-rich glycoprotein. *J. Biol. Chem.* **272**(21): 13541-13547.

Koide T., Foster D., Yoshitake S. and Davie E.W. (1986) Amino acid sequence of human histidine-rich glycoprotein derived from the nucleotide sequence of its cDNA. *Biochemistry* **25**(8): 2220-2225.

Koide T. and Odani S. (1987) Histidine-rich glycoprotein is evolutionarily related to the cystatin superfamily: Presence of two cystatin domains in the N-terminal region, *FEBS Lett*. **216**(1): 17-21.

Komatsu T., Hamamatsu K. and Tsuchida E. (1999) Cross-linked human serum albumin dimer incorporating sixteen (Tetraphenylporphinato)iron(II) derivatives: synthesis, characterization, and O_2-Binding Property, *Macromolecules* **32**(25): 8388-8391.

Kondrat F.D.L., Kowald G.R., Scarff C.A., Scrivens J.H. and Blindauer, C.A. (2012) Resolution of a paradox by native mass spectrometry: facile occupation of all four metal binding sites in the dimeric zinc sensor SmtB. *Chem. Comm.* **49**(8): 813-815.

Kragh-Hansen U. (1981) Molecular aspects of ligand binding to serum albumin. *Pharmacol. Rev.* **33**(1): 17-53.

Kragh-Hansen U., Chuang, V.T.G. and Otagiri M. (2002) Practical aspects of the ligand-binding and enzymatic properties of human serum albumin. *Biol. Pharm. Bull.* **25**(6): 695-704.

Kuo H.W, Chen S.F, Wu C.C, Chen D.R and Lee J.H. (2002) Serum and tissue trace elements in patients with breast cancer in Taiwan. *Biol. Trace Elem. Res.* **89**(1): 1-11.

La Mendola D., Magrì. A., Santoro A.M, Nicoletti V.G and Rizzarelli E. (2012) Copper(II) interaction with peptide fragments of histidine-proline-rich glycoprotein: Speciation, stability and binding details. *J. Inorg. Biochem*. **111**: 59-69.

Lakusta H., Deber C.M., Sarkar, B. (1980) Complexation of Zn(II) to a native sequence tripeptide of human serum albumin studied by 13C nuclear magnetic resonance, *Can. J. Chem.* **58**(8): 757-766.

Lakusta H. and Sarkar B. (1979) Equilibrium studies of zinc(II) and cobalt(II) binding to tripeptide analogues of the amino terminus of human serum albumin. *J. Inorg. Biochem.* **11**(4): 303-315.

Lane L.A. Ruotolo B.T., Robinson C.V., Favrin G. and Benesch J.L.P. (2009) A Monte Carlo approach for assessing the specificity of protein oligomers observed in nano-electrospray mass spectra. *Int. J. Mass Spectrom.* **283**(1-3): 169-177.

Larkin M.A., Blackshields G., Brown N.P., Chenna R., McGettigan P.A., McWilliam H., Valentin F., Wallace I.M., Wilm A., Lopez R., Thompson J.D., Gibson T.J. and Higgins, D.G. (2007) Clustal W and Clustal X version 2.0. *Bioinformatics* **23**(21): 2947-2948.

Lau S.-J. and Sarkar B. (1971) Ternary Coordination complex between human serum albumin, copper (II), and l-histidine*. J. Biol. Chem.* **246**(19): 5938-5943.

Lau S.-J., Kruck T.P.A. and Bibudhendra S. (1974) A peptide molecule mimicking the copper(II) transport site of human serum albumin*. J. Biol. Chem.* **249**(18): 5878-5884.

Leary J.A., Schenauer M.R., Stefanescu R., Andaya A., Ruotolo B.T., Robinson C.V., Thalassinos K., Scrivens J.H., Sokabe M. and Hershey J.W.B. (2009). Methodology for measuring conformation of solvent-disrupted protein subunits using T-WAVE ion mobility MS: An investigation into eukaryotic initiation factors. *J. Am. Soc. Mass Spectrom.* **20**(9): 1699-1706.

Leonard W.J. and Foster J.F. (1961). Changes in optical rotation in the acid transformations of plasma albumin. Evidence for the contribution of tertiary structure to rotatory behavior. *J. Biol. Chem.* **236**(10): 2662-2669.

Leung L.L., Harpel P.C., Nachman, R L. and Rabellino E.M. (1983). Histidine-rich glycoprotein is present in human platelets and is released following thrombin stimulation. *Blood* **62**(5): 1016-1021.

Leung L.L. (1986) Interaction of histidine-rich glycoprotein with fibrinogen and fibrin, *J. Clin. Invest.* **77**(4): 1305-1311.

Leung L.L., Nachman R.L. and Harpel P.C. (1984) Complex formation of platelet thrombospondin with histidine-rich glycoprotein, *J. Clin. Invest.* **73**(1): 5-12.

Levine R. L. (1993) Ischemia: from acidosis to oxidation. *FASEB J.* **7**(13): 1242-1246.

Lijnen H.R., Hoylaerts M., Collen D. (1980) Isolation and characterization of a human plasma protein with affinity for the lysine binding sites in plasminogen. Role in the regulation of fibrinolysis and identification as histidine-rich glycoprotein. *J. Biol. Chem.* **255**(10): 214–22.

Lijnen H.R., Hoylaerts M. and Collen D. (1983) Heparin binding properties of human histidine-rich glycoprotein. Mechanism and role in the neutralization of heparin in plasma. *J. Biol. Chem.* **258**(6): 3803-3808.

Little P.J., Bhattacharya R., Moreyra A.E. and Korichneva I.L. (2010). Zinc and cardiovascular disease. *Nutrition* **26**(11-12): 1050-1057.

Liu J., Wang X., Cai Z. and Lee, F.S.C. (2008) Effect of tanshinone IIA on the noncovalent interaction between warfarin and human serum albumin studied by electrospray ionization mass spectrometry. *J. Am. Soc. Mass Spectrom.* **19**(10): 1568-1575.

Liu L., Bagal D., Kitova E.N., Schnier P.D. and Klassen J.S. (2009). Hydrophobic protein-ligand interactions preserved in the gas phase. *J. Am. Chem. Soc.* **131**(44): 15980-15981.

Loch J.I, Polit A, Bonarek P., Olszewska D., Kurpiewska K., Dziedzicka-Wasylewska M. and Lewiński K. (2012) Structural and thermodynamic studies of binding saturated fatty acids to bovine beta-lactoglobulin. *Int. J. Biol. Macromolec.* **50**(4): 1095-1102.

Loo J.A., Hu P. and Smith R.D. (1994) Interaction of angiotensin peptides and zinc metal ions probed by electrospray ionization mass spectrometry *J Am. Soc. Mass Spectrom.* **5**(11):959-965.

Loo J.A. (1997) Studying noncovalent protein complexes by electrospray ionization mass spectrometry. *Mass Spectrom. Rev.* **16**(1): 1-23.

Loo J.A. (2000) Electrospray ionization mass spectrometry: a technology for studying noncovalent macromolecular complexes. *Int. J. Mass Spectrom.* **200**(1-3): 175-186.

Lowndes S.A and Harris A.L. (2005) The role of copper in tumour angiogenesis. *J Mammary Gland Biol. Neoplasia* **10**: 299-310.

Lu J., Stewart A.J., Sadler P.J, Pinheiro T.J.T. and Blindauer C.A.. (2012a) Allosteric inhibition of cobalt binding to albumin by fatty acids: implications for the detection of myocardial ischemia. *J. Med. Chem.* ***55***(9): 4425-4430.

Lu J., Stewart A.J. Sleep D., Sadler P.J., Pinheiro T.J.T. and Blindauer C.A. (2012b) A molecular mechanism for modulating plasma Zn speciation by fatty acids, *J. Am. Chem. Soc.* **134**(3): 1454-1457.

Lucassen M. and Sarkar B. (1979) Nickel(II)-binding constituents of human blood serum. *J. Toxicol. Environ. Health* **5**(5): 897-905.

Luiken J.J., van Nieuwenhoven F. A., America G., van der Vusse G.J. and Glatz J.F. (1997) Uptake and metabolism of palmitate by isolated cardiac myocytes from adult rats: involvement of sarcolemmal proteins. *J. Lipid Res.* **38**(4): 745-758.

.

Ma X.-H., Qi C.-h., Chen Y. and Han, F.-m. (2008) Studies on the non-covalent binding between tropane alkaloids and human serum albumin by electrospray ion trap mass spectrometry, *Hubei Daxue Xuebao, Ziran Kexueban* **30**(4): 392-395.

Mamyrin B.A, Karataev V.L., Shmikk D.V. and Zagulin V.A. (1973) The mass reflectron, a new non-magnetic time-of-flight spectrometer with high resolution. *Sov. Phys. JETP* **37**(1): 45-48.

Mangani S., Meyer-Klaucke W., Moir A.J., Ranieri-Raggi M., Martini D. and Raggi A. (2003) Characterization of the zinc-binding site of the histidine-proline-rich glycoprotein associated with rabbit skeletal muscle AMP deaminase. *J. Biol. Chem.* **278**(5): 3176-3184.

Manley S.A., Byrns S., Lyon A.W., Brown P. and Gailer J. (2009). Simultaneous Cu-, Fe-, and Zn-specific detection of metalloproteins contained in rabbit plasma by size-exclusion chromatography-inductively coupled plasma atomic emission spectroscopy. *J. Biol. Inorg. Chem.* **14**(1): 61-74.

Maret W. and Sandstead H.H. (2006) Zinc requirements and the risks and benefits of zinc supplementation. *J. Trace Elem. Med. Bio.* **20**(1): 3-18.

Marcotte E.M., Pellegrini M., Yeates T.O. and Eisenberg D. (1999). A census of protein repeats. *J. Mol. Biol.* **293**(1): 151-160.

Martins, E.O. and Drakenberg T.R. (1982) Cadmium(II), zinc(II), and copper(II) ions binding to bovine serum albumin. A ^{113}Cd NMR study. *Inorg. Chim. Acta* **67**: 71-74.

Marx G., Korner G., Mou X. and Gorodetsky R. (1993) Packaging zinc, fibrinogen, and factor XIII in platelet α-granules. *J. Cell. Physiol.* **156**(3): 437-442.

Masuoka J. and Saltman P. (1994) Zinc(II) and copper(II) binding to serum albumin. A comparative study of dog, bovine, and human albumin, *J. Biol. Chem.* **269**(41): 25557-25561.

Mattapalli, H., W. Monteith, Burns, C. and Danell, A. (2009) Zinc deposition during ESI-MS analysis of peptide-zinc complexes. *J. Am. Soc. Mass. Spectrom.* **20**(12): 2199-2205.

McLafferty F.W., Bente P.F., Kornfeld R., Tsai S.-C. and Howe I. (1973). Metastable ion characteristics. XXII. Collisional activation spectra of organic ions. *J. Am. Chem. Soc*. **95**(7): 2120-2129.

McKay A.R., Ruotolo B.T., Ilag L.L. and Robinson C.V. (2006) Mass Measurements of Increased Accuracy Resolve Heterogeneous Populations of Intact Ribosomes. *J. Am. Chem. Soc.* **128**(35): 11433-11442.

Mekmouche Y., Coppel Y., Hochgräfe K., Guilloreau L., Talmard C., Mazarguil H. and Faller P. (2005) Characterization of the Zn^{II} binding to the peptide amyloid-β1–16 linked to alzheimer's disease. *ChemBioChem* **6**(9): 1663-1671.

Mertz W. (1981). The essential trace elements. *Science* **213**: 1332-1338.

Mesleh M.F., Hunter J.M., Shvartsburg A.A., Schatz G.C. and Jarrold M.F. (1996) Structural information from ion mobility measurements: effects of the long-range potential. *J. Phys. Chem.* **100**(40): 16082-16086.

Miller J, McLachlan A.D and Klug A. (1985) Repetitive zinc-binding domains in the protein transcription factor IIIA from Xenopus oocytes. *EMBO J.* **4**(6): 1609-1614.

Morgan W.T. Koskelo P., Koenig H., Conway and T.P. (1978a) Human histidine-rich glycoprotein. II. serum levels in adults, pregnant women and neonates. *Proc. Soc. Exp. Biol. Med.* **158**(4): 647-651.

Morgan W.T. (1978b) Human serum histidine-rich glycoprotein. Interactions with heme, metal ions and organic ligands, *Biochim. Biophys. Acta.* **535**(2): 319-333.

Morgan, W. T. (1981) Interactions of the histidine-rich glycoprotein of serum with metals*. Biochemistry* **20**(5): 1054-1061.

Mothes E. and Faller P. (2007) Evidence that the principal Co^{II}-binding site in human serum albumin is not at the N-terminus: implication on the albumin cobalt binding test for detecting myocardial ischemia. *Biochemistry* **46**(8): 2267-2274.

Muñiz C.S., Gayón J.M.M, Alonso J.I.G and Sanz-Medel A. (2001). Speciation of essential elements in human serum using anion-exchange chromatography coupled to post column isotope dilution analysis with double focusing ICP-MS. *J. Anal. At. Spectrom.* **16**(6): 587-592.

Neumann P.Z. and Sass-Kortsak A. (1967). The state of copper in human serum: evidence for an amino acid-bound fraction. *J. Clin. Invest.* **46**(4): 646-658.

Nicholls K. and Morton P. (May 2010) Investigating the stability of human serum albumin under a range of pH conditions with both time and temperature. [Online] http://www.biopharma.novozymes.com/en/information-centre/posters-and-presentations (Accessed 4th December 2012).

Nordahl E.A., Rydengård V., Morgelin M. and Schmidtchen A. (2005) Domain 5 of high molecular weight kininogen is antibacterial, *J. Biol. Chem.* **280**(41):34832-34839.

Ohyoshi E., Hamada Y., Nakata, K. and Kohata S. (1999) The interaction between human and bovine serum albumin and zinc studied by a competitive spectrophotometry. *J. Inorg. Biochem*. **75**(3): 213-218.

Olsen H.M., Parish C.R. and Altin J.G. (1996) Histidine-rich glycoprotein binding to T-cell lines and its effect on T-cell substratum adhesion is strongly potentiated by zinc. *Immunology* **88**(2): 198-206.

Olsson A.K, Larsson H., Dixelius J., Johansson I., Lee C., Oellig C., Björk I. and Claesson-Welsh L. (2004) A fragment of histidine-rich glycoprotein is a potent inhibitor of tumor vascularization. *Cancer Res.* **64**(2): 599-605.

Öz G., Pountney D.L. and Armitage, I.M. (1998) NMR spectroscopic studies of I = 1/2 metal ions in biological systems, *Biochem. Cell. Biol.* **76**(2-3): 223-234.

Peters T.J. (1995) *All about Albumin: Biochemistry, Genetics and Medical Applications*. Acadamic Press: New York.

Petitpas I., Petersen C.E., Ha C.-E., Bhattacharya A.A., Zunszain P.A., Ghuman J., Bhagavan N.V. and Curry S. (2003) Structural basis of albumin-thyroxine interactions and familial dysalbuminemic hyperthyroxinemia. *Proc. Natl. Acad. Sci. USA* **100**(11): 6440-6445.

Pizzo S.V., Swaim M.W., Roche P.A. and Gonias S.L. (1988) Selectivity and stereospecificity of the reactions of dichlorodiammineplatinum(II) with three purified plasma proteins, *J. Inorg. Biochem.* **33**(1): 67-76.

Poon I.K.H., Hulett M.D. and Parish C.R. (2010) Histidine-rich glycoprotein is a novel plasma pattern recognition molecule that recruits IgG to facilitate necrotic cell clearance via FcγRI on phagocytes. *Blood* **115**(12): 2473-2482.

Poon I.K.H., Patel K.K., Davis D.S., Parish C.R., Hulett M.D. (2011). Histidine-rich glycoprotein: the Swiss Army knife of mammalian plasma, *Blood* **117**(7): 2093-2101.

Porth C. M. (2002). *Pathophysiology: Concepts of altered health states.* 6th Ed. Philadelphia: Lippincott Willliams & Wilkins.

Pringle S.D., Giles K., Wildgoose J.L., Williams J.P., Slade S.E., Thalassinos K., Bateman R.H. Bowers M.T. and Scrivens J.H. (2007) An investigation of the mobility separation of some peptide and protein ions using a new hybrid quadrupole/travelling wave IMS/oa-ToF instrument. *Int. J. Mass Spectrom.* ***261***(1): 1-12.

Przybylski C., Gonnet F., Hersant Y., Bonnaffé D., Lortat-Jacob H. and Daniel R. (2010) Desorption electrospray ionization mass spectrometry of glycosaminoglycans and their protein noncovalent complex. *Anal. Chem.* **82**(22): 9225-9233.

Qi C.-h., Han F.-m., Cao, Y. and Chen, Y. (2006) Studies on noncovalent binding between puerarin and plasma protein by electrospray ion trap mass spectrometry. *Zhongguo Yaoxue Zazhi* **41**(23): 1822-1825.

Qi C.-h., Cao Y., Han F.-m. and Chen, Y. (2007) Study on noncovalent binding between anti-hepatitis B immune ribonucleic acid and human plasma protein by electrospray ion trap mass spectrometry. *Zhongguo Yaoxue Zazhi* **42**(8): 626-629.

Ranieri-Raggi M., Montali U., Ronca F., Sabbatini A., Brown P.E., Moir A.J. and Raggi A. (1997) Association of purified skeletal-muscle AMP deaminase with a histidine-proline-rich-glycoprotein-like molecule. *Biochem. J.* **326** (3): 641-648.

Ray B. and Stearns R.A. (1995) Studies on non-covalent associations of immunosuppressive drugs with serum albumin using pneumatically assisted electrospray ionization mass spectrometry, *Rapid Commun. Mass Spectrom.* **9**(3): 240-244.

Redman B.G., Esper P., Pan Q., Dunn R.L., Hussain H.K., Chenevert T., Brewer G.J. and Merajver S.D. (2003) Phase II trial of Tetrathiomolybdate in patients with advanced kidney cancer. *Clin. Cancer Res.* **9**(5): 1666-1672.

Richieri G.V. and Kleinfeld A.M. (1995) Unbound free fatty acid levels in human serum, *J. Lipid Res.* **36**(2): 229-240.

Richieri G.V., Anel A. and Kleinfeld A.M. (1993). Interactions of long-chain fatty acids and albumin: Determination of free fatty acid levels using the fluorescent probe ADIFAB. *Biochemistry* **32**(29): 7574-7580.

Roboz J., Deng L., Longhua M. and Holland, J.F. (1998) Investigation of suramin-albumin binding by electrospray mass spectrometry. *Rapid Commun. Mass Spectrom.* **12**(19): 1319-1322.

Roepstorff P. and Fohlman J. (1984) Proposal for a common nomenclature for sequence ions in mass spectra of peptides. *Biomed. Mass Spectrom.* **11**(11): 601

Ronish E.W. and Krimm S. (1974) The calculated circular dichroism of polyproline II in the polarizability approximation. *Biopolymers* **13**(8): 1635-1651.

Rowe D.J. and Bobilya D.J. (2000). Albumin facilitates zinc acquisition by endothelial cells*. Proc. Soc. Exp. Biol. Med.* **224**(3): 178-186.

Rowinska-Zyrek M., Witkowska D., Potocki S., Remelli M., and Kozlowski H. (2013) His-rich sequences - is plagiarism from nature a good idea? *New J. Chem.* **37**(1): 58-70

Rózga M., Sokołowska M., Protas A.M. and Bal W. (2007) Human serum albumin coordinates Cu(II) at its N-terminal binding site with 1 pM affinity. *J. Biol. Inorg. Chem*. **12**(6): 913-918.

Ruotolo B.T., Benesch J.L.P., Sandercock A.M., Hyung S.-J. and Robinson C.V. (2008) Ion mobility-mass spectrometry analysis of large protein complexes. *Nat. Protoc.* **3**(7): 1139-1152.

Rydengård V., Andersson Nordahl E. and Schmidtchen A. (2006) Zinc potentiates the antibacterial effects of histidine-rich peptides against *Enterococcus faecalis*. *FEBS J.* **273**(11): 2399-2406.

Rydengård V., Olsson A.K., Mörgelin M. and Schmidtchen A. (2007). Histidine-rich glycoprotein exerts antibacterial activity. *FEBS J.* **274**(2): 377-389

Rydengård V., Shannon O., Lundqvist K., Kacprzyk L., Chalupka A., Olsson A.K, Mörgelin M., Jahnen-Dechent W., Malmsten M., Schmidtchen A.. (2008) Histidine-rich glycoprotein protects from systemic candida infection. *PLoS Pathog.* **4**(8): e1000116.

Sadler P.J., Tucker A. and Viles J.H. (1994) Involvement of a lysine residue in the N-terminal Ni^{2+} and Cu^{2+} binding-site of serum albumins: Comparison with Co^{2+}, Cd^{2+} and Al^{3+}. *Eur. J. Biochem.* **220**(1): 193-200.

Sadler P.J. and Viles J.H. (1996) ^{1}H and ^{113}Cd NMR Investigations of Cd^{2+} and Zn^{2+} Binding Sites on Serum Albumin: Competition with Ca^{2+}, Ni^{2+}, Cu^{2+}, and Zn^{2+}, *Inorg. Chem*. **35**(15): 4490-4496.

Saifer A. and Goldman L. (1961) The free fatty acids bound to human serum albumin. *J. Lipid Res.* **2**(3): 268-270.

Schaller, J., Gerber S., Kämpfer U., Lejon S. and Trachsel C. (2008). *Human Blood Plasma Proteins*. Wiley: Chichester

Schmaier A.H., Kuo A., Lundberg D., Murray, S. and Cines D.B. (1988) The expression of high molecular weight kininogen on human umbilical vein endothelial cells. *J. Biol. Chem.* **263**(31): 16327-33.

Schnitzer J.E. and Oh P. (1994) Albondin-mediated capillary permeability to albumin. Differential role of receptors in endothelial transcytosis and endocytosis of native and modified albumins. *J. Biol. Chem.* **269**(8): 6072-6082.

Scopes, R. K. (1974) Measurement of protein by spectrophotometry at 205 nm. *Anal. Biochem.* **59**(1): 277-282.

Shannon O., Rydengård V., Schmidtchen A., Mörgelin M., Alm P., Sørensen O.E. and Björck L. (2010) Histidine-rich glycoprotein promotes bacterial entrapment in clots and decreases mortality in a mouse model of sepsis. *Blood* **116**(13): 2365-2372.

Shaw C. F., Laib J.E., Savas M.M. and Petering D.H. (1990) Biphasic kinetics of aurothionein formation from gold sodium thiomalate: a novel metallochromic technique to probe zinc(2+) and cadmium(2+) displacement from metallothionein*. Inorg. Chem.* **29**(3): 403-408.

Shaw C.F., Schliesman B., Xiao J., Locke J. Starich M. and Fetter D. (1991) Ligand substitution and redox reactions of the pro-drug auranofin: Albumin-gold-glutathione is a likely metabolite *J. Inorg. Biochem.* **43**(2-3): 594-594.

Shelimov K.B., Clemmer D.E., Hudgins R.R. and Jarrold M.F. (1997). Protein Structure in Vacuo: Gas-Phase Conformations of BPTI and Cytochrome c. *J. Am. Chem. Soc.* **119**(9): 2240-2248.

Shigekiyo T., Yoshida H., Matsumoto K., Azuma H., Wakabayashi S., Saito S., Fujikawa K. and Koide T. (1998) HRG tokushima: molecular and cellular characterization of histidine-rich glycoprotein (HRG) deficiency. *Blood* **91**(1): 128-133.

Shokrzadeh M., Ghaemian A., Salehifar E., Aliakbari S., Saravi S.S., and Ebrahimi P. (2009) Serum zinc and copper levels in ischemic cardiomyopathy. *Biol. Trace Elem. Res.* **127**(2): 116-123.

Shvartsburg A.A. and Jarrold M.F. (1996) An exact hard-spheres scattering model for the mobilities of polyatomic ions. *Chem. Phys. Lett.* **261**(1): 86-91.

Simard J.R., Zunszain P. A., Ha C.-E., Yang J.S., Bhagavan N.V., Petitpas I., Curry S. and Hamilton, J. A. (2005) Locating high-affinity fatty acid-binding sites on albumin by x-ray crystallography and NMR spectroscopy. *Proc. Natl. Acad. Sci. USA* **102**(50): 17958-17963.

Simard J.R., Zunszain P.A., Hamilton J.A. and Curry S. (2006) Location of high and low affinity fatty acid binding sites on human serum albumin revealed by NMR drug-competition analysis. *J. Mol. Biol.* **361**(2): 336-351.

Smith A., Nuiry I. and Morgan W.T. (1985) Proteolysis of histidine-rich glycoprotein in plasma and in patients undergoing thrombolytic therapy. *Thromb. Res.* **40**(5): 653-661.

Sobott F. and Robinson C. V. (2004). Characterising electrosprayed biomolecules using tandem-MS-the noncovalent GroEL chaperonin assembly. *Int. J. Mass Spectrom*. **236**(1-3): 25-32.

Sokolowska M., Wszelaka-Rylik M., Poznaski J. and Bal W. (2009). Spectroscopic and thermodynamic determination of three distinct binding sites for Co(II) ions in human serum albumin. *J. Inorg. Biochem*. **103**(7): 1005-1013.

Spector A.A. (1975) Fatty acid binding to plasma albumin. *J. Lipid Res.* **16**(3): 165-79.

Spector A.A. and Soboroff J.M. (1971) Utilization of free fatty acids complexed to human plasma lipoproteins by mammalian cell suspensions. *J. Lipid Res.* **12**(5): 545-552.

Sterling H.J, Batchelor J.D, Wemmer D.E and Williams E.R. (2010) Effects of buffer loading for electrospray ionization mass spectrometry of a noncovalent protein complex that requires high concentrations of essential aalts*. J. Am. Soc. Mass Spectrom.* **21**(6): 1045-1049.

Stewart A.J., Blindauer C.A., Berezenko S., Sleep D., Sadler P.J. (2003) Interdomain zinc site on human albumin *Proc. Natl. Acad. Sci. USA.* **100**(7): 3701-3706.

Stewart A.J., Blindauer C.A., Berezenko S., Sleep D., Tooth, D. and Sadler, P.J. (2005) Role of Tyr84 in controlling the reactivity of Cys34 of human albumin. *FEBS J.* **272**(2): 353-362.

Stewart A.J., Blindauer C.A. and Sadler P.J. (2009) Plasma fatty acid levels may regulate the Zn^{2+}-dependent activities of histidine-rich glycoprotein. *Biochimie* **91**(11-12): 1518-1522.

Straessle R. (1954). A disulfide dimer of human mercaptalbumin 1a,b. *J. Am. Chem. Soc.* **76**(12): 3138-3142.

Sugio S., Kashima A., Mochizuki S., Noda M. and Kobayashi K. (1999) Crystal structure of human serum albumin at 2.5 Å resolution. *Protein Eng.* **12**(6): 439-446.

Syka J.E.P., Coon J.J., Schroeder M.J., Shabanowitz J. and Hunt D.F. (2004) Peptide and protein sequence analysis by electron transfer dissociation mass spectrometry. *Proc. Natl. Acad. Sci. USA* **101**(26): 9528-9533.

Taguchi K., Chuang, V.T.G., Maruyama T. and Otagiri M. (2012) Pharmaceutical aspects of the recombinant human serum albumin dimer: Structural characteristics, biological properties, and medical applications, *J. Pharm. Sci.* **101**(9): 3033-3046.

Talmard C., Bouzan A. and Faller P. (2007) Zinc binding to amyloid-B: isothermal titration calorimetry and Zn competition experiments with Zn sensors. *Biochem.* **46**(47): 13658-13666.

Thalassinos K., Grabenauer M. Slade S.E., Hilton G.R., Bowers M.T. and Scrivens J.H. (2009) Characterization of phosphorylated peptides using traveling wave-based and drift cell ion mobility mass spectrometry. *Anal. Chem.* **81**(1): 248-254.

The UniProt Consortium (2012) Reorganizing the protein space at the Universal Protein Resource (UniProt). *Nucleic Acids Res.* **40**(D1): D71-D75.

Thulin A., Ringvall M., Dimberg A., Kårehed K., Väisänen T., Väisänen M.R., Hamad O., Wang J., Bjerkvig R., Nilsson B., Pihlajaniemi T., Akerud H., Pietras K., Jahnen-Dechent W., Siegbahn A. and Olsson A.K. (2009). Activated platelets provide a functional microenvironment for the antiangiogenic fragment of histidine-rich glycoprotein. *Mol. Cancer Res.* **7**(11): 1792-1802.

Tibaduiza E.C. and Bobilya D.J. (1996) Zinc transport across an endothelium includes vesicular cotransport with albumin. *J. Cell Physiol.* **167**(3): 539-547.

Tiruppathi C., Finnegan A. and Malik A.B. (1996) Isolation and characterization of a cell surface albumin-binding protein from vascular endothelial cells. *Proc. Natl. Acad. Sci. USA* **93**(1): 250-254.

Tsuchida-Straeten N., Ensslen S., Schäfer C., Wöltje M., Denecke B., Moser M., Gräber S., Wakabayashi S., Koide T. and Jahnen-Dechent W. (2005) Enhanced blood coagulation and fibrinolysis in mice lacking histidine-rich glycoprotein (HRG). *J. Thromb. Haemost.* **3**(5): 865-872.

Van der Vusse G.J. (2009) Albumin as fatty acid transporter, *Drug Metab. Pharmacokinet.* **24**(4): 300-307.

Vanwildermeersch M., Olsson A.-K., Gottfridson E., Claesson-Welsh L., Lindahl U. and Spillmann D. (2006) The anti-angiogenic His/Pro-rich fragment of histidine-rich glycoprotein binds to endothelial cell heparin sulphate in a Zn^{2+} -dependent manner, *J. Biol. Chem.* **281**(15):10298-10304.

Vorum H., Brodersen R., Kragh-Hansen, U., Pedersen A.O. (1992). Solubility of long-chain fatty acids in phosphate buffer at pH 7.4, *Biochim. Biophys. Acta - Lipids and Lipid Metabolism* **1126**(2): 135-142.

Waldron K.J., Rutherford J.C., Ford D. and Robinson N.J. (2009) Metalloproteins and metal sensing. *Nature* **460**(7257): 823-830.

Wastney M.E., Aamodt R. L., Rumble W.F. and Henkin R.I. (1986). Kinetic analysis of zinc metabolism and its regulation in normal humans. *Am. J. Physiol.* **251**(2): R398-R408.

Wilm M. and Mann M. (1996) Analytical properties of the nanoelectrospray ion Source. *Anal. Chem*. **68**(1): 1-8.

Wilm M. (2011) Principles of electrospray ionization. *Mol. Cell. Proteomics* **10**(7): M111.009407

Winston R.L. and Fitzgerald M. C. (1997) Mass spectrometry as a readout of protein structure and function. *Mass Spectrom. Rev.* **16**(4): 165-179.

Wishart D.S., Bigam C.G., Yao J., Abildgaard F., Dyson H.J., Oldfield E., Markley J.L. and Sykes B.D. (1995) ^{1}H, ^{13}C and ^{15}N chemical shift referencing in biomolecular NMR. *J. Biomol. NMR* **6**(2): 135-140.

Wu C., Siems W.F., Klasmeier J. and Hill H.H. (1999) Separation of isomeric peptides using electrospray ionization/high-resolution ion mobility spectrometry. *Anal. Chem.* **72**(2): 391-395.

Wu, L.-L., Gao, H.-W., Gao N.-Y., Chen, F.-F. and Chen L. (2009) Interaction of perfluorooctanoic acid with human serum albumin. *BMC Struct. Biol.* 9(1): 31-37

Wyttenbach T., Grabenauer M., Thalassinos K., Scrivens J.H. and Bowers M.T. (2009) The effect of calcium ions and peptide ligands on the relative stabilities of the calmodulin dumbbell and compact Structures. *J. Phys. Chem. B* **114**(1): 437-447.

Xia Z.F., Horton J.W., Zhao P.Y., Babcock E.E., Sherry A.D. and Malloy C.R. (1996) Effects of ischemia on intracellular sodium and phosphates in the in vivo rat liver. *J. Appl. Physiol.* **81**(3): 1395-1403.

Xie Y., Zhang J., Yin S. and Loo J.A. (2006) Top-down ESI-ECD-FT-ICR mass spectrometry localizes noncovalent protein-ligand binding sites. *J. Am. Chem. Soc.* **128**(45): 14432-14433.

Yamashita M. and Fenn J.B. (1984) Electrospray ion source. Another variation on the free-jet theme. *J. Phys. Chem.* **88**(20): 4451-4459.

Yin S. and Loo J.A. Loo (2011) Top-down mass spectrometry of supercharged native protein-ligand complexes. *Int. J. Mass Spectrom.* **300**(2-3): 118-122.

Zhang J.-C., Claffey K., Sakthivel R., Darzynkiewicz Z., Shaw D.E., Leal J., Wang Y.-C., Lu F.-M. and McCrae K.R. (2000) Two-chain high molecular weight kininogen induces endothelial cell apoptosis and inhibits angiogenesis: partial activity within domain 5. *FASEB J.* **14**(15): 2589-2600.

Zhou Y., Dong J. and Vachet R.W. (2011) Electron transfer dissociation of modified peptides and proteins. *Curr. Pharm. Biotechnol.* **12**(10): 1558-1567.

Zubarev R.A., Kelleher N.L. and McLafferty F.W. (1998) Electron capture dissociation of multiply charged protein cations. a nonergodic process. *J. Am. Chem. Soc.* **120**(13): 3265-3266.

Zubarev R.A., Horn D.M., Fridriksson E.K., Kelleher N.L., Kruger N.A., Lewis M.A., Carpenter B.K. and McLafferty F.W. (2000) Electron capture dissociation for structural characterization of multiply charged protein cations. *Anal. Chem.* **72**(3): 563-573.

Zubarev R., Haselmann K., Budnik B., Kjeldsen F. and Jensen F. (2002) Account: Towards an understanding of the mechanism of electron-capture dissociation: a historical perspective and modern ideas. *Eur. J. Mass Spectrom.* **8**(5): 337-349.

Zubarev R.A. (2004) Electron-capture dissociation tandem mass spectrometry. *Curr. Opin. Biotechnol.* **15**(1): 12-16.

Appendix

Thesis reference: Chapter 2, page 37

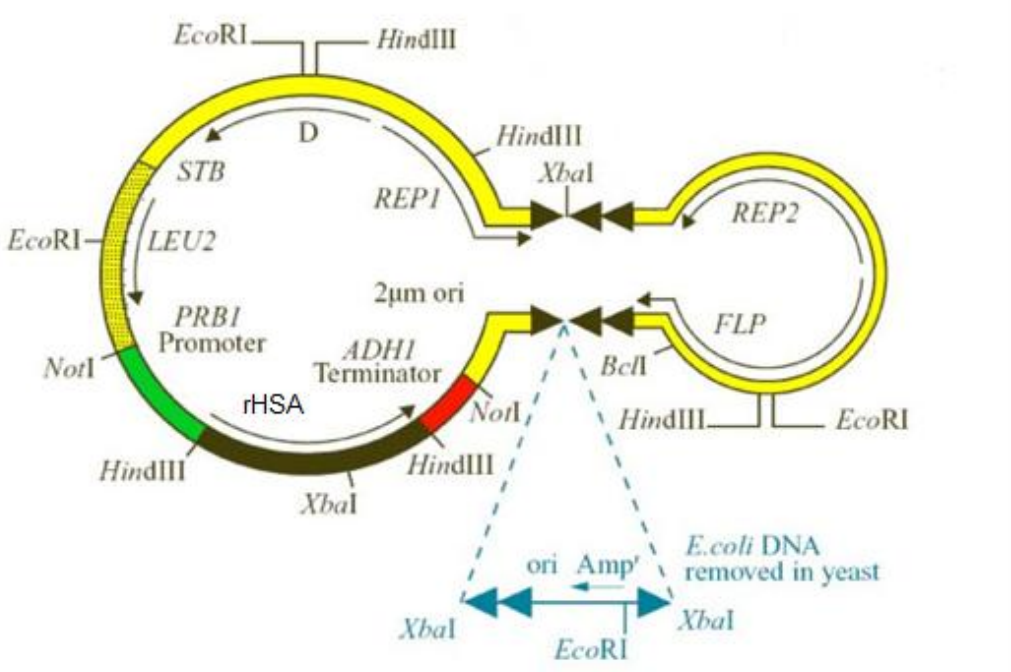

Figure A1 Expression of recombinant albumin in *Saccharomyces cerevisiae*. A 2 μM plasmid for expression of recombinant HSA in yeast which is a safe and alternative product to albumin extracted form blood plasma. The HSA gene (green/black/red) is incorporated between the *STB* and the origin of replication (Evans *et al*., 2010).

Thesis reference: Chapter 3, page 66

Table A1 Comparison of the experimental and theoretical masses observed for HSA. Values are expressed as average masses in Da. Errors in the mass become larger at lower charge states due to peak broadening.

Charge state	Experimental *m/z*	Theoretical *m/z*	Δmass (Da)
16+	4152.96	4153.34	-0.38
17+	3908.68	3909.08	-0.40
18+	3691.60	3691.97	-0.37
19+	3497.36	3497.71	-0.35
20+	3322.93	3322.87	+0.06
21+	3164.60	3164.69	-0.09
22+	3020.91	3020.89	+0.02
23+	2889.74	2889.59	+0.15
24+	2769.39	2769.23	+0.16
25+	2658.53	2658.50	+0.03
26+	2556.33	2556.29	+0.04
27+	2461.59	2461.65	-0.03
28+	2373.77	2373.77	0.00
29+	2292.04	2291.95	+0.09
30+	2215.63	2215.58	+0.05
31+	2144.15	2144.15	0.00
32+	2077.30	2077.17	+0.13
33+	2014.32	2014.26	+0.06
34+	1955.04	1955.05	-0.01
35+	1899.19	1899.22	-0.03
36+	1846.50	1846.49	+0.01
37+	1796.58	1796.61	-0.03
38+	1749.34	1749.36	-0.02
39+	1704.55	1704.53	+0.02
40+	1662.00	1661.94	+0.06
41+	1621.39	1621.43	-0.04
42+	1582.86	1582.85	+0.01
43+	1546.03	1546.06	+0.03
44+	1510.92	1510.94	+0.02
45+	1477.41	1477.39	+0.02

Thesis reference: Chapter 3, page 67

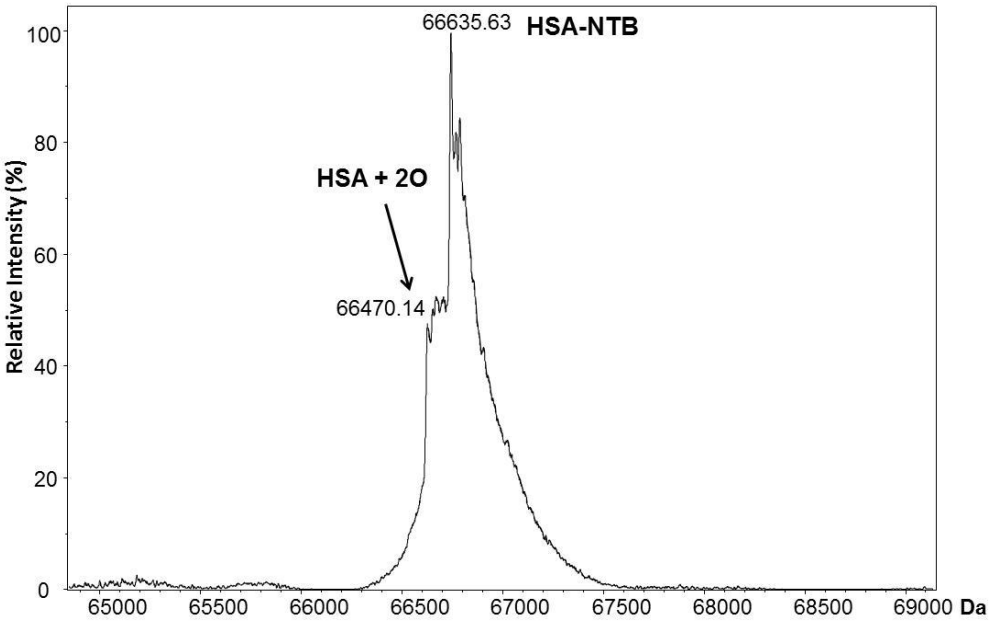

Figure A2 HSA reacted with 40 mol. equiv. DTNB and analysed by ESI-MS. The observed mass was 66,635.63 Da. From the relative intensity of the peaks, it was estimated that 68% of the free thiol was available to react with DTNB. This is in agreement with the thiol assay by UV-Vis spectroscopy. The protocol for reaction with DTNB has previously been described (Stewart *et al*., 2005). The fact that the other species remaining corresponds to HSA + 2O atoms suggests that the oxidation has occurred at Cys34.

Thesis reference: Chapter 3, page 79

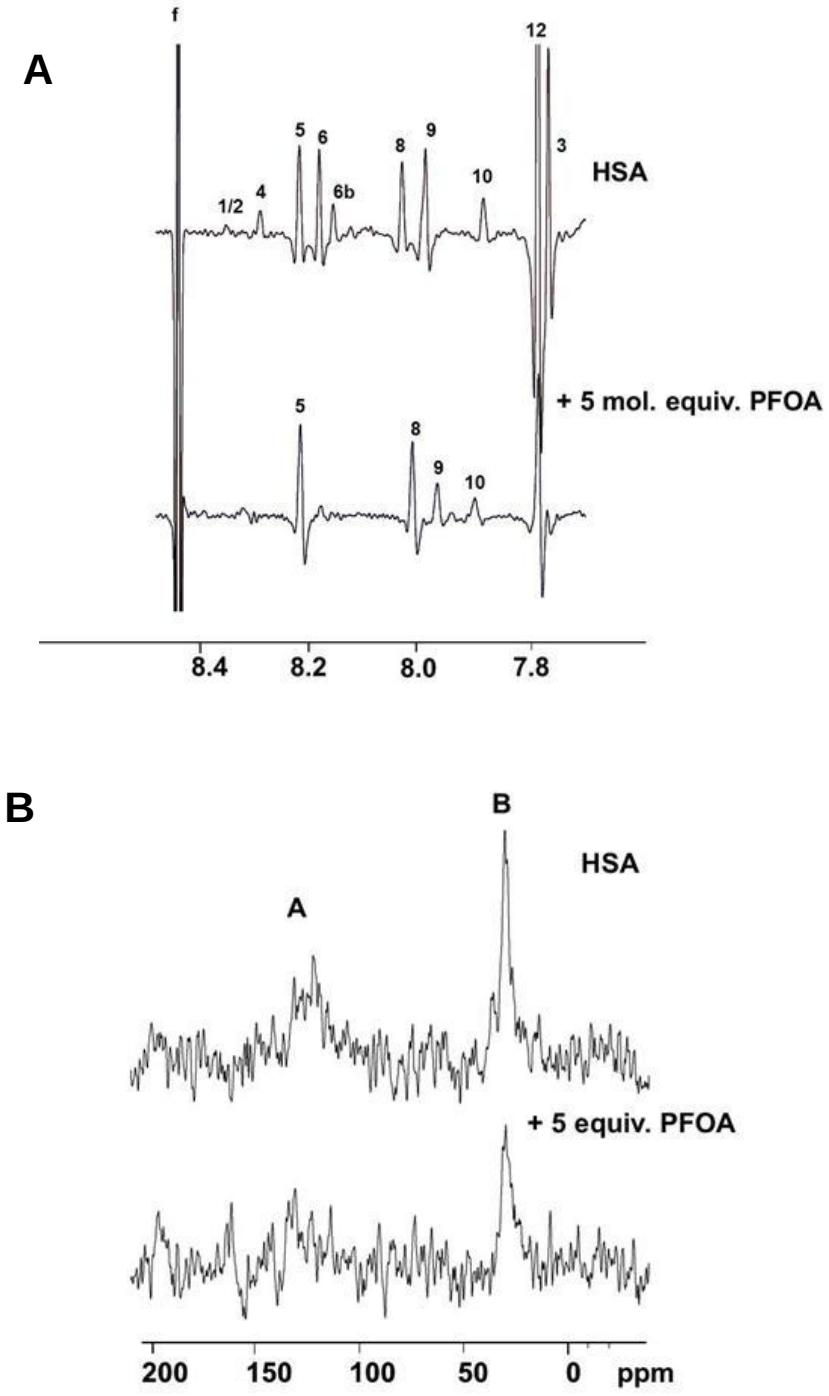

Figure A3 Effect of PFOA binding to HSA on His residues and metal binding. A) 1 mM samples were prepared in 50 mM Tris [D_{11}]-Cl, 50 mM NaCl in 100% D_2O (pH 7.10). Spectra were acquired at 37 °C on a Bruker Avance Ultrashield spectrometer operating at 700 MHz. f = sodium formate at 8.48 ppm which was added as a chemical shift reference. B) 1 mM samples were prepared in 50 mM Tris-Cl, 50 mM NaCl in 10% D_2O (pH 7.4). Spectra were acquired at 37 °C on a Bruker DRX-500 spectrometer operating at 106 MHz for ^{111}Cd. Peaks A and B correspond to Site A and Site B respectively.

Thesis reference: Chapter 4, page 97

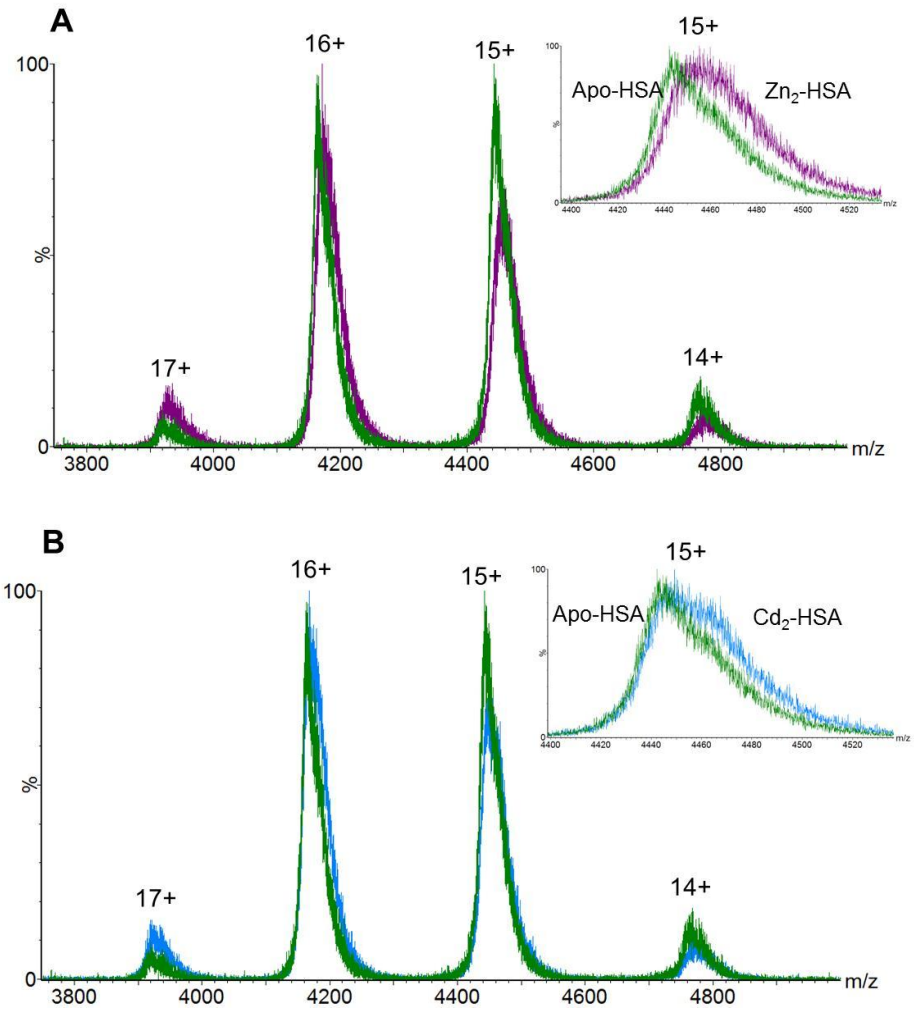

Figure A4. Comparison of spectra obtained for HSA complexes prior to ion mobility experiments. A) HSA with 2. mol. equiv. Zn^{2+} added (*purple*) compared to apo-HSA (*green*). B) HSA with 2. mol. equiv. Cd^{2+} (*blue*). The inset shows a close-up view of the 15+ charge state showing the mass shift observed. Samples were in 200 mM ammonium acetate (pH 7.4). Spectra were obtained on a Synapt HDMS G2 instrument (Waters).

Thesis reference: Chapter 5, page 111 and 115

Table A2 Comparison of the experimental and theoretical masses of charge states observed for HRGP330. Values are expressed as monisotopic masses.

Charge state	Experimental *m/z*	Theoretical *m/z*	∆mass (Da)
3+	1445.00	1445.00	**0.00**
4+	1083.99	1084.00	**0.01**
5+	867.39	867.40	**0.01**
6+	722.99	723.00	**0.01**
7+	619.85	619.86	**0.01**
8+	542.49	542.50	**0.01**

Table A3 Comparison of the experimental and theoretical masses of metalloforms observed for HRGP330. Values are expressed as monoisotopic neutral masses in Da. The italicised numbers are the theoretical values.

Metal ion	Number of metal ions					
	0	**1**	**2**	**3**	**4**	**5**
Zn^{2+}	*4331.98*	*4393.89*	*4455.80*	*4517.71*	*4579.63*	*4641.54*
Zn^{2+}	4331.88	4393.89	4455.79	4517.78	4579.70	4641.64
Cd^{2+}	*4331.98*	*4443.86*	*4555.75*	*4667.64*	*4779.53*	*N/A*
Cd^{2+}	4331.88	4443.81	4555.75	4667.63	4779.54	N/A
Cu^{2+}	*4331.98*	*4392.89*	*4453.80*	*4514.72*	*4575.63*	*4636.54*
Cu^{2+}	4331.88	4392.96	4453.71	4514.68	4575.60	4636.61

Thesis reference: Chapter 5, page 110

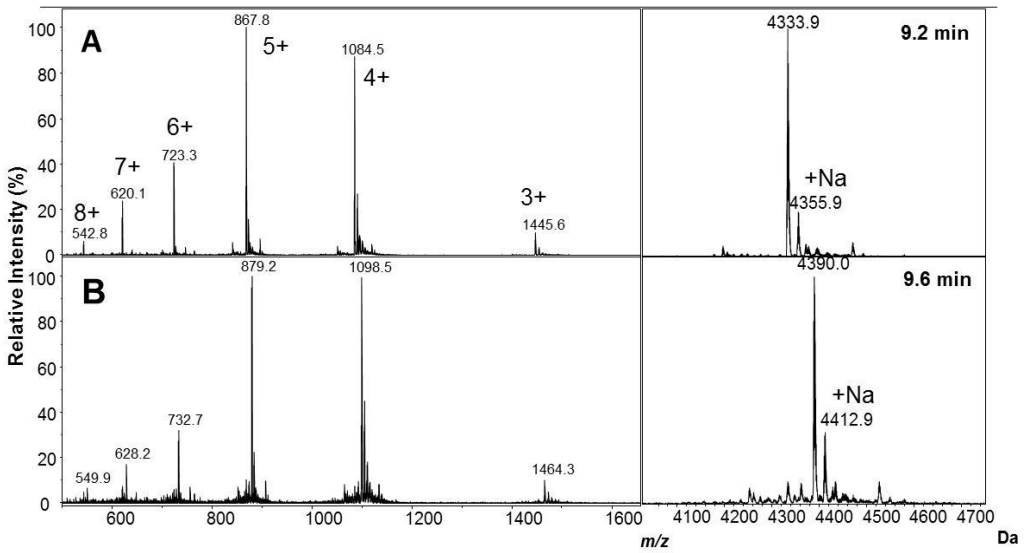

Figure A5 Comparison of products from RP-HPLC of crude HRGP330. A) Peptide that eluted at 9.2 min shows a mass that matches that expected for HRGP330. B) Peptide that eluted at 9.6 min had a mass 4390.0 Da, a mass increase of 56 Da compared to that expected for HRGP330. It is likely that the second peptide still has a protecting group attached as *t*-butyl has a mass of 56 Da.

Thesis reference: Chapter 5, page 116

A

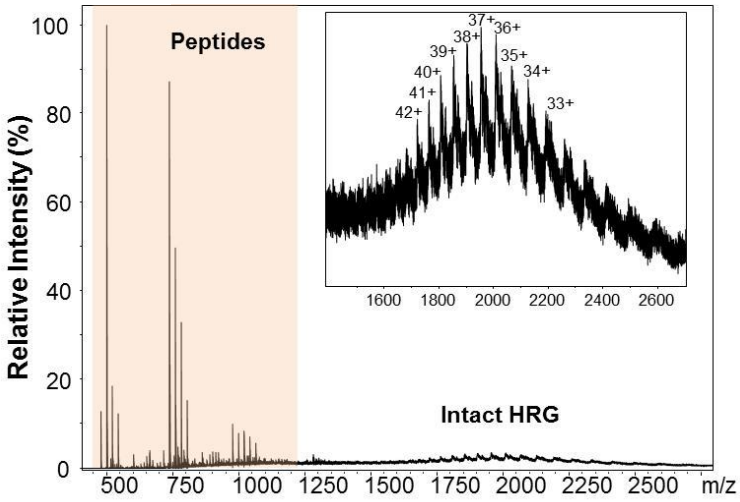

B

Experimental mass	Theoretical mass	Δmass (Da)	Assignment
477.197	477.165	-0.032	(R)CPEE(F)
477.197	477.219	0.022	(F)IEDT(E)
477.197	477.230	0.033	(A)NTKD(S)
477.197	477.249	0.051	(G)QCKV(I)
477.197	477.303	0.106	(C)KTTK(P)
499.178	499.255	0.077	(D)GYLF(Q)
521.160	521.220	0.060	(F)GTNET(H)
521.160	521.224	0.064	(C)PEEF(N)
543.142	543.234	0.092	(H)QHAMG(P)
543.142	543.245	0.102	(Y)YVDF(S)
543.142	543.277	0.135	(P)LPEAN(F)
737.273	737.299	0.025	(I)EDTEPF(R)
737.273	737.340	0.066	(H)QHAMGPP(P)
737.273	737.358	0.084	(V)DFSVRN(C)
737.273	737.358	0.084	(G)PQDLHQ(H)
737.273	737.387	0.113	(S)PVLFDF(I)
759.255	759.298	0.042	(D)FNCTTSS(V)
759.255	759.425	0.169	(P)LAEKALD(L)
759.255	759.425	0.169	(L)AEKALDL(I)
759.255	759.425	0.169	(K)TTKPLAE(K)
759.255	759.425	0.169	(N)TKDSPVL(F)
759.255	759.437	0.182	(I)NKWRR(D)
781.237	781.336	0.099	(S)FDVEASN(L)
781.237	781.340	0.102	(D)VKETDCS(V)
781.237	781.340	0.102	(V)KETDCSV(L)
781.237	781.366	0.129	(F)GFCRADL(S)
803.218	803.379	0.161	(T)NETHRF(P)

Figure A6 ESI-MS of full-length rabbit HRG. A) Low intensity signals are observed for HRG along with peptides visible in the low mass range B) Identification of peptides using FindPept (ExPasy) yields a number of matches that are within 0.2 Da.

Thesis reference: Chapter 5, page 125

Table A4 ^{1}H resonance assignments of HRGP330 recorded at 700 MHz. The spectra were measured at pH 6.20 and 5 °C in 50 mM Tris-D_{11} and 50 mM NaCl.

Residue	NH	Hα	Hβ	Others
D1	8.38	4.51	2.65, 2.51	-
L2	8.43	4.24	1.54	Hδ1 0.81; Hδ2 0.89; γCH 1.403
H3	8.58	4.60	3.06 (Q)	Hδ2 7.04
K6	8.34	4.25	1.69 (Q)	γCH_2 1.29 (Q); εCH2 2.94 (Q)
H7	8.64	-	3.20, 3.12	Hδ2 7.13
S9	8.45	-	3.94, 3.85	-
Q12	8.53	4.23	-	γCH_2 2.27 (Q); Hε21 6.94; Hε22 7.60
E26	8.37	4.20	1.93 (Q)	γCH2 2.14 (Q)
H27	8.63	4.65	-	-
D28	8.40	4.66	2.74, 2.65	-
T29	8.31	4.23	-	γCH_3 1.16
H30	8.53	4.61	3.21, 3.14	Hδ2 7.16
R31	8.19	4.38	1.80, 1.71	δCH_2 3.17 (Q); γCH2 1.54; Hε 7.27
Q32	8.51	4.25	-	γCH2 2.32 (Q); Hε21 6.97; Hε22 7.62
Hs†	8.81	4.64	3.19, 3.13	Hδ2 7.10
Ht†	8.76	4.64	3.20, 3.15	-
Hu†	8.73	4.62	3.15, 3.08	-
Hv†	8.71	4.64	3.11 (Q)	-

† These four His residues (labelled s, t, u and v) are all thought to be after Pro based on strong crosspeaks observed. Therefore they could be His5, His15, His20, His25 or His35.

Thesis reference: Chapter 5, page 127

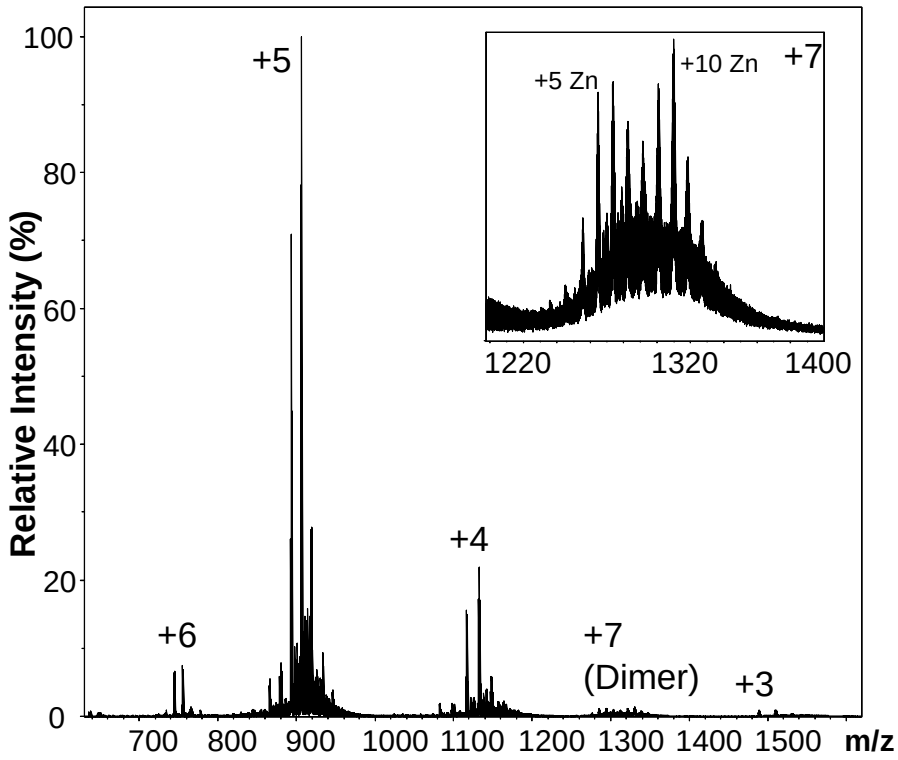

Figure A7 Identification of a Zn^{2+}-bound HRGP330 dimer. The sample was 10 μM HRGP330 in 10 mM ammonium acetate (pH 7.4) that had been incubated with 5 mol. equiv. $Zn(CH_3COO)_2.2H_2O$. The inset shows the +7 charge states of a low intensity Zn^{2+}-bound dimer. The peaks between those labelled in the inset correspond to sequential addition of a Zn^{2+} ion.

Thesis reference: Chapter 5, page 135, 138 and 140

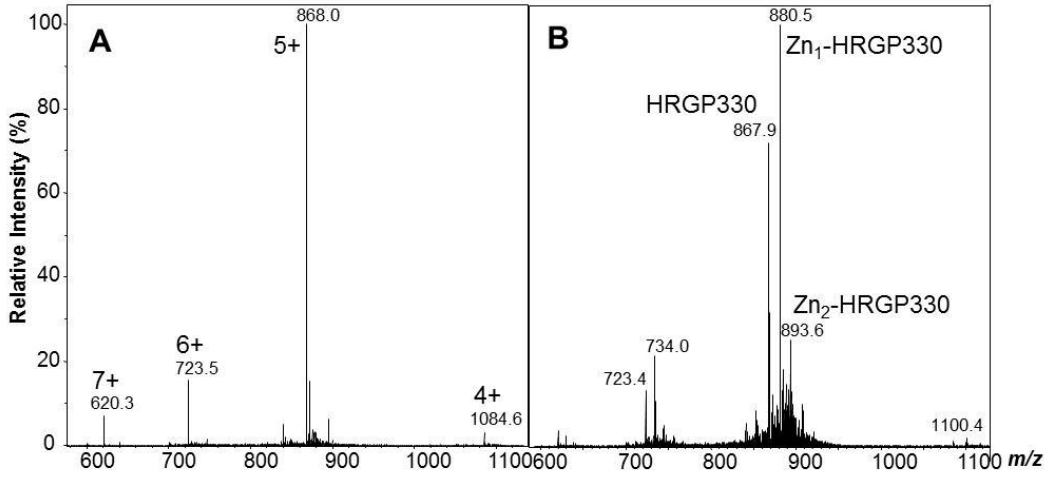

Figure A8 Intact spectrum of HRGP330 prior to top-down MS/MS. A) ESI-MS spectrum of apo-HRGP330 B) ESI-MS spectrum showing Zn_1-HRGP330 and Zn_2-HRGP330. In each case the 5+ charge state was isolated with a width of 4 *m/z* and fragmented by CID and ETD/PTR on an amaZon speed ETD instrument.

Thesis reference: Chapter 5, page 138

Table A5 Summary of Zn^{2+}-bound peptides identified from CID.

Assignment of fragment	Experimental $[M+H]^{1+}$	Theoretical $[M+H]^{1+}$	Δmass (Da)	Experimental + Zn $[M+H]^{1+}$	Theoretical + Zn $[M+H]^{1+}$	Δmass (Da)
y_8	1026.68	1026.49	+0.19	1087.54	1087.40	+0.14
$y1_0$-NH_3	1275.70	1275.57	+0.13	1337.74	1337.50	+0.24
b_{11}	1397.70	1397.64	+0.06	1459.65	1459.55	+0.10
y_{12}	1526.96	1526.71	+0.25	1588.86	1588.62	+0.24
y_{17}	2106.34	2105.97	-0.37	2168.20	2167.89	-0.31
b_{18}	2290.08	2289.93	+0.15	2290.08	2289.93	+0.15
y_{22}	2671.30	2671.22	+0.08	2733.24	2733.14	+0.10
b_{23}	2807.32	2807.28	+0.04	2869.24	2869.19	+0.05
b_{28}	3422.68	3422.52	+0.16	3484.54	3484.43	+0.11
y_{29}	3563.74	3563.60	+0.14	3625.63	3625.51	+0.12
y_{32}	3926.15	3925.80	+0.35	3988.15	3987.71	+0.44
y_{32} –H_2O	3908.12	3907.79	+0.33	3970.00	3969.71	+0.29
y_{33}	4125.12	4124.77	+0.35	4125.12	4124.77	+0.35
b_{33}	4082.02	4081.84	+0.18	4144.04	4143.76	+0.28
y_{34}	4176.65	4175.94	+0.71	4238.30	4237.86	+0.44
y_{34}-NH_3	4158.60	4158.92	-0.32	4220.65	4220.85	-0.20

Thesis reference: Chapter 5, page 144

Table A6 Summary of Zn^{2+}-bound peptides identified from ETD.

Assignment of fragment	Experimental $[M+H]^{1+}$	Theoretical $[M+H]^{1+}$	Δmass (Da)	Experimental + Zn $[M+H]^{1+}$	Theoretical +Zn $[M+H]^{1+}$	Δmass (Da)
z_{13}*	1648.06	1647.75	+0.31	1711.06	1711.56	-0.5
c_{20}	2479.50	2479.15	+0.35	2542.50	2542.65	-0.15
c_{26}	3187.68	3187.46	+0.22	3250.62	3250.96	-0.34
c_{27}	3324.82	3324.52	+0.30	3388.68	3388.02	+0.66
c_{28}	3439.82	3439.54	+0.28	3502.76	3503.04	-0.28
z_{28}*	3410.76	3410.52	+0.24	3473.76	3474.02	-0.26
z_{29}*	3547.82	3548.58	-0.76	3611.62	3612.08	-0.46
z_{30}*	3676.76	3676.68	+0.08	3739.62	3740.18	-0.56
z_{31}*	3812.76	3812.74	+0.02	3876.82	3876.24	+0.58
c_{31}	3833.76	3833.75	+0.01	3986.82	3897.25	+0.57
z_{33}*	4047.94	4047.85	+0.09	4110.82	4111.35	-0.47
z_{34}*	4160.94	4160.94	0.00	4223.82	4224.44	+0.62
c_{34}	4195.94	4195.92	+0.02	4258.94	4259.42	-0.48

*denotes (z+1) and (z+2) ions

Thesis reference: Chapter 6, page 155

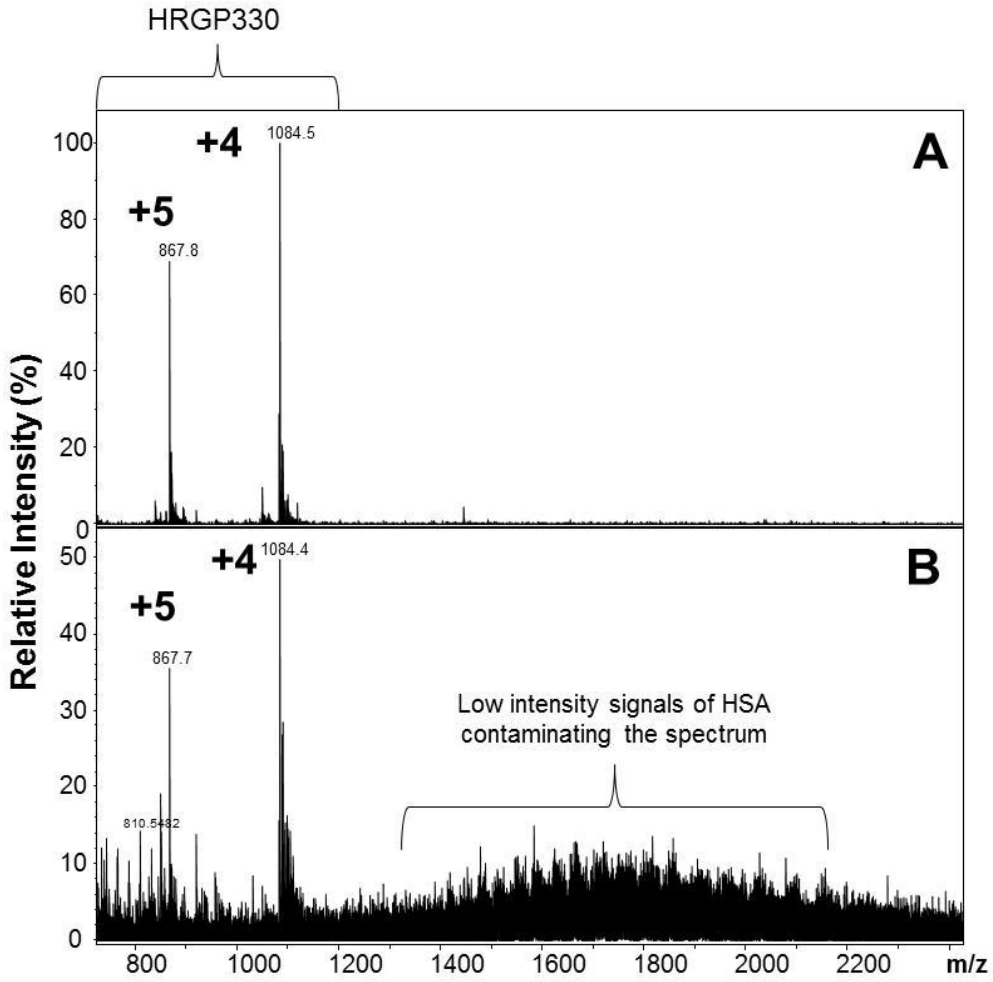

Figure A9 ESI-MS of HRGP330 following incubation with HSA and then separation for analysis. A) 5 μM HRGP330 B) 5 μM HRGP330 following separation from HSA. The HRGP330 can clearly be identified, however, the presence of a small proportion of HSA supressed the HRGP330 charge states considerably. Samples were in 10 mM ammonium acetate (pH 7.4) and spectra were acquired on a maXis-UHR-TOF instrument.